



UNIVERSIDAD NACIONAL AUTÓNOMA DE
MÉXICO

PROGRAMA DE MAESTRÍA Y DOCTORADO EN CIENCIAS
QUÍMICAS

***ESTUDIO DE LA INTERACCIÓN EN FASE GAS DE CÚMULOS SÚPER
PARAMAGNÉTICOS DE ÁTOMOS DE HIERRO CON MOLÉCULAS DE
BENCENO: $Fe_4(benceno)_m$, $m \leq 4$, MEDIANTE TEORÍA DE
FUNCIONALES DE LA DENSIDAD***

TESIS
PARA OPTAR POR EL GRADO DE

MAESTRO EN CIENCIAS

PRESENTA

Q. ISRAEL VALENCIA QUIROZ



TUTOR: Dr. Miguel Castro Martínez

AÑO: 2009



UNAM – Dirección General de Bibliotecas

Tesis Digitales
Restricciones de uso

DERECHOS RESERVADOS ©
PROHIBIDA SU REPRODUCCIÓN TOTAL O PARCIAL

Todo el material contenido en esta tesis está protegido por la Ley Federal del Derecho de Autor (LFDA) de los Estados Unidos Mexicanos (Méjico).

El uso de imágenes, fragmentos de videos, y demás material que sea objeto de protección de los derechos de autor, será exclusivamente para fines educativos e informativos y deberá citar la fuente donde la obtuvo mencionando el autor o autores. Cualquier uso distinto como el lucro, reproducción, edición o modificación, será perseguido y sancionado por el respectivo titular de los Derechos de Autor.

Agradecimientos:

Al CONACyT por la beca otorgada para la realización de los estudios de Maestría, número de becario 223455.

Especial agradecimiento al proyecto CONACYT 60894-CB 2006-1 coordinado por la Dra. Norah Barba Behrens. Los cálculos de este trabajo de tesis fueron realizados en los servidores adquiridos por este proyecto.

La realización de este proyecto se vió ampliamente beneficiado por el Soporte Financiero del Proyecto PAPIIT IN-102308 de DGAPA-UNAM.

Los cálculos de este trabajo de tesis fueron realizados en la supercomputadora Kan-Balam, agradezco profundamente a DGSCA-UNAM por las facilidades de super cómputo asignadas a este proyecto.

A la coordinación del posgrado en Ciencias Químicas por su orientación y grata ayuda.

A las personas involucradas en este equipo de trabajo:

Dr. Jorge Benítez Puebla, Oscar González Antonio, Dr. Alfredo Guevara, Miguel Maynez, Rodrigo Garza, Dra. Inés Nicolás, Dr. Julián Cruz y Dra. Norah Barba Behrens.

A los profesores y miembros de la Facultad de Química por contribuir a mi formación académica y desarrollo personal:

Dra. Josefina de Gyves, M. en C. José Manuel Mendez Stivalet, M. en C. Mercedes Meijueiro, Dra. Silvia Castillo, Dra. Laura Gasque, Dr. David Díaz, Dr. Carlos Bunge, Dr. Hugo Torrens, Dra. Marta Sosa, Q.F.B. Josefina Tenopala.

A los miembros del H. Jurado por sus valiosas observaciones:

Dra. Marcela Betrán Sánchez.

Dr. Roberto Salcedo Pintos.

Dr. Juvencio Robles García.

Dr. Ricardo Gaitán Lozano.

Dr. Gustavo Tavizón Alvarado.

Al departamento de Física y Química Teórica de la Facultad de Química de la UNAM, donde siempre he encontrado apoyo necesario para el desarrollo de mis actividades académicas.

Especialmente a mi asesor de tesis, Dr. Miguel Castro Martínez, quién ha sido mi guía en mi trayectoria académica.

A mi Familia, quienes me han apoyado solidariamente e incondicionalmente con su ayuda en todo momento, Genaro Valencia Santibáñez, Georgina Quiroz Zamora, América Rubí Valencia Quiroz.

Con cariño para Genaro, Georgina y Rubí.

Lugar de realización del trabajo de tesis: Departamento de Física y Química Teórica, División de Estudios de Posgrado, Facultad de Química, Universidad Nacional Autónoma de México.

El resultado de estos trabajos fue presentado en los siguientes congresos:

XII Internacional Materials Research Congreso 2009, Cancún, Quintana Roo, México, Agosto 16-21, 2009. THEORETICAL STUDY OF Fe4-(Benzene) $_m$, $m \leq 4$. Póster.

Primer encuentro académico, QuimiUNAM 2009. Ciudad Universitaria, UNAM, Ciudad de México, Estudio Teórico de las Propiedades Estructurales y Electrónicas de los Complejos Fen-(C₆H₆) $_m$, $n = 4, 6$, y 7 ; y $m \leq 4$. Ponencia. Este trabajo recibió el Premio Luis Ernesto Miramontes Cárdenas, tercer lugar.

Contenido	Página
1. Introducción.	5
2. Hipótesis.	9
3. Objetivos.	10
4. Metodología.	12
5. Resultados.	16
5.1. Especies Aisladas: Fe, Fe ₂ , Fe ₄ y C ₆ H ₆ .	16
5.2. Estado basal de los cúmulos de Fe-bz neutros, cationes y aniones.	21
5.3. Estado basal de los cúmulos de Fe ₄ -bz neutros, aniones y cationes.	24
5.4. Estado basal de los cúmulos de Fe ₄ -bz ₂ neutros, aniones y cationes.	28
5.5. Estado basal de los cúmulos de Fe ₄ -bz ₃ neutros, aniones y cationes.	33
5.6. Estado basal de los cúmulos de Fe ₄ -bz ₄ neutros, aniones y cationes.	38
5.7. Los estados base de los complejos Fe-bz, Fe ₄ -bz, Fe ₄ -bz ₂ , Fe ₄ -bz ₃ y Fe ₄ -bz ₄ .	42
5.7.1. Energías de Unión.	42
5.7.2. Energías de Ionización.	44
5.7.3. Afinidades Electrónicas.	45
5.8. Análisis vibracional.	47
5.8.1. Espectro de infrarrojo del benceno.	47
5.8.2. Espectro de infrarrojo del cúmulo Fe ₄ .	49
5.8.3. Espectro de infrarrojo Fe-bz, neutro catión y anión.	49
5.8.4. Espectro de infrarrojo Fe ₄ -bz neutro, catión y anión.	51
5.8.5. Espectro de infrarrojo Fe ₄ -bz ₂ neutro, catión y anión.	53
5.8.6. Espectro de infrarrojo Fe ₄ -bz ₃ neutro, catión y anión.	55
5.8.7. Espectro de infrarrojo Fe ₄ -bz ₄ neutro.	57
6. Discusión.	58
7. Conclusiones.	71
8. Referencias.	73
9. Apéndice: Artículos publicados en revistas internacionales de riguroso arbitraje	79

1. Introducción

Los cúmulos de los elementos de metales de transición (TM), presentan propiedades estructurales, magnéticas y catalíticas inusuales¹ que en última instancia dependen de su estructura electrónica, diferente de aquella del átomo y del sólido correspondiente, mismas que originan complicados enlaces metal-metal y, en algunos casos, la formación de momentos magnéticos en los sitios atómicos. En particular, los cúmulos pequeños de átomos de hierro, Fe_n, exhiben súper paramagnetismo, debido a que tienen momentos magnéticos mayores que los del sólido.^{2,3} Recientemente ha sido posible efectuar el estudio de la adsorción de moléculas orgánicas sobre cúmulos pequeños de TM_n^{4,5,7}, utilizando técnicas de vaporización láser.⁶ De esta manera, los compuestos neutros Fe_n-(benceno)_m han sido producidos en la fase gaseosa^{5,7} y caracterizados posteriormente, por espectrometría de masas, espectroscopía fotoelectrónica y pruebas de reactividad química. Específicamente se han sintetizado complejos de cúmulos de átomos de hierro, (Fe_n), con benceno (bz), Fe_n-bz_m, n ≤ 7 y m ≤ 4 para los cationes⁷ y n ≤ 9 y m ≤ 4 para los aniones⁸. En ausencia de efectos del disolvente, este tipo de complejos son muy importantes para estudiar las interacciones básicas metal-ligante que determinan las propiedades fisicoquímicas de estos sistemas. En este caso, se espera que el enlace esté dominado por los electrones 3d del cúmulo y la nube π del benceno. Nakajima⁷, Kaya y colaboradores han sugerido que los complejos Fe_n-bz_m pueden formar estructuras tipo “sándwich multicapa” (múltiple-

¹ Bansmann, J.; et al. Magnetic and structural properties of isolated and ensamblated clusters. *Surf. Sci. Rep.* **2005**, 56, 189.

² Billas, I. M. L.; Chatelain, A.; de Heer, W. A. Magnetism from the atom to the bulk in iron, cobalt and nickel clusters. *Science*, **1994**, 265, 1682.

³ Cox, D. M.; Trevor, D. J.; Whetten, R. L.; Rohlfing, E. A.; Kaldor, A. Magnetic behavior of free-iron and iron-oxide clusters. *Phys. Rev. B*, **1985**, 32, 7290.

⁴ Duncan, M. A. Structures, energetic and spectroscopy of gas phase transition metal ion-benzene complexes. *Int. J. Mass Spectrom.* **2008**, 272, 99.

⁵ Nakajima, A.; Kaya, K. A novel network structure of organometallic clusters in the gas phase. *J. Phys. Chem. A*, **2000**, 104, 176.

⁶ Dietz, T. G.; Duncan, M. A.; Powers, D. E.; Smalley, R. Laser production of supersonic metal cluster beams. *J. Chem. Phys.* **1981**, 74, 6511.

⁷ Kurikawa, T.; H. Takeda; M. Hirano, Judai, K; Arita T; Nagao S; Nakajima A; Kaya K. Electronic properties of organometallic Metal-Benzene Complexes [M_n(benzene)_m (M) Sc-Cu)]. *Organometallics*, **1999**, 18, 1430-1438.

⁸ Zheng, W.; Eustis, N. S.; Li, X.; Nilles J. M.; Thomas, O. C.; Bowen, K. H.; Kandalam A. K.; Photoelectron spectroscopic study of iron–benzene cluster anions. *Chem. Phys. Lett.* **2008**, 462, 35-39.

decker) o estructuras tipo “bola de arroz” (rice-ball), esto depende del número de electrones tipo *d* en su capa de valencia. Con base en esta suposición los primeros elementos de la serie de transición (Sc, Ti, V) formarían complejos con geometría de tipo sándwich multicapa con las moléculas de benceno; mientras que, los últimos metales de transición (Fe, Co, Ni) formarían estructuras tipo “bolas de arroz”.

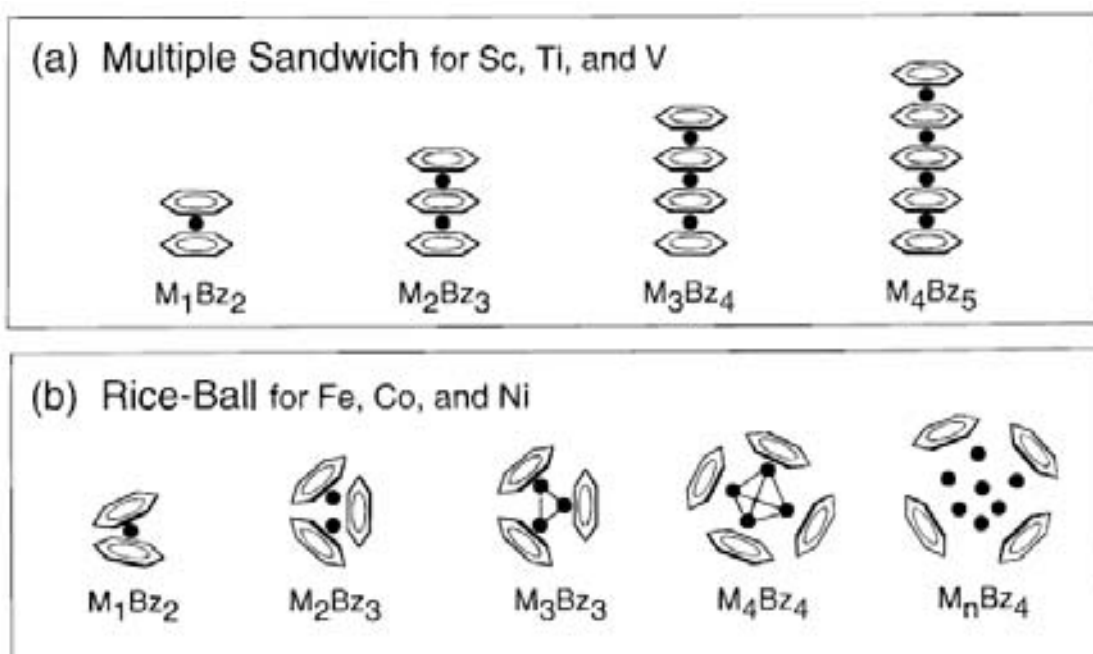


Figura 1. (a) Estructuras propuestas por Kurikawa et al.⁷ para los primeros elementos de la serie de metales de transición Sc, Ti y V; sándwich múltiple. (b) Estructuras propuestas para los últimos elementos de la serie de metales de transición de Fe a Ni; rice-ball.

Los complejos organometálicos formados, a partir de elementos de transición con benceno son los sistemas más pequeños caracterizados, por tener una parte orgánica que es aromática y una parte metálica que puede ser magnética. Para altas concentraciones de benceno, el espectro de masas revela que el número máximo *m* de especies adsorbidas es más pequeño que *n*, permitiendo proponer que los complejos $Fe_n\text{-(benceno)}_m$ tienen estructuras del tipo “bolas de arroz”, que consisten de un cúmulo de Fe_n cubierto con los ligantes de benceno adsorbidos en su superficie. El sistema observado más grande ha sido el cúmulo de Fe_7 que adsorbe cuatro ligantes.^{5,7} Dicha cantidad de especies orgánicas adsorbidas es consistente con la sugerencia de geometrías “bolas

de arroz” para Fe₆ y Fe₇. Sin embargo, la información experimental acerca de cómo las moléculas de benceno interactúan con los cúmulos es aún muy escasa, específicamente en lo que concierne a las propiedades estructurales y electrónicas del benceno coordinado con los cúmulos de hierro. Por otro lado, la adsorción sobre los cúmulos TM_n con ligantes puede evitar su coalescencia, particularmente para el hierro, el cual forma fácilmente cúmulos más grandes o bien, los óxidos correspondientes. Por otra parte, se han estudiado las frecuencias vibracionales -particularmente en el infrarrojo (IR)-, de complejos de átomos de hierro con hidrocarburos aromáticos polí-cíclicos, debido a su alto interés en problemas espectroscópicos en astrofísica. En este trabajo de tesis también se analizaron dichas frecuencias para los complejos Fe_n-(benceno)_m.⁹

En la parte teórica los cálculos para la estructura electrónica de cúmulos de TM_n representan un gran reto para los métodos de la Química Cuántica Computacional, lo que es debido a la abundancia de diferentes estados electrónicos y a la posibilidad de varios isómeros, contenidos estos en un intervalo de energía muy estrecho. Además, surge también la complejidad inherente de los átomos de los elementos de transición, ya que contienen capas de orbitales 3d abiertas de corto alcance, altamente direccionales y orbitales 4s altamente deslocalizados y de largo alcance. Los métodos multirreferenciales, en los cuales, las funciones de onda son tratadas como funciones multiconfiguracionales serían los más adecuados para la descripción correcta de este tipo de sistemas. Sin embargo estos métodos no pueden aplicarse directamente a sistemas de cúmulos de TM_n debido a su alto costo computacional. Solamente se han aplicado al estudio de los dímeros TM₂¹⁰ o al estudio de átomos TM con una molécula de benceno.¹¹ El estudio de los iones TM unidos a la molécula de benceno se ha realizado al nivel denominado “Modified

⁹ Szczepanski, J.; Wang, H.; Vala, M.; Tielens, A. G. G. M.; Eyler, J. R.; Oomens, J. Infrared Spectroscopy of gas-phase complexes of Fe³⁺ and polycyclic aromatic hydrocarbon molecules. *J. ApJ.* **2006**, 646, 666.

¹⁰ Hübner, O.; Sauer, J. Confirmation of 9 Sigma(-)(g) and 8 Sigma(-)(u) ground states of Fe-2 and Fe-2 by CASSCF/MRCI. *Chem. Phys. Lett.* **2002**, 358, 442.

¹¹ Kandalam, A. K.; Jena, P.; Li, X.; Eustis, S. N.; Bowen, K. H. Photoelectron spectroscopy and theoretical studies of [Co-m(pyrene)(n)](-) (m=1,2 and n=1,2) complexes. *J. Chem. Phys.* **2008**, 129, 134308.

Coupled-Pair Functional” (MCPF).¹² Por otra parte, Duncan y colaboradores^{4,13} han estudiado a los complejos de iones de metales de transición coordinados con benceno, mediante el empleo del funcional híbrido B3LYP;^{14,15} el análisis comparativo revela que sus resultados son de una exactitud similar a la obtenida con el método MCPF, y que concuerdan con resultados experimentales.^{4,13} Gutsev and Bauschlicher²⁸ han mostrado que el método BPW91^{16,17} es un esquema apropiado para el estudio de las propiedades estructurales, electrónicas y energéticas de cúmulos pequeños Fe_n , $n \leq 6$. Efectivamente, hemos encontrado que el método BPW91 y las bases orbitales de calidad 6-311++G(2d,2p), constituye una herramienta computacional apropiada para este tipo de complejos. Previamente, y como parte de mi proyecto de posgrado he realizado investigaciones acerca de las propiedades estructurales, electrónicas y energéticas del sistema Fe_7 - (benceno);¹⁸ también he estudiado la interacción de una y dos moléculas de benceno con el cúmulo súper paramagnético de Fe_6 ; para estos complejos, $\text{Fe}_6\text{-}(\text{C}_6\text{H}_6)_{1,2}$, se estudiaron las propiedades estructurales, electrónicas, energéticas y vibracionales. Estos dos temas de investigación, desarrollados durante estos dos años, dieron lugar a un par de publicaciones en el *Journal of Physical Chemistry A*^{19, 20}. De estos estudios, básicamente se ha concluido que existe una disminución en el magnetismo presentado por el cúmulo de Fe_7 cuando se forma el complejo con la molécula de benceno y que existen disminuciones en los momentos magnéticos totales, además, de que se forman interacciones con los electrones tipo *d* del cúmulo de hierro con la nube π del benceno en los enlaces Fe-C y que las coordinaciones de hapticidad igual a seis, η^6 , son las

¹² Baushlicher, C. W.; Partridge, H.; Langhoff, S. R. Theoretical Study of transition-metal ions bound to benzene. *J. Phys. Chem.* **1992**, 96, 3273.

¹³ Jaeger, T. D.; van Heijnsbergen, D.; Klippenstein, S. J.; von Helden, G.; Meijer, G.; Duncan, M. A. Vibrational spectroscopy and density functional theory of transition-metal ion-benzene and dibenzene complexes in the gas phase. *J. Am. Chem. Soc.* **2004**, 126, 10981.

¹⁴ Becke, A. D.; Density Functional Thermochemistry .3. The role of the exact exchange. *J. Chem. Phys.* **1993**, 98, 5648-5652.

¹⁵ Stephens, P. J.; Devlin, F. J.; Chabalowski, C. F.; Frisch, M. J. Ab initio calculation of vibrational absorption and circular-dichroism spectra using density functional force-fields. *J. Phys. Chem.* **1994**, 98, 11623.

¹⁶ Becke, A. D. Density-Functional exchange energy approximation with correct asymptotic behavior. *Phys. Rev. A.* **1988**, 38, 3098.

¹⁷ Perdew, J. P.; Wang, Y. Pair-distribution function and its coupling-constant average for the spin polarized electron-gas. *Phys. Rev. B.* **1992**, 45, 13244.

¹⁸ Valencia, I.; Chávez, V.; Castro, M. Bonding of Benzene with Excited States of Fe_7 , *J. Phys. Chem. A.* **2008**, 112, 5028-5033.

más favorecidas. Por otra parte, el análisis vibracional revela, que se presentan desplazamientos característicos en los espectros de infrarrojo, estos cambios indican que se produce un debilitamiento en los enlaces C-C del benceno, además de una menor energía de unión de los bencenos con el cúmulo de hierro a medida que aumenta el número de bencenos adsorbidos.

En este trabajo se efectuará el estudio teórico de las estructuras tipo rice-ball, de los complejos del cúmulo de Fe_4 contenido hasta 4 moléculas de benceno mediante cálculos del tipo de todos-los-electrones, realizados con la aproximación de gradientes generalizado (GGA, por sus siglas en inglés, generalized gradient approximation) de la teoría de funcionales de la densidad. Como se verá más adelante los resultados obtenidos permitirán la determinación de la geometría de los estados de mínima energía producidos por la interacción del cúmulo de Fe_4 con benceno, así como el análisis de las energías de unión, energías de ionización y afinidades electrónicas. Estos resultados estructurales y electrónicos son útiles para el estudio de las interacciones entre los electrones 3d del cúmulo y la nube π del benceno y para describir el tipo de enlace que existe en estas especies. También estudiaremos los cambios en las frecuencias vibracionales que ocurren en el benceno después del proceso de adsorción. Este trabajo se realizó con el programa computacional Gaussian 03¹⁹.

2. Hipótesis

Como hipótesis de trabajo suponemos que el método elegido, BPW91/6-311++G(2d,2p) describe apropiadamente las complicadas interacciones de intercambio y correlación electrónica que ocurren en este tipo de sistemas, mismos que presentan un reto para los métodos de cálculo de

¹⁹Gaussian 03, Revision E.01, M. J. Frisch, G. W. Trucks, H. B. Schlegel, G. E. Scuseria, M. A. Robb, J. R. Cheeseman, J. A. Montgomery, Jr., T. Vreven, K. N. Kudin, J. C. Burant, J. M. Millam, S. S. Iyengar, J. Tomasi, V. Barone, B. Mennucci, M. Cossi, G. Scalmani, N. Rega, G. A. Petersson, H. Nakatsuji, M. Hada, M. Ehara, K. Toyota, R. Fukuda, J. Hasegawa, M. Ishida, T. Nakajima, Y. Honda, O. Kitao, H. Nakai, M. Klene, X. Li, J. E. Knox, H. P. Hratchian, J. B. Cross, V. Bakken, C. Adamo, J. Jaramillo, R. Gomperts, R. E. Stratmann, O. Yazyev, A. J. Austin, R. Cammi, C. Pomelli, J. W. Ochterski, P. Y. Ayala, K. Morokuma, G. A. Voth, P. Salvador, J. J. Dannenberg, V. G. Zakrzewski, S. Dapprich, A. D. Daniels, M. C. Strain, O. Farkas, D. K. Malick, A. D. Rabuck, K. Raghavachari, J. B. Foresman, J. V. Ortiz, Q. Cui, A. G. Baboul, S. Clifford, J. Cioslowski, B. B. Stefanov, G. Liu, A. Liashenko, P. Piskorz, I. Komaromi, R. L. Martin, D. J. Fox, T. Keith, M. A. Al-Laham, C. Y. Peng, A. Nanayakkara, M. Challacombe, P. M. W. Gill, B. Johnson, W. Chen, M. W. Wong, C. Gonzalez, and J. A. Pople, Gaussian, Inc., Wallingford CT, 2004.

la Química Cuántica Computacional. Esto es, la determinación del estado basal es razonablemente exacta y permitirá efectuar un análisis de los enlaces Fe-C que son los que determinan, en última instancia, las propiedades de este tipo de complejos organometálicos.

En la parte fenomenológica y para el caso específico de los cúmulos de hierro, un elemento tardío en la serie de transición, suponemos que forman complejos estables con benceno del tipo de geometría denominada “bola de arroz”, y de que estas estructuras exhiben las propiedades características que se han determinado experimentalmente para estos compuestos en la fase gaseosa, como son: energías de ionización, afinidad electrónica, momentos magnéticos, etc. En los cálculos realizados en este trabajo de tesis se tomaron diferentes geometrías en las que las moléculas de benceno están dispuestas alrededor del cúmulo magnético de Fe_4 , para cada una de estas estructuras iniciales se probaron al menos tres diferentes multiplicidades para determinar el estado de mínima energía del sistema. Efectivamente, después del proceso de optimización de la geometría, lo que incluye tanto relajamiento estructural como electrónico, se encontró que las geometrías de mínima energía son del tipo bolas de arroz, en donde las moléculas de benceno están dispuestas sobre la superficie del cúmulo de Fe_4 , el cual preserva su estructura, aunque con una distorsión más grande que la que ocurre en el cúmulo libre de Fe_4 , la cual es una geometría tetraédrica distorsionada.

3. Objetivos

Objetivo General

Determinar la geometría del estado basal de los complejos $\text{Fe}_4\text{-bz}_n$, $n \leq 4$, y el modo de coordinación de las moléculas de benceno con el cúmulo de Fe_4 . Y en base a este estado basal, explicar las propiedades del complejo.

Objetivos Particulares

Para los complejos F_4bz_n , $n \leq 4$, determinar:

1. La geometría del estado basal del complejo neutro, anión y catión por medio de cálculos del tipo todos-los-electrones, realizados con el método BPW91/6-311++G(2d,2p), y haciendo uso de facilidades de súper-computo, lo cual es crucial para poder efectuar estos cálculos.
2. Analizar los Orbitales Moleculares para los estados de mínima energía de los complejos, y entender la naturaleza de la unión química de los electrones 3d del cúmulo con la nube π del benceno.
3. Determinar de manera adiabática las propiedades fisicoquímicas tales como, Energía de Ionización, Afinidad Electrónica, Energía de Unión, y ver las tendencias que exhiben estas propiedades a medida que aumenta el número de moléculas absorbidas. El comportamiento de estas propiedades también nos permitirá entender la naturaleza de la estructura electrónica de los complejos.
4. Estudiar el comportamiento del momento magnético durante el proceso de absorción del benceno. Para cada uno de los sistemas esto dará una información muy valiosa acerca de los cambios en la magnetización que experimenta el cúmulo de Fe_4 con la absorción de benceno, se anticipan cambios drásticos de esta propiedad.
5. El cálculo de los Espectros de Infrarrojo, proveerá de una información por lo demás valiosa acerca del cambio que experimental las frecuencias prototípicas del benceno al coordinarse con el cúmulos magnético. En particular, los corrimientos hacia el rojo para algunas de estas frecuencias darán un indicio del debilitamiento que sufren los enlaces C-C del anillo del benceno.

4. Metodología.

Los estados basales (GS) de los complejos $\text{Fe}_n\text{-}(benceno)_m$, $n \leq 4$ y $m \leq 2$, incluyendo los complejos neutros, aniones y cationes fueron determinados por medio de cálculos de todos los electrones realizados con el funcional BPW91^{16,20} que fue usado con el conjunto base 6-311++G(2d,2p). Es necesario puntualizar que el intercambio electrónico, un efecto puramente cuántico, sin análogo clásico, es un orden de magnitud mayor que la energía de correlación. La energía de correlación se define como la energía total exacta del sistema, obtenida de manera experimental, menos la energía de Hartree-Fock sin incluir efectos relativistas. La energía de intercambio ó Hartree-Fock contribuye con un 99% de la energía total, sin embargo, este 1% de imprecisión que la correlación aporta es muy importante en química, porque proporciona valores típicos de la energía involucrada en procesos como ionización, afinidad electrónica, formación y ruptura de enlaces que ocurren en las reacciones químicas, también es importante para cuantificar pequeños efectos magnéticos.

Entre los métodos para el cálculo de las energías de intercambio y correlación electrónica proporcionados por la teoría DFT se cuenta con el funcional BPW91, éste funcional se forma con el funcional de intercambio de Becke (B)¹⁶ y el funcional de correlación¹⁷ desarrollador por Perdew y Wang (PW91). El método de Hartree-Fock considera el intercambio electrónico por la elección del determinante de Slater, el cual representa a la función de onda anti-simétrica de un sistema de n -electrones. Este cálculo corresponde al intercambio electrónico para un sistema inhomogéneo de muchos electrones, que a su vez se puede aproximar al cálculo del intercambio para un gas uniforme de electrones de espín polarizado en un volumen (Jellium), con la aproximación local de la densidad electrónica (LDA). Esta aproximación se generaliza si se consideran las correcciones de gradientes de la densidad electrónica, denominadas como GGA por sus siglas en inglés (generalized gradient approximation), y se aplica a sistemas donde la variación

²⁰ Burrow, P. D.; Michejda, J. A.; Jordan, K. D. Electron transmission study of the temporary negative-ion states of selected benzenoid and conjugated aromatic-hydrocarbons. *J. Chem. Phys.* **1987**, 86, 9.

de la densidad electrónica con la posición es importante, esto es, en sistemas atómicos y/o moleculares en donde la estructura electrónica es muy complicada, como es el caso justamente de sistemas que contienen átomos ó elementos de la serie de transición, tal como los complejos de Fe-benceno a estudiar en esta tesis.

La energía de intercambio de Becke E_x^{B88} se puede expresar explícitamente como:

Energía de Intercambio

$$E_X^{LSDA} = -C_X \sum_{\sigma=\alpha,\beta} \int \rho_{\sigma}^{4/3} d^3 r$$

$$C_X = 3/2(3/4\pi)^{1/3}$$

$$E_X^{B88} = E_X^{LSDA} - b \sum_{\sigma=\alpha,\beta} \int \frac{(\rho^{\sigma})^{4/3} \chi_{\sigma}^2}{1 + 6b \chi_{\sigma} \operatorname{senh}^{-1} \chi_{\sigma}}$$

donde,

$$\chi_{\sigma} \equiv |\nabla \rho^{\sigma}| / (\rho^{\sigma})^{4/3}$$

$$\operatorname{senh}^{-1} x = \ln[x + (x^2 + 1)^{1/2}], b = 0.0042$$

Y la forma explícita para el funcional de la energía de correlación BPW91 es:

PerdewWang – Correlacion

$$r_s = [3/4\pi(n \uparrow + n \downarrow)]^{1/3}$$

$$\zeta = (n \uparrow - n \downarrow) / (n \uparrow + n \downarrow)$$

$$\varepsilon_c(r, \zeta) = \varepsilon_c(r_s, 0) + 1/2 \alpha_c(r_s) \zeta^2 + \dots$$

Donde $n \uparrow$ y $n \downarrow$ son las densidades de espín hacia arriba y hacia abajo y la energía de correlación por electrón ε_c se puede desarrollar de manera logarítmica o mediante derivadas para el parámetro r y la polarización de espín relativa ζ , para expresiones de alta o baja densidad, respectivamente.

Este funcional de densidades de espín corregido por gradiente proporciona una descripción adecuada para el estudio de efectos magnéticos delicados, como podrían ser por ejemplo los que se manifiestan en cúmulos pequeños de átomos de hierro, en donde los resultados experimentales

revelan la presencia de súper paramagnetismo. Los funcionales de correlación y de intercambio local incluyen sólo los valores de las densidades de espín del electrón. Los funcionales corregidos por gradiente incluyen ambos, valores de la densidad del espín del electrón y de sus gradientes.²¹

La base orbital utilizada para los átomos es de calidad 6-311++G(2d,2p)²¹, considerada como una base suficientemente grande, adecuada para la descripción correcta de la correlación electrónica. Se caracteriza porque representa la función contraída tipo gausiana de cada capa interna por seis funciones primitivas gausianas y por tres primitivas más otra gausiana con una primitiva, la función contraída gausiana de cada capa de valencia, además, agrega dos funciones gausianas difusas (++) en todos los átomos, agrega dos funciones tipo *d* sobre los átomos pesados y dos funciones tipo *p*, sobre los átomos de hidrógeno, esto es, los exponentes de estas gausianas son muy pequeños (0.01-0.1). Las funciones contraídas y primitivas para el hierro son (15s11p6d2f)/[10s7p4d2f], mientras que para el Carbono se tiene (12s6p2d)/[5s4p2d], y para el Hidrógeno son (6s2p)/[4s2p].^{22,23,24}.

Se utilizó el software de química cuántica Gaussian-03.¹⁹ Se incluyó un criterio de convergencia estricto para la energía total; minimizada hasta 10^{-8} unidades atómicas. Durante el proceso de atomización de la geometría, las fuerzas fueron optimizadas hasta un corte de 10^{-5} . Estas altas tolerancias son necesarias para la estimación del estado basal, puesto que muchos estados fueron encontrados dentro de un rango muy estrecho de energía. Se empleó una malla ultra fina para estos procesos y para la estimación de las frecuencias de vibración, la cual se realizó bajo la aproximación harmónica para todas las geometrías optimizadas. Con esta metodología se inspeccionaron las regiones de mínima energía de la superficie de energía potencial, PES, para cada complejo neutro y cargado (*n, m*).

²¹ Exploring chemistry with electronic structure methods. Foresman J. Y Frisch A. 2da.Gaussian, Inc., Ed. 1996. pp. 119.

²² Wachters, A. J. H. Gaussian basis set for molecular wavefunctions containing third-row atoms. *J. Chem. Phys.* **1970**, 52, 1033.

²³ Hay, P. J. Gaussian basis sets for molecular calculations – representation of 3d orbitals in transition-metal atoms. *J. Chem. Phys.* **1977**, 66, 4377.

Los estados reportados corresponden a los mínimos de energía verdaderos, lo cual se corrobora con los valores positivos de vibración. También se determinaron los orbitales moleculares MO de las especies neutras optimizadas usando los programas GaussView y ChemCraft. Especialmente, los orbitales moleculares frontera HOMO (Highest Occupied Molecular Orbital), orbital más alto ocupado y LUMO (Lowest Unoccupied Molecular Orbital), orbital más bajo desocupado son importantes para el análisis del enlace químico y los procesos de ionización y afinidad electrónica.

Es de resaltar que el estudio de los cúmulos de MT y de estos cúmulos interactuando con ligantes requiere el uso de funcionales capaces de describir las complicadas interacciones metal-metal y metal-ligante.

La teoría de funcionales de la densidad toma en cuenta la correlación e intercambio de sistemas de varios electrones a través de la aproximación de gradiente generalizado (GGA), por ejemplo la combinación del funcional de intercambio propuesto por Becke¹⁶ y para la correlación desarrollado por Perdew y Wang,¹⁷ junto con el uso de un conjunto base apropiado,²⁴ ha probado ser capaz de determinar el estado basal de la geometría, las propiedades electrónicas, energéticas y electrónicas de sistemas MT o cúmulos presentando complicadas interacciones metal-metal.

18,25,26,28

²⁴ Raghavachari, K.; Trucks, G. W. Highly correlated systems – excitation-energies of 1st row transition metals Sc-Cu. *J. Chem. Phys.* **1989**, 91, 1062.

²⁵ Castro, M. On the interaction of magnetic iron clusters with hydrocarbons: Fe₄-propane. *Chem. Phys. Lett.* **2007**, 435, 322-326.

²⁶ Castro, M. On the bonding of methane with magnetic Fe-4 clusters. *Chem. Phys. Lett.* **2007**, 446, 333-338.

5. Resultados.

5.1. Especies Aisladas: Fe, Fe₂, Fe₄, y C₆H₆.

Los resultados que arrojan los cálculos realizados muestran que el estado basal para el átomo de Fe corresponde a una multiplicidad $M = 2S+1 = 5$, donde S es el espín total, este resultado significa que existen 4 electrones con espines desapareados. La energía en unidades atómicas es de -1263.746419, este valor numérico servirá para obtener los valores de energías de unión, E.U., del cúmulo Fe₄ como E.U. = E(Fe₄)-4E(Fe). Encontramos que los estados excitados corresponden a multiplicidades M = 3 a 0.84 eV y M = 7 a 2.75 eV.

El estado basal del dímero de Fe corresponde a una multiplicidad M = 7 con una distancia de enlace Fe-Fe de 2.01 Å. Con estados excitados M = 9 y M = 5 a 0.49 eV y 0.83 eV. Esta longitud de enlace servirá como referencia al estudiar el enlace Fe-Fe en el cúmulo de Fe₄ sólo y complejado con benceno. El momento magnético por átomo es de 3.0 μ_B . Este valor es más pequeño que el del átomo que es de 4 μ_B . Esto puede deberse a un acoplamiento de los espines de cada átomo, durante el proceso de formación del enlace químico en Fe₂.

En el caso de la molécula de benceno las distancias de enlace C-C corresponden a 1.398 Å, y las distancias C-H corresponden a 1.089 Å. Estos valores se encuentran muy cercanos a los valores experimentales de 1.399 y 1.101 Å²⁷; todos los ángulos de enlace son iguales a 120°.

El estado basal del cúmulo de Fe₄ corresponde a una multiplicidad de M = 15 y el momento magnético por átomo es de 3.5 magnetones de bohr, μ_B , que concuerda con resultados experimentales, ≈ 3.0 μ_B por átomo para cúmulos pequeños de hierro,^{2,3} con una longitud de enlace promedio de 2.352 Å. Este resultado está en acuerdo con el cálculo teórico reportado por Berski²⁸ y asimismo con el de Bauschlicher,²⁹ que utilizó el método BPW91/6-311+G(d). También encontraron un tetraedro

²⁷ Kuchitsu, K. *Structure Data of Free Polyatomic Molecules*, Landolt-Börnstein, New Series, Group II; Springer, Heidelberg

²⁸ S. Berski, G.L. Gutsev, M.D. Mochena, Toward understanding the electron density distribution in magnetic clusters: Insight from the ELF and AIM analyses of ground state Fe-4. *J. Phys. Chem. A.* **2004**, 108, 6025.

²⁹ Gennady, L. G; Bauschlicher C, W, Jr. Electron Affinities, Ionization Energies, and Fragmentation Energies of Fe_n Clusters (n) 2-6): A Density Functional Theory Study. *J. Phys. Chem. A.* **2003**, 107, 7013-7023.

distorsionado para el estado basal de Fe_4 , con longitudes de enlace similares a nuestro resultado; también existe concordancia con el ordenamiento de los estados excitados. El momento dipolar es de 0.0 Debyes, D.

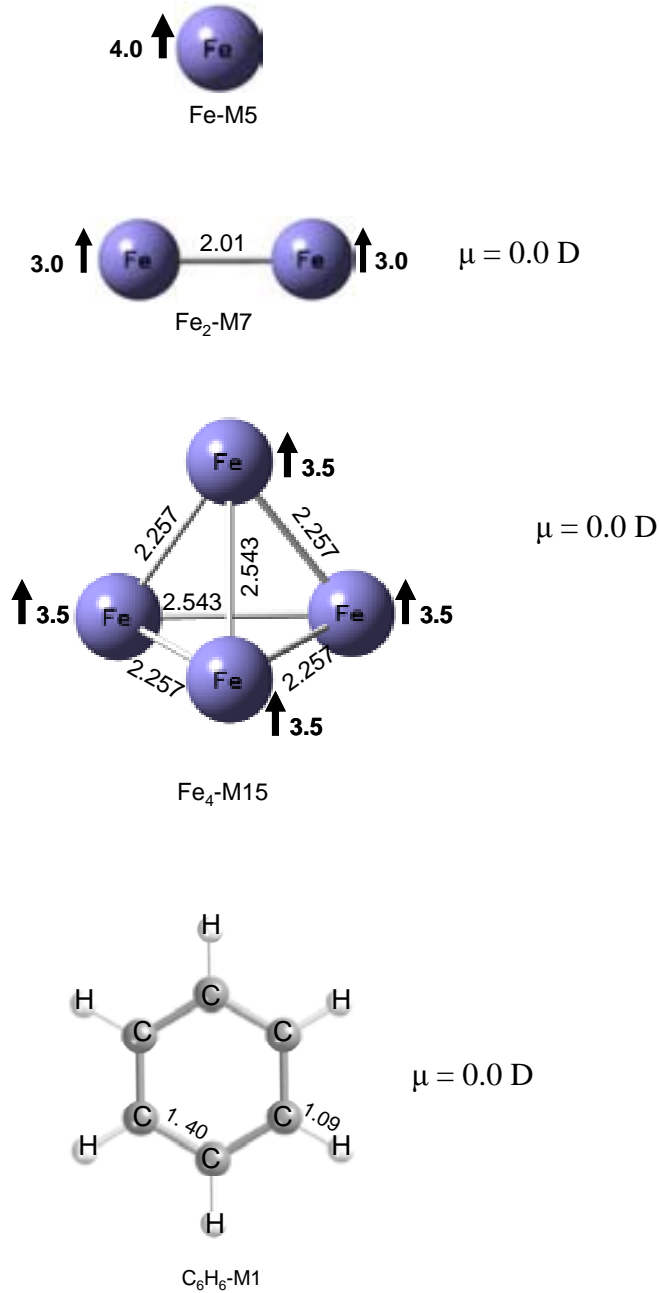


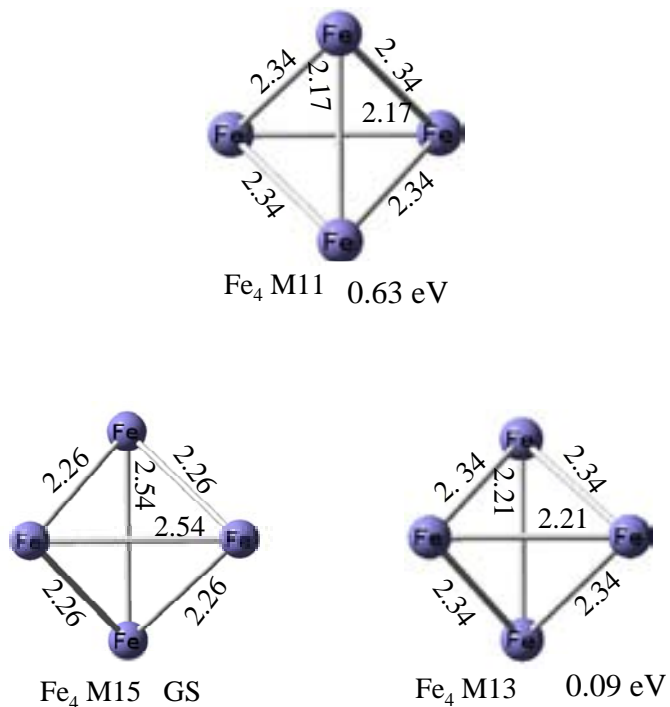
Figura 2. Geometría y multiplicidad calculadas del estado basal para el átomo de Fe, el dímero de Fe, Fe_4 y la molécula de benceno.

La energía de unión del Fe_4 , E.U., se calcula como $E(\text{Fe}_4) - 4E(\text{Fe}) = -7.63 \text{ eV}$ y de -1.91 eV por átomo de Fe. El momento magnético correspondiente es de $3.5 \mu_B$ por cada átomo de hierro,

observamos que es $0.5 \mu_B$ mayor que el del dímero. Este valor se tomará como referencia para observar el efecto de la complejación sucesiva del cúmulo de Fe_4 con las moléculas de benceno.

La multiplicidad correspondiente al anión es $M = 16$ lo que significa un momento magnético de $3.75 \mu_B$ por átomo²⁸, mayor que el del neutro por $0.25 \mu_B$. Las distancias de enlace Fe-Fe van desde 2.32 \AA hasta 2.91 \AA .

La multiplicidad correspondiente al catión es de $M = 12$, es decir, que se redujo con respecto al estado neutro y el momento magnético es de $2.75 \mu_B$ ²⁸. Las distancias de enlace Fe-Fe son de 2.29 \AA .



$$\text{Afinidad electrónica} = 1.77 \text{ eV}$$

$$\text{A. E. exp.} = 1.78(6) \text{ eV}^{30}$$

$$\text{Energía de ionización} = 5.73 \text{ eV}$$

$$\text{E. I. exp} = 6.78 \text{ eV}^{31}$$

Figura 3. Geometría y multiplicidad del estado basal y estados excitados del cúmulo de hierro, Fe_4 .

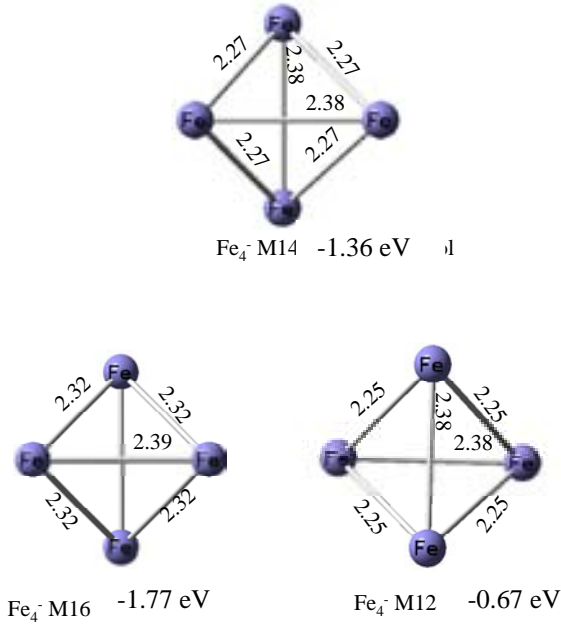


Figura 4. Geometría y multiplicidad del estado basal y estados excitados del anión del cúmulo de Fe_4

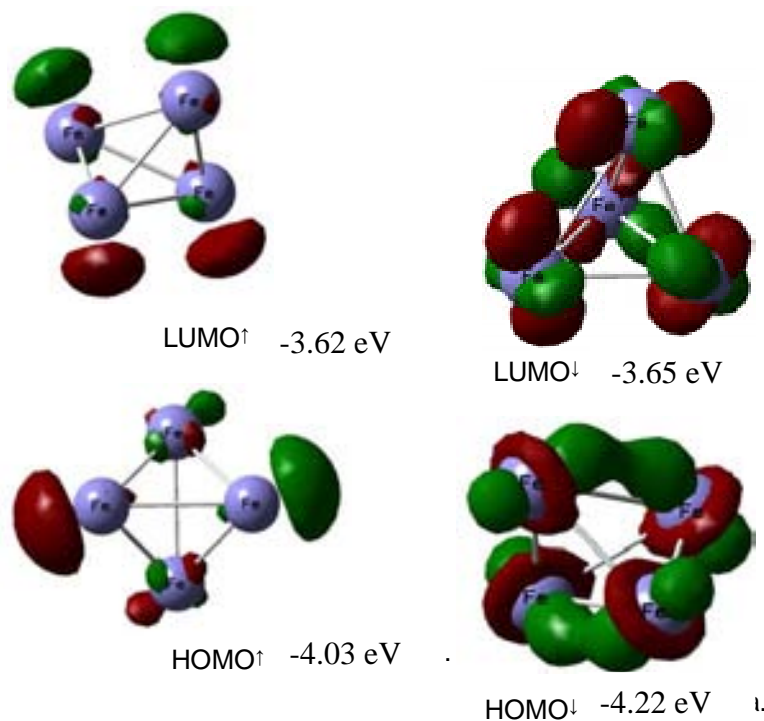


Figura 5. Orbitales moleculares LUMO, HOMO, HOMO-1 de espín mayoritario y LUMO de espín minoritario del cúmulo de Fe_4 .

Hallamos que el estado basal del cúmulo de Fe₄ tiene distancias de enlace Fe-Fe de 2.257 y 2.543 Å, los estados excitados del cúmulo de Fe₄ en la Figura 3 tienen multiplicidades de M = 13 y 11 respectivamente y se encuentran a 8.87 kJ/mol y 60.65 kJ/mol. El primer estado se encuentra a una energía relativamente cercana del estado basal, lo que sugiere que estas dos especies logran coexistir en el experimento, mientras que la especie de multiplicidad M = 11 se encuentra a una energía menos disponible. Estos estados excitados además de los aniones y cationes concuerdan con los calculados por Bauschlicher,²⁸ y con los resultados experimentales reportados por Wang³⁰ y Parks³¹. El anión correspondiente de energía más baja tiene una multiplicidad M = 16, esto indica que el electrón añadido llega al orbital LUMO de espín mayoritario, las distancias de enlace Fe-Fe son de 2.32 y 2.39 Å, los otros dos aniones calculados de multiplicidad M = 12 a una energía relativa de -64.68 kJ/mol y M = 14 a -131.57 kJ/mol se encuentran a valores relativamente altos de energía por lo que se espera que no coexistan con el anión del estado basal. En el caso del catión la geometría de este catión es de un tetraedro perfecto con distancias de enlace Fe-Fe de 2.29 Å. Observamos que existe un reacomodo de los espines de modo que se obtiene como el de menor energía el de multiplicidad igual a 12 cuando el valor esperado era M = 16 o M = 14. Sin embargo este resultado indica que el electrón fue sustraído del orbital HOMO de espín mayoritario, el cual muestra una hibridización 4sp, el cual podría traslapar con los orbitales del ligante,²⁶ en este caso del benceno, y que además el electrón ubicado en el orbital HOMO-1 se reacomoda para ubicarse en el orbital LUMO de espín minoritario. Como se advertirá más adelante este comportamiento no se sigue para los complejos Fe₄-bz_n, n ≤ 4, en los que los orbitales participantes son únicamente los orbitales frontera HOMO y LUMO de espín mayoritario y minoritario. Los estados excitados tienen multiplicidades M = 14 a +590.08 kJ/mol y M = 16 a 653.89 kJ/mol.

³⁰ Wang, L. S.; Li X.; Zhang, H. F.; Probing the electronic structure of iron clusters using photoelectron spectroscopy. *J. Chem. Phys.* **2000**, 262, 56.

³¹ Parks, W. K.; Klots, T. D.; Riley, S. J. Chemical probes of metal cluster ionization-potentials. *J. Chem. Phys.* **1990**, 92, 3813.

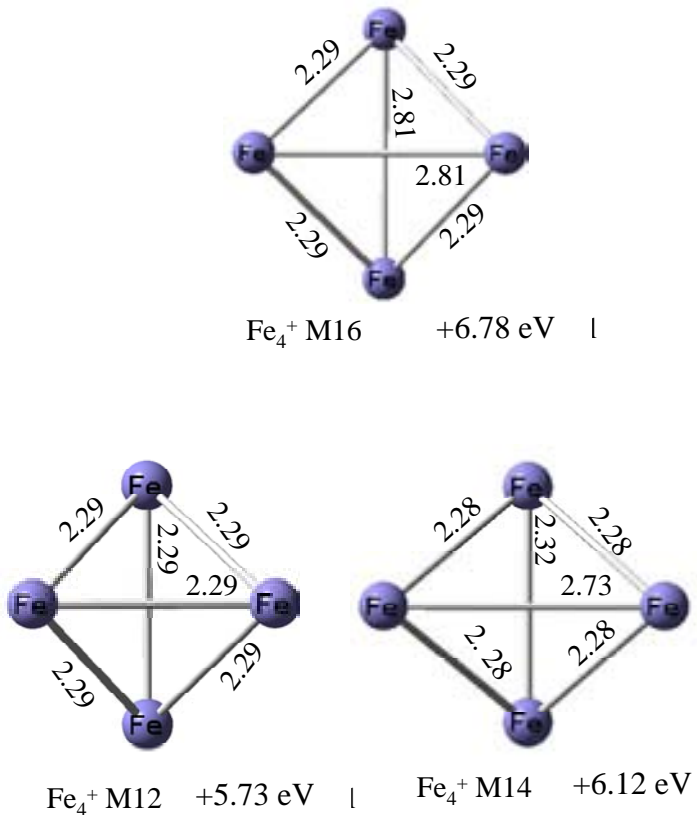
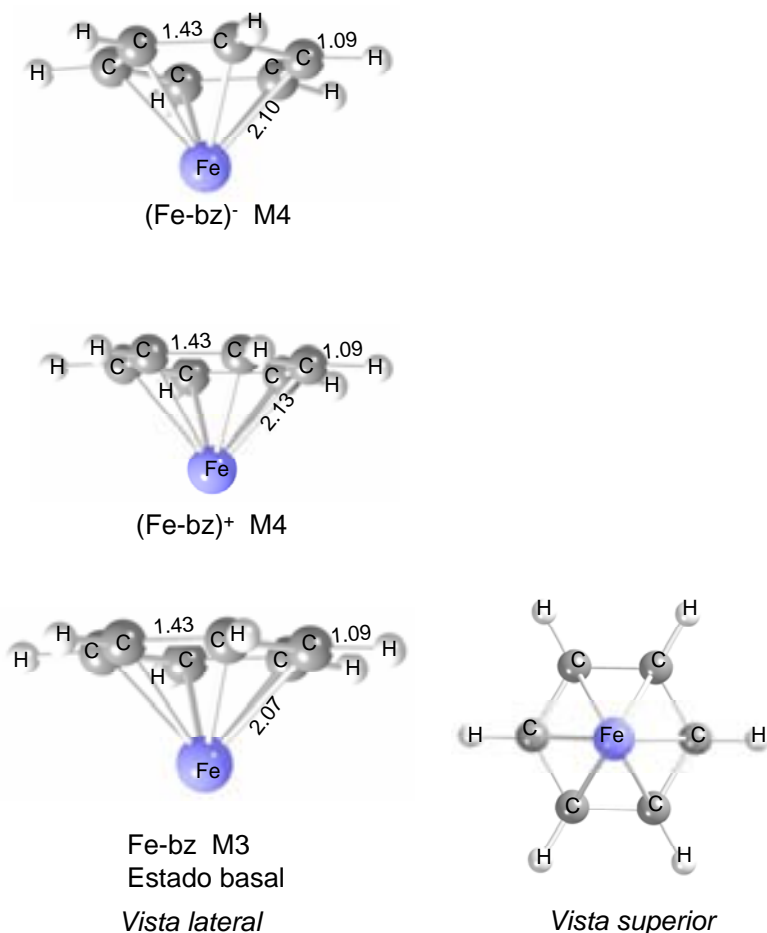


Figura 6. Geometría y multiplicidad del estado basal y estados excitados del catión del cúmulo de Fe_4

5.2. Estado basal de los cúmulos de Fe-bz neutros, cationes y aniones.

Observamos en la Figura 7 que las distancias Fe-C son de 2.07 para el estado basal de Fe-bz y presenta $M = 3$, por lo tanto el momento magnético es de 2 magnetones de bohr, más pequeño que el del átomo aislado, $M = 5$ ($4 \mu_B$). Las distancias Fe-C de 2.07 Å sugieren la formación del enlace Fe-C puesto que son más pequeñas que la suma de los radios de van der Waals, de 1.7 Å para el carbono y de 1.9 Å para el hierro. Esto muestra que el complejo Fe-bz tiene una coordinación igual a 6, η^6 . En el benceno las distancias C-C aumentan de 1.40 a 1.43 Å, y la molécula sigue siendo plana, puesto que los ángulos dihedros son iguales a cero. Las distancias Fe-C crecen en el catión de $M = 4$ a 2.13 Å y a 2.10 Å en el anión $M = 4$, indicando un debilitamiento del enlace Fe-C. Dado que las multiplicidades del anión y del catión son iguales a 4, esto nos indica que los orbitales más disponibles en el caso del anión es el LUMO de espín mayoritario con contribuciones tipo s en el caso del hierro y p_z en el benceno. Para el complejo

neutro el HOMO es de espín minoritario con contribuciones d_z^2 en el átomo de hierro y tipo p y s en los átomos de carbono e hidrógeno. Observamos que los orbitales LUMO y HOMO-n son de antienlace y de no enlace respectivamente, lo que coincide con las mayores distancias Fe-C observadas para el anión y el catión.



Afinidad electrónica = 0.47 eV

A. E. exp. = 0.46 ± 0.1 eV⁸

Energía de ionización = 6.44 eV

E. I. exp = 6.42 ± 0.04 eV⁷

Figura 7. Geometría y multiplicidad para el estado basal del complejo Fe-bz neutro, catión y anión.

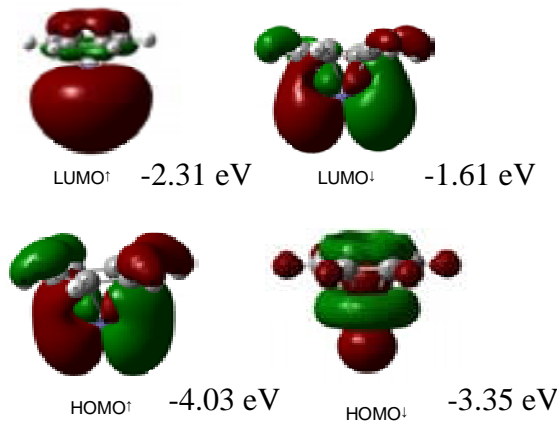


Figura 8. orbitales moleculares del complejo Fe-bz de espín mayoritario y minoritario.

Este diagrama de correlación de orbitales moleculares fue calculado para el complejo Fe-bz debido a que es la estructura más sencilla de calcular, en este diagrama se utilizaron propiedades de simetría para el átomo de hierro se utilizó una simetría octaédrica O_h , mientras que para el benceno se utilizó una simetría D_{6h} . En el caso del complejo Fe-bz se utilizó una simetría C_{6v} .

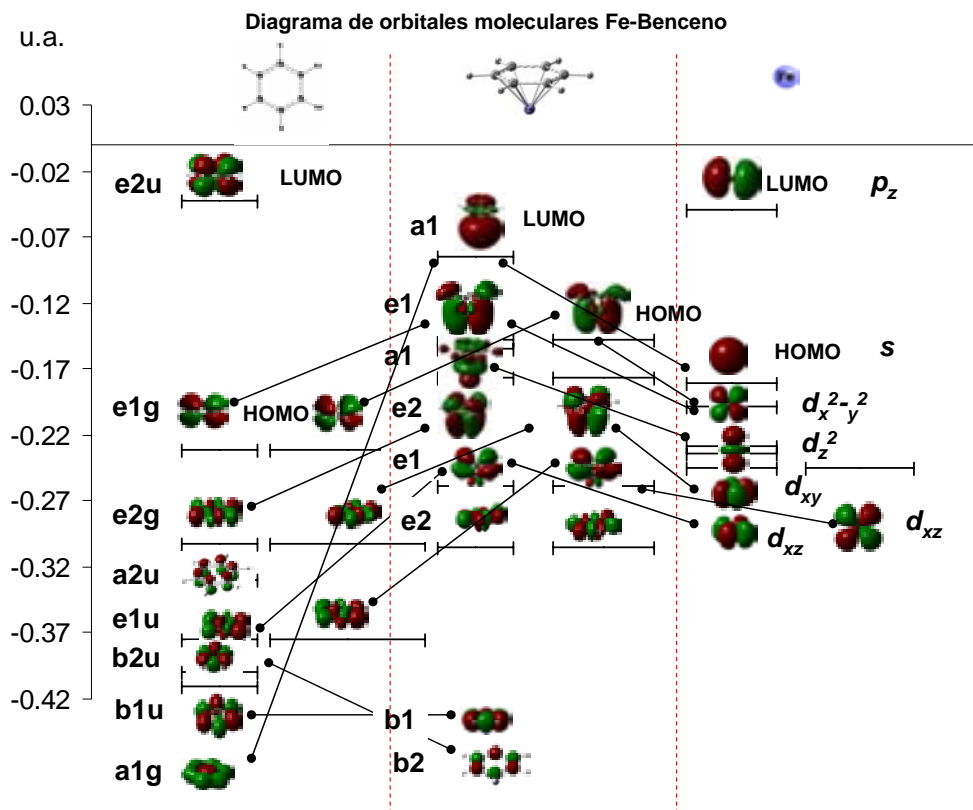


Figura 9. Diagrama de correlación de orbitales moleculares Fe-bz.

5.3. Estado basal de los cúmulos de Fe₄-bz neutros, aniones y cationes.

Observamos en la Figura 10 para el complejo neutro Fe₄-bz que el átomo coordinado al benceno tiene una η^6 , con una distancia Fe-C de 2.10 Å. Las distancias de enlace Fe-Fe son de 2.28 y 2.25 Å. Los estados excitados del cúmulo Fe₄-bz se encuentran a 0.35 eV para M = 13 y 0.46 eV para M = 9, con distancias de enlace Fe-C de 2.16-2.19 Å y 2.09-2.10 Å y longitudes de enlace Fe-Fe de 2.31-2.34 Å y 2.07-2.44 Å respectivamente.

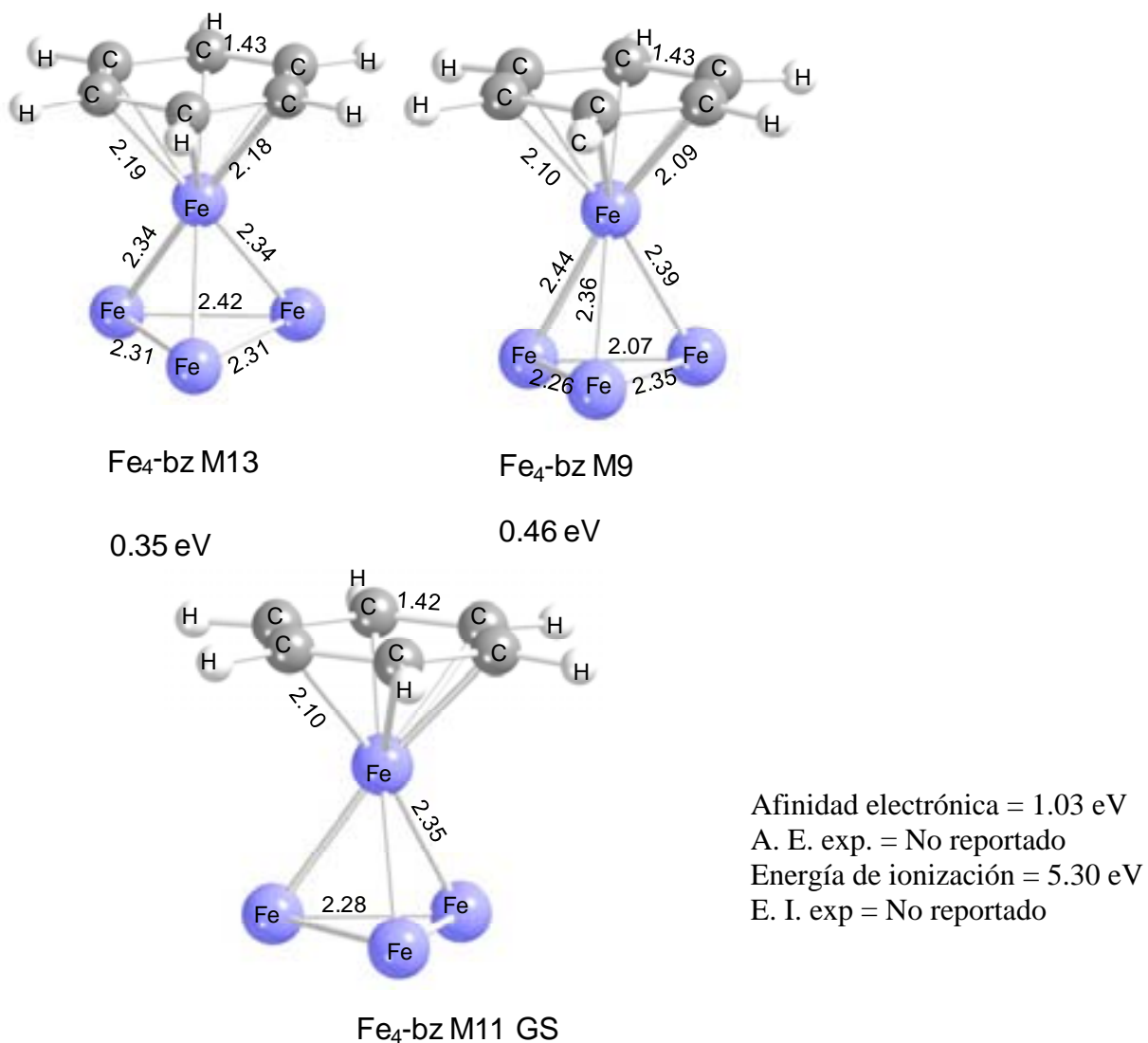


Figura 10. Geometría y multiplicidad para el estado basal y estados excitados del complejo Fe₄-bz neutro.

El anión correspondiente de energía más baja tiene una coordinación η^6 . Las distancias de enlace Fe-C son de 2.08-2.10 Å, y distancias de enlace Fe-Fe de 2.20-2.51 Å. La multiplicidad es igual a 10, a -1.03 eV, esto indica que el electrón añadido llega al orbital LUMO de espín minoritario, los otros dos aniones calculados de multiplicidad M = 12 y M = 8 se encuentran a -0.79 y -0.29 eV. En el caso del catión la multiplicidad del estado basal es igual a 12 a +5.33 eV, lo que indica que el electrón es sustraído del orbital HOMO de espín minoritario. La coordinación es η^6 , distancias de enlace Fe-C de 2.17 Å, y Fe-Fe de 2.28 y 2.34 Å. Los estados excitados M = 10 se encuentran a +5.83 eV y M = 8 a +6.11 eV.

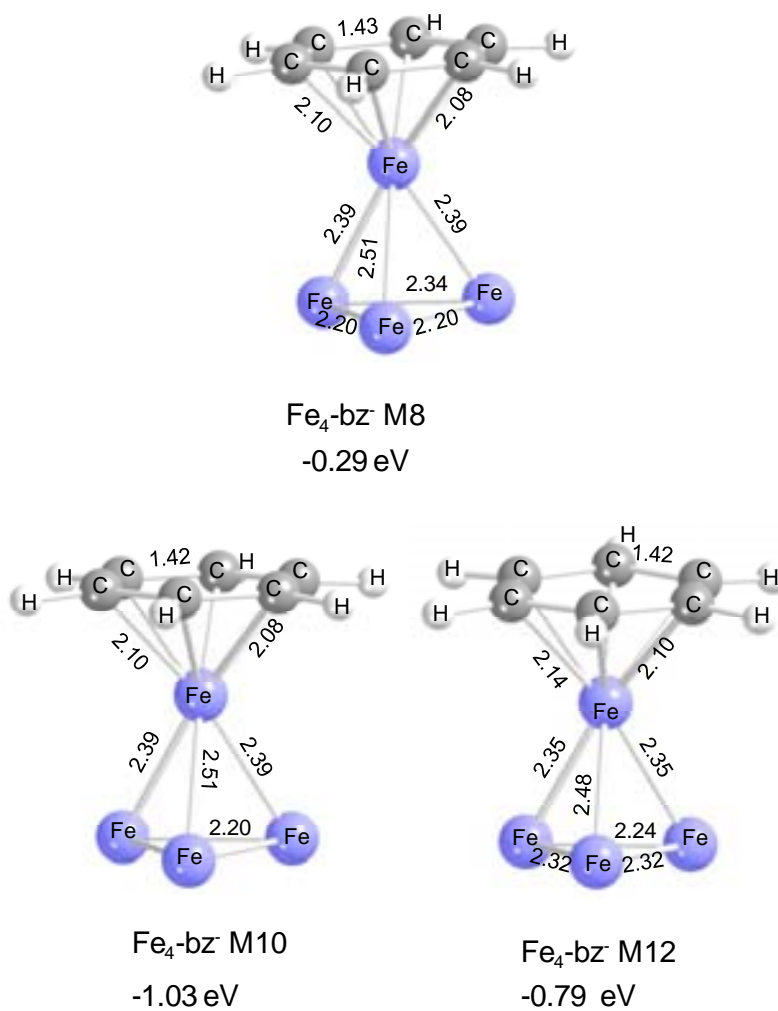


Figura 11. Geometría y multiplicidad para el estado basal y estados excitados del complejo $\text{Fe}_4\text{-bz}$ anión.

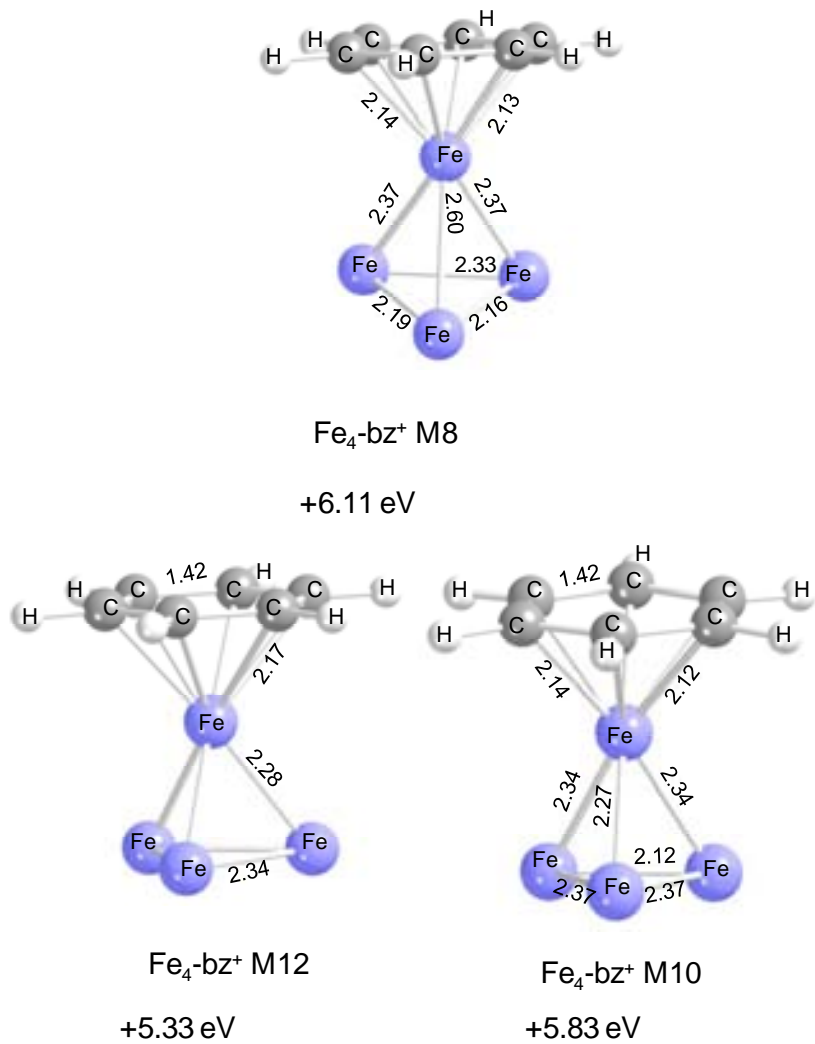


Figura 12. Geometría y multiplicidad para el estado basal y estados excitados del complejo $\text{Fe}_4\text{-bz}$ catión.

Debido a que el estado basal del complejo $\text{Fe}_4\text{-C}_6\text{H}_6$ tiene una multiplicidad $M = 11$, y a que el anión correspondiente tiene una multiplicidad $= 10$, esto significa que el electrón añadido se introdujo en el orbital LUMO de espín beta, reduciendo así la multiplicidad del complejo como se muestra en la Figura 13. Observando las distancias de enlace en el complejo anión podemos predecir el tipo de orbital molecular que fue ocupado, es decir, si las distancias de enlace en el anión son mayores que en el complejo neutro esto nos indicaría que el espín orbital LUMO beta es de antienlace, mientras que si las distancias se contraen en el anión, esto nos diría que este orbital es de enlace.

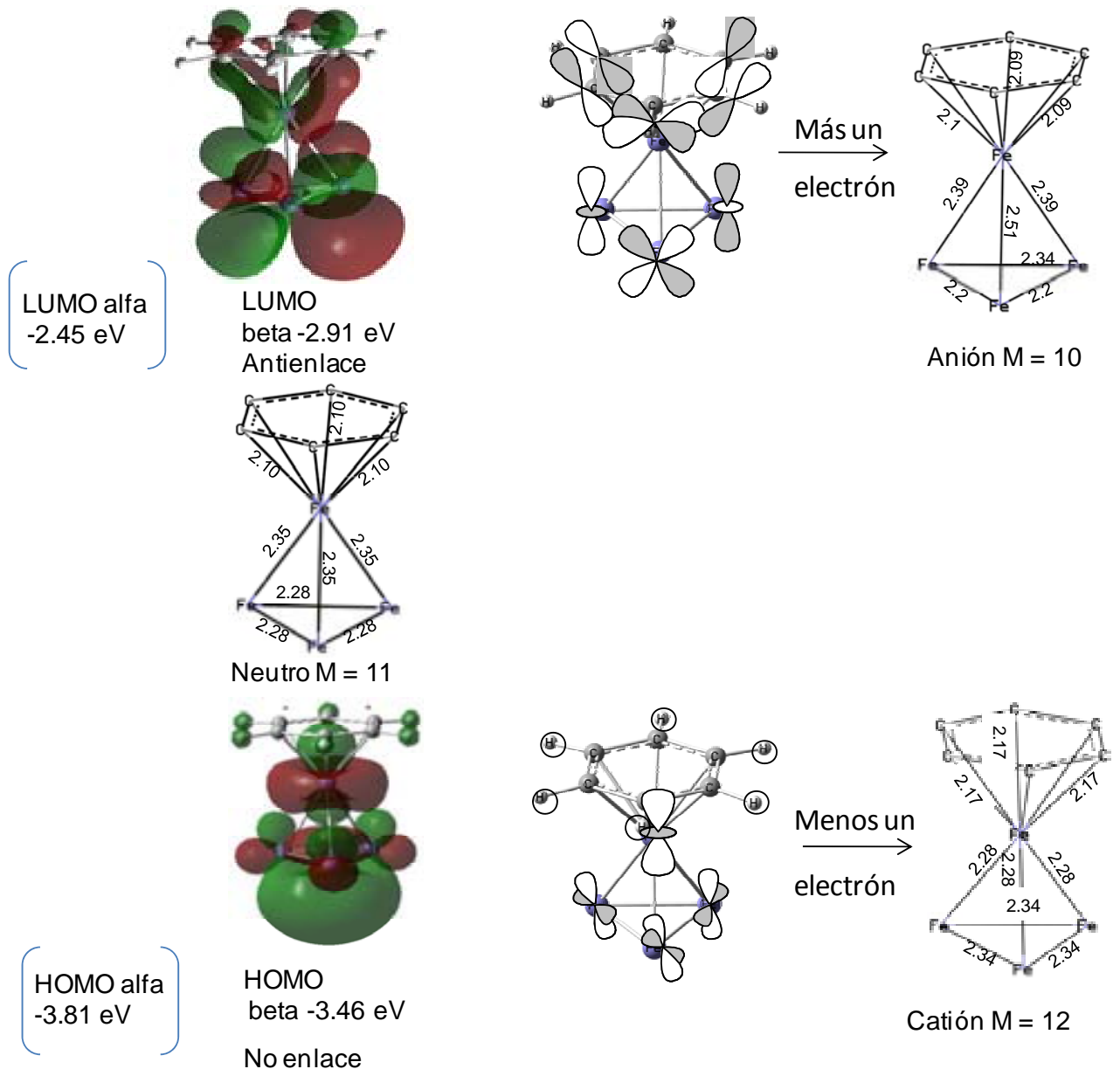


Figura 13. Diagrama de orbitales moleculares del complejo $\text{Fe}_4\text{-bz}$, LUMO de espín minoritario y HOMO de espín minoritario.

De la misma forma podemos hacer una predicción para el catión observando que la multiplicidad correspondiente es $M = 12$, lo que parece indicar que el electrón sustraído se encontraba en el orbital HOMO beta, aumentando así la multiplicidad del catión. En este caso

dependiendo de si las distancias de enlace en el catión son mayores o menores que en el complejo neutro podemos deducir si el espín orbital es de enlace o de no enlace.

Observamos entonces que el espín minoritario es el que participa en la alteración de la estructura electrónica del complejo Fe_4Bz , debido a que se localiza más profundo en energía.

5.4. Estado basal de los cúmulos de $\text{Fe}_4\text{-bz}_2$ neutros, aniones y cationes.

Observamos que el complejo neutro $\text{Fe}_4\text{-bz}_2$ tiene una multiplicidad $M = 7$ correspondiente al estado basal, con coordinaciones η^6 de las dos moléculas de benceno, con distancias de enlace Fe-C de 2.10-2.12 Å para el primer benceno y distancias de enlace Fe-C de 2.11-2.15 Å para el segundo, las distancias de enlace Fe-Fe van de 2.24-2.54 Å, la distancia de enlace que une a los dos átomos de hierro que están coordinados con el benceno es la mayor de todas.

Encontramos que los estados excitados del cúmulo de $\text{Fe}_4\text{-bz}_2$ se encuentran a un valor muy pequeño de 0.02 eV para $M = 9$ lo cual significa que este estado es cuasidegenerado con el estado basal implicando que estos dos estados pudieran estar presentes al mismo tiempo en el experimento de síntesis en la fase gasesosa, con distancias de enlace Fe-C de 2.11-2.14 Å para el primer benceno y 2.12-2.16 Å para el segundo benceno, las distancias de enlace Fe-Fe están entre 2.25 y 2.73 Å. En el segundo estado excitado a 0.28 eV, $M = 5$ las distancias de enlace Fe-C son de 2.10-2.12 Å, y 2.12 Å para el segundo benceno coordinado, y distancias de enlace Fe-Fe de 2.13-2.47 Å.

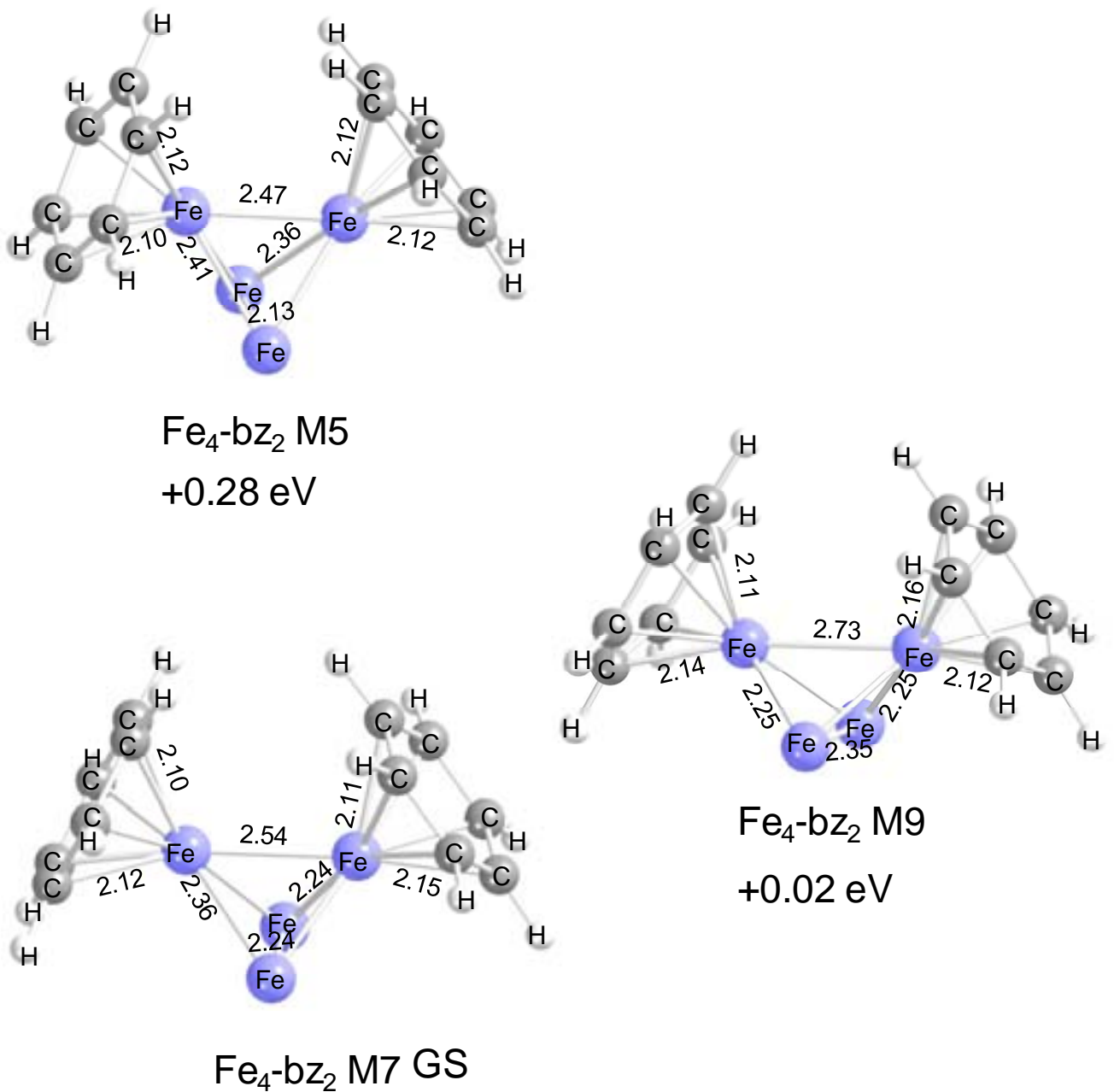


Figura 14. Geometría y multiplicidad para el estado basal y estados excitados del complejo $\text{Fe}_4\text{-bz}_2$ neutro.

El anión correspondiente de energía más baja tiene una multiplicidad $M = 6$, se encuentra a -1.11 eV, esto indica que el electrón añadido llega al orbital LUMO de espín minoritario, las distancias de enlace Fe-C son de 2.08-2.12 Å para el primer benceno y de 2.09-2.12 Å para el segundo benceno, las distancias de enlace Fe-Fe son de 2.11-2.53 Å. Los otros dos aniones calculados de multiplicidad $M = 8$ y $M = 4$ se encuentran a -0.93 y -0.24 eV con respecto al estado basal del complejo neutro.

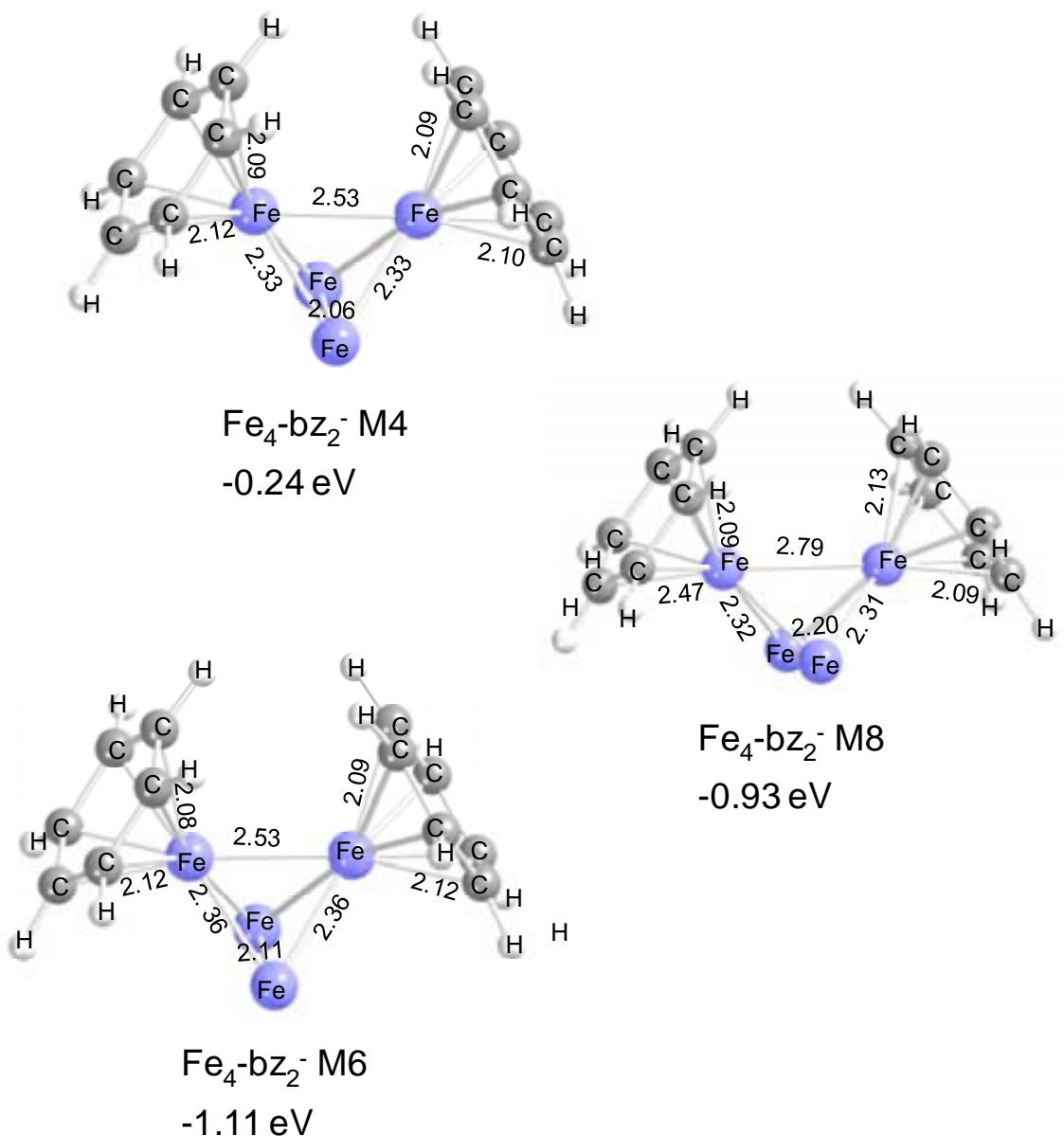


Figura 15. Geometría y multiplicidad para el estado basal y estados excitados del complejo $\text{Fe}_4\text{-bz}_2^-$ anión.

En el caso del catión la multiplicidad del estado basal es igual a 8, se encuentra a 5.06 eV, lo que muestra que el electrón es sustraído del orbital HOMO de espín minoritario. Las distancias de enlace Fe-C van de 2.12-2.14 Å para el primer benceno y de 2.15-2.19 Å para el segundo benceno, las distancias de enlace Fe-Fe son de 2.22-2.51 Å. Los estados excitados del catión corresponden a una multiplicidad $M = 10$ a 5.31 eV y $M = 6$ a 5.64 eV con respecto al estado basal del complejo neutro.

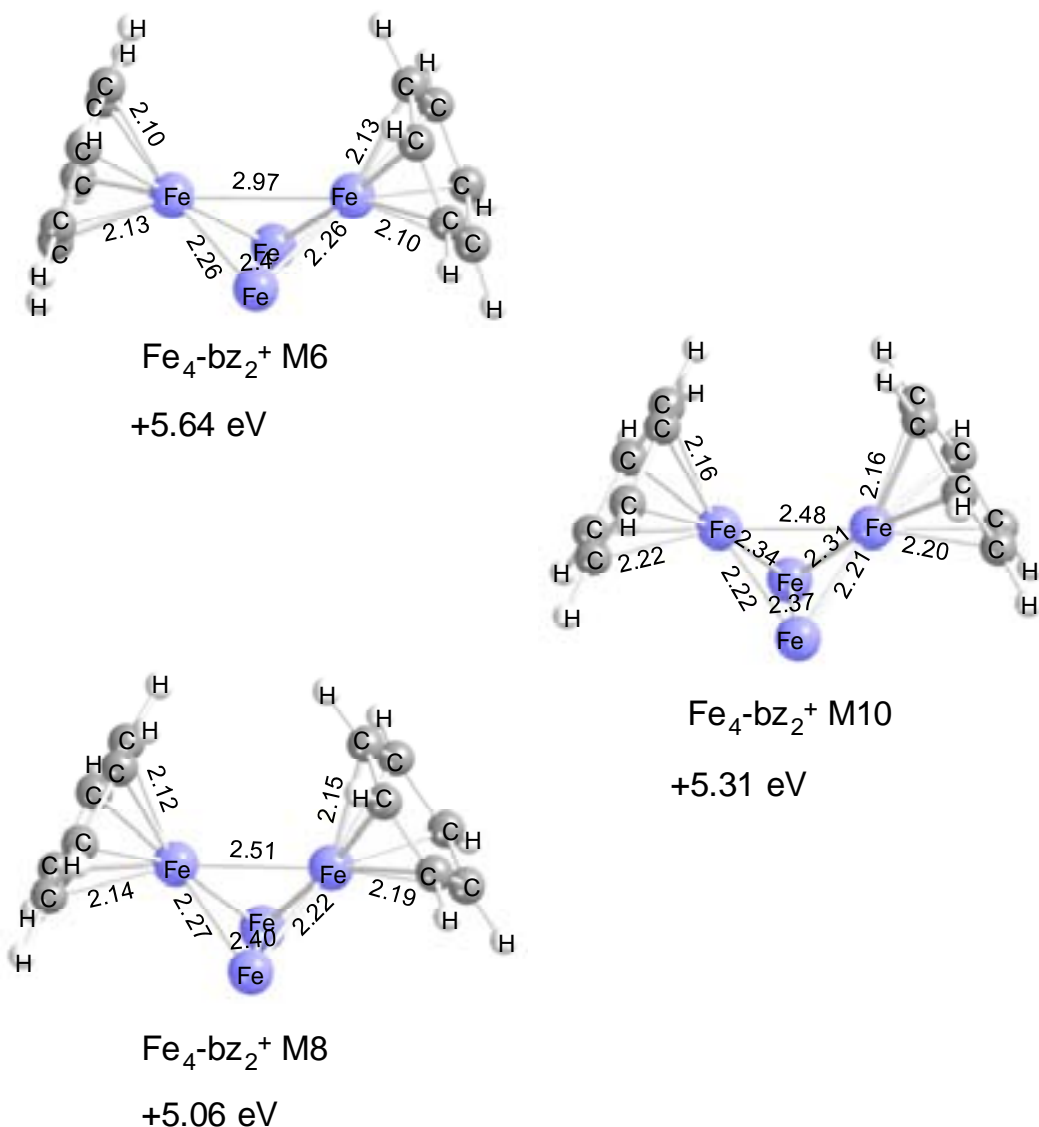


Figura 16. Geometría y multiplicidad para el estado basal y estados excitados del complejo $\text{Fe}_4\text{-bz}_2$ catión.

Debido a que el estado basal del complejo $\text{Fe}_4\text{-bz}_2$ tiene una multiplicidad $M = 7$, y a que el anión correspondiente tiene una multiplicidad igual a 6, esto significa que el electrón añadido se introdujo en el orbital LUMO de espín beta, disminuyendo así la multiplicidad del complejo. Observando las distancias de enlace en el complejo anión podemos predecir el tipo de orbital molecular que fue ocupado, es decir, si las distancias de enlace en el anión son mayores que en el complejo neutro esto nos indicaría que el espín orbital LUMO beta es de antienlace, mientras que si las distancias disminuyen en el anión, esto nos indicaría que este orbital es de enlace.

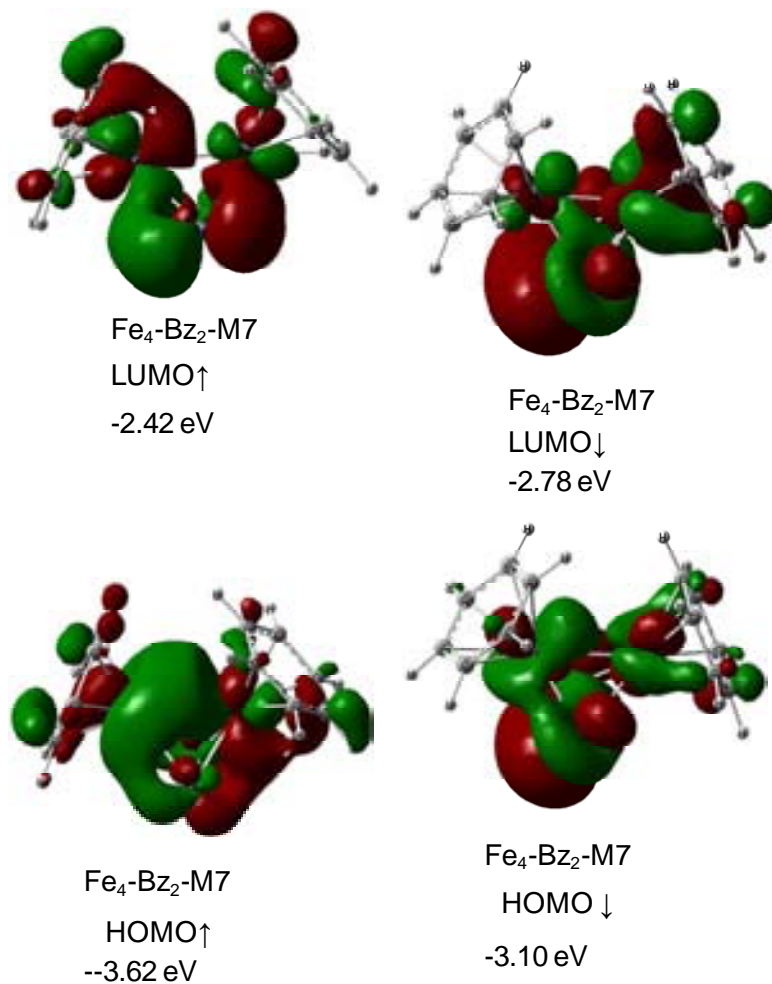


Figura 17. Diagrama de orbitales moleculares del complejo $\text{Fe}_4\text{-bz}_2$, LUMO de espín minoritario y HOMO de espín minoritario

Del mismo modo podemos hacer una predicción para el catión observando que la multiplicidad correspondiente es $M = 8$, lo que significa que el electrón sustraído se encontraba en el orbital HOMO beta, aumentando así la multiplicidad del catión. En este caso dependiendo de si las distancias de enlace en el catión son mayores o menores que en el complejo neutro podemos deducir si el espín orbital es de enlace o de no enlace. Observamos entonces que el espín minoritario es el que participa en la modificación de la estructura electrónica del complejo Fe_4Bz_2 , debido a que se encuentra más profundo en energía.

5.5. Estado basal de los cúmulos de $\text{Fe}_4\text{-bz}_3$ neutros, aniones y cationes.

Observamos para el complejo neutro $\text{Fe}_4\text{-bz}_3$ el estado basal corresponde a una multiplicidad $M = 3$, con coordinaciones de las moléculas de benceno igual a η^6 , las distancias de enlace Fe-C son de 2.09-2.13 Å para el primer benceno, de 2.12-2.14 Å para el segundo benceno y de 2.12-2.18 Å para el tercer benceno, las distancias de enlace Fe-Fe están comprendidas en el intervalo de 2.21-2.64 Å. Los estados excitados del cúmulo de $\text{Fe}_4\text{-bz}_3$ se encuentran a 0.03 eV para el estado con $M = 5$, en donde las distancias de enlace Fe-C son de 2.11-2.12 Å para el primer benceno, de 2.11-2.13 Å para el segundo benceno y de 2.12-2.19 Å para el tercer benceno, las distancias de enlace Fe-Fe van de 2.21-2.58 Å. A 1.02 eV se encuentra el estado $M = 1$, las distancias de enlace Fe-C son de 2.10-2.14 Å para el primer benceno, de 2.10-2.14 Å para el segundo benceno y de 2.10-2.14 Å para el tercer benceno, las distancias de enlace Fe-Fe están comprendidas en el intervalo de 2.12-2.56 Å.

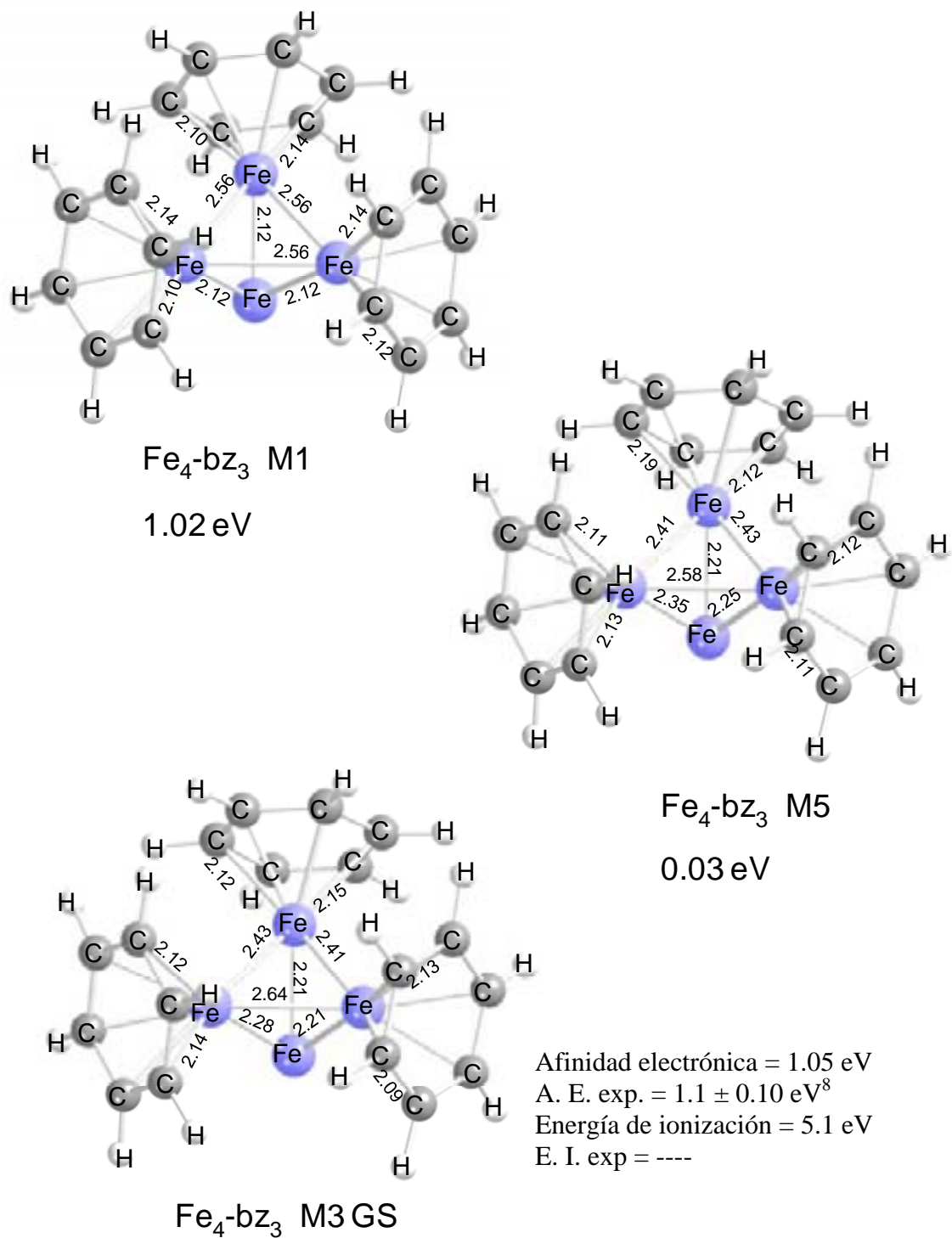


Figura 18. Geometría y multiplicidad para el estado basal y estados excitados del complejo $\text{Fe}_4\text{-bz}_3$ neutro.

El anión correspondiente de energía más baja tiene una multiplicidad de $M = 4$, a -1.31 eV, esto indica que el electrón añadido llega al orbital LUMO de espín mayoritario, las distancias de enlace Fe-C son de 2.10-2.12 Å para el primer benceno, de 2.10-2.12 Å para el segundo y de 2.10-2.12 Å para el tercero. Las distancias de enlace Fe-Fe están comprendidas en el intervalo de 2.22-2.54 Å. el otro anión calculado tiene una multiplicidad $M = 2$ y se encuentra a -0.94 eV.

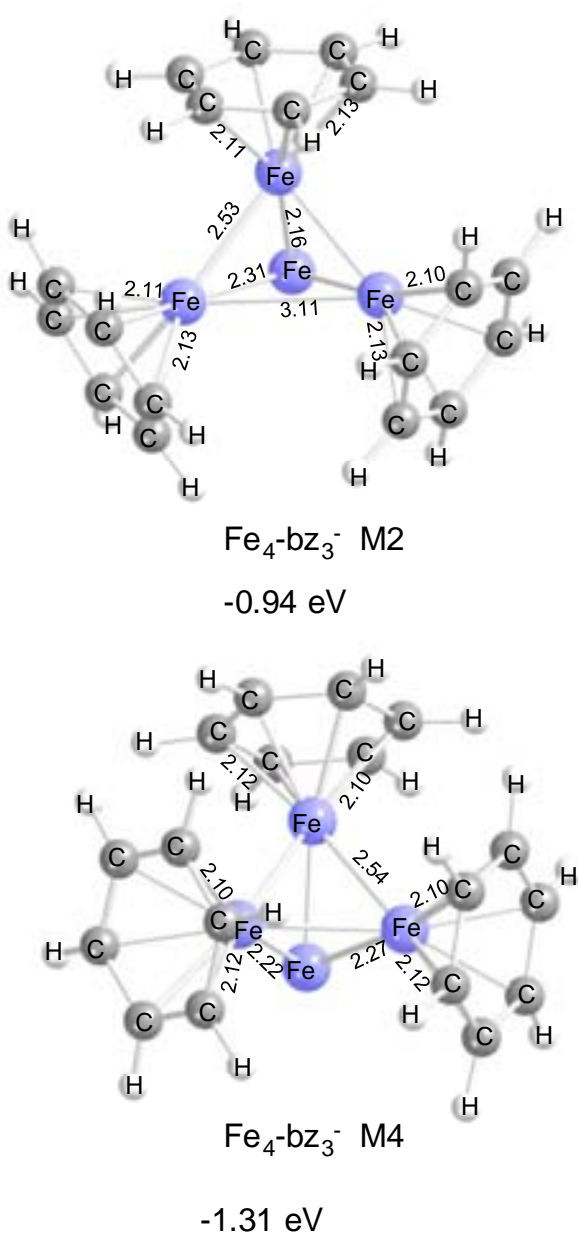


Figura 19. Geometría y multiplicidad para el estado basal y estados excitados del complejo $\text{Fe}_4\text{-bz}_3^-$ anión.

En el caso del catión la multiplicidad del estado basal es igual a 4 a 5.17 eV lo que indica que el electrón es sustraído del orbital HOMO de espín minoritario, las distancias de enlace Fe-C son de 2.13-2.16 Å para el primer benceno, de 2.13-2.16 Å para el segundo benceno y de 2.13-2.16 Å para el tercer benceno, las distancias de enlace Fe-Fe están comprendidas en el intervalo de 2.18-2.57 Å. Un estado excitado del catión corresponde a una multiplicidad $M = 2$ y está ubicado a 5.17 eV, esto indica que es un estado quasi-degenerado del estado basal.

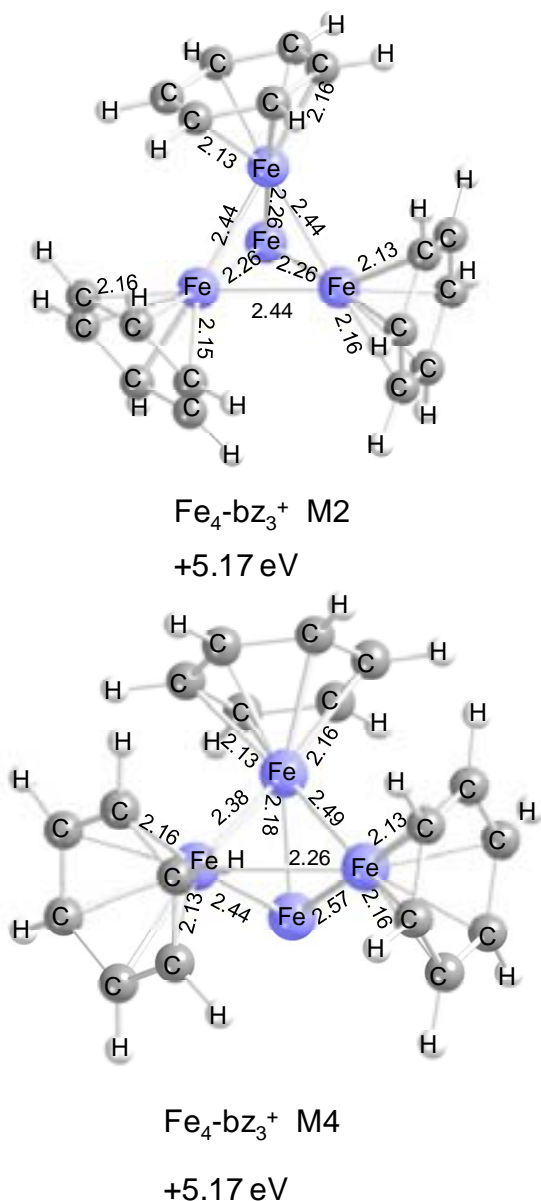


Figura 20. Geometría y multiplicidad para el estado basal y estados excitados del complejo $\text{Fe}_4\text{-bz}_3$ catión.

Debido a que el estado basal del complejo $\text{Fe}_4\text{-bz}_3$ tiene una multiplicidad $M = 3$, y a que el anión correspondiente tiene una multiplicidad = 4, esto significa que el electrón añadido se introdujo en el orbital LUMO de espín mayoritario, aumentando así la multiplicidad del complejo.

Podemos hacer una predicción para el catión observando que la multiplicidad correspondiente es $M = 4$, lo que significa que el electrón sustraído se encontraba en el orbital HOMO de espín minoritario, observamos que este orbital es de enlace Fe-C. Dependiendo de si las distancias de enlace en el catión son mayores o menores que en el complejo neutro podemos deducir si el espín orbital es de enlace o de no enlace. Así que tanto el espín mayoritario como el espín minoritario participan en la modificación de la estructura electrónica del complejo Fe_4Bz_3 .

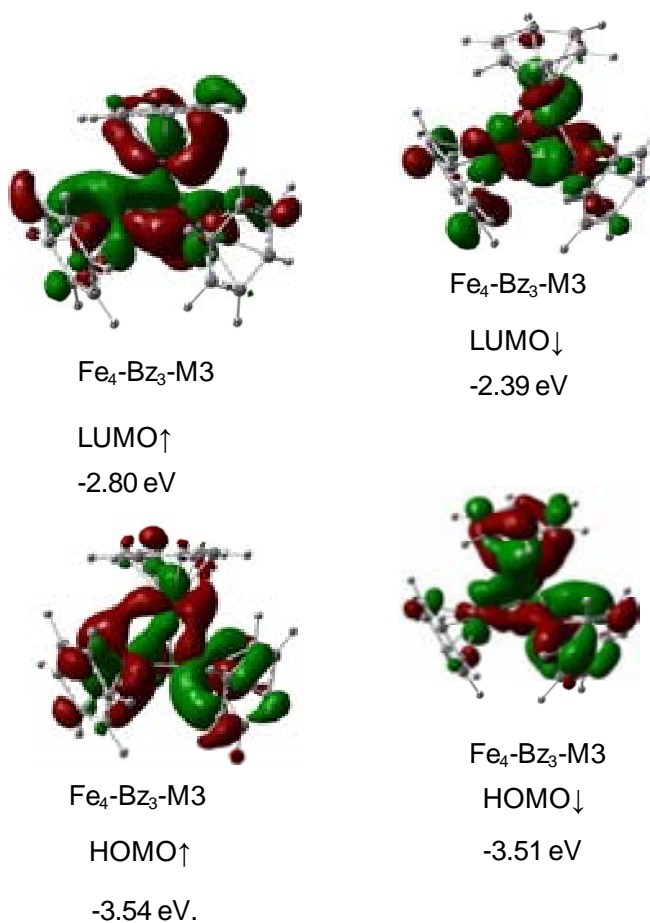


Figura 21. Diagrama de orbitales moleculares del complejo $\text{Fe}_4\text{-bz}_3$, LUMO de espín minoritario y HOMO de espín minoritario.

5.6. Estado basal de los cúmulos de Fe₄-bz₄ neutros, aniones y cationes.

Observamos para el complejo neutro Fe₄-bz₄. El estado basal corresponde a una multiplicidad M = 5, las distancias de enlace Fe-C son de 2.10-2.11 Å para el primer benceno, de 2.16-2.22 Å para el segundo, de 2.16-2.21 Å para el tercero y de 2.17-2.22 Å para el cuarto mientras que las distancias de enlace Fe-Fe son de 2.33 y 2.50 Å.

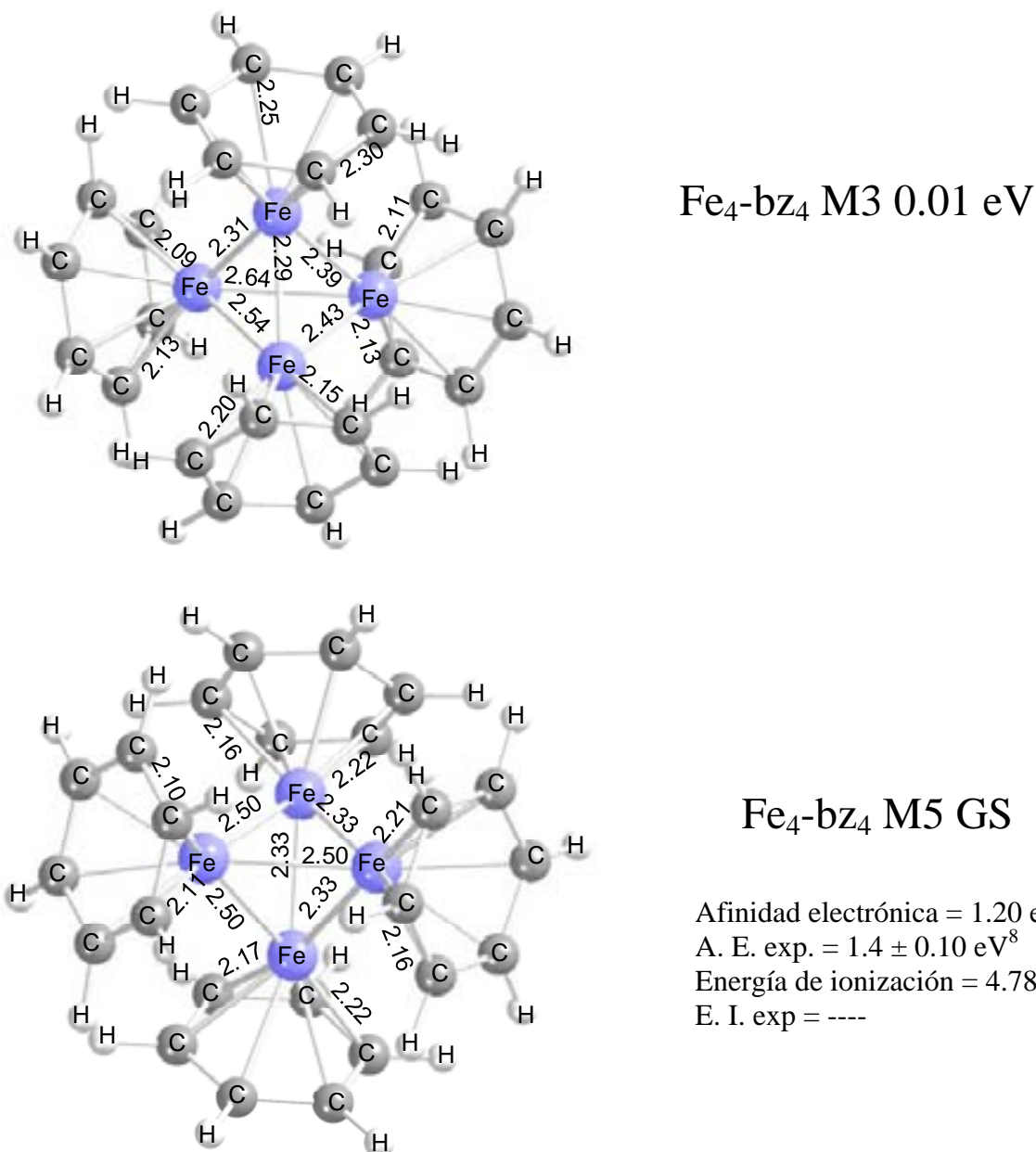


Figura 22. Geometría y multiplicidad para el estado basal Fe₄-bz₄ y del estado excitado.

El anión correspondiente de energía más baja tiene una $M = 4$, a -1.20 eV, esto indica que el electrón añadido se localiza en el orbital LUMO de espín minoritario, el estado excitado correspondiente tiene una multiplicidad $M = 6$ y se encuentra a -1.11 eV, las distancias de enlace Fe-C son de 2.11-2.12 Å para el primer benceno, de 2.12-2.13 Å para el segundo, de 2.11-2.13 Å para el tercero y de 2.22-2.23 Å para el cuarto, las distancias de enlace Fe-Fe son de 2.33 y 2.54 Å.

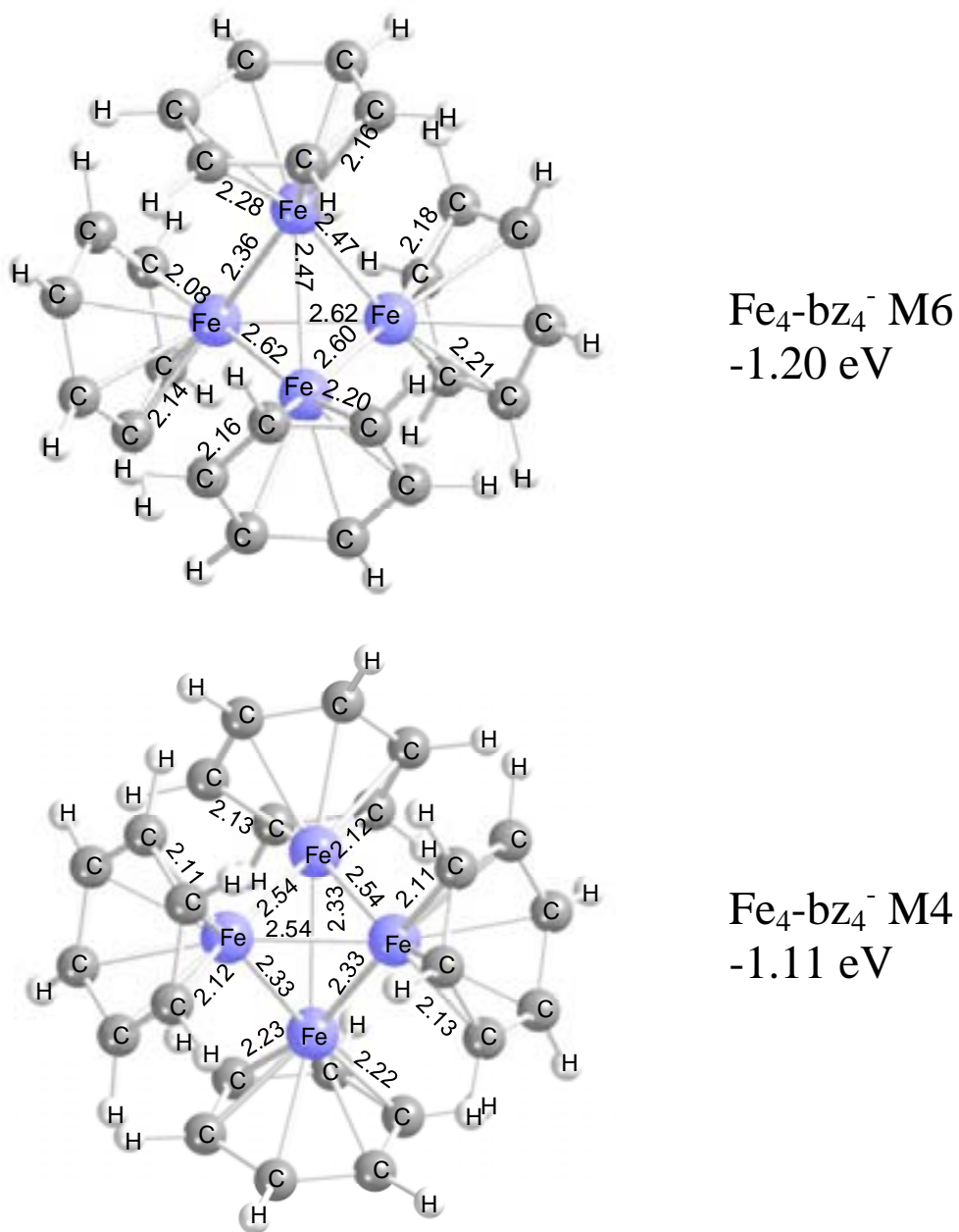


Figura 23. Geometría, multiplicidad, energías del estado basal y excitado del anión $\text{Fe}_4\text{-bz}_4^-$.

En el caso del catión la multiplicidad del estado basal también es igual a 4 en +4.78 eV lo que indica que el electrón es sustraído del orbital HOMO de espín mayoritario. Un estado excitado del catión corresponde a una multiplicidad M igual a 6 y está ubicado a +4.93 eV con respecto al estado basal del complejo neutro, las distancias de enlace Fe-C son de 2.19-2.30 Å para el primer benceno, de 2.11-2.19 Å para el segundo, de 2.24-2.29 Å para el tercero y de 2.12-2.16 Å para el cuarto, las distancias de enlace Fe-Fe son de 2.29 a 2.46 Å.

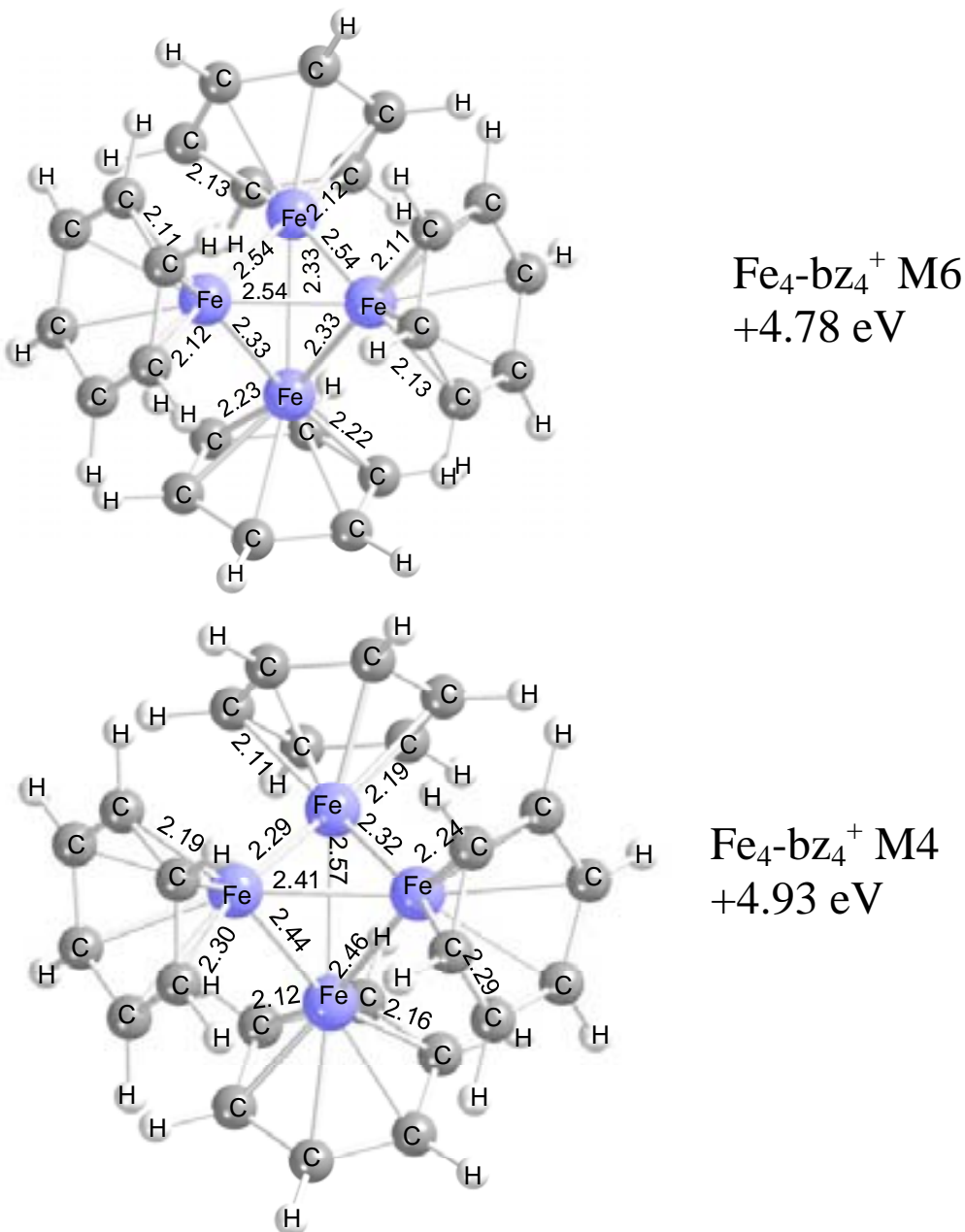


Figura 24. Geometría, multiplicidad, energías del estado basal y excitado del catión $\text{Fe}_4\text{-bz}_4$.

Debido a que el estado basal del complejo $\text{Fe}_4\text{-bz}_4$ tiene una multiplicidad $M = 5$, y a que el anión correspondiente tiene una multiplicidad = 4, esto significa que el electrón añadido se introdujo en el orbital LUMO de espín mayoritario, disminuyendo así la multiplicidad del complejo.

Del mismo modo podemos hacer una predicción para el catión observando que la multiplicidad correspondiente es $M = 4$, lo que significa que el electrón sustraído se encontraba en el orbital HOMO de espín mayoritario, observamos que este orbital es de enlace Fe-C. En este caso dependiendo de si las distancias de enlace en el catión son mayores o menores que en el complejo neutro podemos deducir si el espín orbital es de enlace o de no enlace.

Observamos entonces que el espín mayoritario participa en la modificación de la estructura electrónica del complejo Fe_4Bz_4 .

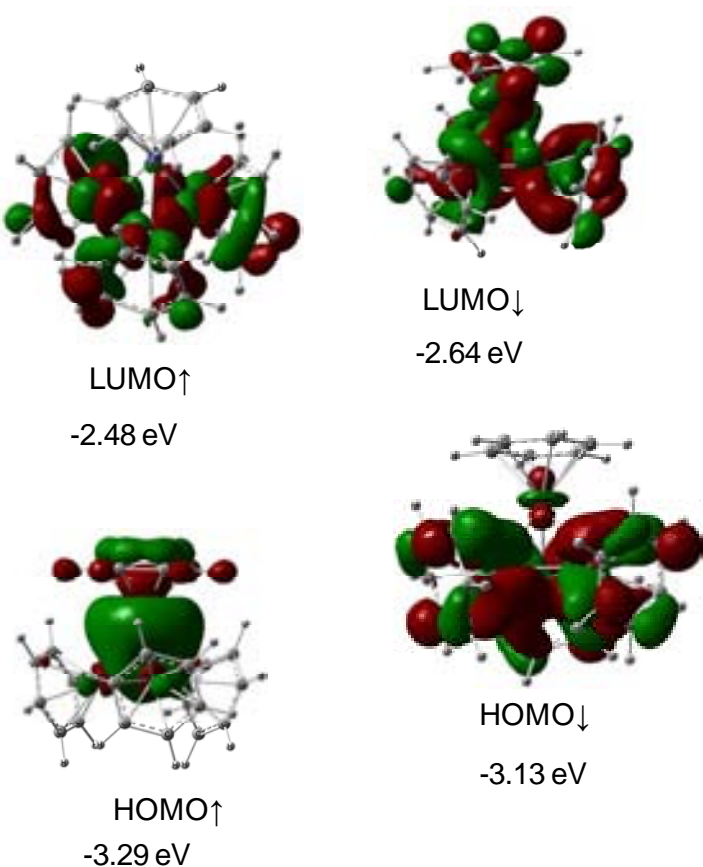


Figura 25. Diagrama de orbitales moleculares del complejo $\text{Fe}_4\text{-bz}_4$, HOMO de espín mayoritario y LUMO de espín minoritario.

5.7. Los estados basales de los complejos Fe-bz, Fe₄-bz, Fe₄-bz₂, Fe₄-bz₃ y Fe₄-bz₄.

5.7.1 Energías de Unión.

En el complejo Fe-bz el momento magnético del átomo de hierro es de $2 \mu_B$; el estado $M = 5$ está localizado a +0.84 eV arriba del estado basal. La energía de unión del benceno con el hierro calculada como $E(Fe)-E(Bz)$ es 1.50 eV. El momento dipolo de este complejo es de 1.77 D, esto muestra la existencia de un importante carácter electrostático en la energía de unión metal-ligante. La determinación experimental del momento dipolar^{32,33} es importante para la caracterización de la unión del benceno con el cúmulo de hierro.

Para el cúmulo Fe₄-bz el estado basal tiene una multiplicidad $M = 11$, lo que significa un momento magnético por átomo de $2.5 \mu_B$, este valor es menor que el momento magnético del Fe₄ que es de $3.5 \mu_B$. La Energía de Unión del benceno con el cúmulo de Fe₄ calculada como $E(Fe_4bz)-[E(Fe_4)+E(Bz)] = 1.71$ eV. El momento dipolo de este complejo es de 0.38 D.

El estado fundamental del complejo Fe₄-bz₂ corresponde a una multiplicidad $M = 7$, que es lo mismo que $1.5 \mu_B$, así, observamos que disminuye el paramagnetismo drásticamente con respecto al complejo Fe₄bz de $2.5 \mu_B$ y con respecto al cúmulo solo de $3.5 \mu_B$ por átomo de Fe, lo que implicaría un apareamiento de los espines electrónicos. El siguiente estado excitado se encuentra a solamente 0.02 eV con una multiplicidad $M = 9$ o sea que es cuasidegenerado con el estado basal; y el estado con multiplicidad igual a $M = 5$ se encuentra también relativamente cercano al

³² Rabilloud, F. Geometry and spin multiplicity of half-sandwich type transition-metal-benzene complexes. *J. Chem. Phys.* **2005**, 122, 134303.

³³ Imura, K.; Ohoyama, H.; Kasai, T.; Structures and its dipole moments of half-sandwich type metal-benzene (1:1) complexes determined by 2-m long electrostatic hexapole. *Chem. Phys.* **2004**, 301, 183.

estado basal 0.28 eV. La Energía de Unión se calcula como $E(Fe_4bz_2) - [E(Fe_4) + 2E(bz)] = 2.65$ eV y 1.33 eV por benceno. El momento dipolo de este complejo es de 0.44 D.

Para el cúmulo $Fe_4\text{-}bz_3$ el estado basal tiene una multiplicidad $M = 3$, lo que significa un momento magnético por átomo de $0.5 \mu_B$, este valor es menor que el momento magnético del Fe_4 que es de $3.5 \mu_B$. La diferencia es de $2.5 \mu_B$, por lo que la complejación del cúmulo de Fe_4 con una molécula de benceno disminuye el súper paramagnetismo del cúmulo de Fe_4 . La energía de unión del benceno con el cúmulo de Fe_4 calculada como $E(Fe_4bz_3) - [E(Fe_4) + 3E(Bz)] = 3.41$ eV o de 1.14 eV por benceno. El momento dipolo de este complejo es de 0.68 D.

Para el cúmulo $Fe_4\text{-}bz_4$ el estado basal tiene una multiplicidad $M = 5$, lo que significa un momento magnético por átomo de $1.0 \mu_B$, este valor es menor que el momento magnético del Fe_4 que es de $3.5 \mu_B$. La diferencia es de $2.5 \mu_B$, por lo que la complejación del cúmulo de Fe_4 con cuatro moléculas de benceno disminuye drásticamente el súper paramagnetismo del cúmulo de Fe_4 . Este resultado muestra que existe un cambio en la tendencia que se había estado observando de ir disminuyendo hasta un valor fijo. Este comportamiento es parecido al reportado por Valencia et al.³⁴ en el que se observa una disminución y un comportamiento tipo plato para el cúmulo saturado con 3 y 4 bencenos. La energía de unión del benceno con el cúmulo de Fe_4 calculada como $E(Fe_4bz_4) - [E(Fe_4) + 4E(Bz)] = 3.51$ eV o 0.88 eV por benceno. El momento dipolo de este complejo es de 1.33 D.

³⁴ Valencia, I.; Castro, M. Theoretical Study of the Structural and Electronic Properties of the $Fe_6\text{-}(C_6H_6)_m$, $m = 3, 4$, complexes, *J. Phys. Chem. A.* **2010**, *114*, 21-28.

Energías de Ionización.

En el complejo Fe-bz el valor de la energía de ionización es de 6.44 eV, este valor concuerda con el reportado experimentalmente de 6.42 ± 0.04 eV⁷.

Para el Fe₄-bz el catión tiene una multiplicidad M = 12, lo que significa que en este caso el momento magnético por átomo es de 2.75 μ_B , es decir 0.25 μ_B mayor que en el caso del complejo neutro, es decir que la eliminación de un electrón, en este caso, aumentó el momento magnético del complejo Fe₄-bz. La energía de ionización calculada de este complejo es de 5.33 eV.

Para el complejo Fe₄-bz₂ el estado de más baja energía correspondiente al catión tiene una multiplicidad M = 8, con un estado neutro de multiplicidad M = 7. La energía de ionización correspondiente es de 5.06 eV.

Para el complejo Fe₄-bz₃ M = 3, el catión tiene una multiplicidad M = 2, es decir que la eliminación de un electrón, en este caso, disminuyó el momento magnético del complejo Fe₄-C₆H₆. La energía de ionización de este complejo es de 5.17 eV.

Para el complejo Fe₄-bz₄ el estado basal M = 5 con un catión que presenta un cuarteto, M = 4, es decir que la eliminación de un electrón, en este caso, disminuyó el momento magnético del complejo Fe₄-bz₄. Observamos que los orbitales activos en este complejo son los orbitales moleculares de espín mayoritario. La energía de ionización de este complejo es de 4.78 eV.

Afinidad electrónica.

En el complejo Fe-bz la afinidad electrónica es de 0.47 eV mientras que el resultado experimental es de 0.46 ± 0.10 eV⁸, por lo que esta concordancia con el experimento es un fuerte indicio de que el estado basal calculado corresponde correctamente al estado basal verdadero.

El anión del Fe₄-bz tiene una multiplicidad $M = 10$, menor que el complejo neutro, por $0.25 \mu_B$. En este caso la adición de un electrón también disminuye el paramagnetismo del complejo Fe₄-bz. La afinidad electrónica correspondiente a este estado es de 1.03 eV; no hay resultado experimental reportado para esta especie.

Para el complejo Fe₄-bz₂, en el caso del anión la multiplicidad $M = 6$, y se encuentra a -106.70 kJ/mol respecto del complejo neutro. Estos resultados también muestran que los orbitales moleculares de espín minoritario son responsables de las interacciones electrónicas del complejo Fe₄bz₂. La afinidad electrónica es de 1.11 eV que es menor que la reportada experimentalmente por Bowen⁸ que es de 1.30 ± 0.10 eV.

Para el complejo Fe₄-bz₃ El anión tiene una multiplicidad $M = 4$, mayor que el complejo neutro. En este caso la adición de un electrón aumenta el paramagnetismo del complejo Fe₄-bz₃. La afinidad electrónica determinada como en los casos anteriores de manera adiabática, es de 1.31 eV, el valor experimental es de 1.1 ± 0.10 eV⁸

Para el complejo Fe₄-bz₄ el anión correspondiente tiene una multiplicidad M igual a 4, menor que el complejo neutro. En este caso la adición de un electrón aumenta el paramagnetismo

del complejo $\text{Fe}_4\text{-bz}_4$. La afinidad electrónica correspondiente a este estado es de 1.20 eV, el valor experimental de 1.4 ± 0.10 eV⁸.

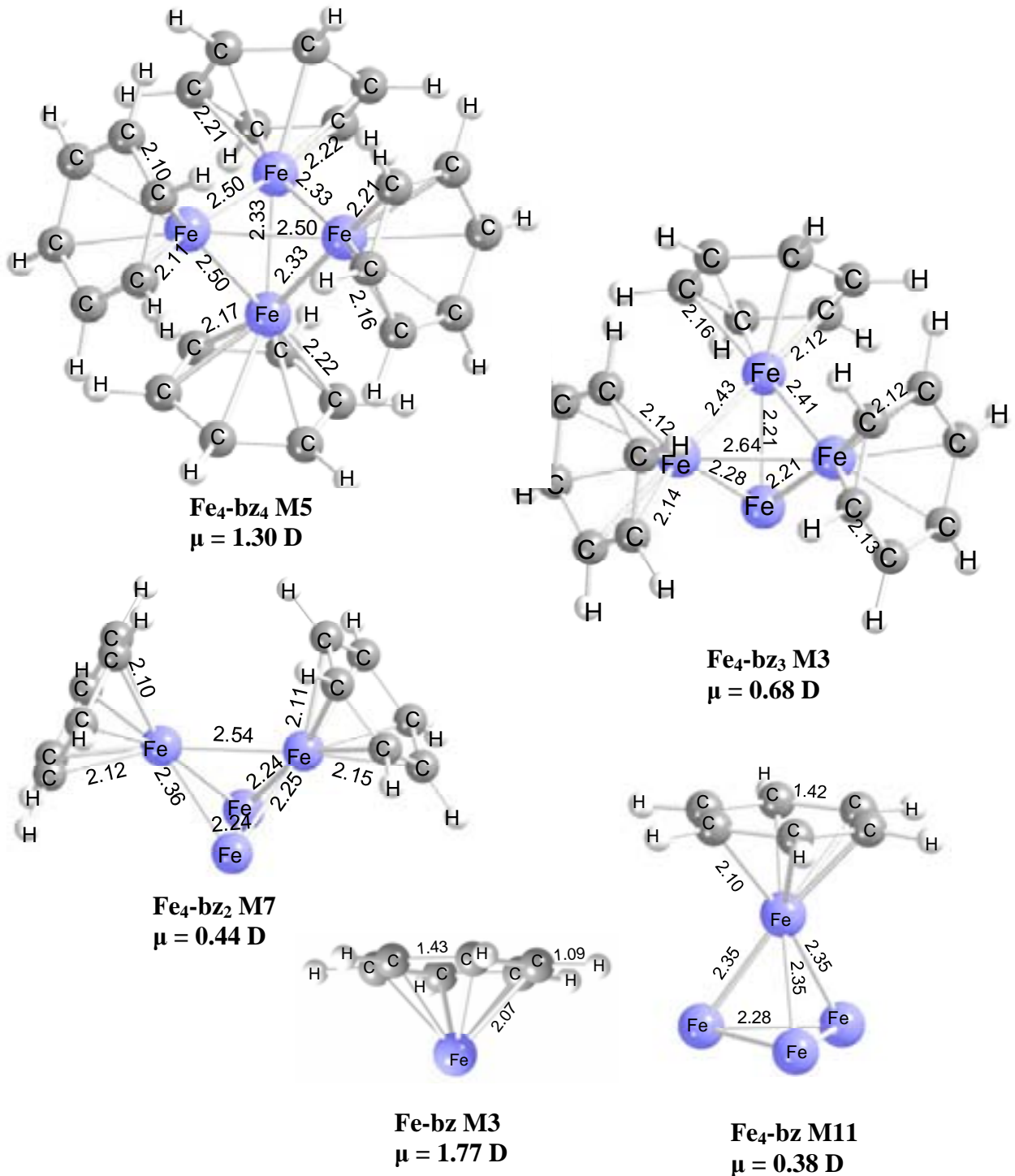


Figura 26. Geometría y multiplicidad del estado basal de los complejos Fe-bz y $\text{Fe}_4\text{-bz}_n$, $n \leq 4$.

Es de resaltar que todos los bencenos presentan una hapticidad igual a 6, a diferencia de los resultados para el complejo $\text{Fe}_6\text{-bz}_4^{34}$ en el que los bencenos adsorbidos están unidos con diferentes hapticidades que van de 6, 5 y 2. El cuarto benceno adsorbido se une con una hapticidad igual a 2, en nuestro caso, se calculó el isómero para este complejo con hapticidad igual a 2 para el cuarto benceno coordinado, sin embargo esta estructura no es la de mínima energía.

5.8. Análisis vibracional.

5.8.1. Espectro de infrarrojo del benceno.

El espectro calculado del benceno, Figura 27, muestra las principales frecuencias de los modos de vibración activos en el infrarrojo, IR, que corresponden a una vibración C-H fuera del plano (out of plane C-H) a 661 cm^{-1} , una torsión C-H en el plano (In plane C-H bending) 1034 cm^{-1} , una distorsión en los carbonos del anillo, (In plane C-ring distortion) a 1472 cm^{-1} y un estiramiento asimétrico C-H en el plano, (asymmetric C-H stretching) a 3121 cm^{-1} .

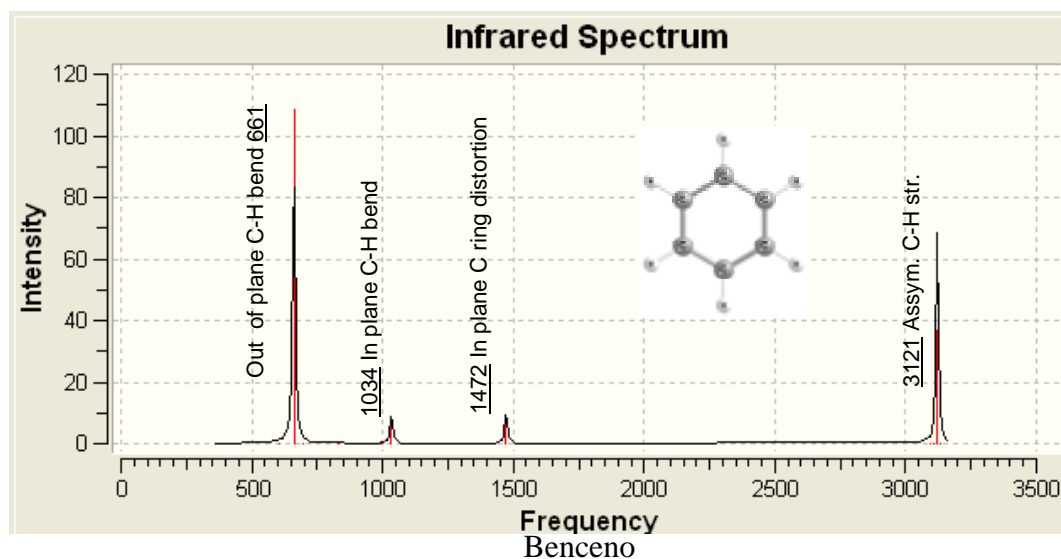


Figura 27. Espectro de infrarrojo de la molécula de benceno.

Los diferentes modos de vibración del benceno⁴⁶ así como la simetría y la nomenclatura se presentan en la Tabla 1 así como la comparación con los valores experimentales de las frecuencias de vibración.³⁵

Tabla 1. Frecuencias e intensidades de los modos de vibración de la molécula de benceno.

teoría	modo	v(cm ⁻¹)	Simetria	I(km/mol)	exp. ^c v(cm ⁻¹)	error(%)	v(cm ⁻¹)	I(km/mol)	Δv(cm ⁻¹)
1	γ(CCC)	394	E2U		410	3.90	388	0.2	-6
2	γ(CCC)	394	E2U		410	3.90	387.8	0.2	-6.2
3	δ(CCC)	603.1	E2G		606	0.48	598.9	0.1	-4.2
4	δ(CCC)	603.2	E2G		606	0.46	598.9	0.1	-4.3
5	γ(C-H)	661.1	A2U	108.7	673	1.77	773.8	15.7	112.7
6	γ(CCC)	699	B2G		703	0.57	596.3	0.3	-102.7
7	γ(C-H)	830.6	E1G		849	2.17	839.3	5.5	8.7
8	γ(C-H)	830.7	E1G		849	2.16	839.6	5.5	8.9
9	γ(C-H)	946.8	E2U		975	2.89	869	0.3	-77.8
10	γ(C-H)	946.8	E2U		975	2.89	869.5	0.3	-77.3
11	γ(C-H)	976.4	B2G		995	1.87	905.4	0.04	-71
12	δ(CCC)	989.9	A1G		992	0.21	956.9	9.46	-33
13	δ(C-C)	997.6	B1U		1010	1.23	987.9	0.04	-9.7
14	δ(C-H)	1034.2	E1U	5.8	1038	0.37	993.8	2.8	-40.4
15	δ(C-H)	1034.2	E1U	5.8	1038	0.37	993.9	2.8	-40.3
16	δ(C-H)	1146.7	B2U		1150	0.29	1135.9	0	-10.8
17	δ(C-H)	1167.3	E2G		1178	0.91	1127.1	0.05	-40.2
18	δ(C-H)	1167.3	E2G		1178	0.91	1127.3	0.05	-40
19	v(C=C)	1330.7	B2U		1310	1.58	1380.9	0	50.2
20	δ(C-H)	1342.9	A2G		1326	1.27	1317	0	-25.9
21	δ(CCC)	1472.4	E1U	6.1	1486	0.92	1426	2.8	-46.4
22	δ(CCC)	1472.4	E1U	6.1	1486	0.92	1426	2.8	-46.4
23	v(C=C)	1588.2	E2G		1596	0.49	1481.8	0.01	-106.4
24	v(C=C)	1588.2	E2G		3047	47.88	1481.8	0.01	-106.4
25	δ(C-H)	3095.9	B1U		3062	1.11	3114.3	0.1	18.4
26	v'(C-H)	3105.5	E2G		3062	1.42	3119.9	0.2	14.4
27	v'(C-H)	3105.6	E2G		3063	1.39	3119.9	0.2	14.3
28	v'(C-H)	3121.1	E1U	36.8	3063	1.90	3130.3	14.2	9.2
29	v'(C-H)	3121.1	E1U	36.8	3063	1.90	3130.3	14.2	9.2
30	δ(C-H)	3131.5	A1G		3068	2.07	3136.3	20.6	4.8

³⁵ Shimanouchi, T. In *Molecular Vibrational Frequencies, NIST, Chemistry WebBook, NIST Standard Reference Database Number 69*; Linstrom, P. J., Mallard, W. G., Eds.; National Institute of Standards and Technology: Gaithersburg, MD, 2007; <http://webbook.nist.gov>.

5.8.2. Espectro de infrarrojo del cúmulo Fe₄.

Para el modo Asymmetric Fe-Fe stretching existen dos bandas activas IR a 126 cm⁻¹ y a 207 cm⁻¹.

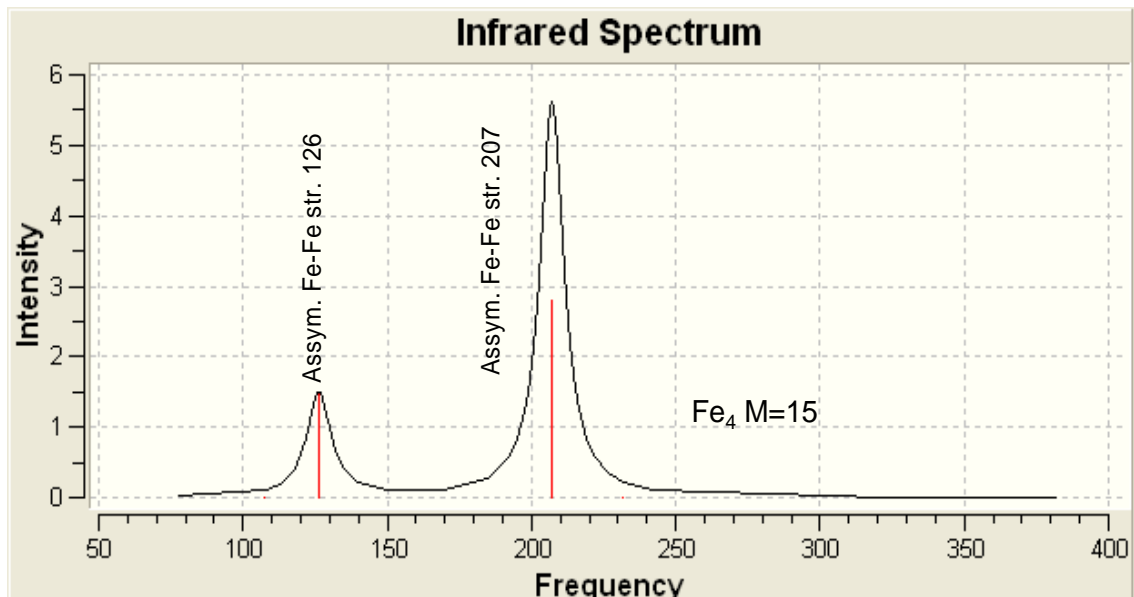


Figura 28. Espectro de infrarrojo del cúmulo de Fe₄.

5.8.3. Espectro de infrarrojo Fe-bz, neutro catión y anión

Para el caso del complejo neutro Fe-bz, observamos que para la vibración Out of plane C-H bending existe un desplazamiento hacia el azul, de 661 cm⁻¹ a 763 cm⁻¹. Para el modo In plane C-H bend existe un desplazamiento hacia el rojo de 1034 cm⁻¹ a 973 cm⁻¹. Para el modo In plane carbon ring distortion desaparece la señal de 1472 cm⁻¹. Para el modo Asymmetric C-H stretching existe un desplazamiento hacia el rojo de 3121 cm⁻¹ a 3104 cm⁻¹.

Para el anion Fe-bz⁻ observamos que para la vibración γ (C-H) existe un desplazamiento hacia el azul, de 661 cm⁻¹ a 761 cm⁻¹. Para el modo δ (C-H) existe un desplazamiento hacia el rojo de 1034 cm⁻¹ a 991 cm⁻¹. Para el modo δ (CCC) existe un desplazamiento hacia el rojo de 1472 cm⁻¹ a 1418 cm⁻¹. Para el modo v' (C-H) existe un desplazamiento hacia el azul de 3121 cm⁻¹ a 3149 cm⁻¹.

Para el caso del cation Fe-bz⁺, observamos que para la vibración γ (C-H) existe un desplazamiento hacia el azul, de 661 cm⁻¹ a 725 cm⁻¹. Para el modo δ (C-H) existe un

desplazamiento hacia el rojo de 1034 cm^{-1} a 970 cm^{-1} . Para el modo $\delta(\text{CCC})$ desaparece la señal.

Para el modo $\delta(\text{CCC})$ existe un desplazamiento hacia el rojo de 3121 cm^{-1} a 3077 cm^{-1} .

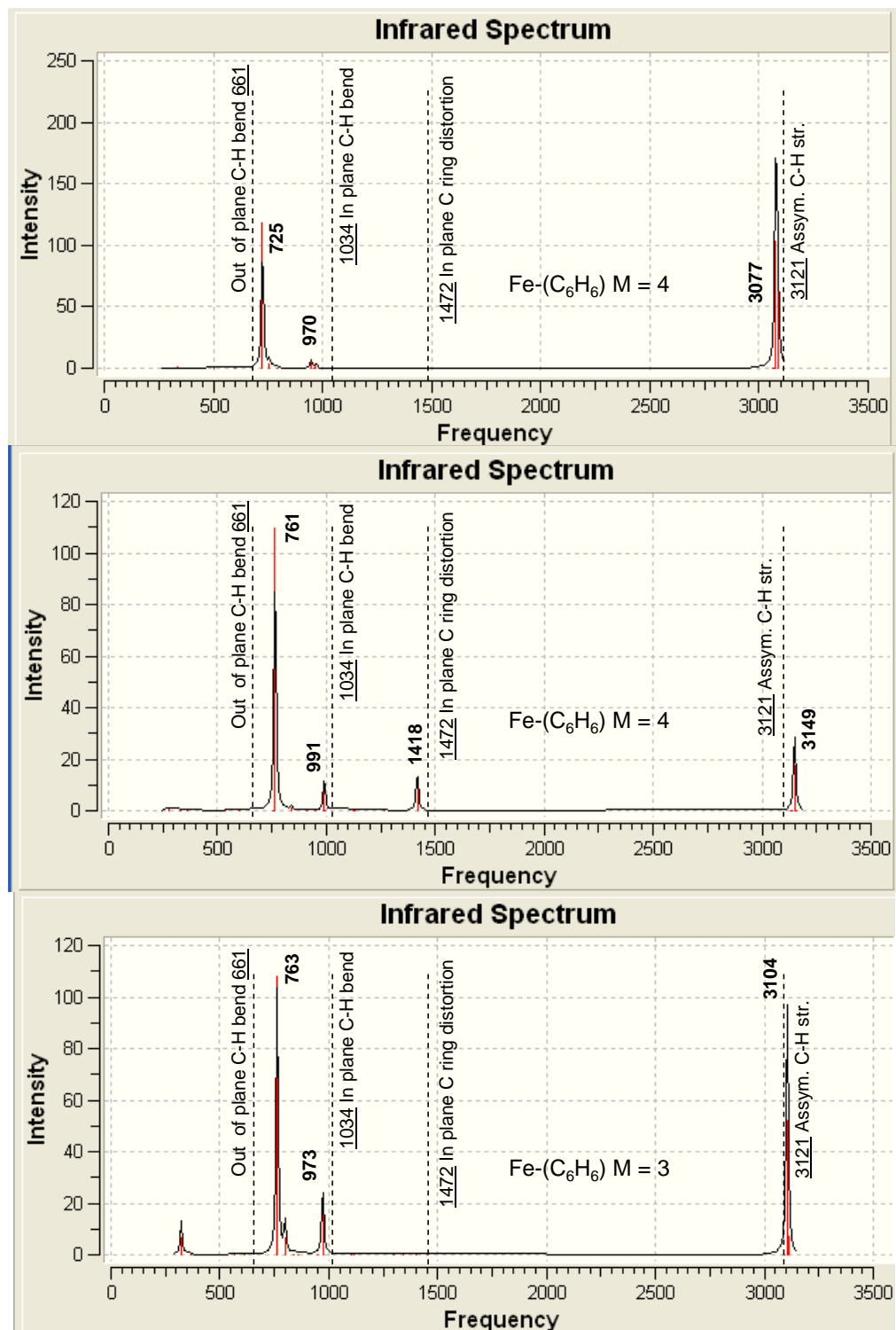


Figura 29. Espectro de infrarrojo del complejo Fe-bz neutro, catión y anión

5.8.4. Espectro de infrarrojo Fe₄-bz neutro, catión y anión.

Para el caso del complejo neutro Fe₄bz, observamos que para la vibración $\gamma(\text{C-H})$ existe un desplazamiento hacia el azul, de 661 cm^{-1} a 774 cm^{-1} . Para el modo $\delta(\text{C-H})$ existe un desplazamiento hacia el rojo de 1034 cm^{-1} a 994 cm^{-1} . Para el modo $\delta(\text{CCC})$ existe un desplazamiento hacia el rojo de 1472 cm^{-1} a 1426 cm^{-1} . Para el modo $\nu'(\text{C-H})$ existe un desplazamiento hacia el azul de 3121 cm^{-1} a 3130 cm^{-1} .

Para el anión Fe₄bz⁻ observamos que para la vibración $\gamma(\text{C-H})$ existe un desplazamiento hacia el azul, de 661 cm^{-1} a 748 cm^{-1} . Para el modo $\delta(\text{C-H})$ existe un desplazamiento hacia el rojo de 1034 cm^{-1} a 985 cm^{-1} . Para el modo $\delta(\text{CCC})$ desaparece la señal. Para el modo $\nu'(\text{C-H})$ existe un desplazamiento hacia el rojo de 3121 cm^{-1} a 3106 cm^{-1} .

Para el caso del cation Fe₄bz⁺, observamos que para la vibración $\gamma(\text{C-H})$ existe un desplazamiento hacia el azul, de 661 cm^{-1} a 748 cm^{-1} . Para el modo $\delta(\text{C-H})$ existe un desplazamiento hacia el rojo de 1034 cm^{-1} a 998 cm^{-1} . Para el modo $\delta(\text{CCC})$ existe un desplazamiento hacia el rojo de 1472 cm^{-1} a 1431 cm^{-1} . Para el modo $\nu'(\text{C-H})$ existe un desplazamiento hacia el azul de 3121 cm^{-1} a 3152 cm^{-1} .

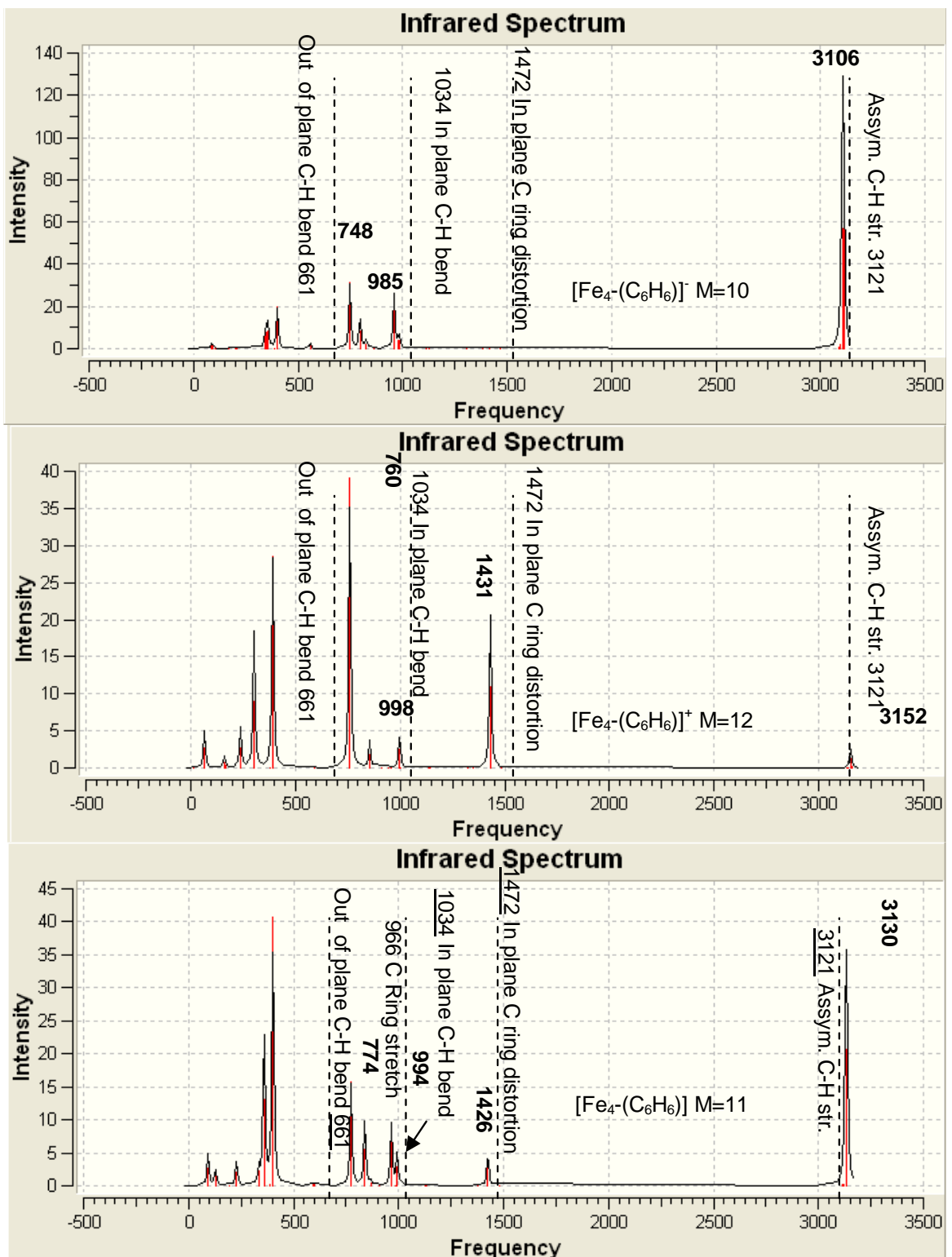


Figura 30. Espectro de infrarrojo del complejo Fe₄-bz neutro, catión y anión

5.8.5. Espectro de infrarrojo Fe₄bz₂ neutro, catión y anión.

Para el caso del complejo neutro Fe₄bz₂, observamos que para la vibración $\gamma(\text{C-H})$ existe un desplazamiento hacia el azul, de 661 cm⁻¹ a 750 cm⁻¹. Para el modo $\delta(\text{C-H})$ existe un desplazamiento hacia el rojo de 1034 cm⁻¹ a 992 cm⁻¹. Para el modo $\delta(\text{CCC})$ existe un desplazamiento hacia el rojo de 1472 cm⁻¹ a 1423 cm⁻¹. Para el modo $\nu'(\text{C-H})$ existe un desplazamiento hacia el azul de 3121 cm⁻¹ a 3129 cm⁻¹.

Para el caso del catión Fe₄bz₂⁺, observamos que para la vibración $\gamma(\text{C-H})$ existe un desplazamiento hacia el azul, de 661 cm⁻¹ a 708 cm⁻¹. Para el modo $\delta(\text{C-H})$ existe un desplazamiento hacia el rojo de 1034 cm⁻¹ a 981 cm⁻¹. Para el modo $\delta(\text{CCC})$ desaparece la señal. Para el modo $\nu'(\text{C-H})$ existe un desplazamiento hacia el azul de 3121 cm⁻¹ a 3152 cm⁻¹.

Para el anión Fe₄bz₂⁻ observamos que para la vibración $\gamma(\text{C-H})$ existe un desplazamiento hacia el azul, de 661 cm⁻¹ a 766 cm⁻¹. Para el modo $\delta(\text{C-H})$ existe un desplazamiento hacia el rojo de 1034 cm⁻¹ a 1001 cm⁻¹. Para el modo $\delta(\text{CCC})$ existe un desplazamiento hacia el rojo de 1472 cm⁻¹ a 1433 cm⁻¹. Para el modo $\nu'(\text{C-H})$ existe un desplazamiento hacia el azul de 3121 cm⁻¹ a 3144 cm⁻¹.

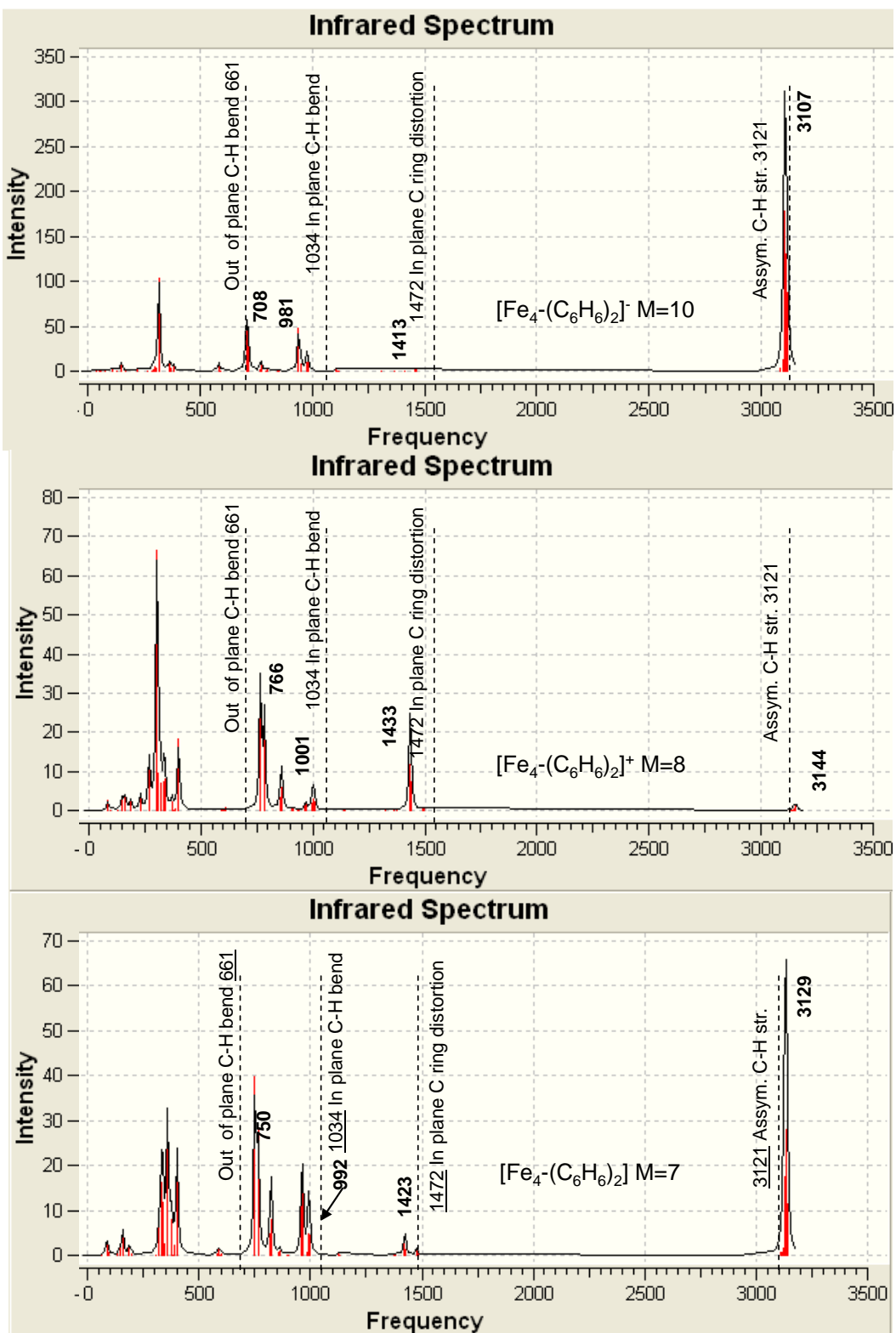


Figura 31. Espectro de infrarrojo del complejo $Fe_4\text{-bz}_2$ neutro, catión y anión

5.8.6. Espectro de infrarrojo Fe₄bz₃ neutro, catión y anión.

Para el caso del complejo neutro Fe₄bz₃, observamos que para la vibración $\gamma(\text{C-H})$ existe un desplazamiento hacia el azul, de 661 cm⁻¹ a 762 cm⁻¹. Para el modo $\delta(\text{C-H})$ existe un desplazamiento hacia el rojo de 1034 cm⁻¹ a 996 cm⁻¹. Para el modo $\delta(\text{CCC})$ existe un desplazamiento hacia el rojo de 1472 cm⁻¹ a 1427 cm⁻¹. Para el modo $\nu'(\text{C-H})$ existe un desplazamiento hacia el azul de 3121 cm⁻¹ a 3130 cm⁻¹.

Para el caso del catión Fe₄bz⁺₃, observamos que para la vibración $\gamma(\text{C-H})$ existe un desplazamiento hacia el azul, de 661 cm⁻¹ a 763 cm⁻¹. Para el modo $\delta(\text{C-H})$ existe un desplazamiento hacia el rojo de 1034 cm⁻¹ a 1004 cm⁻¹. Para el modo $\delta(\text{CCC})$ existe un desplazamiento hacia el rojo de 1472 cm⁻¹ a 1436 cm⁻¹. Para el modo $\nu'(\text{C-H})$ existe un desplazamiento hacia el azul de 3121 cm⁻¹ a 3147 cm⁻¹.

Para el anión Fe₄bz⁻₃ observamos que para la vibración $\gamma(\text{C-H})$ existe un desplazamiento hacia el azul, de 661 cm⁻¹ a 730 cm⁻¹. Para el modo $\delta(\text{C-H})$ existe un desplazamiento hacia el rojo de 1034 cm⁻¹ a 983 cm⁻¹. El modo $\delta(\text{CCC})$ se vuelve inactivo. Para el modo $\nu'(\text{C-H})$ existe un desplazamiento hacia el rojo de 3121 cm⁻¹ a 3102 cm⁻¹.

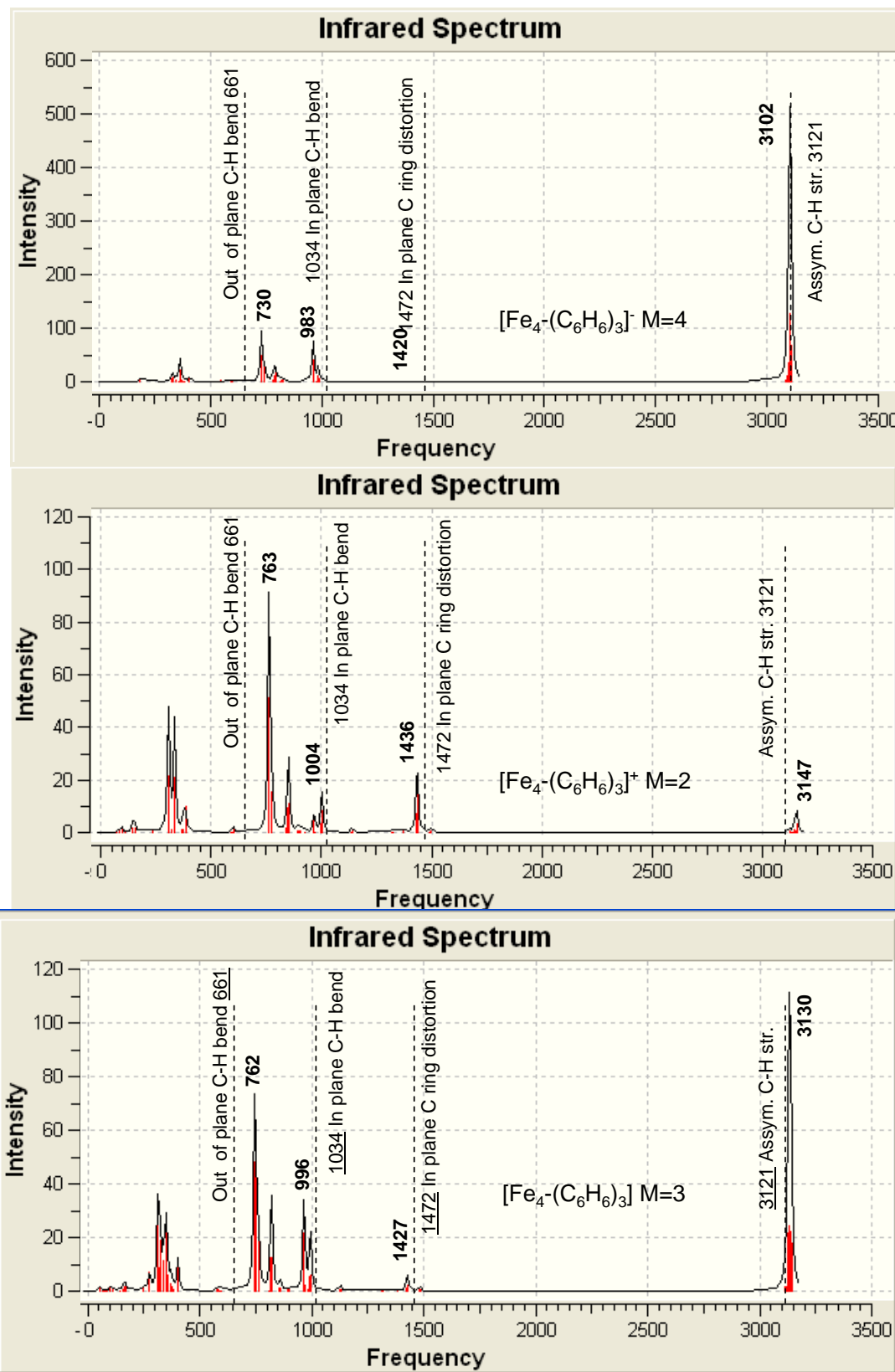


Figura 32. Espectro de infrarrojo del complejo Fe₄-bz₃ neutro, catión y anión

5.8.7. Espectro de infrarrojo Fe₄-bz₄ neutro.

Para el caso del complejo neutro Fe₄bz₄, observamos que para la vibración $\gamma(\text{C-H})$ existe un desplazamiento hacia el azul, de 661 cm^{-1} a 713 cm^{-1} . Para el modo $\delta(\text{C-H})$ existe un desplazamiento hacia el rojo de 1034 cm^{-1} a 1003 cm^{-1} . Para el modo $\delta(\text{CCC})$ existe un desplazamiento hacia el rojo de 1472 cm^{-1} a 1434 cm^{-1} . Para el modo $\nu'(\text{C-H})$ existe un desplazamiento hacia el azul de 3121 cm^{-1} a 3146 cm^{-1} .

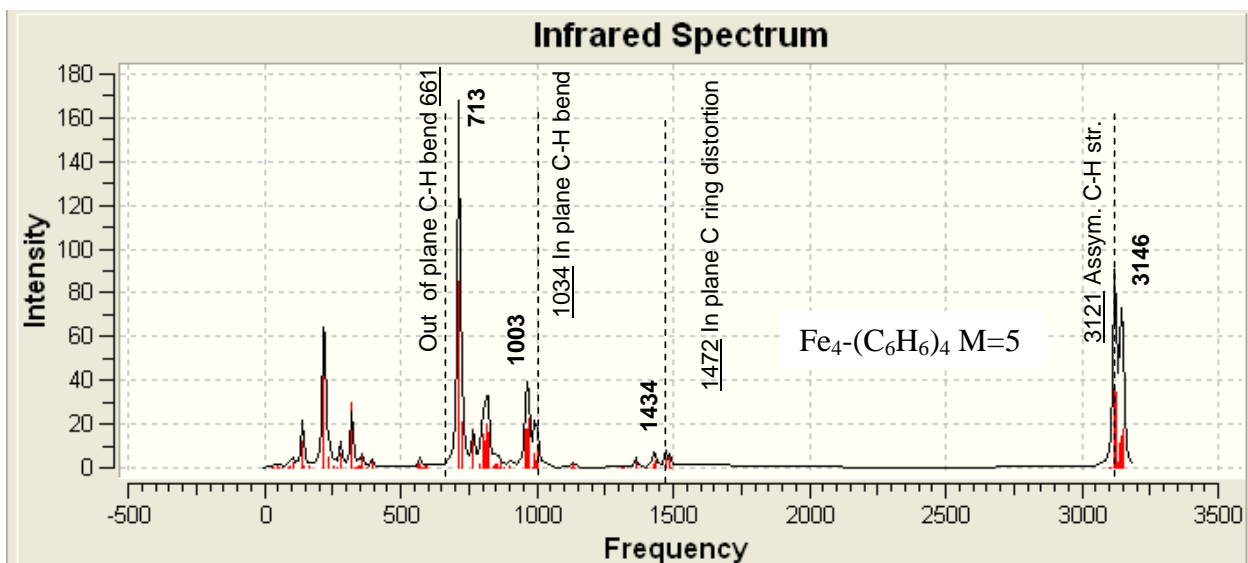


Figura 33. Espectro de infrarrojo del complejo Fe₄-bz₄ neutro.

6. Discusión.

En el complejo Fe-bz el momento magnético del átomo de hierro es de $2 \mu_B$. Este valor es menor que el del átomo de hierro solo, con un momento magnético de $3 \mu_B$. Esto sugiere que existe un rearreglo en la configuración electrónica del átomo de hierro, básicamente del apareamiento del espín en la formación del enlace químico Fe-Fe. De alguna manera este rearreglo electrónico debe contribuir a la formación del enlace Fe-C, ya que el estado $M = 5$ tiene una energía de 0.84 eV arriba del estado basal. Así, podemos decir que la formación del complejo Fe-bz modifica el momento magnético del átomo de hierro disminuyendo el magnetismo.

El complejo neutro Fe-bz muestra un momento dipolo relativamente grande, de 1.77 Debyes, lo que implica contribuciones electrostáticas importantes en la formación del complejo. Pandey et al.³⁶ utilizando métodos de Teoría de Funcionales de la Densidad han encontrado también un estado triplete para el estado basal de Fe-bz, con distancias Fe-anillo de 1.50 Å cercana a nuestro valor, 1.48 Å.

La multiplicidad correspondiente al catión es igual a 4, con un alargamiento de los enlaces Fe-C de 2.07 a 2.13 Å. Esta multiplicidad concuerda con la obtenida por Bauschlicher et al.¹² quien utilizó el método MCP y con los resultados de Jaeger et al.¹³ que utilizó el método B3LYP/6-311++G(d,p) con distancias Fe-anillo de 1.83 y 1.81 Å, respectivamente, las cuales son mayores que nuestro resultado de 1.59 Å. Pandey et al.³⁶ utilizando la aproximación de gradientes generalizados (GGA) también encontró un estado cuarteto para el Fe-bz^+ , con distancias Fe-anillo de 1.59 Å; lo que concuerda con nuestros resultados.

La energía de ionización calculada de 6.44 eV concuerda con los resultados experimentales de 6.42 eV⁷, estos resultados también concuerdan con los resultados teóricos de Pandey et al³⁶ que obtuvo un valor de 6.17 eV y una energía de ionización vertical de 6.25 eV. En el caso del anión Fe-bz^- se obtuvo una multiplicidad $M = 4$.

³⁶ R. Pandey, B. K. Rao, P. Jena, J. M. Newsam. Unique signature of transition metal atoms supported on benzene, *Chem. Phys. Lett.* **2000**, 321, 142.

El valor de la afinidad electrónica adiabática calculada es de 0.43 eV, lo que concuerda con el valor experimental de 0.46 ± 0.1 eV⁸. Pandey también obtuvo resultados teóricos similares. La energía de unión calculada de Fe-bz es de 1.50 eV que es mayor que la energía de unión experimental por aproximadamente 0.70 eV.³⁷ Esto es, a diferencia del buen acuerdo de las afinidades electrónicas el método BPW91 sobreestima esta propiedad.

De acuerdo a los resultados obtenidos para los cúmulos se observa que para todos, disminuye el magnetismo en comparación con el cúmulo de Fe₄ el cual inicialmente tiene un valor de multiplicidad M = 15, mientras que para el cúmulo Fe₄-bz se encuentra un valor de M = 11, para el cúmulo Fe₄-bz₂ M = 7, se alcanza un límite de multiplicidad M = 3 para el complejo Fe₄bz₃ para después volver a subir a M = 5 para el complejo Fe₄bz₄. Aunque los momentos magnéticos de los cúmulos Fe₄-bz_n, n ≤ 4 no han sido reportados, Knickelbein³⁸ ha encontrado recientemente que los momentos magnéticos por átomo de Co medidos para Co₇₋₁₀(C₆H₆)_m son considerablemente más pequeños que aquellos medidos para los cúmulos correspondientes Co_n, claramente apuntando a una perturbación electrónica fuerte del cúmulo de cobalto. Las multiplicidades de espín para los complejos Fe₄-bz_n son consistentes con el comportamiento de los cúmulos de cobalto.

A bajas temperaturas predecimos un momento magnético de $2.5 \mu_B$ para el cúmulo Fe₄-bz, más pequeño que para el cúmulo puro de Fe₄ de $3.5 \mu_B$. A temperaturas más altas como aquellas alcanzadas en los experimentos Stern-Gerlach³⁸ alrededor de 130 K, se espera un momento magnético mayor puesto que la medida puede tener contribuciones del estado M = 13 que se encuentra a 0.35 eV del estado basal.

La naturaleza del enlace metal-ligante en el complejo Fe-bz, estudiada mediante el diagrama de correlación de orbitales moleculares en la que fue necesario imponer condiciones de simetría es para poder correlacionar los orbitales de la misma simetría del benceno con el complejo Fe-bz,

³⁷ Meyer F., Khan I. A., Armentrout P. B. Thermochemistry of transition-metal benzene complexes – binding – energies of M(C₆H₆)(X)(+) (X=1,2) for M = Ti to Cu. *J. Am. Chem. Soc.*, **1995**, 117, 9740.

³⁸ Knickelbein, M. B. Magnetic moments of bare and benzene-capped clusters. *J. Chem. Phys.* **2006**, 125, 044308.

y con el átomo de hierro, nos da una visión de la estructura electrónica en este tipo de complejos, se observa que las principales contribuciones para el orbital LUMO provienen de las interacciones del orbital tipo *s* en el caso del hierro con orbitales tipo *p* y *s* de la molécula de benceno, mientras que las contribuciones de enlace están compuestas por interacciones tipo π por parte del benceno con contribuciones tipo $d_{x^2-y^2}$. Se observa que la mayor contribución al orbital de enlace corresponde a los orbitales e_{1g} , orbitales (π). Esta interacción de enlace es parecida a la del ferroceno, reportada por Rayón y Frenking³⁹, en la que también se observa que las principales contribuciones en el enlace covalente provienen de orbitales tipo π , a diferencia del complejo tipo sándwich cromo bis(benceno), Cr-bz₂ en la que el análisis del diagrama de correlación de orbitales moleculares muestra que la mayor contribución a las interacciones covalentes proviene de orbitales tipo e_{2g} , orbitales (δ), por lo que el complejo cromo bis(benceno) es una molécula con unión de tipo δ .

Por otra parte, las distancias de enlace Fe-C aumentan en longitud en los cúmulos de Fe₄-bz, en comparación con el complejo Fe-bz, esto es debido a que parte de la densidad electrónica del átomo de hierro que inicialmente interactuaba solamente con el benceno ahora tiene que formar enlaces metal-metal con los átomos de hierro del cúmulo.

En la gráfica de la Figura 34 observamos que las distancias aumentan conforme aumenta el número de moléculas de benceno adsorbidas. En el estado basal del complejo Fe₄-bz mostrado en la Figura 10, las distancias Fe-C, 2.10 Å, son ligeramente mayores que las del ferroceno, 2.05 Å. Se observa que para los demás complejos Fe₄-bz_n, $n \leq 4$ las distancias son más pequeñas que las sumas de los radios de van der Waals^{40,41} para el carbono de 1.7 Å y para el hierro de 1.9 Å, sugiriendo la formación de enlaces Fe-C; estas distancias también son más pequeñas que las

³⁹ Rayón M. V., Frenking, G. Bis(benzene)chromium is a delta-bonded molecule and ferrocene is a pi-bonded molecule. *Organometallics*. **2003**, 16, 3304.

⁴⁰ M. Domagala, S. J. Grabowski, K. Urbaniak, G. Młostow, Crystal and molecular structure of (r-2, c-4)-3-benzyl-2,4,5,5-tetraphenyl-1,3-thiazolidine, intramolecular C-H center dot center dot center dot center dot S hydrogen bonds. *J. Mol. Struc. (Theochem)*. **2004**, 690, 69.

⁴¹ G.R. Desiraju, T. Steiner, *The Weak Hydrogen Bond in Structural Chemistry and Biology*, Oxford University Press Inc., New York, 1999.

distancias Fe-C de 2.25-2.38 Å para uniones débiles Fe-C en los complejos $\text{Fe}_4\text{-CH}_4$ y $\text{Fe}_4\text{-C}_3\text{H}_8$.^{25,26} Las distancias de enlace C-C en los complejos $\text{Fe}_4\text{-bz}_n$, $n \leq 4$ muestran que con respecto al benceno libre existe un alargamiento de 0.022-0.023 Å, mientras que las distancias C-H de aproximadamente 1.09 Å no tienen cambios notables.

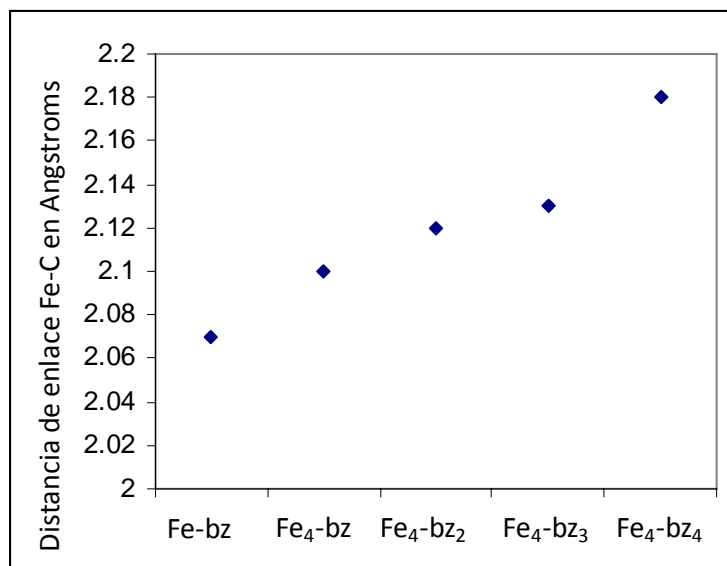


Figura 34. Distancias de enlace promedio Fe-C para los complejos Fe_4bz_n , $n \leq 4$

Este resultado concuerda con los valores de energía de unión de los complejos Fe_4bz_n , $n \leq 4$, en los cuales se puede observar que esta disminuye a medida que aumenta el número de moléculas de benceno en el complejo. Esto es debido principalmente a las repulsiones estéricas y eléctricas entre las moléculas de benceno además de la saturación en la coordinación sobre el cúmulo de hierro.

Observamos que el mayor valor de energía de unión corresponde al complejo $\text{Fe}_4\text{-bz}$, con 1.7 eV seguido por el complejo Fe-bz , con descenso gradual desde $\text{Fe}_4\text{-bz}_2$ hasta $\text{Fe}_4\text{-bz}_4$, exhibiendo este último complejo la menor energía de unión que es de alrededor de 0.88 eV. Podemos comparar estos valores por ejemplo con la energía de unión del benceno sobre una

superficie infinita de Fe(100), en donde el valor es de 4.48 eV.⁴² Simon y Joblin han estudiado mediante métodos TFD la interacción de un solo átomo de hierro con naftaleno ($C_{10}H_8$), pireno (C_6H_{10}) y coroneno los cuales son de interés para estudios en astrofísica.⁴³ Los valores de las energías de unión son de 2.68 eV para el Fe-naphtaleno, 2.85 eV para el Fe-pireno y de 2.59 eV para el coroneno. Se observa que estos valores son muy parecidos a los de Fe_4 -bz por además de que el valor no varía significativamente al cambiar el compuesto policíclico aromático, por lo que existe poca influencia sobre la energía de unión. Como otro ejemplo, se ha estudiado la energía de unión del complejo Fe_2 -coroneno a partir de Fe_2 y coroneno,⁴⁴ la cual es de 4.73 eV.

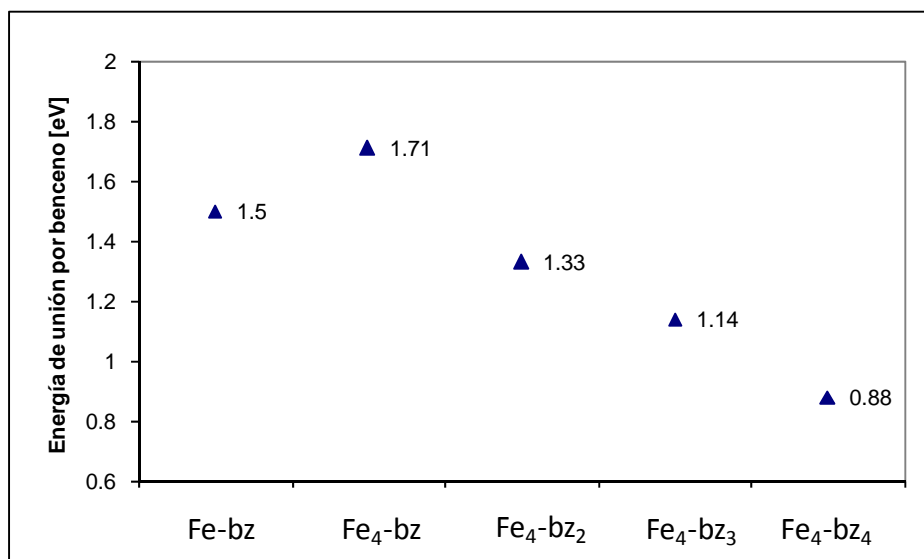


Figura 35. Energías de unión para los complejos Fe_4bz_n , $n \leq 4$

Podemos observar también un cambio en la afinidad electrónica de los complejos Fe_4bz_n , $n \leq 4$. Ésta indica que el cúmulo con 4 moléculas de benceno tiene mayor capacidad para adquirir y estabilizar un electrón adicional que el complejo $Fe-bz$.

⁴² Sun, X.; Suzuki, T.; Kurahashi M. et al. First-principles study on the spin polarization of benzene adsorbed on Fe(100) surface. *J. Appl. Phys.* **2007**, 101, 09G526.

⁴³ Simon, A.; Joblin, C. J. Thermochemistry and infrared Spectroscopy of neutral and cationic iron-polycyclic aromatic hydrocarbon complexes of astrophysical interest. Fundamental density functional theory studies. *J. Phys. Chem. A*, **2007**, 111, 9745.

⁴⁴ Senapati, L.; Nayak, S. K.; Rao, B. K.; Jena, P. Atomic structure, binding energy, and magnetic properties of iron atoms supported on a polyaromatic hydrocarbon. *J. Chem. Phys.* **2003**, 118, 8671.

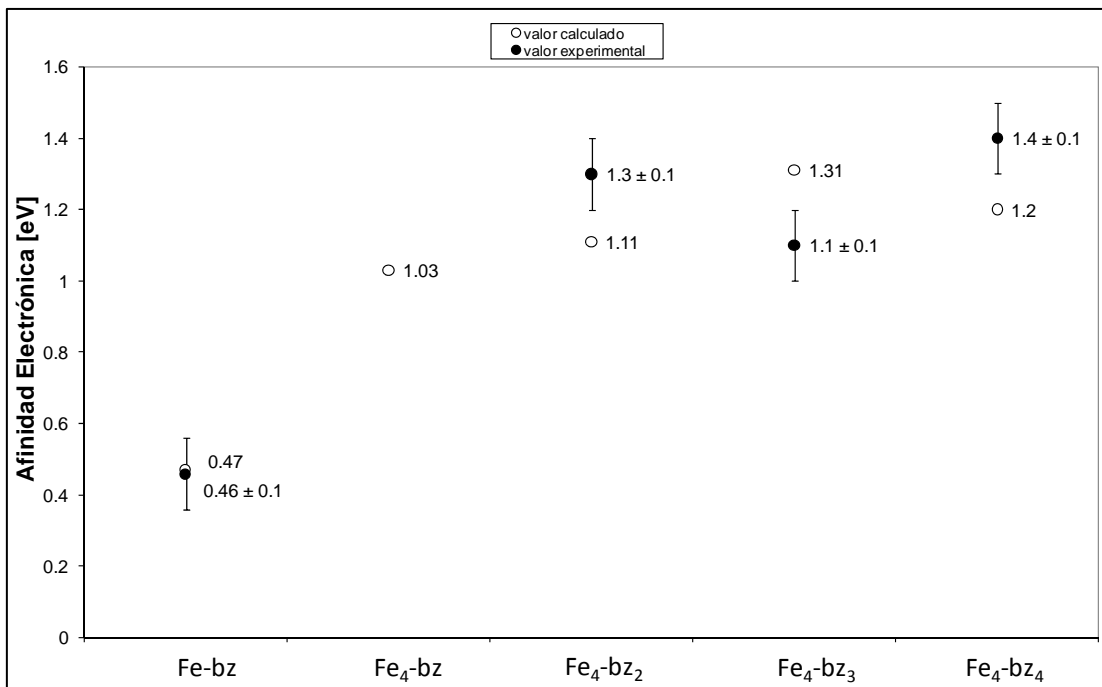


Figura 36. Afinidad electrónica experimental ● y teórica ○ para los complejos Fe_4bz_n , $n \leq 4$

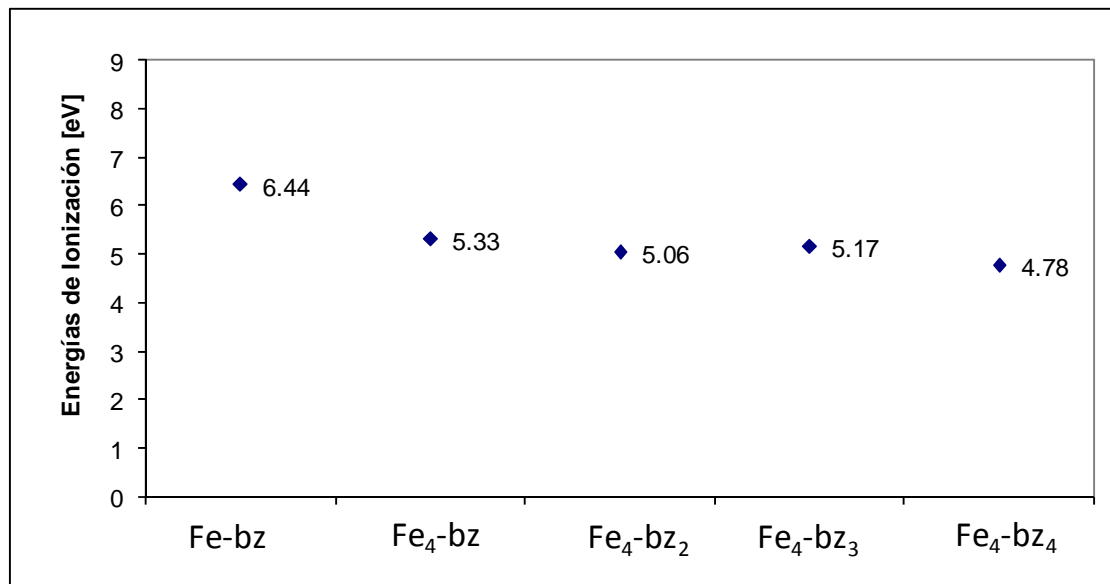


Figura 37. Energías de ionización para los complejos Fe_4bz_n , $n \leq 4$

En el caso de la energía de ionización observamos una disminución en estos valores a medida que aumenta el número de bencenos adsorbidos sobre el cúmulo, esperaríamos que estos valores se relacionaran con el espectro de masas de los cationes, sin embargo, experimentalmente el complejo más estable en forma catiónica es Fe_4bz_3 , el cual esperaríamos que tuviera la menor

energía de ionización, sin embargo tiene una energía de ionización mayor que el de los complejos Fe_4bz_2 y Fe_4bz_4 . La energía de ionización, EI, calculada del benceno es 9.08 eV cercana al valor experimental de 9.24 eV⁴⁵ esta energía es mayor que la del cúmulo Fe_4 con una EI calculada de 5.73 eV. Este comportamiento es parecido al reportado por Valencia et al.⁴⁶ para el cúmulo de Fe_6 con uno y dos bencenos. Esto sugiere que el electrón sustraído de los complejos Fe_4bz_n , corresponde principalmente al cúmulo y en menor medida al benceno. El abatimiento o reducción de la energía de ionización confirma que los electrones más externos de los complejos $\text{Fe}_4\text{-bz}_n$, $n \leq 4$, se encuentran menos enlazados que en el cúmulo Fe_4 libre⁴⁶. Este comportamiento de la disminución de la energía de ionización ha sido observado experimentalmente para los complejos $\text{Sc}_n(\text{Bz})_m$, $\text{Ti}_n(\text{Bz})_m$ y $\text{V}_n(\text{Bz})_m$ mediante el método de fotoionización. Sin embargo, en estos complejos los valores de energía de ionización decaen drásticamente a medida que aumenta el tamaño del cúmulo, a diferencia de los complejos con níquel en los que la energía de ionización decae monótonamente a medida que aumenta el tamaño del cúmulo. La tendencia de la disminución de la energía de ionización es característica para la estructura sándwich múltiple-decker. Este fenómeno en los compuestos tipo sándwich múltiple-decker ha sido estudiado teóricamente mediante cálculos de TFD (B3LYP), los cuales muestran que la ionización tiene lugar en los orbitales moleculares deslocalizados metal-metal mezclados con los orbitales π^* del benceno. En el eje molecular del cúmulo con estructura tipo sándwich ocurre una deslocalización de los orbitales tipo $\delta(\text{e}_{2g})$ del metal a través del LUMO (e_{2g}) del C_6H_6 , lo que da lugar a la drástica disminución en la energía de ionización. Al aumentar el tamaño del cúmulo la estructura tipo sándwich provoca que los electrones se deslocalicen más sobre el eje molecular, mientras que

⁴⁵ (a) Moore, C. E. *Analysis of Optical Spectra*, NSRDS-NBS 34, National Bureau of Standards; National Bureau of Standards: Washington, D.C., 1971. (b) Weast, R. C. *Handbook of Chemistry and Physics*; CRC Press: Boca Raton, FL, 1980; Vol. 61, p E-69. (c) Robinson, J. W. *Handbook of Spectroscopy*; CRC Press: Boca Raton, FL, 1974, Vol. 1, p 257.

⁴⁶ Valencia, I.; Guevara-García, A.; Castro, M. Bonding and Magnetism of $\text{Fe}_6\text{-}(\text{C}_6\text{H}_6)_m$, $m = 1, 2$. *J. Phys. Chem. A* **2009**, *113*, 6222–6238

la estructura tipo “bola de arroz” forma solamente interacciones localizadas d-π sobre los sitios de adsorción del benceno.⁷

En la Figura 38 observamos la variación del momento magnético en los cúmulos a medida que aumenta el número de moléculas de benceno adsorbidas sobre el cúmulo de Fe₄. Este comportamiento muestra que existe una disminución en el momento magnético desde el cúmulo solo que presenta un momento súper paramagnético de 3.5 μ_B por átomo seguido por el complejo Fe₄-bz con 2.5 μ_B hasta Fe₄-bz₃ a 0.5 para después subir a 1 μ_B en el complejo Fe₄-bz₄.

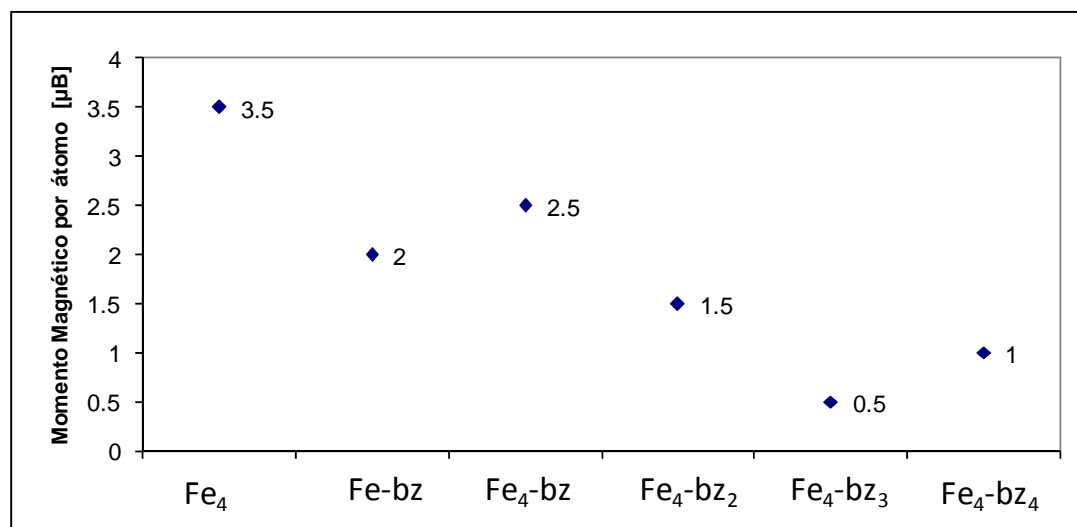


Figura 38. Momento magnético de los complejos Fe₄-bz_m.

De la misma manera para el cúmulo Fe₆-bz_m, m ≤ 4 en la Figura 39 se observa un comportamiento similar, sin embargo el momento magnético más pequeño que se observa es de 2.0 μ_B por átomo, esto parece indicar que además del número de bencenos adsorbidos, el tamaño del cúmulo es un factor que contribuye a la magnetización del cúmulo, además del modo de coordinación de las moléculas de benceno, pues hay que recordar que a diferencia del complejo Fe₄-bz₄ en la que el cuarto benceno tiene una η⁶ en el caso del complejo Fe₆-bz₄ el último benceno adsorbido tiene una η².

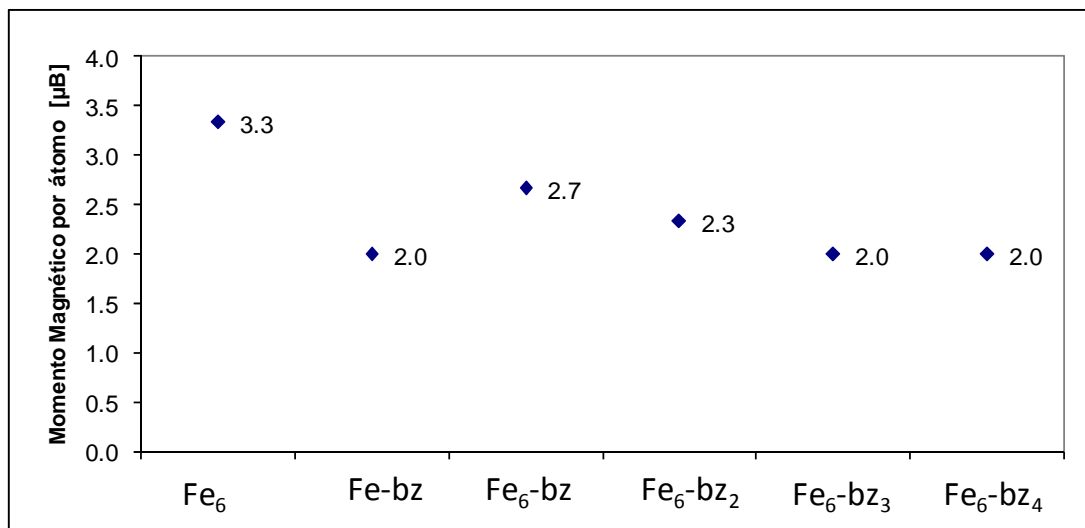


Figura 39. . Momento magnético de los complejos $\text{Fe}_6\text{-bz}_m$.

Las 30 frecuencias calculadas del benceno libre se localizan en el intervalo de 394-3131 cm^{-1} . El valor de vibración de mayor intensidad corresponde al modo de estiramiento completamente simétrico C-H. Los modos vibracionales en los complejos que contienen estiramientos C-H aumentan al ir del benceno libre a los complejos $\text{Fe}_4\text{-bz}_m$ y están desplazadas hacia el azul, mientras que las vibraciones que involucran uniones C-C muestran desplazamientos hacia el rojo. Estos desplazamientos son consistentes con el debilitamiento de los enlaces C-C provocados por la interacción Fe-C en la formación de los complejos Fe_4bz_m .

Análisis vibracional del complejo Fe_4 , C_6H_6 y $\text{Fe}_4\text{-C}_6\text{H}_6$. las frecuencias calculadas para el estado basal del Fe_4 caen en la región de baja frecuencia 108-352 cm^{-1} , y aquellas del benceno en la fase gaseosa están contenidas dentro de 394-3132 cm^{-1} . Esto indica que las frecuencias del Fe_4 y el benceno no traslapan una con otra. Las bandas principales del benceno activas en el infrarrojo se encontraron a 661, 1034 y 1472 cm^{-1} , éstas son ν_{11} (bending C-H fuera del plano), ν_{18} (bending en el plano C-H) y ν_{19} (distorsión del anillo de carbono en el plano). Estos resultados calculados con el funcional BPW91 son solamente ligeramente más pequeños que los

valores experimentales: 673, 1038 y 1486 cm⁻¹.⁴⁷ Otra banda activa para el modo de estiramiento asimétrico C-H fue localizada en 3121 cm⁻¹. Cercano a este modo está el modo de estiramiento C-H, que es inactivo en el infrarrojo y alcanza la mayor frecuencia de 3132 cm⁻¹, para la molécula de benceno libre. Las principales bandas activas del cúmulo de Fe₄ se encuentran a 126, 207, 207 cm⁻¹, con intensidades muy pequeñas de 1.5, 2.8 y 2.8 km/mol respectivamente. Estas frecuencias se deben a modos de estiramiento asimétricos. El modo de estiramiento completamente simétrico del Fe₄ es inactivo en el infrarrojo y está situado a un valor máximo de 352 cm⁻¹ de las frecuencias vibracionales del cúmulo libre.

En el caso del complejo Fe-bz el modo bending fuera del plano es la banda más intensa y también en Fe-bz⁺; de igual manera para el Fe-bz⁻, junto con el modo de estiramiento asimétrico C-H. En estos complejos este modo está desplazado hacia el azul. El bending en el plano C-H está desplazado hacia el rojo en Fe-bz, Febz⁺ y Fe-bz⁻. El modo de distorsión del anillo de carbono en el plano está desplazado hacia el rojo. Estos desplazamientos son similares a los reportados por Jaeger et al.¹³

Para el estado basal del complejo Fe₄-bz, M = 11, las frecuencias se ubican en el intervalo de 12-3136 cm⁻¹. Dos características principales surgen del espectro de IR: (1) éste presenta bandas vibracionales cercanas a las del benceno libre, y (2) algunos modos prohibidos IR del benceno se vuelven activos en el IR en la simetría reducida del complejo, que tiene un momento dipolo de 0.38 D. Específicamente el modo vibracional de mayor intensidad es el modo bending C-H fuera del plano localizado a un valor de 402 cm⁻¹, que es mayor que en el benceno libre; el modo vibracional de estiramiento simétrico del anillo en el benceno libre, a 966 cm⁻¹, se vuelve activo en el complejo. Los modos de distorsión en el plano de los anillos de carbono fueron encontrados a 1426 cm⁻¹ en el complejo Fe₄-bz, mostrando un desplazamiento hacia el rojo y una baja intensidad. El espectro calculado de IR para este complejo en fase gas muestra que, con

⁴⁷ Shimanouchi, T. In *Molecular Vibrational Frequencies, NIST Chemistry WebBook, NIST Standard Reference Database Number 69*; Linstrom, P. J., Mallard, W. G., Eds.; National Institute of Standards and Technology; Gaithersburg, MD, 2007; <http://webbook.nist.gov>

respecto a la molécula de benceno libre, el bending C-H fuera del plano está desplazado hacia el azul, mientras que el bending C-H en el plano está desplazado hacia el rojo. La disminución en la frecuencia de esta banda es indicativa de un debilitamiento en el enlace molecular del benceno. Existen otros modos de distorsión en el plano de los anillos de carbono que no son activos en el benceno libre pero que sí son activos en el complejo y que también están desplazados fuertemente hacia el rojo indicando de igual manera una mayor disminución en la energía del enlace en el anillo de benceno.

En general el espectro de IR del complejo Fe₄-bz muestra que la mayoría de las frecuencias del benceno están desplazadas a valores de menor frecuencia. Una excepción es el desplazamiento hacia el azul para el modo bending C-H fuera del plano el cual es esencialmente un efecto mecánico⁴: la presencia del cúmulo de Fe₄ sobre el anillo de benceno impide el bending del hidrógeno fuera del plano, provocando un aumento en la frecuencia de vibración. A este fenómeno también contribuyen los modos de estiramiento asimétrico C-H, los cuales presentan un ligero desplazamiento hacia el azul, debido principalmente a un ligero incremento en la energía de unión de los enlaces C-H; las distancias C-H en el benceno libre, 1.089 Å, son ligeramente acortadas a 1.087 Å en Fe₄-bz. El modo de estiramiento completamente simétrico C-H fue localizado a la frecuencia más alta 3130 cm⁻¹, del complejo. Esta banda es inactiva en el IR en la molécula libre de benceno pero se vuelve activa en el Fe₄-bz, con un ligero desplazamiento hacia el azul debido a la adsorción del benceno sobre el cúmulo.

Las bandas de 12 a 400 cm⁻¹ corresponden ya sea a Fe₄ o a modos inducidos Fe₄-bz. Por ejemplo, la banda intensa localizada a 400 cm⁻¹ es para un modo bending fuera del plano C-H, acoplado con movimientos oscilatorios, a lo largo de la dirección axial del sitio atómico más cercano.

El espectro del complejo Fe₄-bz₂ muestra el modo vibracional bending C-H fuera del plano a 774 cm⁻¹ con un pico muy intenso, desplazado hacia el azul, al igual que para el complejo

$\text{Fe}_4\text{-bz}$, este menor desplazamiento sugiere un impedimento más pequeño del Fe_6 para este tipo de bending. La modesta banda a 820 cm^{-1} es para los modos bending C-H fuera del plano, estas bandas muestran pequeños desplazamientos hacia el rojo. Bandas débiles aparecen para el bending C-H en el plano a 990 cm^{-1} , y para la distorsión del anillo de carbono en el plano a 1423 cm^{-1} que presenta desplazamientos pequeños hacia el rojo como en el caso de $\text{Fe}_4\text{-bz}$, indicando también un debilitamiento del enlace para las moléculas de benceno en $\text{Fe}_4\text{-bz}_2$. El estiramiento simétrico del anillo de cada molécula de benceno localizado a 900 cm^{-1} de intensidad media está desplazado hacia el rojo más fuertemente que en el complejo $\text{Fe}_4\text{-bz}$. Aquí el estiramiento simétrico de una molécula de benceno está fuera de fase del otro. Cuando el estiramiento simétrico de las moléculas de benceno está en fase, el modo completo es IR inactivo y se ubica a una frecuencia más alta. El modo de estiramiento asimétrico C-H está localizado a 3129 cm^{-1} . El estiramiento simétrico C-H de las moléculas de benceno que están fuera de fase se encuentra a una frecuencia ligeramente mayor de 3134 cm^{-1} , con una fuerte intensidad. En el caso de las vibraciones de baja frecuencia existe una banda muy débil a 590 cm^{-1} para las distorsiones del anillo de carbono. Las vibraciones a 410 cm^{-1} son principalmente debido al bending C-H fuera del plano de los dos bencenos acoplados con movimientos oscilatorios del cúmulo de hierro. Los modos a 370 cm^{-1} se deben a movimientos de tipo swinging de las moléculas de benceno adsorbidas con modos bending de los átomos de hierro.

El espectro IR estimado para el complejo $\text{Fe}_4\text{-bz}_3$ muestra como ya se ha dicho anteriormente 2 propiedades principales. Primero, presenta resonancias vibracionales cercanas a las del benceno libre; y segundo, algunos modos prohibidos en el IR se vuelven activos debido a que el complejo presenta una menor simetría con un momento dipolo de 0.68 D. Estas características son observadas claramente por comparación con el espectro IR del benceno libre, por ejemplo la banda intensa a 762 cm^{-1} debida a la vibración de tipo bending C-H fuera del plano está desplazada hacia el azul con respecto al valor del benceno libre. Estos desplazamientos hacia

el azul son esencialmente efectos mecánicos, debido a que la presencia del cúmulo Fe₄ sobre el benceno impide el modo bending carbono hidrógeno fuera del plano, lo que aumenta la frecuencia de vibración. El modo bending C-H en el plano se localiza a 996 cm⁻¹, desplazado hacia el rojo. La banda de intensidad media a 1427 cm⁻¹ corresponde a distorsiones en el plano del anillo de carbono y está desplazada hacia el rojo. Estos desplazamientos hacia el rojo del bending C-H en el plano y distorsión del anillo de carbono en el plano indican un debilitamiento del enlace en los anillos de benceno. El modo de estiramiento simétrico en el anillo de carbono es inactivo y se ubica a 990 cm⁻¹, sin embargo en el complejo Fe₄-bz₃, este modo está localizado a 967 cm⁻¹, este modo se encuentra fuera de fase, en el caso de la vibración de estiramiento simétrico en el anillo de carbono en fase la frecuencia tiene menor intensidad, casi despreciable y se encuentra a 968 cm⁻¹. Al estar desplazados estos modos hacia el rojo indican un debilitamiento en el enlace de las moléculas de benceno.

Las bandas débiles localizadas a 820 cm⁻¹ corresponden a modos de vibración tipo bending C-H fuera del plano menos simétricos, desplazados hacia el rojo con respecto al valor del benceno libre de 830.7 cm⁻¹, en el que no son activos.

El complejo Fe₄-bz₃ muestra dos bandas intensas, localizadas a las frecuencias más altas a 3130 y 3135 cm⁻¹ para el estiramiento asimétrico C-H.

En el caso del complejo Fe₄-bz₄ el espectro de infrarrojo muestra un incremento grande de los modos vibracionales, IR prohibidos en el benceno, los cuales se vuelven activos en el IR en el complejo. Los modos de vibración C-H fuera del plano están localizados a 713 cm⁻¹; estos modos están desplazados hacia el azul. A diferencia del complejo Fe₆-bz₄³⁴ en la que inesperadamente existe un desplazamiento hacia el rojo debido a que la coordinación de la cuarta molécula de benceno unida al complejo Fe₆ es diferente de seis, es igual a dos y tiene una inclinación. Esto disminuye considerablemente el impedimento mecánico discutido anteriormente para el bending C-H.

El estiramiento simétrico del anillo se encuentra localizado a 972 cm^{-1} , este modo se encuentra desplazado hacia el rojo.

El bending C-H en el plano a 995 cm^{-1} muestra un desplazamiento hacia el rojo de la misma manera, el modo de distorsión del anillo en el plano aparece a 1450 cm^{-1} . El desplazamiento hacia el rojo de estos dos tipos de modos indica un debilitamiento en el enlace molecular de los bencenos.

7. Conclusiones

Con el método BPW91/6-311++G(2d,2p) se determinaron las geometrías de tipo rice-ball para los estados basales de $\text{Fe}_4\text{-}(\text{C}_6\text{H}_6)_m$, $m = 1, 2, 3$, y 4 , en los que los resultados indican que cada una de las moléculas de benceno están unidas a un solo átomo de hierro mediante coordinaciones Fe-C igual a 6 , y en los que se conserva la estructura del Fe_4 , aunque con una geometría más distorsionada que la del cúmulo de Fe_4 libre: un tetraedro menos distorsionado. Podemos afirmar que estos estados calculados corresponden cercanamente a los estados basales verdaderos de los complejos, esto con base en los valores de afinidad electrónica determinados teóricamente, los que concuerdan relativamente bien con los valores experimentales.

Los estados basales de los cúmulos $\text{Fe}_4\text{-bz}_m$ tienen valores de multiplicidad $M = 15$ para Fe_4 , $M = 11$ para el complejo $\text{Fe}_4\text{-bz}$, $M = 7$ para $\text{Fe}_4\text{-bz}_2$, alcanza un límite de baja multiplicidad de $M = 3$ para el complejo $\text{Fe}_4\text{-bz}_3$ y después vuelve a subir a $M = 5$ para el complejo $\text{Fe}_4\text{-bz}_4$. Estos resultados muestran que los efectos magnéticos desempeñan un papel importante en la adsorción de benceno sobre el cúmulo de Fe_4 .

En el caso de la energía de ionización observamos una disminución en estos valores a medida que aumenta el número de bencenos adsorbidos sobre el cúmulo, esto refleja la fuerte interacción de los electrones tipo **d** del cúmulo con la nube **π** del benceno. Además, debido a que

la energía de ionización del cúmulo es menor que la del benceno esto sugiere que en el proceso de ionización en los complejos $\text{Fe}_4\text{-bz}_m$, $m \leq 4$ el cúmulo tiene una mayor participación, lo cual se ve reflejado también en la mayor modificación geométrica del cúmulo y no del benceno. Este resultado concuerda con los valores de energía de unión de los complejos $\text{Fe}_4\text{-bz}_m$, $m \leq 4$, en los cuales se puede observar que también esta energía disminuye a medida que aumenta el número de moléculas adsorbidas de benceno. Esto es debido principalmente a las repulsiones estéricas y eléctricas entre las moléculas de benceno además de la saturación en la coordinación sobre el cúmulo de hierro.

Existen espectros de infrarrojo característicos para cada uno de los complejos Fe_4bz_n neutros, cationes y aniones. En general, los corrimientos hacia el rojo para los modos vibracionales CH in-plane-bending y C-C ring distortion indican un debilitamiento del enlace C-C en el anillo del benceno. También se observa que algunos modos vibracionales que son IR inactivos en benceno libre, se vuelven IR-activos en el complejo. Conversamente, algunos modos que son IR-activos en benceno, se vuelven inactivos en los complejos. Además los espectros calculados pueden servir de guía a los investigadores experimentales para la confirmación de estas estructuras propuestas, debido a que hasta la fecha de realización de este trabajo no se ha realizado estudios experimentales de espectroscopia de infrarrojo para estos complejos.

Referencias

- 1.- Bansmann, J.; et al. Magnetic and structural properties of isolated and ensamblated clusters. *Surf. Sci. Rep.* **2005**, *56*, 189.
- 2.- Billas, I. M. L.; Chatelain, A.; de Heer, W. A. Magnetism from the atom to the bulk in iron, cobalt and nickel clusters. *Science*, **1994**, *265*, 1682.
- 3.- Cox, D. M.; Trevor, D. J.; Whetten, R. L.; Rohlfing, E. A.; Kaldor, A. Magnetic behavior of free-iron and iron-oxide clusters. *Phys. Rev. B*, **1985**, *32*, 7290.
- 4.- Duncan, M. A. Structures, energetic and spectroscopy of gas phase transition metal ion-benzene complexes. *Int. J. Mass Spectrom.* **2008**, *272*, 99.
- 5.- Nakajima, A.; Kaya, K. A novel network structure of organometallic clusters in the gas phase. *J. Phys. Chem. A*, **2000**, *104*, 176.
- 6.- Dietz, T. G.; Duncan, M. A.; Powers, D. E.; Smalley, R. Laser production of supersonic metal cluster beams. *J. Chem. Phys.* **1981**, *74*, 6511.
- 7.- Kurikawa, T.; H. Takeda; M. Hirano, Judai, K; Arita T; Nagao S; Nakajima A; Kaya K. Electronic properties of organometallic Metal-Benzene Complexes [M_n(benzene)_m (M) Sc-Cu)]. *Organometallics*, **1999**, *18*, 1430-1438.
- 8.- Zheng, W.; Eustis, N. S.; Li, X.; Nilles J. M.; Thomas, O. C.; Bowen, K. H.; Kandalam A. K.; Photoelectron spectroscopic study of iron–benzene cluster anions. *Chem. Phys. Lett.* **2008**, *462*, 35-39.
- 9.- Szczepanski, J.; Wang, H.; Vala, M.; Tielens, A. G. G. M.; Eyler, J. R.; Oomens, J. Infrared Spectroscopy of gas-phase complexes of Fe³⁺ and polycyclic aromatic hydrocarbon molecules. *J. ApJ.* **2006**, *646*, 666.
- 10.- Hübner, O.; Sauer, J. Confirmation of 9 Sigma(-)(g) and 8 Sigma(-)(u) ground states of Fe-2 and Fe-2 by CASSCF/MRCI. *Chem. Phys. Lett.* **2002**, *358*, 442.

- 11.- Kandalam, A. K.; Jena, P.; Li, X.; Eustis, S. N.; Bowen, K. H. Photoelectron spectroscopy and theoretical studies of [Co-m(pyrene)(n)](-) (m=1,2 and n=1,2) complexes. *J. Chem. Phys.* **2008**, *129*, 134308.
- 12.- Baushlicher, C. W.; Partridge, H.; Langhoff, S. R. Theoretical Study of transition-metal ions bound to benzene. *J. Phys. Chem.* **1992**, *96*, 3273.
- 13.- Jaeger, T. D.; van Heijnsbergen, D.; Klippenstein, S. J.; von Helden, G.; Meijer, G.; Duncan, M. A. Vibrational spectroscopy and density functional theory of transition-metal ion-benzene and dibenzene complexes in the gas phase. *J. Am. Chem. Soc.* **2004**, *126*, 10981.
- 14.- Becke, A. D.; Density Functional Thermochemistry .3. The role of the exact exchange. *J. Chem. Phys.* **1993**, *98*, 5648-5652.
- 15.- Stephens, P. J.; Devlin, F. J.; Chabalowski, C. F.; Frisch, M. J. Ab initio calculation of vibrational absorption and circular-dichroism spectra using density functional force-fields. *J. Phys. Chem.* **1994**, *98*, 11623.
- 16.- Becke, A. D. Density-Functional exchange energy approximation with correct asymptotic behavior. *Phys. Rev. A.* **1988**, *38*, 3098.
- 17.- Perdew, J. P.; Wang, Y. Pair-distribution function and its coupling-constant average for the spin polarized electron-gas. *Phys. Rev. B.* **1992**, *45*, 13244.
- 18.- Valencia, I.; Chávez, V.; Castro, M. Bonding of Benzene with Excited States of Fe₇. *J. Phys. Chem. A.* **2008**, *112*, 5028-5033.
- 19.- Gaussian 03, Revision E.01, M. J. Frisch, G. W. Trucks, H. B. Schlegel, G. E. Scuseria, M. A. Robb, J. R. Cheeseman, J. A. Montgomery, Jr., T. Vreven, K. N. Kudin, J. C. Burant, J. M. Millam, S. S. Iyengar, J. Tomasi, V. Barone, B. Mennucci, M. Cossi, G. Scalmani, N. Rega, G. A. Petersson, H. Nakatsuji, M. Hada, M. Ehara, K. Toyota, R. Fukuda, J. Hasegawa, M. Ishida, T. Nakajima, Y. Honda, O. Kitao, H. Nakai, M. Klene, X. Li, J. E. Knox, H. P. Hratchian, J. B. Cross, V. Bakken, C. Adamo, J. Jaramillo, R. Gomperts, R. E. Stratmann, O. Yazyev, A. J.

- Austin, R. Cammi, C. Pomelli, J. W. Ochterski, P. Y. Ayala, K. Morokuma, G. A. Voth, P. Salvador, J. J. Dannenberg, V. G. Zakrzewski, S. Dapprich, A. D. Daniels, M. C. Strain, O. Farkas, D. K. Malick, A. D. Rabuck, K. Raghavachari, J. B. Foresman, J. V. Ortiz, Q. Cui, A. G. Baboul, S. Clifford, J. Cioslowski, B. B. Stefanov, G. Liu, A. Liashenko, P. Piskorz, I. Komaromi, R. L. Martin, D. J. Fox, T. Keith, M. A. Al-Laham, C. Y. Peng, A. Nanayakkara, M. Challacombe, P. M. W. Gill, B. Johnson, W. Chen, M. W. Wong, C. Gonzalez, and J. A. Pople, Gaussian, Inc., Wallingford CT, 2004.
- 20.- Burrow, P. D.; Michejda, J. A.; Jordan, K. D. Electron transmission study of the temporary negative-ion states of selected benzenoid and conjugated aromatic-hydrocarbons. *J. Chem. Phys.* **1987**, *86*, 9.
- 21.- Exploring chemistry with electronic structure methods. Foresman J. Y Frisch A. 2da.Gaussian, Inc., Ed. 1996. pp. 119.
- 22.- Wachters, A. J. H. Gaussian basis set for molecular wavefunctions containing third-row atoms. *J. Chem. Phys.* **1970**, *52*, 1033.
- 23.- Hay, P. J. Gaussian basis sets for molecular calculations – representation of 3d orbitals in transition-metal atoms. *J. Chem. Phys.* **1977**, *66*, 4377.
- 24.- Raghavachari, K.; Trucks, G. W. Highly correlated systems – excitation-energies of 1st row transition metals Sc-Cu. *J. Chem. Phys.* **1989**, *91*, 1062.
- 25.- Castro, M. On the interaction of magnetic iron clusters with hydrocarbons: Fe₄-propane. *Chem. Phys. Lett.* **2007**, *435*, 322-326.
- 26.- Castro, M. On the bonding of methane with magnetic Fe-4 clusters. *Chem. Phys. Lett.* **2007**, *446*, 333-338.
- 27.- Kuchitsu, K. *Structure Data of Free Polyatomic Molecules*, Landolt-Börnstein, New Series, Group II; Springer, Heidelberg

- 28.- S. Berski, G.L. Gutsev, M.D. Mochena, Toward understanding the electron density distribution in magnetic clusters: Insight from the ELF and AIM analyses of ground state Fe-4. *J. Phys. Chem. A.* **2004**, *108*, 6025.
- 29.- Gennady, L. G; Bauschlicher C, W, Jr. Electron Affinities, Ionization Energies, and Fragmentation Energies of Fe_n Clusters (n) 2-6): A Density Functional Theory Study. *J. Phys. Chem. A.* **2003**, *107*, 7013-7023.
- 30.- Wang. L. S.; Li X.; Zhang, H. F.; Probing the electronic structure of iron clusters using photoelectron spectroscopy *J. Chem. Phys.* **2000**, *262*, 56.
- 31.- Parks, W. K.; Klots, T. D.; Riley, S. J. Chemical probes of metal cluster ionization-potentials. *J. Chem. Phys.* **1990**, *92*, 3813.
- 32.- Rabilloud, F. Geometry and spin multiplicity of half-sandwich type transition-metal-benzene complexes. *J. Chem. Phys.* **2005**, *122*, 134303.
- 33.- Imura, K.; Ohoyama, H.; Kasai, T.; Structures and its dipole moments of half-sandwich type metal-benzene (1:1) complexes determined by 2-m long electrostatic hexapole. *Chem. Phys.* **2004**, *301*, 183.
- 34.- Valencia, I.; Castro, M. Theoretical Study of the Structural and Electronic Properties of the $\text{Fe}_6\text{-}(\text{C}_6\text{H}_6)_m$, $m = 3, 4$, complexes, *J. Phys. Chem. A.* **2010**, *114*, 21-28
- 35.- Shimanouchi, T. In *Molecular Vibrational Frequencies, NIST, Chemistry WebBook, NIST Standard Reference Database Number 69*; Linstrom, P. J., Mallard, W. G., Eds.; National Institute of Standards and Technology: Gaithersburg, MD, **2007**; <http://webbook.nist.gov>.
- 36.- R. Pandey, B. K. Rao, P. Jena, J. M. Newsam. Unique signature of transition metal atoms supported on benzene, *Chem. Phys. Lett.* **2000**, *321*, 142.
- 37.- Meyer F., Khan I. A., Armentrout P. B. Thermochemistry of transition-metal benzene complexes – binding – energies of $\text{M}(\text{C}_6\text{H}_6)(\text{X})(+)$ ($\text{X}=1,2$) for $\text{M} = \text{Ti}$ to Cu . *J. Am. Chem. Soc.*, **1995**, *117*, 9740.

- 38.- Knickelbein, M. B. Magnetic moments of bare and benzene-capped clusters. *J. Chem. Phys.* **2006**, *125*, 044308.
- 39.- Rayón M. V., Frenking, G. Bis(benzene)chromium is a delta-bonded molecule and ferrocene is a pi-bonded molecule. *Organometallics*. **2003**, *16*, 3304.
- 40.- M. Domagala, S. J. Grabowski, K. Urbaniak, G. Młoston, Crystal and molecular structure of (r-2, c-4)-3-benzyl-2,4,5,5-tetraphenyl-1,3-thiazolidine, intramolecular C-H center dot center dot center dot S hydrogen bonds. *J. Mol. Struc. (Theochem)*. **2004**, *690*, 69.
- 41.- G.R. Desiraju, T. Steiner, The Weak Hydrogen Bond in Structural Chemistry and Biology, Oxford University Press Inc., New York, 1999.
- 42.- Sun, X.; Suzuki, T.; Kurahashi M. et al. First-principles study on the spin polarization of benzene adsorbed on Fe(100) surface. *J. Appl. Phys.* **2007**, *101*, 09G526.
- 43.- Simon, A.; Joblin, C. J. Thermochemistry and infrared Spectroscopy of neutral and cationic iron-polycyclic aromatic hydrocarbon complexes of astrophysical interest. Fundamental density functional theory studies. *J. Phys. Chem. A*, **2007**, *111*, 9745.
- 44.- Senapati, L.; Nayak, S. K.; Rao, B. K.; Jena, P. Atomic structure, binding energy, and magnetic properties of iron atoms supported on a polyaromatic hydrocarbon. *J. Chem. Phys.* **2003**, *118*, 8671.
- 45.- (a) Moore, C. E. *Analysis of Optical Spectra*, NSRDS-NBS 34, National Bureau of Standards; National Bureau of Standards: Washington, D.C., 1971. (b) Weast, R. C. *Handbook of Chemistry and Physics*; CRC Press: Boca Raton, FL, 1980; Vol. 61, p E-69. (c) Robinson, J. W. *Handbook of Spectroscopy*; CRC Press: Boca Raton, FL, 1974, Vol. 1, p 257.
- 46.- Valencia, I.; Guevara-García, A.; Castro, M. Bonding and Magnetism of $\text{Fe}_6\text{-}(\text{C}_6\text{H}_6)_m$, $m = 1, 2$. *J. Phys. Chem. A* **2009**, *113*, 6222–6238

47.- Shimanouchi, T. In *Molecular Vibrational Frequencies, NIST Chemistry WebBook*, NIST Standard Reference Database Number 69; Linstrom, P. J., Mallard, W. G., Eds.; National Institute of Standards and Technology; Gaithersburg, MD, 2007; <http://webbook.nist.gov>

APÉNDICE: Artículos publicados en revistas internacionales de riguroso arbitraje.

- a) Valencia, I.; Chávez, V.; Castro, M. Bonding of Benzene with Excited States of Fe₇, *J. Phys. Chem. A* **2008**, *112*, 5028-5033.
- b) Valencia, I.; Guevara-García, A.; Castro, M. Bonding and Magnetism of Fe₆-(C₆H₆)_m, m = 1, 2. *J. Phys. Chem. A* **2009**, *113*, 6222–6238
- c) Valencia, I.; Castro, M. Theoretical Study of the Structural and Electronic Properties of the Fe₆-(C₆H₆)_m, m = 3, 4, complexes, *J. Phys. Chem. A* **2010**, *114*, 21-28

ARTICLES

Bonding of Benzene with Excited States of Fe₇

Israel Valencia, Victor Chávez, and Miguel Castro*

*Departamento de Física y Química Teórica, DEPg. Facultad de Química,
Universidad Nacional Autónoma de México, México D. F., C. P. 04510, México**Received: December 31, 2007; Revised Manuscript Received: March 19, 2008*

The interaction between high-spin Fe₇ clusters and a benzene molecule was studied using the BPW91/6-311++G(2d,2p) method. The Fe₇–C₆H₆ ground state has a T-shaped structure, similar to that of the benzene dimer, and a multiplicity $M = 2S + 1 = 19$ (S = total spin). The carbon atoms are bonded to a single equatorial iron atom, which experiences a dramatic decrease in its magnetic moment, from 3.1 to $-0.8 \mu_B$; the magnetic moments of other Fe atoms are larger than those in the ground-state Fe₇ cluster. Such unexpected magnetic behavior of the cluster is crucial for adsorption of benzene.

1. Introduction

Nowadays, significant advances have been made in the synthesis, characterization, and understanding of small transition metal (TM) clusters.^{1,2} This has been accomplished using state-of-the-art experimental techniques for an accurate study of low-energy states of size-selected clusters. It was found that they present unexpected reactivity, magnetic, and optical properties, which strongly depend on size and, finally, on the electronic structure of the TM clusters, which is unique and different from that of the atom and bulk limits. For example, iron clusters show superparamagnetism³ and act as catalysts in the synthesis of carbon nanotubes^{4,5} and in reactions where the activation of the C–H bond is crucial.⁶ Overall, these findings open new avenues in material science, as there is the possibility of forming novel materials with specific properties using clusters as building blocks.^{7–9} But, and markedly for iron, the clusters coalesce to form bigger units when assembled.⁹ This problem can be avoided by coating the cluster with ligands, implying the study of the effects of ligands on the original attributes of the cluster. Also, a fundamental issue that is yet to be solved is the geometry of these particles. Due to their small size, insight into this property should rely on indirect methods as the chemical approach, under the assumption that cluster geometry is unaltered by the adsorbed species. However, there are limited experimental and theoretical attempts to study the effects of ligands on the behavior of clusters. For iron clusters, such studies have been done recently using small ligands such as H₂O for Fe_n, $n \leq 4$,¹⁰ C₂H₂ and CCH₂ for Fe_n, $n \leq 4$,¹¹ CH₄ for Fe_n, $n \leq 15$,^{12–14} and C₂H₆ for Fe₄.¹⁵

The objective of this work is to study interactions of benzene with a superparamagnetic Fe₇ cluster using density functional theory with generalized gradient approximation (DFT–GGA). We will specially focus on the magnetic behavior of Fe₇ upon benzene adsorption. It will be shown that the excited states of Fe₇ are more capable of adsorbing benzene than the ground state. The bonding of benzene, or its derivatives, with TM clusters may explain the origin of the existence of novel benzene–cluster

geometries.¹⁶ In advance, C₆H₆–Fe₇ has a T-shaped structure as that found for a low-lying state of the benzene dimer.

The electronic structure calculations on TM clusters pose a considerable theoretical challenge, since due to the open d-shell structure they usually have many spin states lying within a narrow energy range. Even though multireference methods, where electronic wave functions are treated as multiconfigurational functions, are more suitable and needed for the correct characterization of this kind of system, their use is limited because of their high computational cost. These methods have been only applied to the study of TM dimers¹⁷ or, regarding the present case, to the study of a TM atom interacting with a benzene moiety.¹⁸ On the other hand, DFT–GGA techniques with the use of appropriate basis sets allow the characterization of the ground-state properties for bigger clusters containing several TM atoms. Indeed, as refs 1, 2, and 5–10 show, DFT has succeeded in describing the electronic properties of magnetic TM clusters as well as the interaction of these particles with small molecules. So, a DFT-based method, described below, was chosen for the study of Fe₇–C₆H₆.

2. Methodology

The ground states (GS) of Fe₇, C₆H₆, and Fe₇–C₆H₆ were determined by means of DFT all-electron calculations, realized with the functional of Becke for exchange¹⁹ and that of Perdew and Wang for correlation.²⁰ This approach is referred to as BPW91, which is used in concert with 6-311++G(2d,2p) basis sets (15s11p6d2f)/[10s7p4d2f] for Fe, (12s6p2d)/[5s4p2d] for C, and (6s2p)/[4s2p] for H.^{21–23} The Gaussian-03 code was employed.²⁴ The BPW91/6-311++G(2d,2p) method is appropriate for the study of small iron clusters interacting with hydrocarbons.^{14,15} A strict convergence criterion was used for the total energy, minimized up to 10^{-8} au. Without imposing symmetry constraints and for several different spin states, defined by the total number of unpaired electrons, or the total spin, S , several candidate structures were fully optimized with a 10^{-5} au threshold for the rms force. An ultrafine grid was used for these steps and for the vibrational analysis, which was performed under the harmonic approximation for all the

* Corresponding author. E-mail: castro@quetzal.pquim.unam.mx

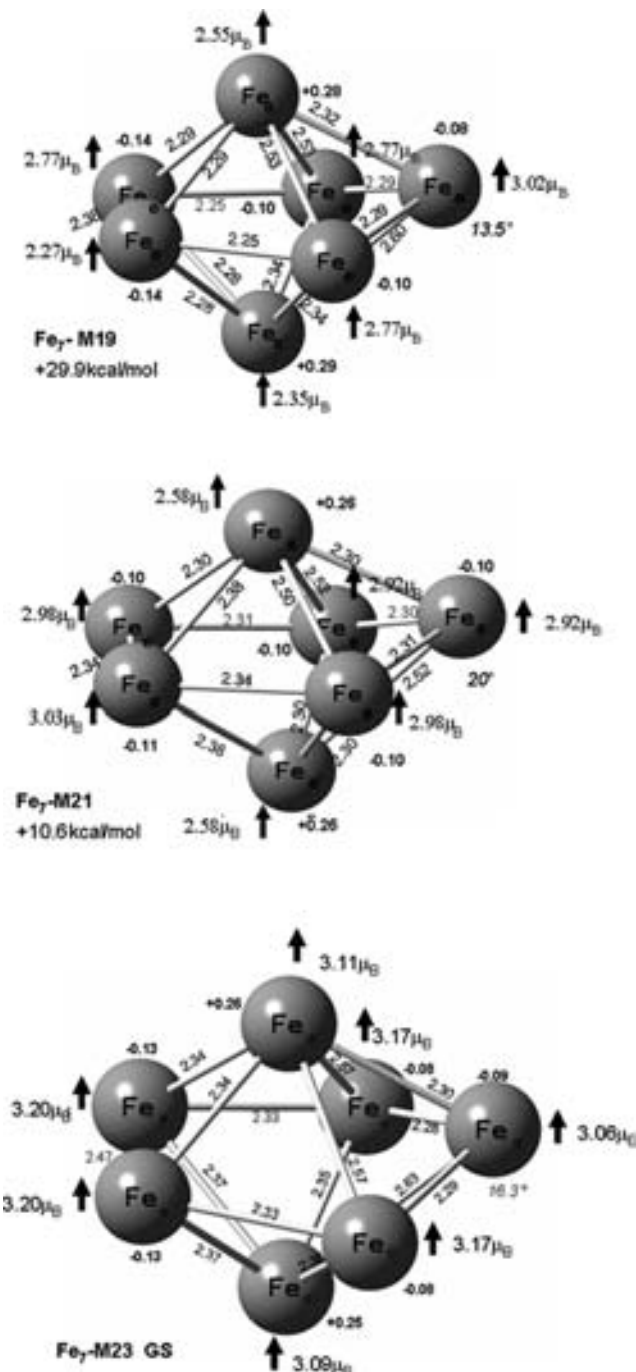


Figure 1. Bond lengths, in angstroms, atomic charges, and magnetic moments, in μ_B , for the $M = 23$, 21, and 19 states of Fe₇. Also is indicated the dihedral angle for the atom Fe_e.

optimized geometries. All the located states in Figures 1 and 2 are local minima, since they have positive frequencies, on the potential energy surface. Mulliken populations were obtained to determine the magnetic moments and charge-transfer effects for the Fe₇–C₆H₆ interaction. These parameters are very useful for the analysis of the magnetic behavior of Fe₇ during the adsorption of benzene. As will be shown, the magnetic effects are crucial for the bonding of benzene with Fe₇.

3. Results and Discussion

The GS of benzene has C–C and C–H distances of 1.398 and 1.089 Å, respectively, close to the experimental values,²⁵ 1.399 and 1.101 Å; all bond angles are equal to 120°. The GS

of Fe₇ is a distorted pentagonal bipyramid, see Figure 1, with a multiplicity $M = 2S + 1 = 23$, where S is the total spin. This structure has one of the atoms of the five-membered ring located 16.3° out of the plane formed by the other four. The unpaired electrons form magnetic moments of 3.1–3.2 bohr magnetons (μ_B) at the atomic sites. The equatorial atoms have negative charges, −0.08 to −0.13 electrons (e), which are compensated by the charges, +0.26 e, of the axial sites. These results are in agreement with previous DFT studies.^{26,27} Furthermore, the calculated GS of Fe₇⁺ has $M = 24$ and lies 5.99 eV over the neutral GS, which is in concordance with the experimental ionization energy, 5.76 ± 0.05 eV, for Fe₇.²⁸ Similarly, addition of one extra electron yields, after full relaxation, an $M = 22$ GS for Fe₇[−]; the adiabatic electron affinity, 1.60 eV, is close to the observed value, 1.50 ± 0.05 eV.²⁹ Indeed, it is strongly believed that the GS of Fe₇ is a distorted pentagonal bipyramid with $M = 23$, as its estimated density of states²⁶ follows closely the features of the photoelectron spectrum.²⁹ However, as will be shown, the GS is not a highly reactive state. The $M = 21$ state lies 10.6 kcal/mol over the GS. Note that $M = 19$, 30 kcal/mol above the GS, is undeniably a higher energy state; its charge distribution is similar to that of the $M = 21$ and 23 states, with shorter bond lengths and smaller magnetic moments it also presents an inhomogeneous magnetization, ≈2.8–3.0 μ_B at the equatorial sites and 2.55 μ_B at the axial ones. At this level of theory, this $M = 19$ higher energy state presents a negative frequency, which may be due to its highly compact structure. Furthermore, since the equatorial atoms have a smaller coordination number, NC = 4, than the axial sites, NC = 5, they are more suitable for bonding with benzene, mainly those of the $M = 21$ and 19 states, as they have smaller magnetic moments (lesser amount of unpaired electrons at those sites).

The $M = 19$ excited state of Fe₇, through an equatorial atom Fe_e, adsorbs benzene, forming the Fe_{7e}–C₆H₆ $M = 19$ GS (**I**), in which benzene and the pentagonal bipyramid lie in a T-shaped geometry similar to that of the C₆H₆ dimer,³⁰ see Figure 2. Moreover, the Fe_{7e}–C₆H₆ $M = 21$ state (**III**) is quasi-degenerate with the GS, since it lies less than 1.0 kcal/mol above, whereas the Fe₇ GS forms the Fe_{7e}–C₆H₆ $M = 23$ state (**III**), located 4.4 kcal/mol above **I**. Thus, the $M = 19$ and 21 Fe₇ excited states, remarkably the former, are considerably stabilized by the benzene adsorption. In fact, this process reverses the order of the magnetic states of Fe₇. Besides, carbon bonding at one axial Fe_a atom yields parallel Fe₇–C₆H₆ higher energy states, considerably above the T-shaped GS.

Up to here, the spin multiplicity for the GS of the bare Fe₇ cluster was determined. As quoted, the $M = 23$ assignment is validated by the estimated ionization energy, electron affinity, and density of states, which compare well with their experimental counterparts. Moreover, the calculated spin multiplicity, $M = 19$, for the GS of Fe₇–C₆H₆ indicates a significant reduction or quenching, from 3.1 to 2.6 μ_B , of the average atomic magnetic moment for the coated Fe₇ cluster. Though the magnetic moment of Fe₇–C₆H₆ has not yet been reported, Knickelbein³¹ has recently found that the moments per Co atom measured for Co_{7–10}(C₆H₆)_m are markedly smaller than those measured for the corresponding pure Co_n clusters, clearly pointing to a strong electronic perturbation of the underlying Co_n cluster. Our spin-multiplicity assignment for Fe₇–C₆H₆ is consistent with such magnetic behavior. At low temperatures we predict an atomic moment of 2.6 μ_B for Fe₇–C₆H₆, smaller than 3.1 μ_B for pure Fe₇. At higher temperatures, as those reached in Stern–Gerlach experiments,³¹ 130 K, a higher magnetic moment is expected as the measurement may have

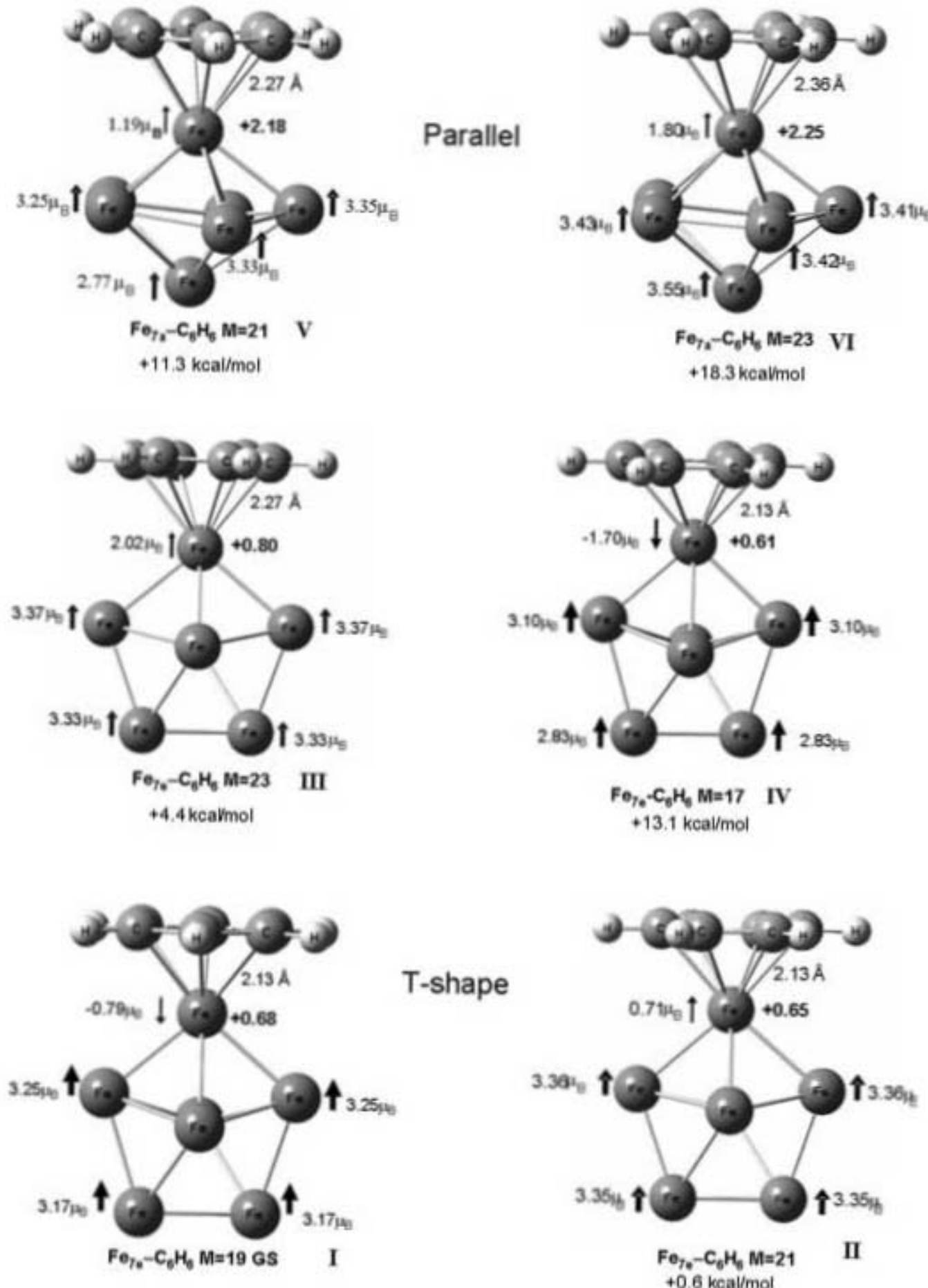


Figure 2. Bond lengths, in angstroms, atomic charges, and magnetic moments, in μ_B , for the lowest energy states of $\text{Fe}_7\text{-C}_6\text{H}_6$.

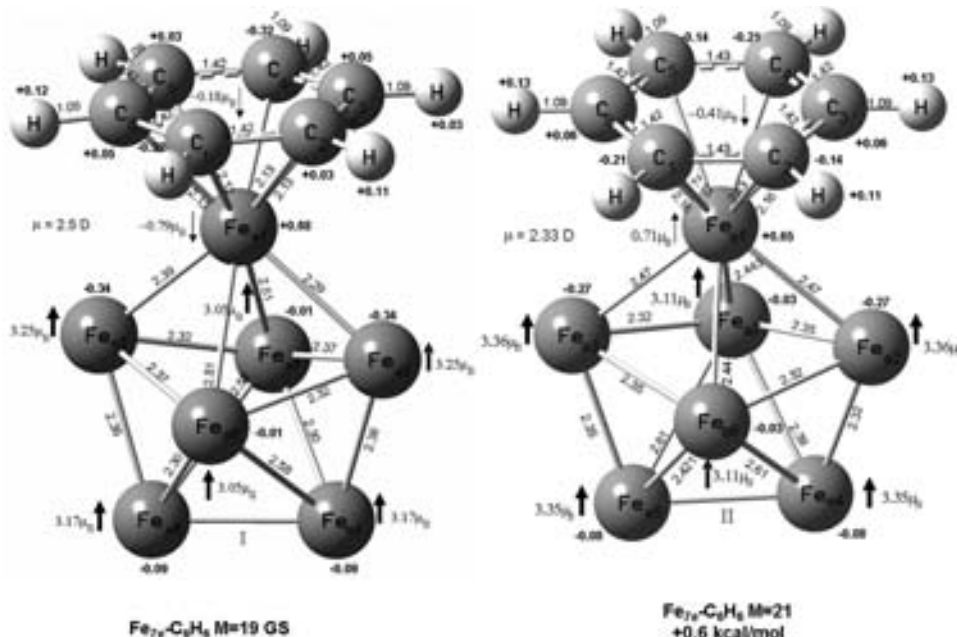


Figure 3. Bond lengths, in angstroms, atomic charges, dipole moments, in debyes, and magnetic moments, in μ_B , for the $\text{Fe}_{7e}-\text{C}_6\text{H}_6$ $M = 19$ GS and for **II**.

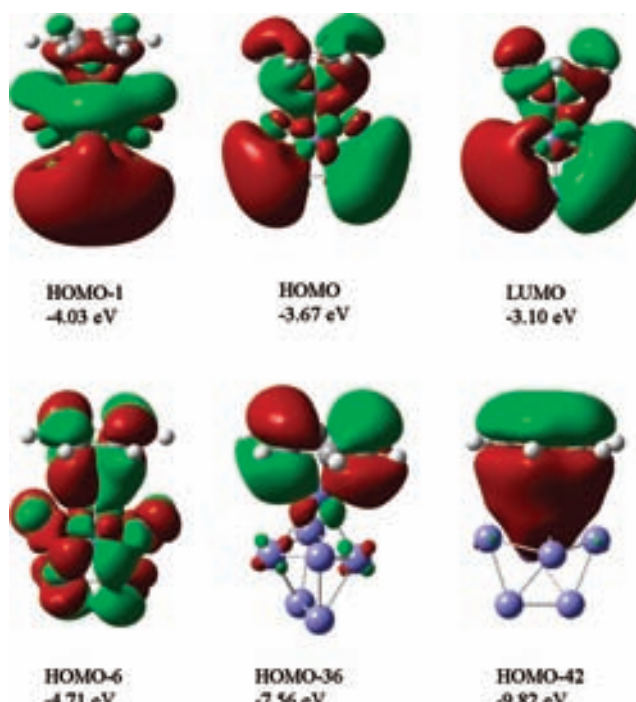


Figure 4. Contour plots for LUMO^\dagger , HOMO^\dagger , and other deeper MOs of **II**.

contributions from the $M = 21$ and 23 states, lying only 1 and 4 kcal/mol above the GS, respectively.

In the $\text{Fe}_{7e}-\text{C}_6\text{H}_6$ GS, shown in Figure 3 together with state **II**, the C–Fe_e distances, 2.116–2.129 Å, are slightly longer than those of ferrocene (2.045 Å), prototypical of C–Fe covalent bonds;³² a similar pattern holds for **II**, as its C–Fe_e lengths are 2.161–2.130 Å. For both cases, these distances are smaller than the sum of the van der Waals radii of C (1.7 Å) and Fe (1.9 Å), suggesting C–Fe bond formation; they are also shorter than the C–Fe distances, 2.253–2.381 Å, for weak C–Fe bonding in Fe_4-CH_4 and $\text{Fe}_4-\text{C}_3\text{H}_8$.^{14,15} As shown below, C–Fe bonds are formed in $\text{Fe}_7-\text{C}_6\text{H}_6$. The C–C distances in **I** (1.420–1.421 Å) or **II** (1.419–1.426 Å) show, with respect to free benzene,

a lengthening of 0.022–0.023 Å or 0.021–0.028 Å, whereas the C–H bonds, ≈ 1.087 Å, have minor shrinks.

The contour plots of the highest occupied molecular orbital (HOMO), the lowest unoccupied MO (LUMO), and other deeper MOs of majority spin for **II** are shown in Figure 4. HOMO, HOMO-1, HOMO-6, and HOMO-10 have bond signatures between the 3d-electrons of Fe_{e1} and the π -cloud of C₆H₆; they also contribute largely to the other Fe atoms, for example, HOMO has large spots on Fe_{e4} and Fe_{e5} and HOMO-1 on the six Fe_{e2}–Fe_{e7} sites. These kinds of MOs show how the bonding is accomplished between Fe₇ and C₆H₆, and they also reveal a polarization from Fe_{e1} toward the other Fe sites, with an increase in their negative charge and spin density, more clearly on the

Fe sites directly bonded to Fe_{e1}. Other MOs, not shown in Figure 4, also have this type of σ -bond, formed between the π - and the 3d-electrons. Also, the LUMO presents C–Fe_e bonding, with contributions to C₆H₆ and to Fe_{e2}–Fe_{e5}. The HOMO–LUMO gap in bare benzene is 5.1 eV, and in **II** it is much smaller, 0.57 eV; because in **II**, both MOs have contributions from C₆H₆, the adsorption on Fe₇ renders a softer benzene moiety. Furthermore, HOMO-42 depicts that, aside from overlapping strongly with the electrons of Fe_{e1}, the symmetric π MO of benzene remains delocalized around the ring. A similar C–Fe_e bonding is also displayed by the MOs of **I**; the main difference is that they are located at a deeper orbital energies.

Subtracting the GS energies of Fe₇ $M = 23$ and C₆H₆ from that of Fe₇–C₆H₆ $M = 19$ GS, a binding energy (BE), including zero-point energy (ZPE), of 16.8 kcal/mol is obtained. The BE of **II** is 16.2 kcal/mol. On experimental grounds, the dissociation energy of Fe–benzene is estimated to be greater than 0.7 eV or 16.1 kcal/mol; our values are consistent with this finding for a single Fe atom^{16,33,34} and with the estimated BE of benzene, 1.07 eV or 24.67 kcal/mol, on an infinite Fe(100) surface.³⁵

From C₆H₆ to Fe₇, a small transfer of charge (0.2 e) occurs through the C–Fe_e bonds. This charge does not reside on Fe_{e1}. As indicated by the population analysis, Fe_{e1} has a charge of +0.68 e, whereas the other iron atoms have a whole negative charge of −0.90 e. The results of this strong electronic polarization of Fe₇ in **I** show how an acidic response of Fe₇ is accomplished: the (directly) bonded Fe_{e1} atom to benzene has a positive charge. Overall, this movement of charge reduces the repulsion between the “3d” electrons (mostly of majority spin in the bare cluster) localized at Fe_{e1} and the π -electrons of C₆H₆. In fact, benzene adsorption produces a dramatic decrease, and even a change of direction, of the magnetic moment at Fe_{e1}, because it is moved from 2.77 μ_B , in bare Fe₇, up to −0.79 μ_B in **I**. This decrease is compensated by the other iron atoms of the cluster, since they reach high magnetic moments (3.25 μ_B), as those of the high-spin Fe₇ $M = 23$ GS, 3.20 μ_B . Also in the opposite direction, the carbon atoms have a whole magnetic moment of −0.18 μ_B . An analogous behavior is presented by the quasi-degenerate state **II**. It has a positive charge of +0.65 e and a small magnetic moment of 0.71 μ_B at the Fe_{e1} site. In this case, four iron atoms reach magnetizations (3.36 μ_B) even greater than those of the Fe₇ $M = 23$ GS. Moreover, also the carbon atoms have a whole magnetic moment of 0.41 μ_B , but in the opposite direction. In brief, the repulsion between the Fe_{e1} 3d- and the π -electrons diminishes through a transfer of charge, associated with transference of magnetic moments, from Fe_{e1} toward the other Fe sites, leaving Fe_{e1} positively charged and with a smaller magnetic moment. These results agree with the finding that the magnetic moment of a single Fe atom is reduced from 4 to 2 μ_B when adsorbed in benzene.^{34,36} Truly, **I** and **II** have the smallest magnitudes of the magnetic moments at the Fe sites, directly bonded to the carbon atoms, than the higher energy states **III** (2.02 μ_B), **IV** (1.70 μ_B), **V** (1.19 μ_B), and **VI** (1.80 μ_B).

It should be mentioned that we have also performed geometry optimization using the smaller 6-311+G(d) basis set (15s11p6d1f)/[10s7p4d1f] for Fe, (12s6p1d)/[5s4p1d] for C, and (5s)/[3s] for H; such set has been used for the study of Fe_n interacting with NO.³⁷ The obtained results indicate a similar order for the Fe₇–C₆H₆ low-lying states. The structure **I**, Figure 2, remains as the GS, while the structures **II**, **III**, **IV**, **V**, and **VI** are located 0.9, 5.1, 13.7, 11.8, and 19.4 kcal/mol above the GS. Moreover, in **I**, the iron atom, Fe_{e1}, bonded directly to benzene, presents a magnetic moment of −0.68 μ_B , whereas in **II**, Fe_{e1} has 0.73

μ_B ; these values are close to those obtained with the 6-311++G(2d,2p) basis set.

Even more, a natural bond order³⁸ analysis also indicates a magnetic moment of −0.43 μ_B for the Fe_{e1} atom of the GS structure **I**. Similarly, a value of 0.88 μ_B was obtained for the Fe_{e1} atom of **II**. Thus, in the Fe₇–C₆H₆ GS, the magnetic moment of the Fe atom carrying the benzene molecule shows an opposite direction from that of the other Fe atoms.

The calculated 30 vibrational frequencies of free benzene fall in the 3131–394 cm^{−1} range. And those of the states **I** and **II** fall within the 3142–16 cm^{−1} and 3144–9 cm^{−1} gaps. In all cases, the upper value corresponds to the full symmetric C–H stretching, having an increase of 11 or 13 cm^{−1}. Indeed, the modes involving C–H displacements are increased from C₆H₆ to Fe₇–C₆H₆, whereas the vibrations containing C–C movements show reductions of −11 up to −111 cm^{−1}. This softening is consistent with the weakening of the C–C bonds, due to the C–Fe bonding, observed for benzene in Fe₇–C₆H₆.

4. Conclusions

The $M = 19$ and 21 excited states of Fe₇ adsorb benzene forming the lowest energy states of Fe₇–C₆H₆ with a T-shaped geometry and with the carbon atoms bonded to a single Fe_{e1} atom. However, the Fe₇–C₆H₆ $M = 23$ state lies only 4.4 kcal/mol over the $M = 19$ GS. Thus, in these coated Fe₇ clusters the $M = 23$ –19 magnetic states are contained within a gap of 4.4 kcal/mol, indicating a significant decrease from that, 30 kcal/mol, of the free clusters. These results show how the magnetic effects play a crucial role in the absorption of C₆H₆ by Fe₇. This process produces a strong polarization on Fe₇, yielding a positive charge, +0.65 or +0.68 e, and a severe reduction of the magnetic moment, 0.7 or 0.8 μ_B , at the iron atom, Fe_{e1}, bonded directly with the carbon atoms, whereas other iron atoms have an increase of charge and of magnetic moments. Such charge and magnetic polarization reduces the repulsion between the 3d-electrons of Fe_{e1} and the π -electrons of benzene, facilitating the Fe₇–C₆H₆ bonding through an acid behavior of Fe₇ and through C–Fe σ bond formation.

Acknowledgment. Financial support from Project PAPIIT IN-107905 from DGAPA-UNAM is acknowledged. The access to the supercomputer facilities at DGSCA-UNAM is strongly appreciated.

References and Notes

- (1) Bansmann, J. *Surf. Sci. Rep.* **2005**, *56*, 189.
- (2) Alonso, J. A. *Chem. Rev.* **2000**, *100*, 637.
- (3) Khanna, S. N.; Linderoth, S. *Phys. Rev. Lett.* **1991**, *67*, 742.
- (4) Nikolaev, P.; Bronikowski, M. J.; Bradley, R. K.; Rohmund, F.; Colbert, D. T.; Smith, K. A.; Smalley, R. E. *Chem. Phys. Lett.* **1999**, *313*, 91.
- (5) Satishkumar, B. C.; Govindaraj, A.; Sen, R.; Rao, C. N. R. *Chem. Phys. Lett.* **1998**, *293*, 47.
- (6) Schnabel, P.; Irion, M. P.; Weil, K. G. *J. Phys. Chem.* **1991**, *95*, 9688.
- (7) Eberhardt, W. *Surf. Sci.* **2002**, *500*, 242.
- (8) Chen, B.; Castlemann, A. W., Jr.; Ashman, C.; Khanna, S. N. *Int. J. Mass Spectrom.* **2002**, *220*, 171.
- (9) Vystavel, T.; Koch, S. A.; Palasantzas, G.; De Hosson, J. Th. M. *J. Mater. Res.* **2005**, *20*, 1785.
- (10) Gutsev, G. L.; Mochena, M. D.; Bauchlicher, C. W., Jr *Chem. Phys.* **2005**, *314*, 291.
- (11) Chrétien, S.; Salahub, D. R. *J. Chem. Phys.* **2003**, *119*, 12279.
- (12) Liyanage, R.; Zhang, X.-G.; Armentrout, P. B. *J. Chem. Phys.* **2001**, *115*, 9747.
- (13) (a) Chiodo, S.; Kondakova, O.; Michelini, M. C.; Russo, N.; Sicilia, E.; Irigoras, A.; Ugalde, J. M. *J. Phys. Chem. A* **2004**, *108*, 1077. (b) Chiodo, S.; Rivalta, I.; Michelini, M. C.; Russo, N.; Sicilia, E.; Ugalde, J. M. *J. Phys. Chem. A* **2004**, *110*, 12501.

- (14) Castro, M. *Chem. Phys. Lett.* **2007**, *435*, 322.
(15) Castro, M. *Chem. Phys. Lett.* **2007**, *446*, 333.
(16) Kurikawa, T.; Takeda, H.; Hirano, M.; Judai, K.; Arita, T.; Nagano, S.; Nakajima, A.; Kaya, K. *Organometallics* **1999**, *18*, 1430.
(17) Hübner, O.; Sauer, J. *Chem. Phys. Lett.* **2002**, *358*, 442.
(18) Rabillo, F. *J. Chem. Phys.* **2005**, *122*, 134303.
(19) Becke, A. D. *Phys. Rev. A* **1988**, *38*, 3098.
(20) Perdew, J. P.; Wang, Y. *Phys. Rev.* **1992**, *45*, 13244.
(21) Wachters, A. J. H. *J. Chem. Phys.* **1970**, *52*, 1033.
(22) Hay, P. J. *J. Chem. Phys.* **1977**, *66*, 4377.
(23) Raghavachari, K.; Trucks, G. W. *J. Chem. Phys.* **1989**, *91*, 1062.
(24) Frisch, M. J.; Trucks, G. W.; Schlegel, H. B.; Scuseria, G. E.; Robb, M. A.; Cheeseman, J. R.; Montgomery, J. A., Jr.; Vreven, T.; Kudin, K. N.; Burant, J. C.; Millam, J. M.; Iyengar, S. S.; Tomasi, J.; Barone, V.; Mennucci, B.; Cossi, M.; Scalmani, G.; Rega, N.; Petersson, G. A.; Nakatsuji, H.; Hada, M.; Ehara, M.; Toyota, K.; Fukuda, R.; Hasegawa, J.; Ishida, M.; Nakajima, T.; Honda, Y.; Kitao, O.; Nakai, H.; Klene, M.; Li, X.; Knox, J. E.; Hratchian, H. P.; Cross, J. B.; Bakken, V.; Adamo, C.; Jaramillo, J.; Gomperts, R.; Stratmann, R. E.; Yazyev, O.; Austin, A. J.; Cammi, R.; Pomelli, C.; Ochterski, J. W.; Ayala, P. Y.; Morokuma, K.; Voth, G. A.; Salvador, P.; Dannenberg, J. J.; Zakrzewski, V. G.; Dapprich, S.; Daniels, A. D.; Strain, M. C.; Farkas, O.; Malick, D. K.; Rabuck, A. D.; Raghavachari, K.; Foresman, J. B.; Ortiz, J. V.; Cui, Q.; Baboul, A. G.; Clifford, S.; Cioslowski, J.; Stefanov, B. B.; Liu, G.; Liashenko, A.; Piskorz, P.; Komaromi, I.; Martin, R. L.; Fox, D. J.; Keith, T.; Al-Laham, M. A.; Peng, C. Y.; Nanayakkara, A.; Challacombe, M.; Gill, P. M. W.; Johnson, B.; Chen, W.; Wong, M. W.; Gonzalez, C.; Pople, J. A. *Gaussian 03*, revision D.01; Gaussian, Inc.: Wallingford, CT, 2004.
(25) Kuchitsu, K. *Structure Data of Free Polyatomic Molecules*; Landolt-Börnstein, New Series, Group II; Springer: Heidelberg, 1992; Vol. 21.
(26) Castro, M. *Int. J. Quantum Chem.* **1997**, *64*, 223.
(27) Bobadova-Parvanova, P.; Jackson, K. A.; Srinivas, S.; Horoi, M.; Kohler, C.; Seifert, G. *J. Chem. Phys.* **2002**, *116*, 3576.
(28) Yand, S.; Knickelbein, M. B. *J. Chem. Phys.* **1990**, *93*, 1533.
(29) Wang, L.-S.; Li, X.; Zhang, H.-F. *Chem. Phys.* **2000**, *262*, 53.
(30) Sinnokrot, M. O.; Valeev, E. F.; Sherill, C. D. *J. Am. Chem. Soc.* **2002**, *124*, 10887.
(31) Knickelbein, M. B. *J. Chem. Phys.* **2006**, *125*, 044308.
(32) (a) Wilkinson, G.; Rosenblum, M.; Whiting, M. C.; Woodward, R. B. *J. Am. Chem. Soc.* **1952**, *74*, 2125. (b) Dunitz, J. D.; Orgel, L. E.; Rich, A. *Acta Crystallogr.* **1956**, *9*, 373.
(33) Mayer, F.; Khan, I. A.; Armentrout, P. B. *J. Am. Chem. Soc.* **1995**, *117*, 9740.
(34) Pandey, R.; Rao, B. K.; Jena, P.; Newsam, J. M. *Chem. Phys. Lett.* **2000**, *321*, 142.
(35) Sun, X.; Suzuki, T.; Kurashashi, M.; Shang, J. W.; Yamauchi, Y. *J. Appl. Phys.* **2007**, *101*, 09G256.
(36) Pandey, R.; Rao, B. K.; Jena, P.; Blanco, M. A. *J. Am. Chem. Soc.* **2001**, *123*, 3799.
(37) Gutsev, G. L.; Mochena, M. D.; Johnson, E.; Bauchlicher, C. W., Jr. *J. Chem. Phys.* **2006**, *125*, 194312.
(38) Reed, A. E.; Curtiss, L. A.; Weinhold, F. *Chem. Rev. (Washington, DC, U.S.)* **1988**, *88*, 899.

JP712184W

Bonding and Magnetism of $\text{Fe}_6-(\text{C}_6\text{H}_6)_m$, $m = 1, 2$

Israel Valencia, Alfredo Guevara-García, and Miguel Castro*

Departamento de Física y Química Teórica, DEPg, Facultad de Química, Universidad Nacional Autónoma de México, México D. F., C. P. 04510, México

Received: May 29, 2008; Revised Manuscript Received: April 20, 2009

The interactions of one and two benzene molecules with the superparamagnetic Fe_6 cluster were studied by means of gradient-corrected density functional theory. The ground state, GS, of bare Fe_6 presents a distorted octahedral structure with $2S = 20$; S is the total spin. For the calculated $2S = 16$ GS of the neutral $\text{Fe}_6-\text{C}_6\text{H}_6$ complex, as well as in the positive and negative ions both with $2S = 15$, the benzene unit is adsorbed on one axial Fe_a atom. The $2S = 14$ GS for $\text{Fe}_6-(\text{C}_6\text{H}_6)_2$ resembles a sandwich structure, with the metal Fe_6 cluster separating the benzene rings that are bonded symmetrically on the two axial sites of Fe_6 . The binding is accounted for by electrostatic interactions and by $3d-\pi$ bonds, as revealed by the molecular orbitals. Though each $\text{C}-\text{Fe}$ bond is weak, η^6 coordinations were indicated by the topology of the electronic density. The $3d-\pi$ bonding is reflected by the adiabatic ionization energies and electron affinities, which are smaller than those of bare Fe_6 . The computed IR spectra show vibrational bands near those of bare benzene; some forbidden IR modes in benzene and in Fe_6 become IR active in $\text{Fe}_6-(\text{C}_6\text{H}_6)_{1,2}$. The results show a strong perturbation of the electronic structure of Fe_6 . The decrease of its magnetic moment implies that the magnetic effects play an important role in the adsorption of benzene.

1. Introduction

Transition metal (TM) clusters present unusual structural, magnetic, and catalytic properties,¹ which finally depend on their electronic structure, different from those of the atom and bulk limits, that originate complicated metal–metal bonds and, in some cases, the formation of magnetic moments on the atomic sites. Particularly, small iron clusters, Fe_n , exhibit superparamagnetism because they have bigger moments than that of the bulk.^{2,3} Very recently, using laser vaporization techniques,⁴ the study for the adsorption of organic molecules on small TM clusters has been addressed.^{5–7} In this way, neutral $\text{Fe}_n-(\text{benzene})_m$ species were produced in the gas phase,^{6,7} which were characterized mainly by mass spectrometry. Under high concentration of benzene, the mass spectrum revealed that the maximum m number of adsorbed moieties is smaller than n , allowing the proposal that $\text{Fe}_n-(\text{benzene})_m$ has rice-ball structures consisting of an Fe_n cluster fully covered by benzene. The biggest observed system was Fe_7 , being saturated with four benzenes, and was followed by Fe_6 which also adsorbs four ligands.^{6,7} Such an amount of adsorbed moieties is consistent with the suggestion of rice-ball geometries for Fe_6 and Fe_7 . However, relatively little experimental information is known on how the benzene molecules interact with iron clusters, specifically regarding the electronic and structural properties of the benzene adsorbed iron particles. In fact, rice-ball patterns were indicated for $\text{Fe}_n-(\text{C}_6\text{H}_6)_m$, but definitive experimental structural information is still elusive for these species. On the other hand, the coating of TM clusters with ligands may avoid their coalescence, mostly for iron, when one tries to link such particles, which is important for the design of new materials, with desired magnetic and/or catalytic properties, using TM clusters as building blocks. This implies also the study of the effects that ligands produce on the original attributes of the

cluster, but little is known about this issue. Furthermore, the magnetic properties of complexes of TMs and polycyclic aromatic hydrocarbons (PAH), as extended systems of benzene, have raised considerable interest in recent years and motivated several theoretical and experimental studies.^{8–10} Specifically, the IR properties of Fe–benzene compounds have been studied,⁵ as well as those of PAH for astrophysical purposes.^{11–14}

On the theoretical side, electronic structure calculations on TM clusters pose a considerable challenge, which is due to the abundance of low-lying electronic states, the possibility of multiple isomers, and the complicated nature of the TM atoms (occupying open 3d shells of short-range and close in energy, highly delocalized 4s orbitals). Even though multi-reference methods, where electronic wave functions are treated as multiconfigurational functions, are suitable and needed for the correct characterization of these kind of systems, their use is limited because of their expensive computational cost. These methods have been only applied to the study of TM dimers¹⁵ or, regarding the present research, to the study of TM atoms interacting with a single benzene molecule.¹⁶ The study of the TM ions bound to one benzene molecule has been realized at the modified coupled-pair (MCP) functional level.¹⁷ More recently, Duncan and co-workers^{5,18} have studied the TM–benzene ions with the use of the hybrid B3LYP functional;^{19,20} they found good agreement with the MCP results as well as with experimental data.^{5,18} It should be remarked that the study of TM clusters and of TM clusters interacting with molecules requires the use of functionals able to describe the complicated metal–metal interactions and the metal–ligand ones. In this regard, density functional theory (DFT), accounting for exchange correlation of many electron systems through the general gradient dependent approximation (GGA), for example the combination of the exchange functional proposed by Becke²¹ and the one for correlation developed by Perdew and Wang,²² jointly with the use of appropriate basis sets,²³ have proved to be

* To whom correspondence should be addressed. E-mail: castro@quetzal.pqum.unam.mx.

able to determine the ground state (GS) geometry and the electronic and energetic properties of TM systems or clusters presenting complicated metal–metal interactions.^{24–27} In fact, DFT–GGA based methods allow the characterization of the GS properties for bigger clusters containing several TM atoms. As refs 24–27 show, DFT has succeeded in describing the electronic properties of magnetic TM clusters as well as the interaction of these particles with small molecules.

Specifically, Gutsev and Bauschlicher²⁴ have shown that the BPW91 method^{21,22} is an appropriate GGA–DFT scheme for an accurate study of the structural, electronic, and energetic properties of small Fe_n , $n \leq 6$, clusters.²⁴ In their study, the requirement of more strict convergence criteria for the total energy and atomic forces, as well as the requirements of ultrafine grids, was pointed out.²⁴ The BPW91 approach and the 6311++G(2d,2p) orbital basis sets were employed, and the interactions of the superparamagnetic Fe_4 cluster with propane²⁵ and methane²⁶ were studied. More recently, we have also studied, with the BPW91/6311++G(2d,2p) method, the bonding and magnetic properties of the relatively small Fe_7 cluster interacting with a single benzene molecule.²⁷ In this last study, we have observed that calculations on $\text{Fe}_7-(\text{C}_6\text{H}_6)_1$ were quite computationally expensive, limiting the study of the adsorption process when two or more benzene moieties were considered.

The objective of this work is to study, by means of first principles all-electron calculations, performed with GGA–DFT, the interactions of benzene molecules with the magnetic Fe_6 cluster. It will be shown that the obtained results allow the determination of the geometry for the low-lying states that are produced from the interaction of the Fe_6 cluster with one and two benzene moieties, as well as the analysis of bond dissociation energies, ionization energies, and electron affinities. These structural and electronic results are useful for the study of the interactions between the 3d electrons of the cluster and the π cloud of benzene and to depict the type of bonding that occurs in the $\text{Fe}_6-(\text{C}_6\text{H}_6)_m$ species. We will also address the vibrational frequencies suffered by benzene in the adsorption process. The mono- and dibenzene complexes containing one TM atom have been studied extensively.⁵ It will be shown that $\text{Fe}_6-(\text{C}_6\text{H}_6)_2$, resembling some features of ferrocene,^{28,29} possesses unusual energetic and magnetic properties caused by the d– π bonding.

2. Methodology

The low-lying states of the Fe_6 cluster, benzene, and $\text{Fe}_6-(\text{benzene})_m$ ($m = 1, 2$) complexes as well as those for the corresponding single positively and negatively charged species were determined with the aid of DFT all-electron calculations performed with the BPW91 functional,^{21,22} which was used in concert with 6-311++G(2d,2p) basis sets (15s11p6d2f)/[10s7p4d2f] for Fe, (12s6p2d)/[5s4p2d] for C, and (6s2p)/[4s2p] for H.²³ The Gaussian-03 quantum chemistry software was used.³⁰ Here, also a strict convergence criterion was used for the total energy, minimized up to 10^{-8} au. Without imposed symmetry constraints and for different spin states, several candidate structures were fully optimized with a 10^{-5} au threshold for the root mean square (rms) force. An ultrafine grid was used for these steps and for the vibrational analysis, which was performed under the harmonic approximation for all optimized geometries. With this methodology, the regions of true minima states of the potential energy surface for each complex were searched. That is, the reported states in Figures 1–4 are true local minima because they have positive frequencies.

3. Results and Discussion

3a. Lowest Energy States Fe_6 , Fe_6^+ , and Fe_6^- . The GS of Fe_6 is a distorted octahedron of D_{2h} symmetry, shown in Figure 1, with a multiplicity $M = 2S + 1 = 21$; S is the total spin corresponding to a $^{21}\text{A}_u$ electronic state. The unpaired electrons form a magnetic moment of 20 bohr magnetons (μ_B) or 3.3 μ_B per atom. These results are in agreement with those reported by Gutsev and Bauschlicher,²⁴ Bobadova-Parvanova et al.,³¹ as well as with our previous results.³² Then, Fe_6 is a small cluster presenting high magnetic moment and geometry of relatively high symmetry. Experimentally, the Stern–Gerlach measurements are indicative of superparamagnetism in small iron clusters, as they have moments of $\approx 3.0 \mu_B$ per atom, bigger than the bulk value, $2.2 \mu_B$.²³ The DFT results quoted above are consistent with such experimental findings. Table 1 contains some higher energy states of Fe_6 . The average equilibrium bond length, R_{eq} , is also indicated, showing a shortening as the multiplicity decreases. The $M = 19$ state (3.0 μ_B /atom) lies nearest to the GS and may contribute, depending on temperature, on the measured moment. The other states may contribute negligibly as they lie at higher energies. Electron detachment from the $M = 21$ GS of Fe_6 yields, after full relaxation, an $M = 22$ GS for the Fe_6^+ ion, with an adiabatic ionization energy (IE) of 6.15 eV, which is near the experimental result, 5.96 ± 0.05 eV.³³ The GS geometry of Fe_6^+ is shown in Figure 2, as well as the highest occupied molecular orbital of minority spin, HOMO^\downarrow , from which the electron was deleted. Some higher energy states of Fe_6^+ are also indicated in Table 1. Assuming that one electron deletion from the excited states occurs either from the related HOMO^\downarrow , yielding an $M - 1$ state, or from HOMO^\uparrow , yielding an $M + 1$ state (M is the multiplicity of the parent neutral), and choosing the one of lowest energy, one finds that the IE for the higher energy states differs notably from the experiment; the departure increases as the energy of the state increases (see Table 1, in parentheses, the multiplicity of the produced Fe_6^+ ion is also indicated.). Attachment of one electron yields an $M = 20$ GS for Fe_6^- . Occupation was done on the lowest unoccupied molecular orbital, LUMO^\downarrow ; see Figure 2. The estimated adiabatic electron affinity (AE), 1.61 eV, matches with the measured value, 1.58 ± 0.06 eV.³⁴ As is shown in Table 1, the estimated EAs for the higher energy states, assuming the $M \pm 1$ rule quoted above, differ significantly from the experimental value. The importance of the spin effects in the accurate estimation of EAs and IEs for small iron clusters is exemplified by these results. The geometry of benzene is shown in Figure 1; its calculated IE, 9.08 eV, bigger than that of Fe_6 , is close to the observed value, 9.24 eV.³⁵

3b. Lowest Energy States of $\text{Fe}_6-(\text{C}_6\text{H}_6)$ and $\text{Fe}_6-(\text{C}_6\text{H}_6)_2$. The GS of $\text{Fe}_6-\text{C}_6\text{H}_6$ has C_{2v} symmetry with $M = 17$, yielding an $^{17}\text{A}_2$ electronic state, where the benzene molecule is adsorbed on one axial Fe_a atom, as shown in Figure 3. Note that the bonding of one axial iron atom with the carbon atoms of the benzene ring lengthens considerably the separations of Fe_a with the iron atoms in the equatorial plane; still, the structure of the whole Fe_6 cluster is preserved in this monobenzene compound. Concerning benzene, the bond lengths of the carbon atoms are slightly increased, from 1.40 to 1.42 Å, and the planarity is mostly maintained, since the dihedral angle in the ring is 1.1°. As shown in Table 2, the $M = 15$ state is quasidegenerate with the GS; other states lie at higher energies. Then, benzene adsorption reverses the order of the low-lying states of Fe_6 , quenches the moment by about 4 μ_B , and forms a dipole moment of 2.37 Debyes (D). This last feature implies important electrostatic contributions in the Fe_6 –benzene bonding.

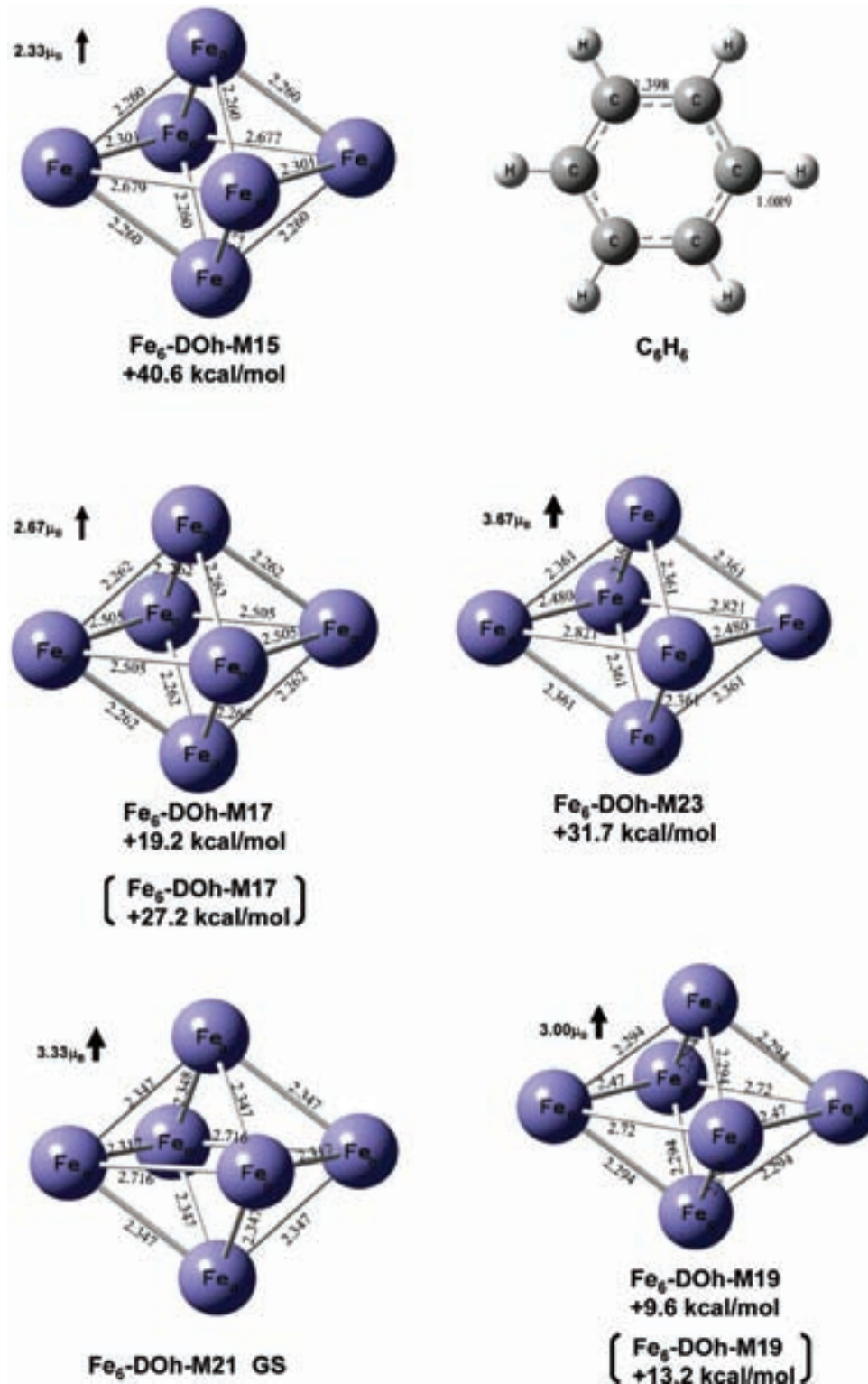


Figure 1. Lowest energy states for Fe₆. Bond lengths, in Å, and average magnetic moments per atom, in μ_B , are indicated. Also the calculated ground state for benzene is shown.

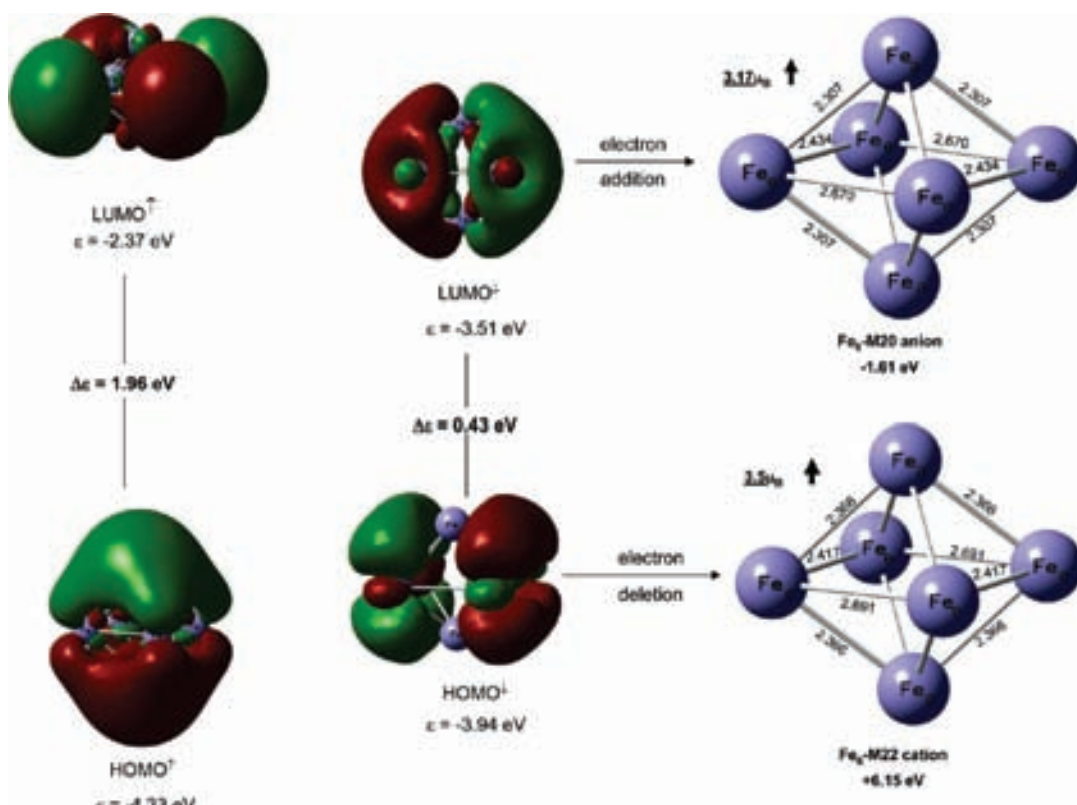
The GS of Fe₆-(C₆H₆)₂ has D_{2h} symmetry with $M = 15$, corresponding to the ${}^1\text{B}_{2g}$ electronic state, and the carbon atoms of the benzene molecules are bonded symmetrically, as depicted in Figure 4a, to the axial Fe atoms. These C-Fe η^6 coordinations produce a high compact structure, since the bond lengths among the equatorial Fe_e sites, aside from being equal to each other, 2.287 Å, are shorter than those of bare Fe₆, 2.716 and 2.317 Å. In Table 2 are reported other higher energy states of the axial isomers. The adiabatic IE and EA determined for the GSs of

the complexes also are indicated there. Figure 4b shows the second lowest isomer, lying 5 kcal/mol over the GS, which comes from the bonding of one benzene to one axial Fe atom, and the other attached to one equatorial Fe site, producing, due to repulsion between the benzene units, a less symmetric and a more open geometry. Other axial-equatorial (AE) isomers lie at higher energies (see Table 2 and Figure 4b); they are distinguished by strong structural changes on the original geometry of the Fe₆ cluster. Then, these results show that the

TABLE 1: Lowest Energy States of the Fe_6 , Fe_6^- , and Fe_6^+ Clusters, Computed with the BPW91/6-311++G(2d,2p) Method^a

multiplicity	ΔE (kcal/mol)	R_{eq} (Å)	IE (eV)	ΔIE (eV)	EA (eV)	ΔEA (eV)
Fe_6						
21	0.0	2.404	6.15 (22) ^b	0.19	1.61 (20) ^c	0.03
19	9.6	2.394	5.72 (20) ^b	0.24	2.18 (20) ^c	0.60
17	19.2	2.343	5.45 (18) ^b	0.51	2.40 (18) ^c	0.82
23	31.7	2.458				
15	40.6	2.336	5.35 (16) ^b 5.96 ± 0.05^d	0.61	2.25 (16) ^c 1.58 ± 0.06^e	0.67
Fe_6^+						
22	0.00	2.429				
20	3.5	3.201				
18	11.3	3.170				
16	22.1	2.345				
14	29.3	2.304				
Fe_6^-						
20	0.00	2.389				
18	8.8	2.366				
22	18.7	2.437				
16	24.9	2.311				

^a Relative energies, ΔE , and average equilibrium bond lengths, R_{eq} , are indicated, as well as adiabatic ionization energies, IE, and electron affinities, EA, for each state. Also, the difference of the estimated IE and EA is shown, with respect to the experimental values. ^b Multiplicity of the Fe_6^+ cluster. ^c Multiplicity of the Fe_6^- cluster. ^d Experimental value from ref 33. ^e Experimental value from ref 34.

**Figure 2.** Contour plots for the HOMO and LUMO orbitals of the GS of neutral Fe_6 . Also, the GS structures for the lowest energy states of the anion and cation are shown.

GS geometry of the Fe_6 –dibenzene complex resembles some kind of sandwich geometry, with the metal Fe_6 unit separating the two benzene rings. Consistently, a dipole moment equal to zero was obtained for this symmetric structure. On the other hand, Zheng et al.³⁶ have pointed out the possibility of sandwich structures for the dibenzene complexes of the Fe_2 , Fe_3 , and Fe_4 clusters. The present results show how the Fe_6 cluster adsorbs two benzene molecules producing such kind of structures.³⁶ Thus, adsorption of two benzene moieties quenches the moment, by $6 \mu_B$, more strongly than one adsorption. For low temperatures, near 0 K, a value of $2.3 \mu_B$ per atom is predicted for

$\text{Fe}_6-(\text{C}_6\text{H}_6)_2$. These results agree with the experimental finding that the moments of small magnetic cobalt clusters are reduced considerably by the adsorption of benzene.³⁷

3c. Bonding Molecular Orbitals of $\text{Fe}_6-\text{C}_6\text{H}_6$ and $\text{Fe}_6-(\text{C}_6\text{H}_6)_2$. In $\text{Fe}_6-\text{C}_6\text{H}_6$ and $\text{Fe}_6-(\text{C}_6\text{H}_6)_2$, the C–Fe contacts, 2.106–2.118 and 2.133–2.138 Å, respectively, are a bit longer than those of ferrocene,³⁸ 2.045 Å, prototypical of C–Fe covalent bonds, but they are shorter than the sum of the van der Waals radii of C (1.7 Å) and Fe (1.9 Å), suggesting C–Fe bonding, which, aside from the electrostatic attractive interactions quoted above, is due to the covalent bond formation arising

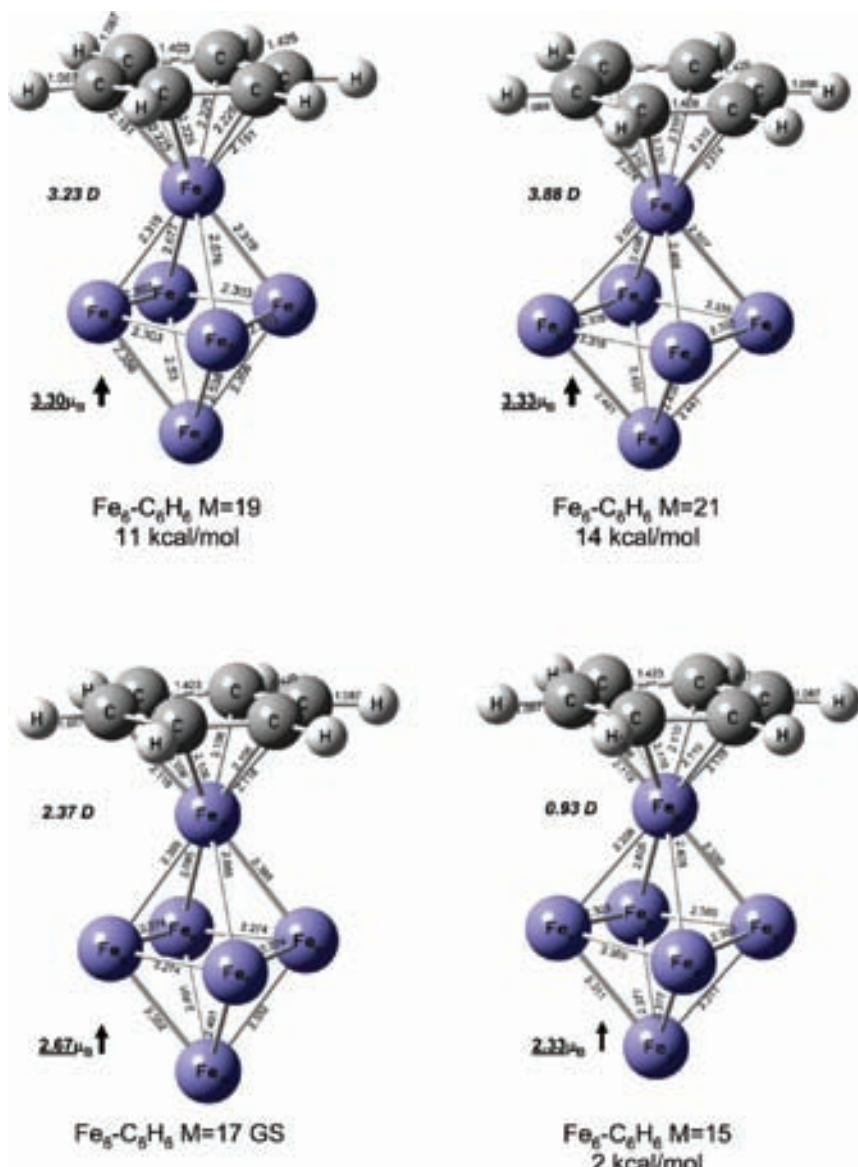


Figure 3. Bond lengths, in Å, average magnetic moments per atom, in μ_B , and dipole moments, in Debyes, for the lowest energy states of $\text{Fe}_6\text{-C}_6\text{H}_6$.

from the orbitals, mainly of 3d type, of the cluster and the π cloud of benzene, as will be described below.

The C–Fe bond formation was analyzed by the contour plots of the molecular orbitals (MO), of majority spin, of the $\text{Fe}_6\text{-}(\text{C}_6\text{H}_6)_2$ GS. Those MOs with bond signatures between the 3d electrons of the Fe_a sites and the π cloud of benzene are shown in Figure 5. Specifically, HOMO shows weak C–Fe bonding, while HOMO–7 and HOMO–12 indicates clear bond formation between the 3d orbitals of the Fe_a atoms and the π electrons. In HOMO–11, both axial and equatorial atoms are involved in the $\text{Fe}_6\text{-C}_6\text{H}_6$ bond formation, and in HOMO–39, apart from a markedly C– Fe_a bonding, the symmetric π MO of benzene remains delocalized around the ring. Other MOs (see Figure 6) are polarized from the Fe_a sites toward the Fe_e atoms, signifying transference of electrons into the equatorial plane. Some electronic delocalization around that plane is depicted by HOMO–3, HOMO–5, and HOMO–23. These MOs show bonding behavior in the square, and they produce a shortening of the $\text{Fe}_e\text{-Fe}_e$ bond lengths. In Figure 1 of the Supporting Information section, the MOs of spin down showing C–Fe bonding are reported; those with $\text{Fe}_a\text{-Fe}_e$ polarization

and delocalization in the equatorial plane are also reported there in Figure 2. As shown in panels a and b of Figure 3 of the Supporting Information, the formations of 3d– π bonds are also accomplished in $\text{Fe}_6\text{-C}_6\text{H}_6$. This kind of bonding and the electrostatic contributions accounts for the relatively short, 2.106–2.118 Å, C–Fe contacts of $\text{Fe}_6\text{-C}_6\text{H}_6$.

Both, LUMO and HOMO of $\text{Fe}_6\text{-}(\text{C}_6\text{H}_6)_{1,2}$ have signatures on the benzene units (see Figure 5 and Figure 3a of the Supporting Information), and their gaps, 0.79 and 0.74 eV, are notably smaller than that of bare benzene, 5 eV, suggesting an increase of the softness for the adsorbed benzene.

As mentioned, some MOs of $\text{Fe}_6\text{-}(\text{C}_6\text{H}_6)_2$ show bonding behavior in the square ring, producing a shortening of the $\text{Fe}_e\text{-Fe}_e$ distances. Effectively, the $\text{Fe}\text{-Fe}$ bond lengths in the equatorial plane have the same value, 2.274 Å for $\text{Fe}_6\text{-C}_6\text{H}_6$ and 2.287 Å for $\text{Fe}_6\text{-}(\text{C}_6\text{H}_6)_2$, and they are shorter than the distances in the rectangular plane of the GS of Fe_6 ; they also are shorter than the average for the $M = 17$ (2.57 Å) and $M = 15$ (2.49 Å) states of Fe_6 . These results are indicative of an increase of the metal–metal bonding in the square planes of $\text{Fe}_6\text{-C}_6\text{H}_6$ and of $\text{Fe}_6\text{-}(\text{C}_6\text{H}_6)_2$. Besides, the whole $\text{Fe}\text{-Fe}$

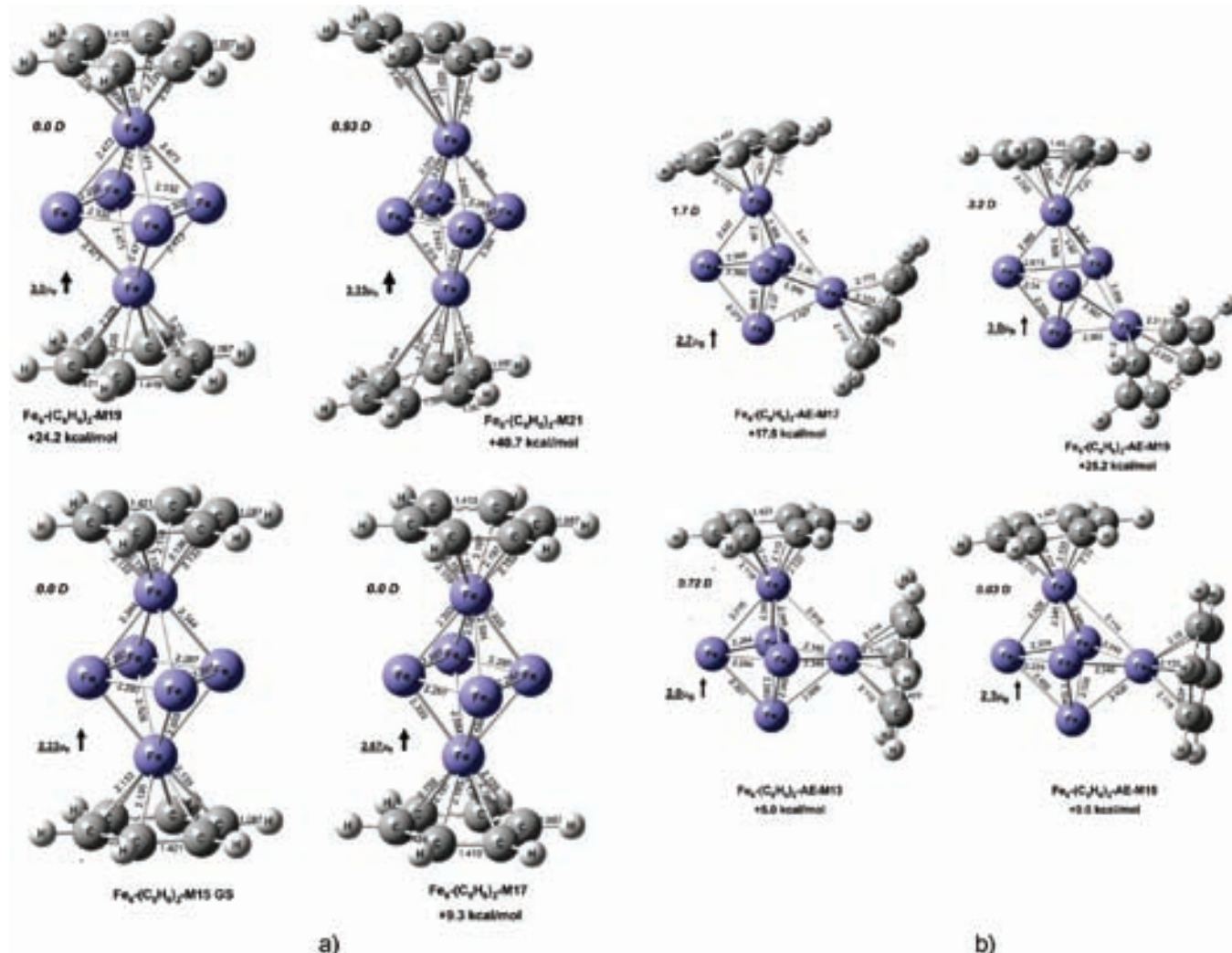


Figure 4. (a) Bond lengths, in Å, average magnetic moments per atom, in μ_{B} , and dipole moments, in Debyes, for the lowest energy states of the axial–axial isomers of $\text{Fe}_6-(\text{C}_6\text{H}_6)_2$. (b) Bond lengths, in Å, average magnetic moments per atom, in μ_{B} , and dipole moments, in Debyes, for the low-lying states of the axial–equatorial isomers of $\text{Fe}_6-(\text{C}_6\text{H}_6)_2$.

TABLE 2: Lowest Energy States of the $[\text{Fe}_6-(\text{C}_6\text{H}_6)_m]$, $m = 1, 2$ Complexes^a

multiplicity	ΔE (kcal/mol)	IE (eV)	EA (eV)
$\text{Fe}_6-\text{C}_6\text{H}_6$			
17	0.0	5.31 (16) ^b	1.44 (16) ^c
15	2.0		
19	11		
21	14		
$\text{Fe}_6-(\text{C}_6\text{H}_6)_2$			
axial isomers			
15	0.00	4.90 (16) ^b	0.86 (16) ^c
17	9.3		
19	24.2		
21	40.7		
axial-equatorial isomers			
13	5.0		
15	9.0		
17	17.5		
19	25.2		

^a Relative energies, adiabatic ionization energies, and electron affinities are indicated. ^b Multiplicity of the lowest energy state of $[\text{Fe}_6-(\text{C}_6\text{H}_6)_m]^+$, $m = 1$ or 2. ^c Multiplicity of the lowest energy state of $[\text{Fe}_6-(\text{C}_6\text{H}_6)_m]^-$, $m = 1$ or 2.

average distance (2.385 Å) of Fe_6 in $\text{Fe}_6-(\text{C}_6\text{H}_6)_2$ is somewhat shorter than that of free Fe_6 , 2.404 Å. Thus, aside from the

quenching of the magnetization, a shrinking of Fe_6 is produced in the dibenzene complex.

Up to here, the results show that the Fe_6 –benzene bonding is due to the electrostatic contributions and to the covalent bonds arising from the 3d orbitals and the π cloud. Below, it will be determined if each carbon atom effectively is bonded to the Fe_a sites, yielding η^6 coordinations or lower ones, and the strength of the Fe–C bonds, expected to be weak, since a small lengthening, ≈ 0.02 Å, was found for the C–C bond lengths in $\text{Fe}_6-(\text{C}_6\text{H}_6)_{1,2}$.

The $\text{Fe}_6-\text{C}_6\text{H}_6$ and $\text{Fe}_6-(\text{C}_6\text{H}_6)_2$ GSs are true minima on the potential energy surface, where all atomic forces are zero, because full optimization produces positive frequencies. For such equilibrium structures, the theory of atoms in molecules (AIM) has proved to be useful for depicting the bond formation through the topological analysis of the electronic density, ρ , and the Laplacian, $\nabla^2\rho$.³⁹ Taken as input the GS wave function of $\text{Fe}_6-\text{C}_6\text{H}_6$ and $\text{Fe}_6-(\text{C}_6\text{H}_6)_2$, AIM⁴⁰ defines bond critical points (BCP) for the C–Fe contacts as well as gradient paths originating at BCP and terminating at the C and Fe nucleus, which is the topological criteria⁴¹ for a bond formation between the C and Fe centers. Figure 7 contains the AIM results for $\text{Fe}_6-(\text{C}_6\text{H}_6)_2$; a similar picture was found for $\text{Fe}_6-\text{C}_6\text{H}_6$. Consequently, these C–Fe bonds originate the formation of

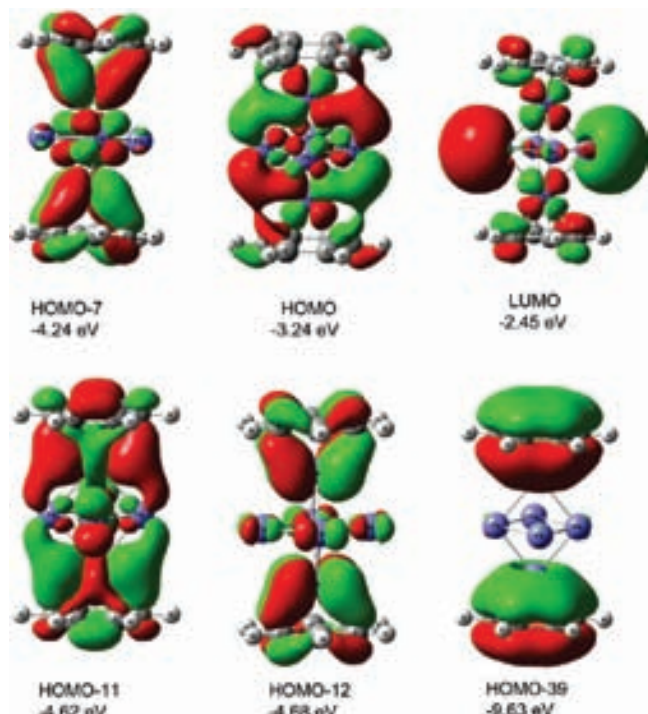


Figure 5. Contour plots for the C–Fe_a bonding molecular orbitals of the Fe₆–(C₆H₆)₂ GS.

Fe–C–C rings, for which AIM yields the related ring critical points, RCP. Critical points and C–Fe bond paths are shown in Figure 7. Then, C–Fe η^6 coordinations occur in the mono- and dibenzene complexes. Note that the positive $\nabla^2\rho$ values show a locally depleted electronic density on the C–Fe bonds. For Fe₆–(C₆H₆)₂, AIM reveals the formation of twelve Fe–Fe bonds in the compact Fe₆ region, where apart from the BCPs and RCPs, a cage critical point, CCP, also appears. These AIM results are consistent with the analysis of the MOs discussed above, which indicate, with respect to the GS of the free Fe₆ cluster, an increase of the bonding in the Fe₆ region of the Fe₆–(C₆H₆)₂ complex, accounting for the shortening of the average Fe–Fe distance of the coated cluster. Also, some MOs showed electron delocalization in the equatorial plane of the Fe₆ region of the complex. Consistently, the $\nabla^2\rho$ values indicate a lesser concentrated electronic density for the Fe_e–Fe_e bonds in the equatorial plane than for the axial–equatorial iron bonds; see Figure 7. See also Figure 4, for Fe₆–C₆H₆, in the Supporting Information.

3d. Ionization Energies, Electron Affinities, and Bond Dissociation Energies. Electron detachment was also considered. After a full, structural, and electronic relaxation, an $M = 16$ GS was found for [Fe₆–(C₆H₆)₂]⁺, with an adiabatic IE of 5.31 eV. The [Fe₆–(C₆H₆)₂]⁺ ion presents also $M = 16$ but with a more diminished IE, of 4.90 eV. These low ionization energies, which are smaller than those of bare Fe₆ (6.15 eV) and benzene (9.08 eV), are clear signatures of d–π interactions.⁷ They also suggest that the electron is mainly deleted from the Fe₆ moiety. This is just the case for Fe₆–(C₆H₆)₂ where the electron is removed from the HOMO[†], reported in Figure 1 of the Supporting Information, which shows strong contributions on the Fe₆ region, mostly on the equatorial plane. Also, note that the IE decreases as more benzene moieties are added. The IEs of Fe₆–(C₆H₆)_m ($m = 1, 2$) have not yet been measured, but the determined IEs for Fe–(C₆H₆)_m ($m = 1, 2$), >6.42 and 5.18 ± 5 eV,⁷ respectively, are clearly smaller than the IE for the bare Fe atom, 7.87 eV, and they also decrease from $m = 1$ to

$m = 2$. Our results for Fe₆–(C₆H₆)_{1,2} follow this experimental tendency. (We have obtained an IE of 6.44 eV for Fe–C₆H₆, which is in line with the measurements of Kurikawa et al.,⁷ indicating a value greater than 6.42 eV.) The difference of IE for Fe₆ and Fe–(C₆H₆)₂, 1.25 eV, suggest significant delocalization of the most external electrons of Fe₆ through the Fe₆–(C₆H₆)₂ adduct, which is accomplished through the network of the 3d–π bonds. It is interesting to compare these findings with the results of Senapati et al.⁸ for iron atoms supported on coronene (C₂₄H₁₂), a PAH compound. Specifically, for Fe–coronene and Fe₂–coronene, the adiabatic IEs, 5.51 and 5.54 eV, respectively, are near to the values quoted above, 5.31 and 4.90 eV for (Fe₆–C₆H₆)_{1,2}. They also are smaller than those of the separated species, Fe (7.64 eV), Fe₂ (6.55 eV), and coronene (7.19 eV), with the peculiarity that the IE of Fe–coronene is closer to that of coronene, while for Fe₂–coronene it is closer to Fe₂, signifying that in the former case the electron is removed from coronene, whereas in Fe₂–coronene, the detachment is done from the Fe₂ cluster.⁸ This last behavior is similar to our present results for the Fe₆–C₆H₆ complexes, on which electron deletion mainly occurs from Fe₆.

Moreover, addition of one electron gives the [Fe₆–C₆H₆][–] and [Fe₆–(C₆H₆)₂][–] ions, both with $M = 16$ GSs and with smaller adiabatic electron affinities, 1.44 and 0.86 eV, respectively, than that of Fe₆, 1.61 eV; note the larger decrease for the Fe₆–(C₆H₆)₂ adduct. (It should be mentioned that we have obtained an adiabatic EA of 0.47 eV for Fe–C₆H₆, which is in close agreement with the experimental value, 0.46 ± 0.1 eV, determined recently by Zheng et al. for this isolated complex in the gas phase, by means of negative ion photoelectron spectroscopy techniques.³⁶) This and the reduction of the IE confirm that the most external electrons of the neutral and charged [Fe₆–(C₆H₆)_m] ($m = 1, 2$) complexes are less bonded than those of the bare Fe₆ cluster. Indeed, the HOMO of [Fe₆–(C₆H₆)₂][–] is very similar to the LUMO[†] of the neutral, lying over the whole adduct, with huge contributions on the equatorial plane of Fe₆; see Figure 5.

When one subtracts the GS energies of Fe₆ and C₆H₆ from that of Fe₆–(C₆H₆)₂, a bond dissociation energy (BDE), including zero point energy corrections, of 47.9 kcal/mol was obtained, or ≈24 kcal/mol per benzene, yielding a bond strength of about 4 kcal/mol for each C–Fe bond. Similarly, the calculated BDE for Fe₆–C₆H₆ is 19.9 kcal/mol or 0.86 eV. The BDEs for the neutral and charged Fe₆–(C₆H₆)_{1,2} complexes are reported in Table 3. Besides, with respect to the Fe₆–C₆H₆ GS, the BDE for the second benzene is 28.1 kcal/mol. Thus, in a sequential addition, the BDE for the second step shows an enhancement, which is indicative of a bigger stability for the Fe₆–(C₆H₆)₂ adduct. These results give insight that the structures of Fe_n(C₆H₆)_m, as inferred from spectroscopic and chemical probe studies, consist of an Fe_n cluster surrounded by a strongly adsorbed layer of benzene molecules.^{6,7} Moreover, on experimental grounds, the BDE of Fe–C₆H₆ is estimated to be greater than 16.1 kcal/mol; our values are consistent with this finding for a single Fe atom^{7,42,43} and with the BDE of benzene, 24.7 kcal/mol, on an infinite Fe(100) surface.⁴⁴ On the other hand, Simon and Joblin have studied, with DFT methods, the interaction of a single iron atom with naphthalene (C₁₀H₈), pyrene (C₁₆H₁₀), and corenene, which are of interest for astrophysics.¹² They found that the BDEs for neutral Fe–naphthalene (0.64 eV), Fe–pyrene (0.68 eV), and Fe–coronene (0.62 eV) hardly change with the PAH compound. A standard value of 0.6 eV or 13.8 kcal/mol was indicated for the binding energy between iron and neutral PAH, which is relatively close to the BDE for Fe–C₆H₆ mentioned above.

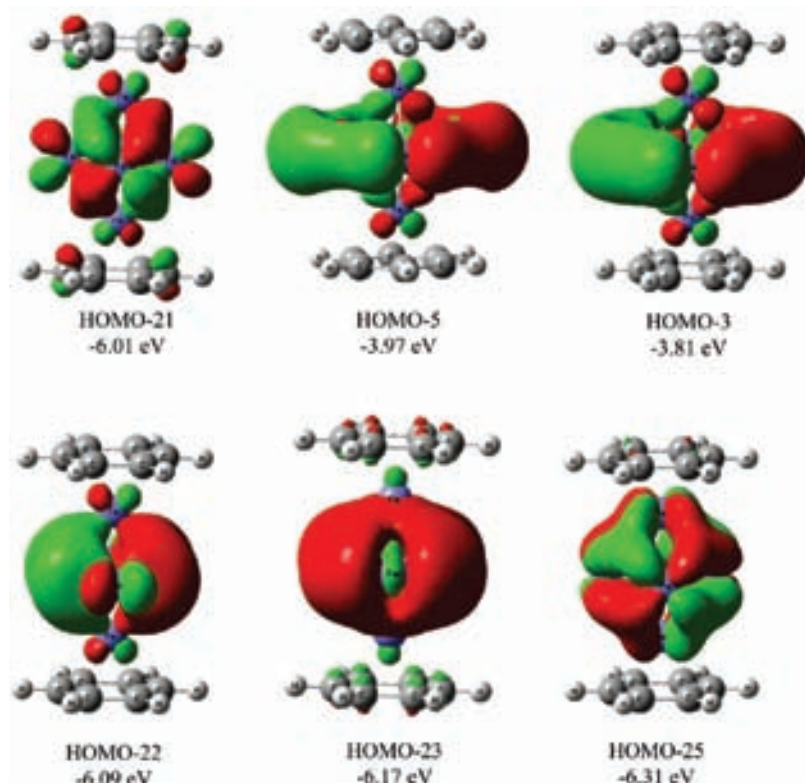


Figure 6. Contour plots for the molecular orbitals of $\text{Fe}_6-(\text{C}_6\text{H}_6)_2$. They show polarization from the axial toward the equatorial iron atoms and delocalization in the equatorial plane.

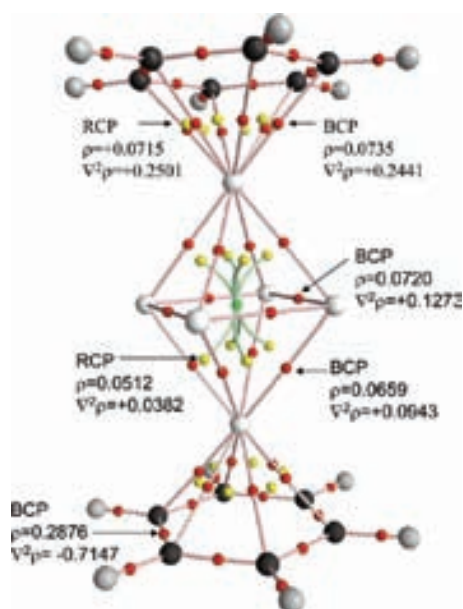


Figure 7. Molecular graph for the GS of $\text{Fe}_6-(\text{C}_6\text{H}_6)_2$. The density (ρ), in e au^{-3} , and Laplacians ($\nabla^2\rho$), in e au^{-5} , for the BCPs of the C–Fe and Fe–Fe contacts and the RCPs of the Fe–C–C and Fe–Fe–Fe rings are indicated.

Furthermore, a BDE of 24.7 kcal/mol has been estimated for Fe_2 –coronene, producing Fe_2 and coronene,⁸ which is markedly close to our results for the $\text{Fe}_6-(\text{C}_6\text{H}_6)_{1,2}$ complexes.

Assuming an Fe_6^+ + benzene dissociation channel, which is reasonable because the IE of Fe_6 is smaller than that of benzene, an adiabatic BDE of 1.68 eV or 38.8 kcal/mol was obtained for $[\text{Fe}_6-(\text{C}_6\text{H}_6)]^+$. Likewise, a BDE of 3.32 eV or 76.6 kcal/mol (1.66 eV or 38.3 kcal/mol per benzene) was found for $[\text{Fe}_6-(\text{C}_6\text{H}_6)_2]^+$. These binding energies are bigger than those

TABLE 3: Adiabatic Bond Dissociation Energies per Benzene Molecule, for the Neutral and Charged Species of the $[\text{Fe}_6-(\text{C}_6\text{H}_6)_m]$ ($m = 1$ and 2) Complexes

complex	products	BDE (kcal/mol)
$\text{Fe}_6-\text{C}_6\text{H}_6$	$\text{Fe}_6 + \text{C}_6\text{H}_6$	19.9
$\text{Fe}_6-(\text{C}_6\text{H}_6)_2$	$\text{Fe}_6 + 2\text{C}_6\text{H}_6$	24.0
$[\text{Fe}_6-\text{C}_6\text{H}_6]^+$	$\text{Fe}_6^+ + \text{C}_6\text{H}_6$	38.8
$[\text{Fe}_6-(\text{C}_6\text{H}_6)_2]^+$	$\text{Fe}_6^+ + 2\text{C}_6\text{H}_6$	38.3
$[\text{Fe}_6-\text{C}_6\text{H}_6]^-$	$\text{Fe}_6^- + \text{C}_6\text{H}_6$	16.9
$[\text{Fe}_6-(\text{C}_6\text{H}_6)_2]^-$	$\text{Fe}_6^- + 2\text{C}_6\text{H}_6$	16.2

of the neutrals and are accounted for by an increase of the electrostatic contributions. That is, the benzene moieties are more strongly adsorbed on Fe_6^+ than on Fe_6 . Experimentally,⁴² the determined BDEs for $[\text{Fe}-(\text{C}_6\text{H}_6)_m]^+$ ($m = 1$ and 2) are equal to 2.15 ± 0.10 and 1.94 ± 0.17 eV, respectively; they are close to each other, with the latter slightly smaller. Our results for Fe_6 closely follow this energetic behavior. As expected, the binding energy between the Fe_6^+ cluster and the benzene molecule is lower than the corresponding energy for Fe^+ . This is because of the Fe–Fe bonding interactions that the axial Fe atom, coordinated directly to benzene, presents in the $[\text{Fe}_6-(\text{C}_6\text{H}_6)]^+$ complex. Due to the metal–metal bonding, the interaction of TM clusters with benzene produce bonding patterns different from those observed in single TM ions. These results should be compared with the BDEs for $[\text{Fe}-\text{naphthalene}]^+$ (2.77 eV), $[\text{Fe}-\text{pyrene}]^+$ (2.60 eV), and $[\text{Fe}-\text{coronene}]^+$ (2.59 eV), which are significantly bigger than the BDE of $[\text{Fe}_6-(\text{C}_6\text{H}_6)_{1,2}]^+$, 1.68–1.66 eV. This difference could be partially accounted for by the fact that in Fe–PAH the electron is deleted from the PAH moieties, because these bare PAH molecules have smaller IEs than the Fe atom, while in $\text{Fe}_6-\text{C}_6\text{H}_6$ it is deleted from the Fe_6 cluster. In fact, for the $\text{Fe}_2^+ + \text{coronene}$ dissociation channel, Senapati et al.⁸ have determined a BDE of 2.08 eV for $[\text{Fe}_2-\text{coronene}]^+$, which is

more closer to our BDE results for $[\text{Fe}_6-(\text{C}_6\text{H}_6)_{1,2}]$, although other dissociation paths were found to be more favorable for $[\text{Fe}_6-\text{coronene}]^+$.

For the $[\text{Fe}_6-\text{C}_6\text{H}_6]^-$ ion, an adiabatic BDE of 16.9 kcal/mol was obtained under the assumption of an $\text{Fe}_6^- + \text{benzene}$ dissociation, which is in line with the well-known feature that benzene does not bind an additional electron. In the same way, a BDE of 1.41 eV or 32.42 kcal/mol (0.70 eV or 16.21 kcal/mol per benzene) was found for $[\text{Fe}_6-(\text{C}_6\text{H}_6)_2]^-$, dissociating into $\text{Fe}_6^- + 2 \text{ benzene}$, while dissociation into $[\text{Fe}_6-\text{C}_6\text{H}_6]^- + \text{benzene}$ yields a considerable smaller BDE, 0.67 eV or 15.5 kcal/mol. These binding energies are smaller than those of the neutrals and cations. Hence, on the $[\text{Fe}_6-(\text{C}_6\text{H}_6)_{1,2}]^-$ complexes the benzene molecules are less strongly adsorbed on the Fe_6 core, which is accounted for by the repulsion of Fe_6^- with the π cloud.

Then, in $\text{Fe}_6-(\text{C}_6\text{H}_6)_m$ ($m = 1, 2$), there is a considerable relaxation of the electronic structure of Fe_6 , as shown by the strong changes of the IEs, EAs, and magnetic moments. As shown above, the adsorption of benzene notably quenches the magnetization of Fe_6 , $4 \mu_B$ for $m = 1$ and $6 \mu_B$ for $m = 2$. The coating of the cluster switch on a spin paired process, which apart from the C–Fe bond formation also produces an increase of the metal–metal bonding. The shortening of the Fe–Fe distances found for $m = 2$ indicate that such bonding truly increases. The decrease of the atomic magnetic moments is closely connected with the reduction of the repulsive interactions between the 3d electrons of Fe_6 and the π cloud of benzene. Smaller moments on the Fe atoms mean that there are smaller amounts of 3d electrons at those sites, resulting in a reduction of the repulsion with the π electrons. These results agree in that the moment of an Fe atom is reduced from 4 to $2 \mu_B$ when adsorbed in benzene.^{43,45} Thus, magnetic effects are crucial for the bonding of C_6H_6 with Fe_6 .

3e. Vibrational Analysis: Fe_6 , C_6H_6 , and $\text{Fe}_6-\text{C}_6\text{H}_6$. The computed frequencies for the GS of Fe_6 fall in the low-frequency 54–336 cm^{-1} region, and those for benzene in the gas phase are contained within 394–3132 cm^{-1} . Thus, the gaps of the frequencies for the free Fe_6 and benzene species do not overlap each other. The estimated IR spectra for the Fe_6 , C_6H_6 , and $\text{Fe}_6-\text{C}_6\text{H}_6$ species are shown in Figure 8. The main IR-active bands of benzene were found at 661, 1034, and 1472 cm^{-1} , they are for the ν_{11} (out-of-plane C–H bend), ν_{18} (in-plane C–H bend), and ν_{19} (in-plane carbon ring distortion) vibrational resonances, respectively. These BPW91 results are only slightly smaller than the experimental values: 673, 1038, and 1486 cm^{-1} .⁴⁶ Another IR-active band for the asymmetric C–H stretching mode was located at 3121 cm^{-1} ; see Figure 8b. Close to this mode is positioned the fully symmetric C–H stretching mode, which is IR inactive and reaches the highest frequency, 3132 cm^{-1} , for the bare benzene molecule. The complete list of the calculated vibrational frequencies for benzene is shown in Table 4, together with the reported experimental values; intensities, in km/mol, are also indicated. Overall, the theoretical estimations show relatively small errors, the biggest departures, of 3.9%, occur for the in-plane C–H bending and the in-plane carbon ring distortions. Regarding Fe_6 , its main active IR bands, shown in Figure 8a, were found at 245, 254, and 300 cm^{-1} , with quite small intensities of 1.3, 3.6, and 1.6 km/mol, respectively. These frequencies account for asymmetric stretching modes. Another two vibrations, lying at 54 and 147 cm^{-1} , have negligible contributions to the IR spectrum. It should be mentioned that the full symmetric stretching mode of Fe_6 , which

is IR inactive, is situated at the top value, 336.3 cm^{-1} , of the vibrational frequencies for this isolated cluster.

For the $M = 17$ GS of $\text{Fe}_6-\text{C}_6\text{H}_6$, the frequencies fall in the 11–3142 cm^{-1} range. Two main features emerges from its IR spectrum: (1) it presents vibrational bands near those of the free benzene molecule, and (2) some forbidden IR modes of benzene become IR active in the reduced symmetry of the complex, which has a dipole moment of 2.37 D. These kinds of frequencies are reported in Table 4 and also are indicated in Figure 8c. Specifically, the strongest resonance is for the out-of-plane C–H bend mode lying at a higher value, 775 cm^{-1} , than in bare benzene; the shift to the blue is of 114 cm^{-1} . The notorious bands at 833–838 cm^{-1} , IR inactive in free benzene, present also this kind of C–H bend mode; they become IR active in the complex with small shifts in their frequencies, of 2.8 and 6.9 cm^{-1} . Also the symmetric ring stretching vibrational mode lying at 968 cm^{-1} is now IR active, with a shift of –22.3 cm^{-1} . Although smaller than the 775 cm^{-1} band, relatively strong resonances are shown (see Figure 8c) by the in-plane C–H bend modes, centered at 992 and 1000 cm^{-1} , presenting reductions of –42 and –34.4 cm^{-1} , respectively. The in-plane carbon ring distortion modes were found at 1426 and 1431 cm^{-1} in the $\text{Fe}_6-\text{C}_6\text{H}_6$ complex, showing also noticeable reductions, –46.2 and –41.9 cm^{-1} , and a weak band. Thus, the calculated IR spectrum for this complex in the gas phase shows that, with respect to the bare benzene molecule, the out-of-plane C–H bend is shifted to the blue by 114 cm^{-1} , while the in-plane C–H bend and the in-plane carbon ring distortion are shifted to the red, by –42 to –34.4 cm^{-1} and –46.2 to –41.9 cm^{-1} , respectively. The frequency decrease of the last two bands is indicative of a weakened molecular bonding in the benzene moiety. Other non-IR active in-plane carbon ring distortions are more strongly diminished, by about –100 cm^{-1} , indicating a bigger decrease of the bonding in the benzene ring. For instance, the mode lying at 1588.2 cm^{-1} in free benzene is moved to 1488.2 cm^{-1} in the $\text{Fe}_6-\text{C}_6\text{H}_6$ complex. Indeed, the IR spectrum of $\text{Fe}_6-\text{C}_6\text{H}_6$ (see Figure 8c) shows that most of the frequencies of benzene are moved to lower values. One exception is the blue shift for the out-of-plane C–H bend, which is essentially a mechanical effect:⁵ the presence of the Fe_6 cluster over the benzene ring impedes the out-of-plane hydrogen bend, driving the frequency higher. Even more, the C–H asymmetric stretching modes, at 3136 cm^{-1} , present also a small shift to the blue, of 14 cm^{-1} , that is mainly accounted for by the slight increase of the bonding in the C–H bonds; the C–H distances in free benzene, 1.089 Å, are slightly shortening to 1.087 Å, in $\text{Fe}_6-\text{C}_6\text{H}_6$. The full symmetric C–H stretching mode was located at the highest frequency, 3142 cm^{-1} , of the complex; it is IR inactive in free benzene but turns IR active in $\text{Fe}_6-\text{C}_6\text{H}_6$, with a small shift to the blue, 11 cm^{-1} , and a strong resonance. Hence, the C–H stretching modes suffer small shifts to the blue upon adsorption.

The bands within 67–400 cm^{-1} correspond either to Fe_6 or to induced Fe_6 –benzene modes. For example, the strong (30.7 km/mol) resonance at 398 cm^{-1} is for an out-of-plane C–H bend, tied with oscillatory movements, along the axial direction, of the nearest Fe site. Similar details were found at 383 cm^{-1} but with 7.4 km/mol. The 336–345 cm^{-1} band is for swinging modes of benzene around the nearest Fe_a atom, with this one showing oscillations in a parallel direction to the benzene ring. At 327.4 cm^{-1} , the symmetric stretching of Fe_6 holds, showing a negligible intensity, 0.6 km/mol, and a shift of –9 cm^{-1} . The peaks at 262–281 cm^{-1} are for asymmetric stretching modes of Fe_6 in the equatorial plane, they are shifted to the blue by 17

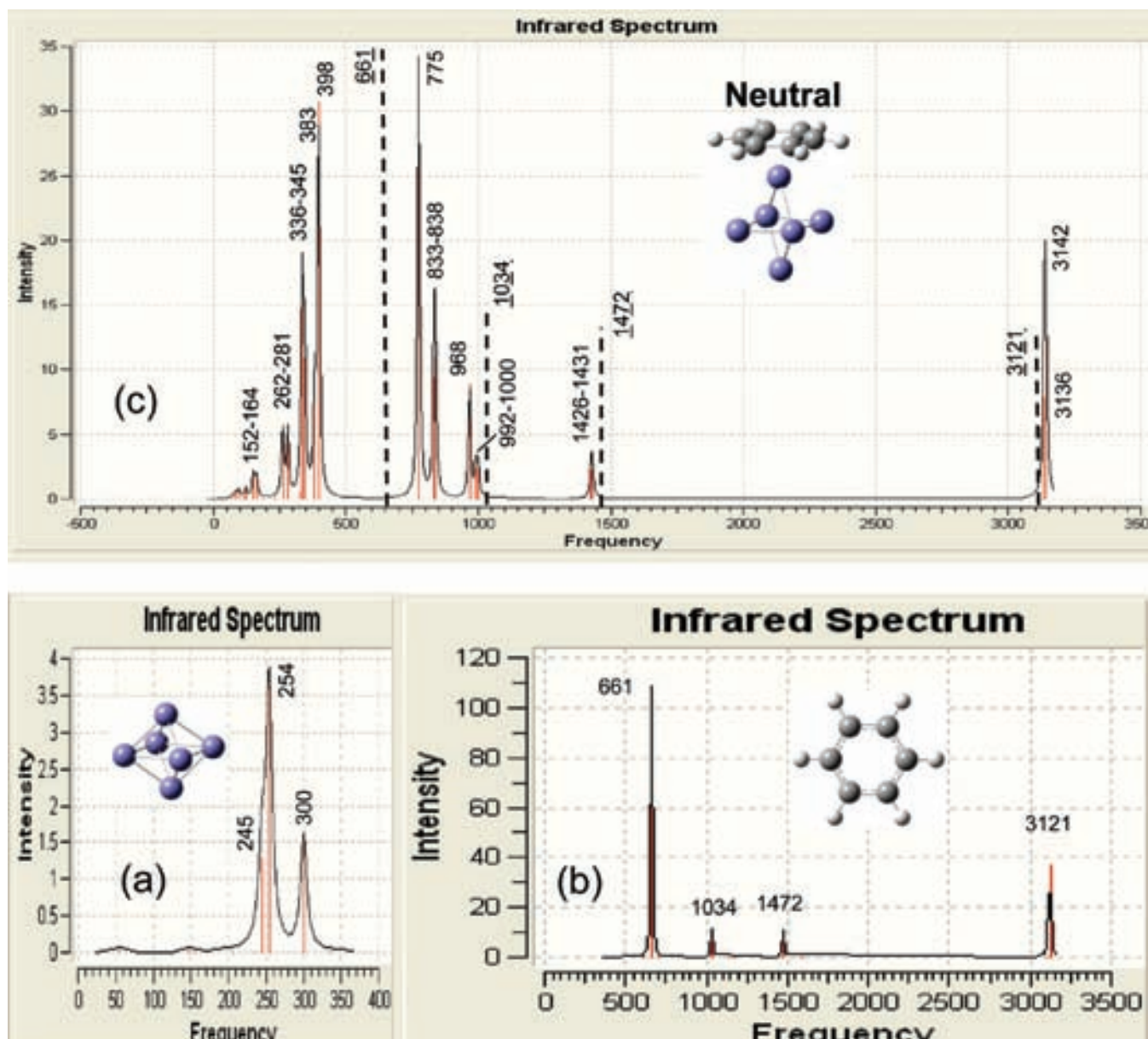


Figure 8. Calculated IR spectra for the neutral Fe_6 (c), C_6H_6 (a), and $\text{Fe}_6-\text{C}_6\text{H}_6$ (b) species.

and 27 cm^{-1} , with respect to bare Fe_6 . As quoted above, the IR-active asymmetric stretching of free Fe_6 lies at 300 cm^{-1} ; this mode lies at 232 cm^{-1} in the complex and is IR inactive. At 164 cm^{-1} , a symmetric stretching of Fe_6 holds, and at 152 cm^{-1} appears a swinging of benzene, with the nearest Fe site oscillating in a parallel direction of the benzene ring.

3f. Vibrational Analysis: Fe_6^+ , C_6H_6^+ , and $[\text{Fe}_6-\text{C}_6\text{H}_6]^+$. The calculated IR spectra of Fe_6^+ , C_6H_6^+ , and $[\text{Fe}_6-\text{C}_6\text{H}_6]^+$ are reported in Figure 9. The results, Figure 9b, show that C_6H_6^+ possess more IR-active bands than neutral benzene. The out-of-plane C–H bend, in-plane C–H bend, and in-plane carbon ring distortion modes, located at 657 (82), 1045 (10), and 1416 – 1502 cm^{-1} (105.2 – 46.3), are also IR active as in neutral benzene; from this reference, they are shifted by -4 , 11 , and -56 to $+30 \text{ cm}^{-1}$. (Values in parentheses are for the intensities in km/mol .) The C–H asymmetric stretching modes, at 3144 and 3152 cm^{-1} , also remain IR active, and they are shifted to the blue by 23 – 31 cm^{-1} . Another IR-active C–H asymmetric stretching appears at 3125 cm^{-1} , with a minor intensity, and shows a shift of 29.5 cm^{-1} , with respect to neutral benzene, where it is IR inactive. These three CH frequencies originate

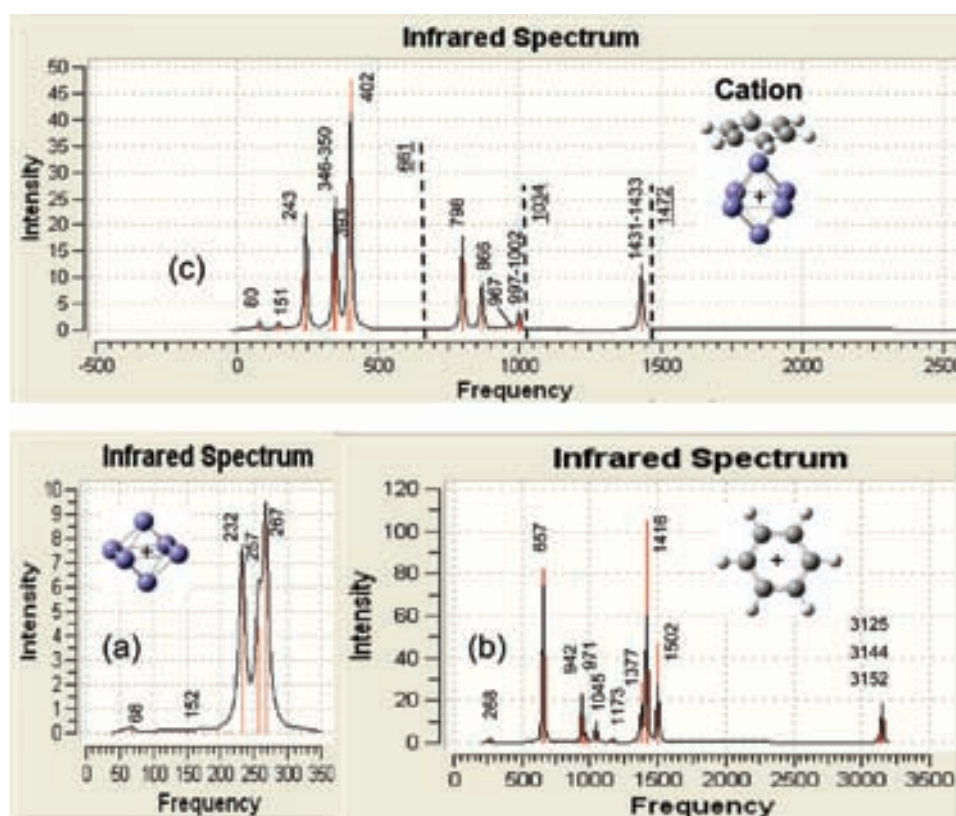
the upper band for the IR spectrum of the C_6H_6^+ ion. The band at 1377 cm^{-1} is for an in-plane carbon ring distortion, shifted to the blue by 47 cm^{-1} , with respect to the IR-inactive mode in C_6H_6 . An in-plane C–H bend mode positioned at 942 cm^{-1} shows a modest intensity and also contributes to the IR spectrum; weaker bands appear at 971 and 268 cm^{-1} , which are for out-of-plane C–H bends. Contrary to C_6H_6 and C_6H_6^+ , the IR spectrum for the Fe_6^+ ion is not quite different from that of the neutral Fe_6 cluster. Indeed, as shown in Figures 8a and 9a, the Fe_6^+ ion also presents three main IR-active bands, having higher intensities and shifted to lower frequencies, which are for the vibrational modes described above for Fe_6 .

The IR spectrum for the $[\text{Fe}_6-\text{C}_6\text{H}_6]^+$ cation is shown in Figure 9c, and in Table 5 are reported the vibrational frequencies that the benzene molecule presents in this complex. Since the IE of Fe_6 , 6.15 eV , is considerably smaller than that of benzene, 9.08 eV , it is expected that electron detachment from $\text{Fe}_6-\text{C}_6\text{H}_6$ mainly occurs from the Fe_6 fragment, producing an $[\text{Fe}_6-\text{C}_6\text{H}_6]^+$ ion that could be viewed as an Fe_6^+ moiety joined to benzene. Indeed, the IR spectrum of $[\text{Fe}_6-\text{C}_6\text{H}_6]^+$ reveals the presence of vibrational bands, which are nearer to those of neutral benzene

TABLE 4: Estimated Vibrational Frequencies and Intensities for Bare Benzene^a

mode	benzene			benzene in Fe ₆ —C ₆ H ₆				
	theory		exp. ^c	error (%)	benzene in Fe ₆ —C ₆ H ₆			
	ν (cm ⁻¹)	I (km/mol)			ν (cm ⁻¹)	I (km/mol)	$\Delta\nu$ (cm ⁻¹)	
1	γ (CCC)	394 ^b		410	3.9	383.1	7.4	-10.9
2	γ (CCC)	394		410	3.9	384.5		-9.5
3	δ (CCC)	603.1		606	0.48	598.7		-4.4
4	δ (CCC)	603.2		606	0.49	597.8		-5.4
5	γ (C—H)	661.1	108.7	673	1.77	775.1	34.3	114
6	γ (CCC)	699		703	0.57	586.3		-112.7
7	γ (C—H)	830.6 ^b		849	2.17	833.4	9.4	2.8
8	γ (C—H)	830.7 ^b		849	2.17	837.6	10.9	6.9
9	γ (C—H)	946.8		975	2.89	875.4		-71.4
10	γ (C—H)	946.8		975	2.89	876.2		-70.7
11	γ (C—H)	976.4		995	1.9	904		-72.4
12	δ (CCC)	989.9 ^b		992	2.02	967.5	8.9	-22.3
13	δ (C—C)	997.6		1010	1.23	988.7		-8.9
14	δ (C—H)	1034.2	5.8	1038	3.85	992.1	2.4	-42
15	δ (C—H)	1034.2	5.8	1038	3.85	999.8	2.5	-34.4
16	δ (C—H)	1146.7		1150	2.61	1137.1		-9.6
17	δ (C—H)	1167.3		1178	0.94	1129.3		-38
18	δ (C—H)	1167.3		1178	0.94	1131.4		-35.9
19	ν (C=C)	1330.7		1310	1.58	1389.4		-58.8
20	δ (C—H)	1342.9		1326	1.27	1317.7		-25.3
21	δ (CCC)	1472.4	6.1	1486	0.92	1426.2	2.3	-46.2
22	δ (CCC)	1472.4	6.1	1486	0.92	1430.5	2.3	-41.9
23	ν (C=C)	1588.2		1596	0.49	1488.2		-100
24	ν (C=C)	1588.2		1596	0.49	1484.2		-104
25	δ (C—H)	3095.9		3047	1.60	3119.6		23.7
26	ν' (C—H)	3105.5		3062	1.42	3125.2		19.7
27	ν' (C—H)	3105.6		3062	1.42	3125.8		20.2
28	ν' (C—H)	3121.1	36.8	3063	1.89	3135.7	7.9	14.6
29	ν' (C—H)	3121.1	36.8	3063	1.89	3135.8	7.6	14.7
30	δ (C—H)	3131.5 ^b		3068	2.07	3142.2	12.4	10.7

^a The values that benzene presents in the Fe₆—C₆H₆ complex are shown. The experimental values for benzene and the errors of the calculations are also indicated. The nomenclature is as follows: “out of plane bending” (γ), “in plane bending” (δ), “symmetric stretching” (ν), and “asymmetric stretching” (ν'). ^b IR active in the neutral Fe₆—C₆H₆ complex. ^c Experimental values from ref 46.

Figure 9. Calculated IR spectra for the Fe₆⁺ (c), C₆H₆⁺ (a), and [Fe₆—C₆H₆]⁺ (b) cations.

than to those of C₆H₆⁺; see Table 5. The dashed lines in Figure 9c are for IR-active modes of neutral benzene. The results also

indicate that some IR-inactive modes of free benzene become IR active in the reduced symmetry of the complex. Conversely,

TABLE 5: Calculated Frequencies and Intensities for the Bare Benzene⁺ Ion^a

mode	bare benzene ⁺		benzene in $[\text{Fe}_6-\text{C}_6\text{H}_6]^+$			
	ν (cm ⁻¹)	I (km/mol)	ν (cm ⁻¹)	I (km/mol)	$\Delta\nu$ (cm ⁻¹) ^d	$\Delta\nu$ (cm ⁻¹) ^e
1	$\delta(\text{CCC})$	240.3		595.3	355	-7.8
2	$\gamma(\text{CCC})$	268	2.6	392.8	124.8	-1.1
3	$\gamma(\text{CCC})$	322.3		391	68.7	-2.9
4	$\gamma(\text{C}-\text{H})$	324.6		605.1	280.6	-93.9
5	$\delta(\text{CCC})$	584.8		596.1	11.3	-7.0
6	$\gamma(\text{C}-\text{H})$	657.1	82.1	797.9	140.9	+136.8
7	$\gamma(\text{C}-\text{H})$	754.3 ^b		866.2	5.3	+35.5
8	$\gamma(\text{C}-\text{H})$	875.4 ^b		867.2	4.7	+86.5
9	$\delta(\text{C}-\text{H})$	925.2		996.9	2	-34.3
10	$\delta(\text{C}-\text{H})$	941.7	23.4	1001.5	1.7	-32.7
11	$\delta(\text{CCC})$	955.5 ^b		967.1	1.3	-22.8
12	$\gamma(\text{C}-\text{H})$	971.1 ^c	4.3	911.9	-59.2	-34.9
13	$\gamma(\text{C}-\text{H})$	982.8		909.8	-73	-37.0
14	$\delta(\text{CCC})$	985.6	0.1	998.9	0.5	+1.3
15	$\gamma(\text{C}-\text{H})$	1000.8		929.6	-71.2	-46.8
16	$\delta(\text{C}-\text{H})$	1045	10.1	1136.6	91.6	30.7
17	$\delta(\text{C}-\text{H})$	1173.3 ^c	2	1144.3	-29	-2.4
18	$\delta(\text{C}-\text{H})$	1187.5		1137.6	-49.9	-29.7
19	$\delta(\text{C}-\text{H})$	1333.8		1493.4	159.6	-94.8
20	$\delta(\text{C}-\text{H})$	1351.8		1322.6	-29.2	-20.4
21	$\delta(\text{CCC})$	1377.4	28.8	1382.5	5.2	+51.9
22	$\delta(\text{CCC})$	1416.3	105.2	1433.2	6.8	-39.2
23	$\delta(\text{CCC})$	1502.4	46.3	1431	6.5	-41.4
24	$\nu(\text{C}=\text{C})$	1619.8 ^b		1491.3	0.1	-96.9
25	$\nu'(\text{C}-\text{H})$	3125.4 ^c	1.8	3130.7	5.3	+34.8
26	$\nu(\text{C}-\text{H})$	3129.1		3134.5	5.3	+29.0
27	$\nu(\text{C}-\text{H})$	3141		3137.0	-39.6	+31.4
28	$\nu'(\text{C}-\text{H})$	3144 ^c	8.7	3144.8	-0.8	+23.7
29	$\nu'(\text{C}-\text{H})$	3152.4 ^c	16.4	3146.7	-5.7	+25.6
30	$\nu(\text{C}-\text{H})$	3155.3 ^b		3151.8	0.2	+20.3

^a The values that benzene presents in the $[\text{Fe}_6-\text{C}_6\text{H}_6]^+$ complex are shown. The nomenclature is the same as in Table 4. ^b IR active in the $\text{Fe}_6-\text{C}_6\text{H}_6^+$ complex. ^c IR inactive in the $\text{Fe}_6-\text{C}_6\text{H}_6^+$ cation. ^d With respect to the benzene⁺ cation. ^e With respect to neutral benzene.

some high frequency IR-active modes of bare benzene become IR inactive. We proceed with the description of these features. At 798 cm⁻¹, the band for the out-of-plane C–H bending is located with a smaller intensity (18 km/mol) but shifted to the blue, by 137 cm⁻¹ with respect to C_6H_6 , more strongly than in the neutral $\text{Fe}_6-\text{C}_6\text{H}_6$ complex (114 cm⁻¹), which is a signature of a stronger mechanical effect in $[\text{Fe}_6-\text{C}_6\text{H}_6]^+$: the presence of the Fe_6^+ cluster over the benzene ring increases the impediment for the out-of-plane hydrogen bending, because an additional electrostatic repulsion between Fe_6^+ and the H^{δ+} atoms now appears, i.e., the C–H bond has some polar behavior. In fact, of the studied neutral and charged species, this mode in this complex presents the largest shift to the blue. At 997–1002 cm⁻¹, the in-plane C–H bends were found with minor intensities but with similar shifts to the red, -32.7 to -34.3 cm⁻¹, as those of neutral $\text{Fe}_6-\text{C}_6\text{H}_6$, -34.4 to -42 cm⁻¹. The weak band at 967 cm⁻¹ is for the symmetric ring stretching, which is IR inactive in C_6H_6^+ , at 956 cm⁻¹, and in neutral C_6H_6 , at 990 cm⁻¹. At 866.2 cm⁻¹, a modest resonance for an out-of-plane C–H bending of four CH units is located; this mode is IR inactive in neutral benzene, at 830.7 cm⁻¹, and in C_6H_6^+ , at 754.3 cm⁻¹. So, this mode is shifted to the blue by 35.5 cm⁻¹ and by 112 cm⁻¹. See Table 5. The upper band, 1431–1433 cm⁻¹, is for two in-plane carbon ring distortions with modest intensities, 6.8 km/mol, and is shifted to the red by ≈-40 cm⁻¹, with respect to the neutral benzene molecule.

Up to here, these results indicate that the out-of-plane C–H bend, the in-plane C–H bend, and the in-plane carbon ring distortion modes of benzene, in the $[\text{Fe}_6-\text{C}_6\text{H}_6]^+$ complex, are shifted by +137, -32.7 to -34.3, and -40 cm⁻¹, respectively. The displacement to the red for the last two bands is indicative of a weakening of the molecular bonding in the benzene moiety. On the other hand, the observed IR spectrum for positively charged TM atoms binding to benzene in the condensed phase

also shows similar vibrational shifts; that is, with respect to the neutral benzene molecule, the out-of-plane C–H bend occurs at higher frequencies while the in-plane C–H bend and the in-plane carbon ring distortion are moved to the red.⁵ Lastly, the IR spectrum for C_6H_6 and C_6H_6^+ shows that the asymmetric C–H stretching modes, lying at highest frequencies, are IR active; see Figures 8b and 9b. However, these modes becomes IR inactive in the $[\text{Fe}_6-\text{C}_6\text{H}_6]^+$ cation.

At a low frequency, 402 cm⁻¹, the strongest band of this complex is located, which exhibits similar features as the mode lying at 398 cm⁻¹ of the neutral $\text{Fe}_6-\text{C}_6\text{H}_6$ complex. With a smaller intensity, an analogous behavior was found for the mode lying at 393 cm⁻¹. The notorious band at 346–350 cm⁻¹ mimics the vibrational modes of $\text{Fe}_6-\text{C}_6\text{H}_6$ lying at 336–345 cm⁻¹. The modest band positioned at 243 cm⁻¹ accounts for two asymmetric stretching modes between two equatorial Fe atoms of the cluster, coupled with swinging movements of benzene. The small band at 151.2 cm⁻¹ (1.4 km/mol) accounts for the symmetric stretching of the Fe_6^+ fragment. Finally, the bands at 78–79.5 cm⁻¹ are swinging modes of benzene around the Fe_6^+ cluster.

3g. Vibrational Analysis: Fe_6^- , C_6H_6^- , and $[\text{Fe}_6-\text{C}_6\text{H}_6]^-$. The IR spectrum of the C_6H_6^- ion, Figure 10b, is similar to that of neutral benzene. Effectively, with enhanced resonances, only the out-of-plane C–H bend (676.4 cm⁻¹), the in-plane C–H bend (1029 cm⁻¹), the in-plane carbon ring distortion (1469 cm⁻¹), and the asymmetric C–H stretching (3056.2 cm⁻¹) modes are IR active. With respect to the neutral, the first mode shows a small shift to the blue, of 15 cm⁻¹, the second and third shifts have minor reductions, -5 and -3 cm⁻¹, and the last one is more clearly moved, by -65 cm⁻¹, to the red. So, one electron addition produces relatively small changes on the IR spectrum of benzene, mainly accounted for by the fact that the electron goes into a higher energy nonbonding orbital. As

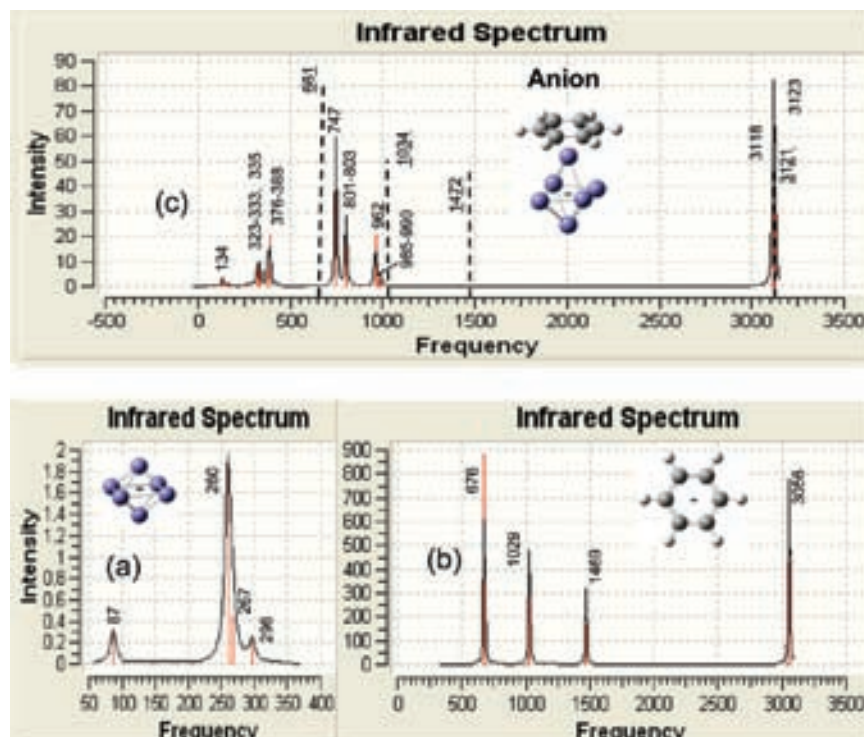


Figure 10. Calculated IR spectra for the Fe_6^- (c), $\text{Fe}_6-\text{C}_6\text{H}_6^-$ (a), and $[\text{Fe}_6-\text{C}_6\text{H}_6]^-$ (b) anions.

in the neutral Fe_6 cluster, the IR spectrum for the Fe_6^- anion, Figure 10a, also possesses three IR-active modes lying at 296, 267, and 260 cm⁻¹, with noticeably smaller intensities; the first two are shifted to the blue by 23 and 6 cm⁻¹, and the last one is shifted by -4 cm⁻¹. Also, with a small intensity, a peak appears at 87 cm⁻¹, being shifted to the blue by 32 cm⁻¹. The symmetric stretching of Fe_6 , 338 cm⁻¹, is IR inactive with a minor shift of 2 cm⁻¹. Thus, most of the IR bands of Fe_6^- are slightly shifted to higher values, which reflects the fact that it is more stable, by 1.61 eV, than the neutral, with an increase in the bonding, since the average bond length of the Fe_6^- anion, 2.389 Å, is shorter than that of Fe_6 , 2.404 Å.

The IR spectrum for the $[\text{Fe}_6-\text{C}_6\text{H}_6]^-$ anion is shown in Figure 10c, and in Table 6 are indicated the frequencies that the benzene moiety presents in this complex. The added electron to $\text{Fe}_6-\text{C}_6\text{H}_6$, $M = 17$, goes into its LUMO¹ orbital (shown in Figure 5 of the Supporting Information) to yield the $M = 16$ state for $[\text{Fe}_6-\text{C}_6\text{H}_6]^-$; since the LUMO has a major contribution on Fe_6 , such an electron mainly resides on the metallic part of the complex. Then, it will be more appropriate to evaluate the shifts of benzene, in $[\text{Fe}_6-\text{C}_6\text{H}_6]^-$, with respect to neutral bare benzene, instead of choosing the C_6H_6^- anion. However, similar results are obtained for both references. See Table 6. For example, the IR-active out-of-plane C–H bend, at 747 cm⁻¹, showing also a strongest band (as in $\text{Fe}_6-\text{C}_6\text{H}_6$, C_6H_6 , and C_6H_6^-) is shifted to the blue by 71 or by 86 cm⁻¹. Two other out-of-plane C–H bend modes, at 801 and 803 cm⁻¹, were found also to be IR active with moderate intensities and shifted to the red by ≈ -30 cm⁻¹; see Table 6 and Figure 10c. As quoted, the IR-active in-plane C–H bend lies at a similar frequency, 1034 and 1029 cm⁻¹, in free neutral and negative benzene; in $[\text{Fe}_6-\text{C}_6\text{H}_6]^-$, this mode was found at the 985–990 cm⁻¹ weak band and is clearly shifted to the red, with respect to both C_6H_6 and C_6H_6^- . Likewise, the in-plane carbon ring distortion (IR active in bare neutral and anionic benzene species) was found at 1419 and 1422 cm⁻¹ in $[\text{Fe}_6-\text{C}_6\text{H}_6]^-$ and is essentially IR inactive, because these frequencies have minor

intensities; see Table 6. Either from bare C_6H_6 or C_6H_6^- , this mode is shifted to the red, by ≈ -50 cm⁻¹. The shift to the red for the in-plane C–H bend and the in-plane carbon ring distortion, by -44 to -49 cm⁻¹ and by -50 cm⁻¹, respectively, also implies a weakening of the molecular bonding for benzene in the $[\text{Fe}_6-\text{C}_6\text{H}_6]^-$ complex. Note that these shifts are slightly bigger than those of $\text{Fe}_6-\text{C}_6\text{H}_6$ and $[\text{Fe}_6-\text{C}_6\text{H}_6]^+$; thus, in $[\text{Fe}_6-\text{C}_6\text{H}_6]^-$, a (slightly) bigger reduction for the molecular bonding of benzene occurs. The experimental determination of these frequency displacements will be valuable to confirm or deny this tendency. Moreover, the symmetric ring stretching, IR inactive in bare benzene and C_6H_6^- and lying at 990 cm⁻¹ in both cases, becomes IR active in $[\text{Fe}_6-\text{C}_6\text{H}_6]^-$, at 962 cm⁻¹, with a notorious band and becomes shifted to the red by a slightly bigger value, -28 cm⁻¹, than in the other complexes. We now move to the highest frequencies; the asymmetric C–H stretching band, at 3118 cm⁻¹, remains IR active with a negligible decrease, of -3.4 cm⁻¹, with respect to the free benzene molecule but clearly is shifted to the blue, by 61.5 cm⁻¹, with respect to the bare C_6H_6^- anion. A similar picture holds for the symmetric C–H stretching, which is IR inactive in bare C_6H_6 and C_6H_6^- but turns IR active in the complex at 3123.8 cm⁻¹, which shows the strongest band. At low frequencies, the modes lying at 376–388, 335, and 323–333 cm⁻¹ mimic the 383–398, 327, and 336–345 cm⁻¹ modes, respectively, of neutral $\text{Fe}_6-\text{C}_6\text{H}_6$ described above. At 260 cm⁻¹ with 1.8 km/mol, an asymmetric stretching of bare Fe_6^- was found; in neutral Fe_6 , this mode lies at 254 cm⁻¹ with 3.6 km/mol, and this mode is located at 293 cm⁻¹ in $\text{Fe}_6-\text{C}_6\text{H}_6^-$, where it is IR inactive. Lastly, at the bottom of the IR spectrum of $[\text{Fe}_6-\text{C}_6\text{H}_6]^-$ lies the 134 cm⁻¹ (3.4 km/mol) band, which is for the symmetric stretching of the Fe_6 moiety; this mode is IR inactive in neutral Fe_6 , lying at 116 cm⁻¹, and in the Fe_6^- anion, at 147 cm⁻¹.

3h. Vibrational Analysis: $\text{Fe}_6-(\text{C}_6\text{H}_6)_2$, $[\text{Fe}_6-(\text{C}_6\text{H}_6)_2]^+$, and $[\text{Fe}_6-(\text{C}_6\text{H}_6)_2]^-$. The IR spectrum of $\text{Fe}_6-(\text{C}_6\text{H}_6)_2$ is shown in Figure 11a. In this case, the out-of-plane C–H bend also presents a very strong resonance at 752 cm⁻¹ but is shifted to

TABLE 6: Calculated Frequencies and Intensities for the Bare Benzene⁻ Ion^a

mode	bare benzene ⁻ anion			benzene in $[\text{Fe}_6-\text{C}_6\text{H}_6]^-$			
	ν (cm ⁻¹)	I (km/mol)	ν (cm ⁻¹)	I (km/mol)	$\Delta\nu$ (cm ⁻¹) ^d	$\Delta\nu$ (cm ⁻¹) ^e	
1	$\gamma(\text{CCC})$	364.5		377.8	13.3	-16.1	
2	$\gamma(\text{CCC})$	364.6 ^b		387.7	20.6	-6.2	
3	$\delta(\text{CCC})$	593.3		597.8	4.5	-5.4	
4	$\delta(\text{CCC})$	593.7		597.8	4.1	-5.3	
5	$\gamma(\text{C}-\text{H})$	676.4	879.0	747.4	59.7	71.0	86.3
6	$\gamma(\text{CCC})$	690.3		557.2		-133.1	-141.8
7	$\gamma(\text{C}-\text{H})$	833.5 ^b		802.6	15.0	-31.0	-28.1
8	$\gamma(\text{C}-\text{H})$	834.2 ^b		801.2	16.4	-32.9	-29.4
9	$\gamma(\text{C}-\text{H})$	946.0		836.1		-109.9	-110.7
10	$\gamma(\text{C}-\text{H})$	946.2		837.3		-108.9	-109.5
11	$\gamma(\text{C}-\text{H})$	982.1		872.5		-109.6	-103.9
12	$\delta(\text{CCC})$	988.3		978.4		-9.9	-19.2
13	$\delta(\text{CCC})$	990.0 ^b		962.0	20.8	-28.0	-27.9
14	$\delta(\text{C}-\text{H})$	1029.1	391.0	985.3	2.8	-43.8	-48.9
15	$\delta(\text{C}-\text{H})$	1029.2	385.0	989.9	2.8	-39.2	-44.3
16	$\delta(\text{C}-\text{H})$	1132.1	0.1	1128.5	0.1	-3.6	-18.2
17	$\delta(\text{C}-\text{H})$	1145.6		1121.6	0.1	-23.9	-45.7
18	$\delta(\text{C}-\text{H})$	1145.6		1119.2		-26.4	-48.1
19	$\delta(\text{CCC})$	1336.7		1386.5		49.8	55.8
20	$\delta(\text{C}-\text{H})$	1339.7		1311.2		-28.4	-31.7
21	$\delta(\text{CCC})$	1469.3 ^c	166.5	1419.4	0.2	-50.0	-53.2
22	$\delta(\text{CCC})$	1469.4 ^c	165.4	1422.0	0.3	-47.5	-50.5
23	$\nu'(\text{C}=\text{C})$	1579.5		1474.9		-104.6	-113.2
24	$\nu'(\text{C}=\text{C})$	1579.6		1473.6		-106.0	-114.7
25	$\nu'(\text{C}-\text{H})$	3034.2		3100.6		66.4	4.7
26	$\nu(\text{C}-\text{H})$	3046.3 ^b		3123.8	52.5	77.5	-7.7
27	$\nu'(\text{C}-\text{H})$	3053.8		3106.4		52.6	0.9
28	$\nu'(\text{C}-\text{H})$	3053.9		3107.8		53.9	2.2
29	$\nu'(\text{C}-\text{H})$	3056.2	415.5	3117.7	31.3	61.5	-3.4
30	$\nu'(\text{C}-\text{H})$	3056.2	430.9	3117.0	30.1	60.8	-4.0

^a The values that benzene presents in the $[\text{Fe}_6-\text{C}_6\text{H}_6]^-$ complex are shown. The nomenclature is the same as in Table 4. ^b IR active in the $\text{Fe}_6-\text{C}_6\text{H}_6^+$ complex. ^c IR inactive in the $\text{Fe}_6-\text{C}_6\text{H}_6^+$ ion. ^d With respect to the C_6H_6^+ ion. ^e With respect to neutral benzene.

the blue by a smaller amount, 91 cm⁻¹, than in $\text{Fe}_6-\text{C}_6\text{H}_6$, 114 cm⁻¹, suggesting a smaller impediment of Fe_6 for this type of bending. The modest band at 822–823 cm⁻¹ is for out-of-plane C–H bend modes, showing small shifts, -9 to -8 cm⁻¹. Weak bands appear for the in-plane C–H bend, at 990–991 cm⁻¹, and for the in-plane carbon ring distortion, at 1424–1426 cm⁻¹, which present shifts similar to the red, -43 and -46 cm⁻¹, as those found for $\text{Fe}_6-\text{C}_6\text{H}_6$, indicating also a weakening of the bonding for the benzene molecules in $\text{Fe}_6-(\text{C}_6\text{H}_6)_2$. Besides, the symmetric ring stretching of each benzene, lying at 947 cm⁻¹ with a prominent band (35 km/mol), is shifted to the red more strongly, by -53 cm⁻¹, than in the neutral and charged monobenzene complexes, $[\text{Fe}_6-\text{C}_6\text{H}_6]^{\pm}$, where it is shifted by -22 to -28 cm⁻¹. Here, the stretching of one benzene molecule is out of phase from the other one. When the symmetric ring stretching modes of the two benzene units are in phase, the whole mode is IR inactive and lies at a higher frequency, 961 cm⁻¹, with a smaller displacement, -29 cm⁻¹. With a modest intensity, 23 km/mol, an asymmetric C–H stretching is located at 3134 cm⁻¹. The symmetric C–H stretching modes of the two benzene units, in the out-of-phase way, lie at 3140 cm⁻¹ and show a strongest resonance, 44 km/mol. The in-phase symmetric C–H stretching mode is non-IR active and is situated quite close, at 3141 cm⁻¹. We now address the low-frequency part; the weak band at 583 cm⁻¹ is for in-plane carbon ring distortions. The resonance at 375 cm⁻¹ is mainly for out-of-plane C–H bend modes of the two benzenes coupled with oscillatory movements of the two axial Fe_a atoms along the axial direction. The 313–318 cm⁻¹ band is for swinging movements of the benzene units tied with bending modes of the axial Fe sites. At 289 cm⁻¹, the strongest band of $\text{Fe}_6-(\text{C}_6\text{H}_6)_2$ lies here; the two axial Fe_a atoms oscillate rigidly (their internuclear length does not change) along the axial direction and are coupled with out-of-plane C–H bend modes of the benzene moieties. The

285–259 cm⁻¹ band, 4.5–1 km/mol, is for in-plane distortions of the iron equatorial sites tied with swinging modes of benzene. The small band at 178 cm⁻¹, 1.4 km/mol, shows swinging movements of benzene tied with bend modes of the two axial Fe atoms. Similar features are observed at 132 cm⁻¹. Lastly, the weak band at 89 cm⁻¹, with 4.9 km/mol, is for a stretching of the whole Fe_6 cluster with the two benzene moieties.

The estimated IR spectrum for $[\text{Fe}_6-(\text{C}_6\text{H}_6)_2]^+$ is shown in Figure 11b. Here, the out-of-plane C–H bend, 772 cm⁻¹, shows a bigger shift to the blue, 111 cm⁻¹, than that of neutral $\text{Fe}_6-(\text{C}_6\text{H}_6)_2$, 91 cm⁻¹. This tendency is similar to that observed for $[\text{Fe}_6-\text{C}_6\text{H}_6]^+$ and $\text{Fe}_6-\text{C}_6\text{H}_6$, which present shifts to the blue of 137 and 114 cm⁻¹, respectively. Note that these last two complexes are the ones that present the biggest displacement to the blue for this mode. The in-plane C–H bending lies at 996 cm⁻¹; this weak band is shifted to the red by about the same amount, -38 cm⁻¹, as in $[\text{Fe}_6-\text{C}_6\text{H}_6]^+$, -34.3 to -32.7 cm⁻¹. The magnitude of these shifts are slightly smaller than those of the neutral $\text{Fe}_6-(\text{C}_6\text{H}_6)_{1,2}$ complexes, quoted above. Also the in-plane carbon ring distortion of $[\text{Fe}_6-(\text{C}_6\text{H}_6)_2]^+$ falls at about the same value, 1431 cm⁻¹, as that of $[\text{Fe}_6-\text{C}_6\text{H}_6]^+$, 1431–1433 cm⁻¹, producing a shift to the red of -42 cm⁻¹. Thus, these results show that the frequency shifts in $[\text{Fe}_6-(\text{C}_6\text{H}_6)_2]^+$ are equal to +111, -38, and -42 cm⁻¹, for the out-of-plane C–H bend, in-plane C–H bend, and in-plane carbon ring distortion, respectively. The shifts to the red for the last two modes are indicative of a decrease of the molecular bonding for the benzene moieties in the $[\text{Fe}_6-(\text{C}_6\text{H}_6)_2]^+$ complex. Further, in the out-of-phase way, the symmetric ring stretching of the two benzene moieties was located at 953 cm⁻¹, and showing a weak band, it was also shifted to the red, by -47 cm⁻¹. The in-phase symmetric ring stretching of the benzene moieties is IR inactive and lies at 962 cm⁻¹. Note that these last frequencies are close to those of the $\text{Fe}_6-(\text{C}_6\text{H}_6)_2$

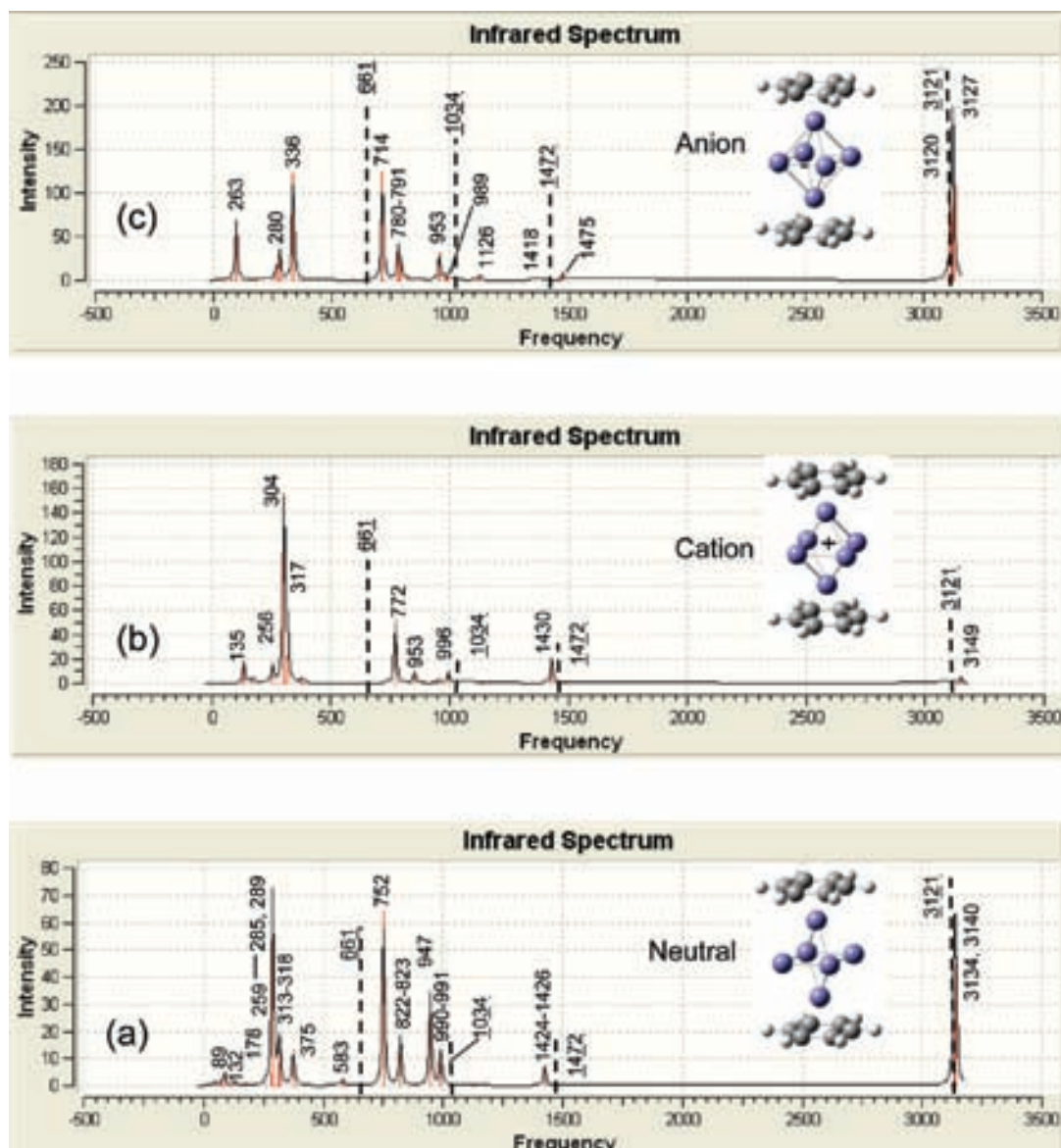


Figure 11. Calculated IR spectra for $[Fe_6-(C_6H_6)_2]$ (a), $[Fe_6-(C_6H_6)_2]^+$ (b), and $[Fe_6-(C_6H_6)_2]^-$ (c).

adduct, 947 and 961 cm^{-1} . On the other hand, for the dibenzene $Fe^+(C_6H_6)_2$ complex the displacements for the out-of-plane C–H bend, in-plane C–H bend, and in-plane carbon ring distortion have been determined by means of the FELIX free electron laser technique. As shown in Figure 12 of ref 5, the measured values, of about +93, −67, and −40 cm^{-1} , follow a tendency similar to those obtained for $Fe_6^{+-(C_6H_6)_2}$ in the present work: +111, −38, and −42 cm^{-1} , which shows encouragement since it means that the shifts of the $Fe_6^{+-(C_6H_6)_{1,2}}$ ions could be determined by the FELIX method or probably also by the use of infrared multiple-photon dissociation (IRMPD) spectroscopy, applied successfully to the study of Fe–PAH ions.¹¹

The small peak in the IR spectrum of $[Fe_6-(C_6H_6)_2]^+$ lying at 3149 cm^{-1} corresponds to the symmetric C–H stretching of the benzene molecules, in the out-of-phase way; note the absence of this feature in the IR spectrum of $[Fe_6-C_6H_6]^+$. The in-phase symmetric C–H stretching is IR inactive and lies at the top frequency, 3150 cm^{-1} , of the complex. At low frequencies, the band at 317 cm^{-1} is for swinging modes of the benzene molecules coupled with oscillatory movements, in a parallel direction to the benzene rings, of the two axial iron atoms. At 304 cm^{-1} , the strongest band is positioned, which is quite similar

to the vibrational mode of $Fe_6-(C_6H_6)_2$ at 289 cm^{-1} . The small band at 256 cm^{-1} mimics the mode of $Fe_6-(C_6H_6)_2$ lying at 285 cm^{-1} . Lastly, the small peak at 135 cm^{-1} is for a stretching mode of the whole Fe_6 cluster with the two benzene molecules.

Of the studied species, $[Fe_6-(C_6H_6)_2]^-$ shows the smallest shift to the blue, 53 cm^{-1} , for the out-of-plane C–H bend, lying at 714 cm^{-1} with the strongest resonance (see Figure 11c), implying the smallest impediment for this type of vibrational mode, which is partially accounted for by the fact that in this complex occurs the longest Fe–C distances, 2.14–2.17 Å, as compared for example with those of $Fe_6-(C_6H_6)_2$, which are limited within 2.13–2.14 Å. The modest band lying at 780–791 cm^{-1} also corresponds to out-of-plane C–H bend modes, but they involve the bending of only four or three CH units. The in-plane C–H bend is located at 989 cm^{-1} with a negligible band, 1 km/mol, and shifted to the red by −45 cm^{-1} . Unexpectedly, another in-plane C–H bend lies at 1126 cm^{-1} with a higher intensity, 6.3 km/mol, but shifted to the blue by 92 cm^{-1} . Also, with a negligible band, 1.6 km/mol, the in-plane carbon ring distortion is located at 1418 cm^{-1} , yielding a negative shift of −54 cm^{-1} . Another in-plane carbon ring distortion lies at about the same frequency, 1475 cm^{-1} , as that of bare benzene, 1472

cm^{-1} ; its intensity, 8.7 km/mol, is also quite similar (see Table 4). Then, showing very weak resonances, the in-plane C–H bend and the in-plane carbon ring distortion modes are shifted to the red by -45 and -54 cm^{-1} , respectively, suggesting also a weakening of the molecular bonding of the benzene ligands in the $[\text{Fe}_6-(\text{C}_6\text{H}_6)_2]^-$ complex.

As shown above, the in-plane carbon ring distortion is IR inactive in $[\text{Fe}_6-\text{C}_6\text{H}_6]^-$ and, in $[\text{Fe}_6-(\text{C}_6\text{H}_6)_2]^-$, though the band is quite weak, the IR activity of this mode is recovered. Furthermore, the symmetric ring stretching mode of the two benzene molecules, in the out-of-phase way, is situated at the same frequency, 953 cm^{-1} , and shows also the same shift to the red, -47 cm^{-1} , as in $[\text{Fe}_6-(\text{C}_6\text{H}_6)_2]^+$, but with an enhanced resonance; see Figure 11c. Similarly, the in-phase symmetric ring stretching of the rings, at 956 cm^{-1} , is IR inactive. Centered at 3120 cm^{-1} is located a strong band for three asymmetric C–H stretching modes. Closely, at 3127 cm^{-1} , lies the strongest resonance of $[\text{Fe}_6-(\text{C}_6\text{H}_6)_2]^-$, which is for the (out-of-phase) symmetric C–H stretching modes of the benzene moieties; these last two frequencies show minor shifts to the red, -1 and -5 cm^{-1} , respectively, with respect to neutral benzene. At low frequencies, 336 cm^{-1} , the strongest band for the IR spectrum of $[\text{Fe}_6-(\text{C}_6\text{H}_6)_2]^-$ also appears, which is for a similar mode as that located at 304 cm^{-1} for $[\text{Fe}_6-(\text{C}_6\text{H}_6)_2]^+$ and at 289 cm^{-1} for $\text{Fe}_6-(\text{C}_6\text{H}_6)_2$, which also show the strongest resonances. With a modest intensity, the band situated at 280 cm^{-1} mimics the vibrational mode lying at 256 cm^{-1} for $[\text{Fe}_6-(\text{C}_6\text{H}_6)_2]^+$ and at 285 cm^{-1} for $\text{Fe}_6-(\text{C}_6\text{H}_6)_2$. At the bottom of the spectrum, 263 cm^{-1} , lies a modest band, which accounts for swinging modes of benzene coupled with oscillatory movements, in a parallel direction to the benzene rings, of a square defined by two axial and two equatorial iron atoms.

4. Conclusions

The interactions of one and two benzene molecules with the magnetic Fe_6 cluster were studied with the BPW91/6311++G(2d,2p) method. The theoretical results for the IE and EA of Fe_6 are in close agreement with the experimental values, which gives support in that the $M = 21$ distorted octahedral structure is the GS of this cluster, and that the chosen method describes properly the metal–metal interactions in this kind of magnetic particles. Other spin states of Fe_6 produce EAs and IEs that differs significantly from the experimental results. It was found that the adsorption of benzene considerably reduces the magnetic moment of Fe_6 . The total magnetic moments for the GS of $\text{Fe}_6-\text{C}_6\text{H}_6$, $16 \mu_B$, and $\text{Fe}_6-(\text{C}_6\text{H}_6)_2$, $14 \mu_B$, are quenched by about 4 and 6 μ_B , respectively, as compared with the bare Fe_6 cluster, $20 \mu_B$. Also, adsorption of two benzenes produces a shrinking of Fe_6 , indicating an increase of the metal–metal bonding. Thus, magnetic effects are crucial in the adsorption of C_6H_6 by Fe_6 . The estimated adiabatic BDEs per benzene: 20 – 24 kcal/mol for $\text{Fe}_6-(\text{C}_6\text{H}_6)_{1,2}$, $\approx 38 \text{ kcal/mol}$ for $[\text{Fe}_6-(\text{C}_6\text{H}_6)_{1,2}]^+$, and 16 – 17 kcal/mol for $[\text{Fe}_6-(\text{C}_6\text{H}_6)_{1,2}]^-$, give insight that the $\text{Fe}_n(\text{C}_6\text{H}_6)_m$ structures, as proposed experimentally, consist of an Fe_n core surrounded by adsorbed benzene molecules.⁷ The BDEs are accounted for by electrostatic and by $3d$ – π covalent contributions. Though each C–Fe bond is weak, 3 – 6 kcal/mol , η^6 coordinations on these compounds were confirmed by the topological properties of the electronic density. Consistently, the decrease of the IEs is a clear signature of d – π interactions; the EAs are also diminished. The calculated IR spectra for the complexes present vibrational bands near those of the free benzene molecule, and some forbidden IR modes in benzene become IR active in the complexes. Conversely, some

IR-active modes in benzene become inactive in the $[\text{Fe}_6-(\text{C}_6\text{H}_6)_{1,2}]^{+,-}$ charged complexes.

The out-of-plane C–H bend modes are displaced to the blue by 91 – 114 cm^{-1} for $\text{Fe}_6-(\text{C}_6\text{H}_6)_{1,2}$, 111 – 137 cm^{-1} for $[\text{Fe}_6-(\text{C}_6\text{H}_6)_{1,2}]^+$, and 53 – 86 cm^{-1} for $[\text{Fe}_6-(\text{C}_6\text{H}_6)_{1,2}]^-$; in each case, the smaller value is for $m = 2$. Thus, the cations (anions) show the biggest (smallest) impediment for this type of C–H bending. The in-plane C–H bend modes are shifted to the red by similar quantities in these compounds: -34 to -43 cm^{-1} for $\text{Fe}_6-(\text{C}_6\text{H}_6)_{1,2}$, -32 to -38 cm^{-1} for $[\text{Fe}_6-(\text{C}_6\text{H}_6)_{1,2}]^+$, and -44 to -49 cm^{-1} for $[\text{Fe}_6-(\text{C}_6\text{H}_6)_{1,2}]^-$. Analogously, the in-plane carbon ring distortions are shifted to the red by -42 to -47 cm^{-1} for $\text{Fe}_6-(\text{C}_6\text{H}_6)_{1,2}$, -40 to -42 cm^{-1} for $[\text{Fe}_6-(\text{C}_6\text{H}_6)_{1,2}]^+$, and -50 to -54 cm^{-1} for $[\text{Fe}_6-(\text{C}_6\text{H}_6)_{1,2}]^-$. The frequency decrease for these two vibrational modes is indicative of a weakening of the bonding in the benzene molecule. Shifted also to the red, the symmetric ring stretching exemplifies clearly a forbidden IR mode of benzene, located at 990 cm^{-1} , that becomes IR active after adsorption; it was found at 962 and 968 cm^{-1} in the monobenzene complexes and at 947 and 953 cm^{-1} in the species containing two benzenes. Furthermore, the in-plane carbon ring distortion and the asymmetric C–H stretching are IR active in benzene; they become IR inactive in $[\text{Fe}_6-\text{C}_6\text{H}_6]^-$ and in $[\text{Fe}_6-\text{C}_6\text{H}_6]^+$, respectively. Then, in this contribution, we addressed the study of the interactions of one and two benzene ligands with the magnetic Fe_6 cluster. This is one of the first studies that deals with this size of iron clusters bonded to benzene. We hope that this research will motivate experimental and theoretical studies on this regime of cluster size, necessary to deeply understand the properties of the Fe_n –(benzene) $_m$ systems.

Acknowledgment. Financial support from Project PAPIIT IN-102308 from DGAPA-UNAM is acknowledged. Supercomputer facilities from DGSCA-UNAM are appreciated. A.G.-G. deeply acknowledges DGAPA-UNAM for his postdoctoral fellowship.

Supporting Information Available: Contour plots for the C– Fe_a bonding MOs of spin down of $\text{Fe}_6-(\text{C}_6\text{H}_6)_2$ are contained in Figure 1 and those, also of spin down, presenting polarization from the axial toward the equatorial iron atoms, and delocalization in the equatorial plane are reported in Figure 2. Some contour plots for the C– Fe_a bonding MOs of majority spin of $\text{Fe}_6-\text{C}_6\text{H}_6$ are reported in Figures 3a,b. The molecular graph for the GS of $\text{Fe}_6-\text{C}_6\text{H}_6$ is contained in Figure 4; there, the density, ρ , in $e \text{ au}^{-3}$, and laplacian, $\nabla^2\rho$, in $e \text{ au}^{-5}$, are indicated for the BCPs of the C–Fe and Fe–Fe contacts and the RCPs for the Fe–C–C and Fe–Fe–Fe rings. The contour plots for the HOMO and LUMO orbitals of $\text{Fe}_6-\text{C}_6\text{H}_6$ are reported in Figure 5. This material is available free of charge via the Internet at <http://pubs.acs.org>.

References and Notes

- (1) Bansmann, J.; et al. *Surf. Sci. Rep.* **2005**, *56*, 189.
- (2) Billas, I. M. L.; Chatelain, A.; de Heer, W. A. *Science* **1994**, *265*, 1682.
- (3) Cox, D. M.; Trevor, D. J.; Whetten, R. L.; Rohlfing, E. A.; Kaldor, A. *Phys. Rev. B* **1985**, *32*, 7290.
- (4) Dietz, T. G.; Duncan, M. A.; Powers, D. E.; Smalley, R. *J. Chem. Phys.* **1981**, *74*, 6511.
- (5) Duncan, M. A. *Int. J. Mass Spectrom.* **2008**, *272*, 99.
- (6) Nakajima, A.; Kaya, K. *J. Phys. Chem. A* **2000**, *104*, 176.
- (7) Kurikawa, T.; et al. *Organometallics* **1999**, *18*, 1430.
- (8) Senapati, L.; Nayak, S. K.; Rao, B. K.; Jena, P. *J. Chem. Phys.* **2003**, *118*, 8671.

- (9) Kandalam, A. K.; Jena, P.; Li, X.; Eustis, S. N.; Bowen, K. H. *J. Chem. Phys.* **2008**, *129*, 134308.
- (10) Li, X.; Eustis, S. N.; Bowen, K. H.; Kandalam, A. *J. Chem. Phys.* **2008**, *129*, 124312.
- (11) Szczepanski, J.; Wang, H.; Vala, M.; Tielens, A. G. G. M.; Eyler, J. R.; Oomens, J. *ApJ.* **2006**, *646*, 666.
- (12) Simon, A.; Joblin, C. *J. Phys. Chem. A* **2007**, *111*, 9745.
- (13) Wang, Y.; Szczepanski, J.; Vala, M. *Chem. Phys.* **2007**, *342*, 107.
- (14) Simon, A.; Joblin, C.; Polfer, N.; Oomens, J. *J. Phys. Chem. A* **2008**, *112*, 8551.
- (15) Hübner, O.; Sauer, J. *Chem. Phys. Lett.* **2002**, *358*, 442.
- (16) Rabilloud, F. *J. Chem. Phys.* **2005**, *122*, 134303.
- (17) Bauschlicher, C. W.; Partridge, H.; Langhoff, S. R. *J. Phys. Chem.* **1992**, *96*, 3273.
- (18) Jaeger, T. D.; van Heijnsbergen, D.; Klippenstein, S. J.; von Helden, G.; Meijer, G.; Duncan, M. A. *J. Am. Chem. Soc.* **2004**, *126*, 10981.
- (19) Becke, A. D. *J. Chem. Phys.* **1993**, *98*, 5648–5652.
- (20) Stevens, P. J.; Devlin, F. J.; Chablowski, C. F.; Frisch, M. J. *J. Phys. Chem.* **1994**, *98*, 11623.
- (21) Becke, A. D. *Phys. Rev. A* **1988**, *38*, 3098.
- (22) Perdew, J. P.; Wang, Y. *Phys. Rev.* **1992**, *45*, 13244.
- (23) Raghavachari, K.; Trucks, G. W. *J. Chem. Phys.* **1989**, *91*, 1062.
- (24) Gutsev, G. L.; Bauschlicher, C. W., Jr. *J. Phys. Chem. A* **2003**, *107*, 7013.
- (25) Castro, M. *Chem. Phys. Lett.* **2007**, *435*, 322–326.
- (26) Castro, M. *Chem. Phys. Lett.* **2007**, *446*, 333–338.
- (27) Valencia, I.; Chávez, V.; Castro, M. *J. Phys. Chem.* **2008**, *112*, 5028.
- (28) Kealy, T. J.; Pauson, P. L. *Nature* **1951**, *168*, 1039.
- (29) Wilkinson, G.; Rosenblum, M.; Whiting, M. C.; Woodward, R. B. *J. Am. Chem. Soc.* **1952**, *74*, 2125.
- (30) Frisch, M. J.; Gaussian 03, Revision D.01; Gaussian Inc.: Wallingford, CT, 2004.
- (31) Bobadova-Parvanova, P.; Jackson, K. A.; Srinivas, S.; Horoi, M.; Kohler, C.; Seifert, G. *J. Chem. Phys.* **2002**, *116*, 3576.
- (32) Castro, M. *Int. J. Quantum Chem.* **1997**, *64*, 223.
- (33) Yand, S.; Knickelbein, M. B. *J. Chem. Phys.* **1990**, *93*, 1533.
- (34) Wang, L.-S.; Li, X.; Zhang, H.-F. *Chem. Phys.* **2000**, *262*, 53.
- (35) (a) Moore, C. E. *Analysis of Optical Spectra*, NSRDS-NBS 34, National Bureau of Standards; National Bureau of Standards: Washington, D.C., 1971. (b) Weast, R. C. *Handbook of Chemistry and Physics*; CRC Press: Boca Raton, FL, 1980; Vol. 61, p E-69. (c) Robinson, J. W. *Handbook of Spectroscopy*; CRC Press: Boca Raton, FL, 1974, Vol. 1, p 257.
- (36) Zheng, W.; Eustis, S. N.; Li, X.; Nilles, J. M.; Thomas, O. C.; Bowen, K. H.; Kandalam, A. K. *Chem. Phys. Lett.* **2008**, *462*, 35.
- (37) Knickelbein, M. B. *J. Chem. Phys.* **2006**, *125*, 044308.
- (38) Dunitz, J. D.; Orgel, L. E.; Rich, A. *Acta Crystallogr.* **1956**, *9*, 373.
- (39) Bader, R. F. W. *Atoms in Molecules. A Quantum Theory*; Oxford University Press: New York, NY, 1990.
- (40) AIM2000; designed by Friedrich Biegler-König; University of Applied Sciences: Bielefeld, Germany, 2000.
- (41) Popelier, P. *Atoms in Molecules. An Introduction*, 1st ed.; Prentice-Hall, Pearson Education Limited: Edinburgh Gate, Essex, England, 2000.
- (42) Mayer, F.; Khan, I. A.; Armentrout, P. B. *J. Am. Chem. Soc.* **1995**, *117*, 9740.
- (43) Pandey, R.; Rao, B. K.; Jena, P.; Newsam, J. M. *Chem. Phys. Lett.* **2000**, *321*, 142.
- (44) Sun, X.; et al. *J. Appl. Phys.* **2007**, *101*, 09G256.
- (45) Pandey, R.; Rao, B. K.; Jena, P.; Blanco, M. A. *J. Am. Chem. Soc.* **2001**, *123*, 3799.
- (46) Shimanouchi, T. In *Molecular Vibrational Frequencies, NIST Chemistry WebBook, NIST Standard Reference Database Number 69*; Linstrom, P. J., Mallard, W. G., Eds.; National Institute of Standards and Technology: Gaithersburg, MD, 2007; <http://webbook.nist.gov>.

JP811065W

Theoretical Study of the Structural and Electronic Properties of the $\text{Fe}_6-(\text{C}_6\text{H}_6)_m$, $m = 3, 4$, Complexes

Israel Valencia and Miguel Castro*

Departamento de Física y Química Teórica, DEPg. Facultad de Química, Universidad Nacional Autónoma de México, México D.F., C.P. 04510, México

Received: June 30, 2009; Revised Manuscript Received: November 23, 2009

The adsorption of benzene on the magnetic Fe_6 cluster was studied by means of first principles all-electron calculations done with gradient corrected density functional theory. In the $M = 2S + 1 = 13$ (S is the total spin) ground state (GS) of $\text{Fe}_6-(\text{C}_6\text{H}_6)_3$ each benzene is bonded with one Fe atom, forming η^6 coordinations with C–Fe contacts of 2.12–2.17 Å; though the Fe_6 cluster structure is preserved, it presents more distortion than in bare Fe_6 . The $M = 13$ GS of $\text{Fe}_6-(\text{C}_6\text{H}_6)_4$ shows a more distorted geometry with three η^6 and one η^2 coordinations, as the bonding with the fourth benzene was reduced to two C–Fe bonds. Thus, $\text{Fe}_6-(\text{C}_6\text{H}_6)_4$ may be viewed as a Fe_6 core covered by a layer of benzene molecules. The d– π bonding interactions are clearly reflected by the estimated adiabatic ionization energies (4.60 and 4.42 eV for $m = 3$ and 4, respectively), because they are significantly smaller than that of bare Fe_6 , 6.15 eV. The adiabatic electron affinities also are diminished clearly, 1.02 and 1.13 eV, for $m = 3$ and 4, respectively, as compared to that of Fe_6 , 1.61 eV. The magnetic moments of the $\text{Fe}_6-(\text{C}_6\text{H}_6)_{3,4}$ complexes are strongly quenched, by 8.0 magneton bohrs (μ_B), with respect to the value, 20.0 μ_B , of the isolated Fe_6 cluster. Lastly, the vibrational spectra show IR bands placed near those of free benzene and several forbidden IR modes of benzene turn IR active in the reduced symmetry of the complexes.

1. Introduction

The study of transition metal (TM) clusters interacting with organic molecules is nowadays an active field of research because it is important for the design and synthesis of novel compounds presenting unusual structural, electronic, and magnetic properties.^{1,2} Recently, the state-of-the-art of laser vaporization techniques makes feasible the synthesis in the gas phase of TM–clusters–benzene complexes for all of the 3d metals,³ which, in the absence of solvent effects, are important for the study of the fundamental interactions determining their structural and physicochemical properties. Indeed, some of these small systems, those involving a single TM atom and benzene units, have been the focus as basic models for the study of d– π bonding interactions.³ Once obtained in the gas phase, the complexes are characterized by mass spectrometry, photoionization spectroscopy, chemical probe experiments, and IR methods.^{1–4} So far, the results are consistent with two types of geometries for the $\text{TM}_n-(\text{benzene})_m$ complexes, multiple-decker sandwich structures for early TMs and clusters fully covered with benzene moieties for late transition metals.^{1,2} Besides, the observed ionization energies, IEs, and electron affinities, EAs, provide some insight on their electronic structure.^{1–4} The $\text{Fe}_6-(\text{C}_6\text{H}_6)_4$ complex was observed by mass spectrometry by Kurikawa et al.; see the (6, 4) peak in Figure 2 of ref 1. Recently, Zheng et al.⁴ have determined the mass spectrum of iron–benzene anions, $\text{Fe}_n-(\text{C}_6\text{H}_6)_m^-$, $n = 1–7$ and $m = 1–5$; a relatively intense peak was found for $\text{Fe}_6-(\text{C}_6\text{H}_6)_4^-$, confirming the formation of the neutral (6, 4) complex; the spectrum reveals also a more intense peak for $[\text{Fe}_6-(\text{C}_6\text{H}_6)_3]^-$ and a smaller one for $\text{Fe}_6-(\text{C}_6\text{H}_6)_5^-$. Their photoelectron spectroscopy results also allowed the determination of the EA of $\text{Fe}_6-(\text{C}_6\text{H}_6)_4$.⁴ However,

there are not reported experimental results for the EAs, IEs, binding energies, and vibrational frequencies for all the $\text{Fe}_6-(\text{C}_6\text{H}_6)_m$, $m = 1, 2, 3$, and 4, compounds. Also a fundamental issue that is yet to be solved is the geometry of these complexes, since it is not known the structural details of bond lengths and bond angles, confirming the proposed structures and accounting for the observed electronic, magnetic, and energetic behaviors. Overall, the knowledge of these properties is important for the design of new materials using this kind of TM_n-L_m compounds as building blocks.^{5–7}

On the other hand, theoretical calculations have proved to be useful for the accurate determination of the ground state geometry of magnetic TM clusters^{8–10} and of TM clusters interacting with organic and inorganic ligands (L); also they are able to determine the electronic and energetic properties of this kind of TM_n-L_m compound.^{11–13} In a previous report, we have addressed the structural, electronic, magnetic, energetic, and vibrational properties of the $\text{Fe}_6-(\text{C}_6\text{H}_6)_{1,2}$ complexes.¹³ The objective of this work is to study, by means of first principles all-electron calculations, realized with the generalized gradient approximation (GGA) of density functional theory (DFT), the adsorption of three and four benzene molecules on the surface of the magnetic Fe_6 particle. Neutral and charged $[\text{Fe}_6-(\text{C}_6\text{H}_6)_{3,4}]^\pm$ compounds will be addressed. The obtained results will allow determining the geometry for the low-lying states of these complexes as well as the estimation of adiabatic ionization energies, electron affinities, and binding energies. An analysis of the magnetic moments and vibrational frequencies also will be presented. This theoretical study will provide insight on the tendencies of these properties as the number of adsorbed benzene molecules on the Fe_6 cluster increases.

* Corresponding author. E-mail: castro@quetzal.pquim.unam.mx

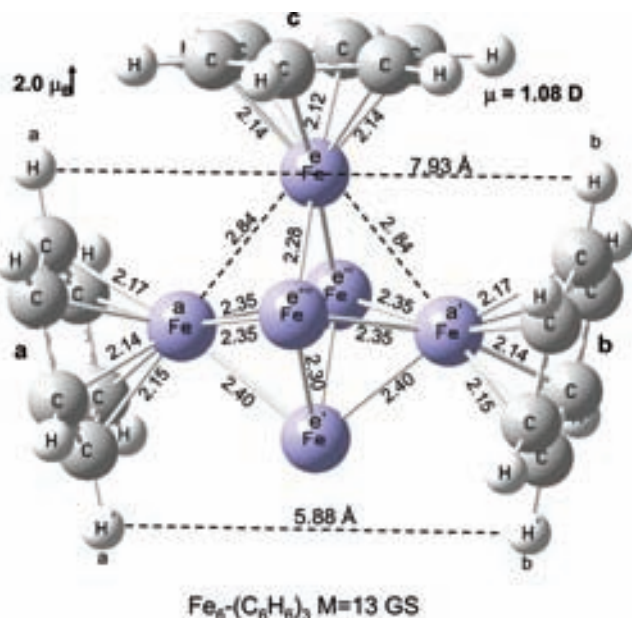


Figure 1. Bond lengths, in Å, average magnetic moments per atom, in μ_B , and dipole moments, in Debyes, for the $M = 13$ GS geometry of $\text{Fe}_6-(\text{C}_6\text{H}_6)_3$.

2. Methodology

The ground states (GS) of the magnetic Fe_6 cluster, benzene, and $\text{Fe}_6-(\text{benzene})_m$, $m = 3$ and 4, complexes as well as those for the corresponding single positively and negatively charged compounds were determined by means of DFT all-electron calculations, performed with the functional of Becke for exchange¹⁴ and that of Perdew and Wang for correlation.¹⁵ This approach is referred to as BPW91, which is used in concert with 6-311++G(2d,2p) basis sets [15s11p6d2f]/[10s7p4d2f] for Fe, [12s6p2d]/[5s4p2d] for C, and [6s2p]/[4s2p] for H.^{16–18} The Gaussian-03 quantum chemistry code was used.¹⁹ Comparing with available experimental data, we have found that BPW91/6-311++G(2d,2p) is useful for the study of small iron clusters interacting with benzene molecules.^{12,13} Strict convergence criterion was used for the total energy; minimized up to 10^{-8} au. Without imposing symmetry constraints and for several states of different multiplicities, $M = 2S + 1$ (S is the total spin), several candidate structures were fully optimized by choosing a 10^{-5} au threshold for the rms force. An ultrafine grid was used for these steps and for the vibrational analysis, which was performed under the harmonic approximation for all the optimized geometries. The located states reported in Figures 1 and 2 are true local minima on the potential energy surface, because they have positive frequencies. The molecular orbitals, MO, of the neutral GSs were also analyzed to obtain insight of the Fe–C bond formation. Particularly, the highest occupied MO (HOMO) and the lowest unoccupied MO (LUMO) are important for the analysis of the electron detachment and addition processes.

3. Results and Discussion

3a. Lowest Energy States of Fe_6 , Fe_6^+ , and Fe_6^- . The GS of Fe_6 is of high multiplicity, $M = 21$, in a distorted octahedral geometry, and the magnetic moment, 3.3 bohr magnetons (μ_B) per atom, agrees with the experimental results, $\approx 3.0 \mu_B$ per atom, for small iron clusters.^{20,21} The geometry of Fe_6 is shown in Figure 1 of ref 13. The Fe_6^+ ion has $M = 22$ and the IE, 6.15 eV, is near the observed value, 5.96 ± 0.05 eV.²² The GS

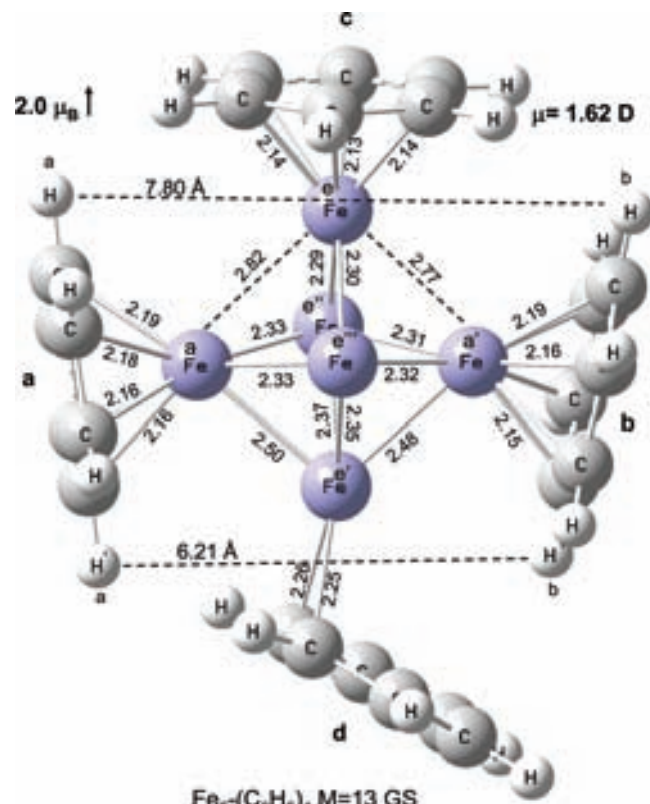


Figure 2. Ground state geometry for the $\text{Fe}_6-(\text{C}_6\text{H}_6)_4$ compound.

of Fe_6^- is of lower multiplicity, 20, and the EA, 1.61 eV, matches with the experiment, 1.58 ± 0.06 eV.²³ The estimated IE of benzene, 9.08 eV, is bigger than that of Fe_6 and near to the observed value, 9.24 eV.²⁴ These results will be used to discuss the IEs and EAs of the $\text{Fe}_6-(\text{C}_6\text{H}_6)_{3,4}$ complexes.

3b. Lowest Energy States of $\text{Fe}_6-(\text{C}_6\text{H}_6)_3$, $[\text{Fe}_6-(\text{C}_6\text{H}_6)_3]^-$, and $[\text{Fe}_6-(\text{C}_6\text{H}_6)_3]^+$. The GS geometry of $\text{Fe}_6-(\text{C}_6\text{H}_6)_3$ has C_{2v} symmetry, defining a $^{13}\text{B}_1$ electronic state, with $2.0 \mu_B$ per atom (see Figure 1) and with the benzene moieties disposed in a distorted way on the surface of the Fe_6 cluster, and a dipole moment of 1.08 debyes (D) is formed, suggesting important electrostatic character in the metal–ligand binding. The experimental determination of the dipole moment, as discussed by Rabilloud²⁵ and Imura et al.,²⁶ will provide insight on the nature of the bonding and on the assigned GS of this complex. The $M = 11$ and $M = 15$ states (see Table 1a) were found to be 16.9 and 31.2 kJ/mol over the GS. Thus, adsorption of three benzenes quenches more strongly, by $8.0 \mu_B$, the magnetic moment of the complex than the $m = 1$ and 2 cases, which show reductions of 4.0 and $6.0 \mu_B$, respectively.¹³

The lowest energy state of the $[\text{Fe}_6-(\text{C}_6\text{H}_6)_3]^-$ ion shows a geometry similar to that of the neutral complex (see Table 1b), but with a higher spin of $M = 14$ or $2.2 \mu_B$ per atom. The $M = 12$ state was located quite close in energy, 16.3 kJ/mol above, whereas the $M = 16$ state lies 54.4 kJ/mol above the GS (see Table 1a). Also the GS geometry of the $[\text{Fe}_6-(\text{C}_6\text{H}_6)_3]^+$ cation resembles closely the GS structure of the neutral complex (see Table 1b), presenting a spin state of $M = 12$. The $M = 10$ and 14 states were found at about 30 kJ/mol above the GS. Note that $[\text{Fe}_6-(\text{C}_6\text{H}_6)_3]^-$ has a bigger magnetic moment than the neutral, and $[\text{Fe}_6-(\text{C}_6\text{H}_6)_3]^+$ has a smaller one. This behavior differs from that of the mono- and dibenzene species,¹³ which, in both cases the anions and cations have the same multiplicity, $M = 16$.

TABLE 1

a. Lowest Energy States of Neutral and Charged Fe ₆ -(C ₆ H ₆) ₃ Complexes ^a				
multiplicity	ΔE (kJ/mol)	IE (eV)	EA (eV)	
	Fe ₆ -(C ₆ H ₆) ₃			
13	0.0	4.60	1.02	
11	16.9			
15	31.2			
	[Fe ₆ -(C ₆ H ₆) ₃] ⁻			
14	0.0			
12	16.3			
16	54.4			
	[Fe ₆ -(C ₆ H ₆) ₃] ⁺			
12	0.0			
10	31.8			
14	29.3			
b. Internuclear Distances, in Å, for the Ground States of Neutral and Charged Fe ₆ -(C ₆ H ₆) ₃ Complexes ^b				
bond	benzene	Fe ₆ -(C ₆ H ₆) ₃	[Fe ₆ -(C ₆ H ₆) ₃] ⁻	[Fe ₆ -(C ₆ H ₆) ₃] ⁺
Fe _a -C	a	2.14–2.17	2.12–2.15	2.15–2.17
Fe _{a'} -C	b	2.14–2.17	2.12–2.16	2.15–2.17
Fe _e -C	c	2.12–2.14	2.16	2.12–2.13
Fe _e -Fe _a		2.84	2.96	2.73
Fe _e -Fe _{a'}		2.84	2.96	2.73
Fe _e -Fe _{e''}		2.28	2.34	2.32
Fe _e -Fe _{e'''}		2.28	2.34	2.32
Fe _{e'} -Fe _{e''}		2.30	2.29	2.32
Fe _{e'} -Fe _{e'''}		2.30	2.29	2.32
Fe _a -Fe _{e'}		2.35	2.38	2.32
Fe _a -Fe _{e'''}		2.35	2.38	2.32
Fe _{a'} -Fe _{e''}		2.35	2.38	2.32
Fe _{a'} -Fe _{e'''}		2.35	2.38	2.32
Fe _a -Fe _{e'}		2.40	2.40	2.37
Fe _{a'} -Fe _{e'}		2.40	2.40	2.37
H _a -H _b		7.93	7.68	7.81
H' _a -H' _b		5.88	6.09	5.79

^a Relative energies, adiabatic ionization energies, and electron affinities are indicated. ^b Also are shown the H_a-H_b and H'_a-H'_b separations. Labels correspond to Figure 1.

Addition of a third benzene to Fe₆-(C₆H₆)₂, disturbs considerably the structural pattern of the *m* = 2 adduct.¹³ First, the Fe-C contacts, for the opposite lying **a** and **b** benzene moieties, are increased from 2.13–2.14 to 2.14–2.17 Å, whereas the Fe-C distances for the third **c** benzene are contained in the shorter 2.12–2.14 Å range. Second, a strong distortion is produced on the original distorted octahedral shape of Fe₆. For example, the two axial atoms, Fe_a, bonded to **a** and **b**, and the two equatorial atoms, Fe_e, bonded to the Fe_a sites with bond lengths of 2.35 Å, no longer define a plane (the dihedral angle is 16.7°), since the Fe_e site, bonded with benzene **c**, has two big Fe_e-Fe_a distances, of 2.84 Å, and two shorter ones, of 2.28 Å, with those Fe_e sites; see Figure 1. Effectively, **a** and **b** are tilted in such manner to reduce the repulsion with benzene **c**. Consistent with the more symmetric geometry of Fe₆-(C₆H₆)₂, the two rhombi formed by the two Fe_a atoms and two Fe_e sites define, each one, a plane; also the rhombus formed by the four equatorial atoms defines a plane. However, on Fe₆-C₆H₆, the equatorial rhombus is nonplanar, since the dihedral angle is 4.7°, indicating a less symmetric structure.¹³ These structural features of Fe₆-(C₆H₆)₃ are also clearly revealed by the H-H distances between **a** and **b**, presenting shorter, 5.88 Å for H'_a-H'_b, and longer, 7.93 Å for H_a-H_b, separations, as compared to those of Fe₆-(C₆H₆)₂, where both are equal to 6.78 Å;¹³ the H'_a-H'_b

separation may originate steric hindrance for the adsorption of a fourth benzene. Despite such highly distorted geometry, the Fe-C contacts suggest the formation of three η^6 (six Fe-C bonds are formed for each ligand) coordinations for the GS of this complex.

Most of the structural features quoted above for the neutral are also shown by the charged species. On the [Fe₆-(C₆H₆)₃]⁻ anion, the two Fe_a-Fe_e distances, 2.96 Å, are even more lengthened than those in the neutral, 2.84 Å, and the bond lengths in the distorted equatorial plane are elongated from 2.35 to 2.38 Å; see Table 1b. These results imply that the added electron increases the repulsion of the third **c** benzene with the other two. Further, the Fe_e-C contacts are enlarged, from 2.12–2.14 to 2.16 Å; the opposite occurs on the two sets of Fe_a-C contacts, which are shortened from 2.14–2.17 to 2.12–2.16 Å. Besides, the [Fe₆-(C₆H₆)₃]⁺ ion shows the most compact geometry of the *m* = 3 species, as most of the metal-metal distances are shortened, with respect to those of the neutral; see Table 1b. For example, the two Fe_a-Fe_e distances are shortened from 2.84 to 2.73 Å and the Fe_e-Fe_e bond lengths are reduced from 2.35 to 2.32 Å. These results show the sensitivity of the structural parameters of the Fe₆-(C₆H₆)₃ complex on the electronic charge.

3c. Lowest Energy States of Fe₆-(C₆H₆)₄, [Fe₆-(C₆H₆)₄]⁻, and [Fe₆-(C₆H₆)₄]⁺. Without imposing symmetry constraints on the full relaxation procedure, structural and electronic, Fe₆-(C₆H₆)₄ reaches a lowest energy state with *M* = 13, shown in Figure 2, and with the benzene molecules adsorbed asymmetrically on the Fe₆ cluster, originating a dipole moment, 1.62 D, bigger than that of the Fe₆-tribenzene compound. The **c** ligand presents relatively short Fe-C contacts, 2.13–2.14 Å, appropriate for the formation of η^6 coordination, whereas longer Fe-C contacts, of 2.15 up to 2.19 Å, are formed for the somewhat tilted **a** and **b** rings, indicating slightly distorted η^6 coordination for each benzene moiety. Attachment of the fourth **d** benzene yields two short Fe-C contacts, of 2.25–2.26 Å, which may originate the formation of Fe-C bonds, and four longer Fe-C contacts, 3.12–3.80 Å, denying clearly such bond formation. Thus, the fourth benzene molecule is bonded to the cluster through η^2 (two Fe-C bonds are formed) coordination. In a similar geometry and also with two short Fe-C contacts, but of different lengths, 2.10 and 2.28 Å, for the fourth benzene, the *M* = 11 state lies only 14.4 kJ/mol above the GS. As shown in Table 2a, the *M* = 15 state is located higher in energy.

The GS of the [Fe₆-(C₆H₆)₄]⁻ ion shows a geometry similar to that of the neutral complex (see Table 2b), but with a higher multiplicity, *M* = 14 or 2.2 μ_B per atom. At a slightly higher energy, 13.0 kJ/mol, was located the *M* = 12 state. As reported in Table 2a, the *M* = 16 state of this negative ion lies at a considerable higher energy. The GS of [Fe₆-(C₆H₆)₄]⁺ presents a magnetic moment of 1.8 μ_B per atom (*M* = 12) and a geometry resembling that of the neutral compound; see Table 2b. The *M* = 10 and 14 states of the positive ion were found at about 35 kJ/mol above the GS; see Table 2a. Note that the magnetic moment of [Fe₆-(C₆H₆)₄]⁻ is equal to that of the [Fe₆-(C₆H₆)₃]⁻ anion; a similar behavior occurs for the *m* = 4 and *m* = 3 positive ions.

On the [Fe₆-(C₆H₆)₄]⁻ anion, the two Fe-C contacts, 2.16 and 2.17 Å, of the fourth benzene are clearly shorter than those of the neutral; those of **a** and **b** are shortened a little bit, and the Fe-C bonds of **c** are slightly enlarged. The metal-metal distances are notably lengthened. For example, two Fe_e-Fe_a distances are moved from 2.77–2.82 to 2.89–2.93 Å; other

TABLE 2

a. Lowest Energy States of Neutral and Charged $\text{Fe}_6-(\text{C}_6\text{H}_6)_4$ Complexes ^a			
multiplicity	ΔE (kJ/mol)	IE (eV)	EA (eV)
	$\text{Fe}_6-(\text{C}_6\text{H}_6)_4$		
13	0.0	4.42	1.13
11	14.4		
15	31.2		
			1.10 ± 0.1^b
	$[\text{Fe}_6-(\text{C}_6\text{H}_6)_4]^-$		
14	0.0		
12	13.0		
16	70.3		
	$[\text{Fe}_6-(\text{C}_6\text{H}_6)_4]^+$		
12	0.0		
10	33.9		
14	37.2		

b. Internuclear Distances, in Å, for the Ground States of Neutral and Charged $\text{Fe}_6-(\text{C}_6\text{H}_6)_4$ Complexes ^c				
bond	benzene	$\text{Fe}_6-(\text{C}_6\text{H}_6)_4$	$[\text{Fe}_6-(\text{C}_6\text{H}_6)_4]^-$	$[\text{Fe}_6-(\text{C}_6\text{H}_6)_4]^+$
Fe_a-C	a	2.16–2.19	2.14–2.17	2.18–2.20
$\text{Fe}_{a'}-\text{C}$	b	2.15–2.19	2.13–2.17	2.16–2.17
Fe_e-C	c	2.13–2.14	2.15–2.16	2.11–2.13
$\text{Fe}_{e'}-\text{C}$	d	2.25–2.26	2.16–2.17	2.33
Fe_e-Fe_a		2.82	2.93	2.78
$\text{Fe}_e-\text{Fe}_{a'}$		2.77	2.89	2.64
$\text{Fe}_e-\text{Fe}_{e''}$		2.29	2.29	2.33
$\text{Fe}_e-\text{Fe}_{e'''}$		2.30	2.30	2.34
$\text{Fe}_{e'}-\text{Fe}_{e''}$		2.37	2.37	2.36
$\text{Fe}_{e'}-\text{Fe}_{e'''}$		2.35	2.35	2.36
$\text{Fe}_a-\text{Fe}_{e''}$		2.33	2.34	2.31
$\text{Fe}_a-\text{Fe}_{e'''}$		2.33	2.34	2.31
$\text{Fe}_{a'}-\text{Fe}_{e''}$		2.31	2.33	2.30
$\text{Fe}_{a'}-\text{Fe}_{e'''}$		2.32	2.33	2.30
$\text{Fe}_a-\text{Fe}_{e'}$		2.50	2.51	2.46
$\text{Fe}_{a'}-\text{Fe}_e$		2.48	2.50	2.46
H_a-H_b		7.80	7.63	7.61
$\text{H}'_a-\text{H}'_b$		6.21	6.29	6.10

^a Relative energies, adiabatic ionization energies, and electron affinities are indicated. ^b Experimental value, from ref 4. ^c Also are shown the H_a-H_b and $\text{H}'_a-\text{H}'_b$ separations. Labels correspond to Figure 2.

small enlargements can be observed in Table 2b. Thus, $[\text{Fe}_6-(\text{C}_6\text{H}_6)_4]^-$ shows a more open geometry than the neutral complex.

On $[\text{Fe}_6-(\text{C}_6\text{H}_6)_4]^+$, the two Fe_e-C contacts of the fourth benzene are equal to 2.33 Å, and they are the longest ones observed on these complexes producing the formation of Fe–C bonds. The Fe_a-C contacts of **a**, 2.18–2.20 Å, are now different from those of **b**, 2.16–2.17 Å. Two Fe_e-Fe_a distances, 2.64 and 2.78 Å, are shorter than those of the neutral, 2.77 and 2.82 Å, and the other two Fe_e-Fe_a bond lengths, 2.46 Å, are a little bit shorter (see Table 2b), whereas the Fe_e-Fe_e bond lengths, 2.30–2.31 Å, are also slightly shortened. That is, $[\text{Fe}_6-(\text{C}_6\text{H}_6)_4]^+$ presents a slightly more compact geometry than the neutral compound.

3d. Bonding Molecular Orbitals of $\text{Fe}_6-(\text{C}_6\text{H}_6)_3$ and $\text{Fe}_6-(\text{C}_6\text{H}_6)_4$. In Figure 3 are shown the contour plots of the HOMO and LUMO, of major-spin (\uparrow), of $\text{Fe}_6-(\text{C}_6\text{H}_6)_3$; other MOs, lower in energy than the HOMO, indicative of Fe–C bonding, are reported in Figure 1S of the Supporting Information. The LUMO † shows an antibonding behavior between the equatorial Fe_e atom and benzene **c**; since this MO is the one

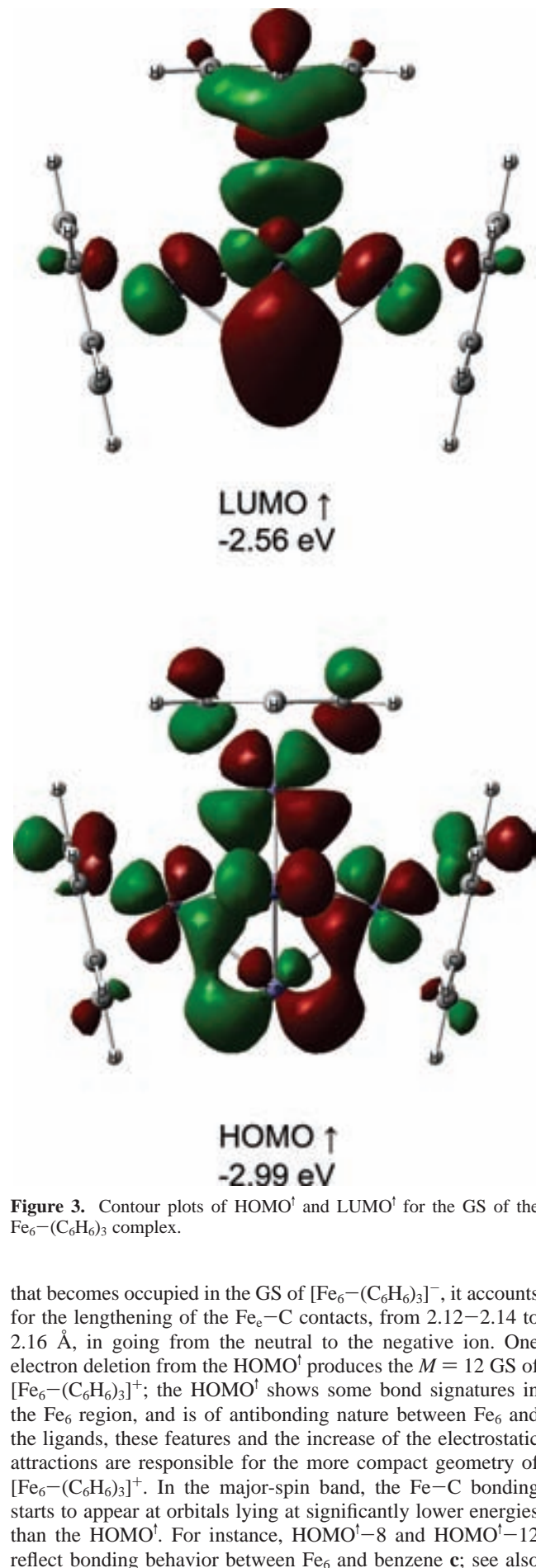


Figure 3. Contour plots of HOMO † and LUMO † for the GS of the $\text{Fe}_6-(\text{C}_6\text{H}_6)_3$ complex.

that becomes occupied in the GS of $[\text{Fe}_6-(\text{C}_6\text{H}_6)_3]^-$, it accounts for the lengthening of the Fe_e-C contacts, from 2.12–2.14 to 2.16 Å, in going from the neutral to the negative ion. One electron deletion from the HOMO † produces the $M = 12$ GS of $[\text{Fe}_6-(\text{C}_6\text{H}_6)_3]^+$; the HOMO † shows some bond signatures in the Fe₆ region, and is of antibonding nature between Fe₆ and the ligands; these features and the increase of the electrostatic attractions are responsible for the more compact geometry of $[\text{Fe}_6-(\text{C}_6\text{H}_6)_3]^+$. In the major-spin band, the Fe–C bonding starts to appear at orbitals lying at significantly lower energies than the HOMO † . For instance, HOMO † -8 and HOMO † -12 reflect bonding behavior between Fe₆ and benzene **c**; see also

HOMO-15[†] and HOMO-18[†] in Figure 1S in the Supporting Information. The MOs of minor-spin (\downarrow) containing signatures of Fe-C bond formation are reported in Figure 2S of the Supporting Information. The HOMO[†] and HOMO-1[†] contain bond signatures between the axial Fe_a atoms and **a** and **b**. Continuing up to HOMO-9[†] also appear bond signatures of Fe₆ with the benzene moieties.

In Figure 4 are shown the LUMO[†] and HOMO[†] for the GS of Fe₆-(C₆H₆)₄; other MOs, of major spin, presenting bond signatures of Fe₆ with the benzene molecules are reported in Figure 3S of the Supporting Information. The LUMO orbital, which is the one that is occupied in the GS of the [Fe₆-(C₆H₆)₄]⁻ anion, shows bond signatures between two C atoms of benzene **d** and the equatorial Fe sites. Becoming unoccupied in the GS of the [Fe₆-(C₆H₆)₄]⁺ ion, the HOMO[†] shows highly localized 3d contributions on the Fe sites, yielding a nonbonding behavior. As shown in Figure 3S, HOMO-1[†] and HOMO-3[†] record bonding interactions of Fe₆ with the **a**, **b**, and **c** ligands; HOMO-5[†] and HOMO-6[†] have signatures of Fe-C bonding with two C sites of benzene **d**. In addition, HOMO-23[†], HOMO-29[†], HOMO-30[†], HOMO-31[†], HOMO-38[†], HOMO-45[†], HOMO-48[†], and HOMO-53[†], reported in Figure 4S of the Supporting Information present this type of bonding. Thus, the MOs of major-spin suggest that only two Fe-C bonds are formed with the fourth moiety. Also reported in Figure 4S, HOMO-9[†], HOMO-12[†], and HOMO-13[†] contain bonding behavior of Fe₆ with the two **a** and **b** ligands. The bonding of Fe₆ with **a**, **b**, and **c** is exemplified by HOMO-11[†] and HOMO-37[†]. Lastly, HOMO-49[†], HOMO-50[†], and HOMO-53[†] reflect bond signatures of Fe₆ with the four benzene moieties. Thus, these MOs show how the benzene molecules are bonded to the cluster.

3e. Bond Dissociation Energies. For the Fe₆-(C₆H₆)_m \rightarrow Fe₆ + mC₆H₆ dissociation, including zero point energy, ZPE, and according to the difference of the GSs total energies, [E(Fe₆) + mE_t(C₆H₆)] - E_t(Fe₆-(C₆H₆)_m), an adiabatic bond dissociation energy, BDE, of 274.9 or 91.6 kJ/mol per benzene unit was found for Fe₆-(C₆H₆)₃, implying a bond strength of 15.5 kJ/mol for each C-Fe bond of this tribenzene compound that presents η^6 coordinations. Moving now to Fe₆-(C₆H₆)₄ and following a similar procedure, a BDE of 297.9 kJ/mol was found for this complex where there are two different types of C-Fe coordination modes, three η^6 and one η^2 , making the estimation of the BDE per benzene molecule more involved; very approximately it is 74.5 kJ/mol, which is clearly smaller than the corresponding results for the $m = 1-3$ compounds reported in Table 3. Note that the BDEs of Fe₆-(C₆H₆)_m, third column of Table 3, have the sum of all bond energies. In general, the BDEs per benzene unit decreases as m increases, but a maximum occurs at $m = 2$, implying a relatively high stability for Fe₆-(C₆H₆)₂. For the Fe₆-(C₆H₆)_m \rightarrow Fe₆-(C₆H₆)_{m-1} + C₆H₆ rupture, the sequential BDE was obtained according to the difference of the GS total energies: [E(Fe₆-(C₆H₆)_{m-1}) + E_t(C₆H₆)] - E_t(Fe₆-(C₆H₆)_m). As shown in Table 3, also for the $m = 1$ to $m = 2$ sequential addition, the BDE for the second moiety shows a highest value, 117.2 kJ/mol. Similarly, in a sequential way the BDE for the third ligand is 74.5 kJ/mol, and that for the fourth moiety is very small, 23.4 or 11.7 kJ/mol per each C-Fe bond. This weak bonding is due to the fact that Fe₆ forms only two longer C-Fe bonds, of 2.26 Å, with benzene **d**. On these grounds, a smaller binding energy is expected for the fifth adsorbed unit, signifying that Fe₆ could adsorb a maximum of four or at most five benzene moieties, which is consistent with the mass spectrometry results of

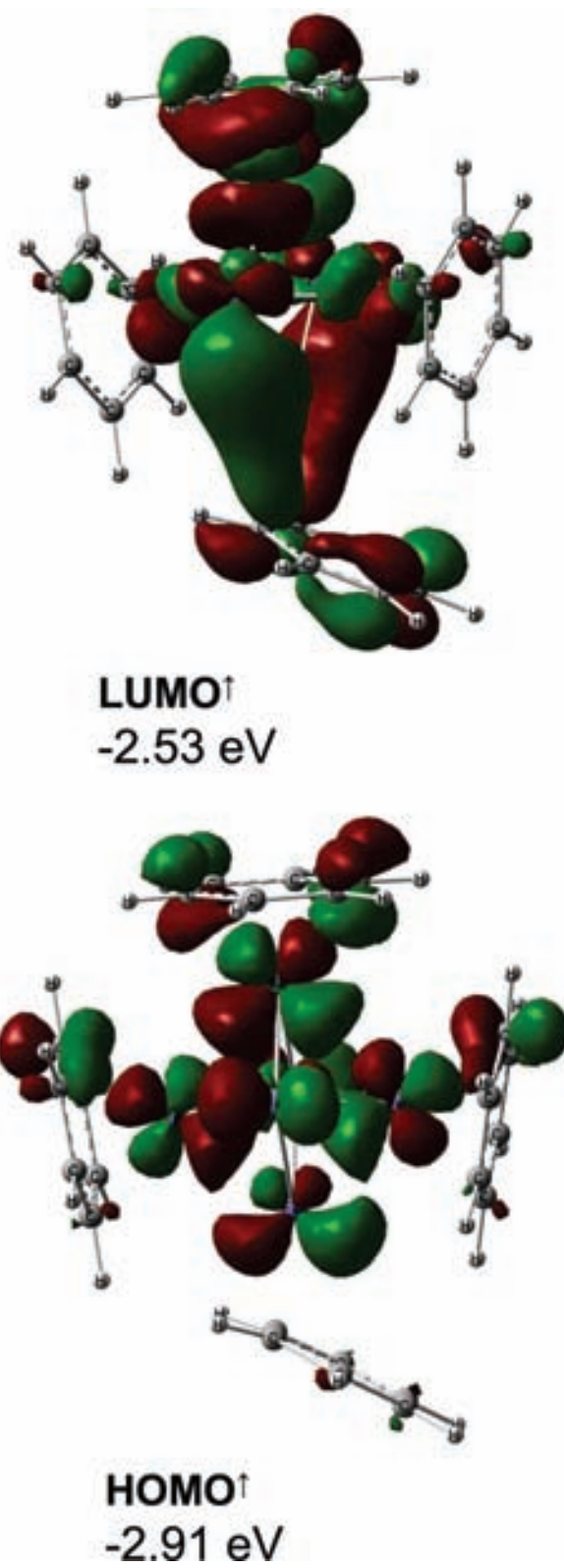


Figure 4. Contour plots of LUMO[†] and HOMO[†] for the GS of the Fe₆-(C₆H₆)₄ complex.

Kurikawa et al. and Zheng et al., quoted in the Introduction. Within the limitations of the studied structures, our results seem to be in the right direction, regarding the location of the GS geometries of Fe_n-(C₆H₆)_m, which, as found on experimental grounds, consist of an Fe_n core surrounded by a relatively strongly adsorbed layer of benzene.^{1,2} By this last reason only this type of rice-ball geometries was addressed in this work. In

TABLE 3: Sum of Adiabatic Bond Dissociation Energies, BDEs, BDEs per Benzene Unit, and Sequential BDEs for the Neutral and Charged Species of the $\text{Fe}_6-(\text{C}_6\text{H}_6)_m$, $m = 1-4$, Complexes^a

complex	products	BDE (kJ/mol) sum	BDE (kJ/mol) per benzene unit	BDE (kJ/mol) sequential
$\text{Fe}_6-\text{C}_6\text{H}_6$	$\text{Fe}_6 + \text{C}_6\text{H}_6$	83.3	83.3	83.3
$\text{Fe}_6-(\text{C}_6\text{H}_6)_2$	$\text{Fe}_6 + 2\text{C}_6\text{H}_6$	200.8	100.4	117.2
$\text{Fe}_6-(\text{C}_6\text{H}_6)_3$	$\text{Fe}_6 + 3\text{C}_6\text{H}_6$	274.9	91.6	74.5
$\text{Fe}_6-(\text{C}_6\text{H}_6)_4$	$\text{Fe}_6 + 4\text{C}_6\text{H}_6$	297.9	74.5	23.4
$[\text{Fe}_6-\text{C}_6\text{H}_6]^+$	$\text{Fe}_6^+ + \text{C}_6\text{H}_6$	162.3	162.3	162.3
$[\text{Fe}_6-(\text{C}_6\text{H}_6)_2]^+$	$\text{Fe}_6^+ + 2\text{C}_6\text{H}_6$	320.5	160.2	157.8
$[\text{Fe}_6-(\text{C}_6\text{H}_6)_3]^+$	$\text{Fe}_6^+ + 3\text{C}_6\text{H}_6$	416.7	138.9	95.4
$[\text{Fe}_6-(\text{C}_6\text{H}_6)_4]^+$	$\text{Fe}_6^+ + 4\text{C}_6\text{H}_6$	456.9	114.2	40.3
$[\text{Fe}_6-\text{C}_6\text{H}_6]^-$	$\text{Fe}_6^- + \text{C}_6\text{H}_6$	70.7	70.7	70.7
$[\text{Fe}_6-(\text{C}_6\text{H}_6)_2]^-$	$\text{Fe}_6^- + 2\text{C}_6\text{H}_6$	135.6	67.8	64.8
$[\text{Fe}_6-(\text{C}_6\text{H}_6)_3]^-$	$\text{Fe}_6^- + 3\text{C}_6\text{H}_6$	228.4	76.1	92.8
$[\text{Fe}_6-(\text{C}_6\text{H}_6)_4]^-$	$\text{Fe}_6^- + 4\text{C}_6\text{H}_6$	261.1	65.3	35.4

^a The results for $m = 1$ and 2 are from ref 13.

this regard, a more complete study should consider also the multiple-decker sandwich states to determine, undoubtedly, the GSs of these compounds. Lastly, the BDE of $\text{Fe}-\text{C}_6\text{H}_6$ is estimated to be greater than 67.4 kJ/mol; our theoretical results are consistent with this experimental value for a single Fe atom^{1,27,28} and with the binding energy of benzene, 103.3 kJ/mol, on an infinite $\text{Fe}(100)$ surface.²⁹

Assuming $[\text{Fe}_6-(\text{C}_6\text{H}_6)_m]^+ \rightarrow \text{Fe}_6^+ + m\text{C}_6\text{H}_6$, dissociation paths, which is reasonable because the IE of Fe_6 is smaller than that of benzene, adiabatic BDEs of 416.7 and 456.9 kJ/mol, or 138.9 and 114.2 kJ/mol per ligand, were found for $m = 3$ and 4, respectively. These results are reported in Table 3, together with those for $m = 1$ and 2. These BDEs are bigger than those of the neutrals, accounted for by the increase of the electrostatic contributions. The BDE per benzene unit decreases as the adsorption of benzene increases, which is clearer from $m = 3$ to $m = 4$, with a fall of 24.7 kJ/mol. A similar behavior is exhibited by the sequential BDEs (see Table 3), but with bigger reductions from $m = 2$ to $m = 3$, of 62.4 kJ/mol, and from $m = 3$ to $m = 4$, of 55.1 kJ/mol, yielding a relatively small binding energy, of 40.3 kJ/mol, for the fourth benzene molecule. Experimentally,²⁷ the BDEs for $\text{Fe}^+-(\text{C}_6\text{H}_6)_m$, $m = 1$ and 2, are equal to 207.5 ± 9.6 and 187.0 ± 16.3 kJ/mol, respectively; they are close to each other, with the latter slightly smaller; our results for Fe_6^+ closely follow this trend. As expected, the binding energy for $\text{Fe}_6^+-\text{benzene}$ is lower than that of $\text{Fe}^+-\text{benzene}$, because, aside from the bonding with benzene, the Fe atoms are also bonded with the other atoms in the cluster.

For the $[\text{Fe}_6-(\text{C}_6\text{H}_6)_m]^- \rightarrow \text{Fe}_6^- + m\text{C}_6\text{H}_6$ dissociations, the BDEs are 228.4 and 261.1 kJ/mol, for $m = 3$ and 4, respectively. Those for $m = 1$ and 2 are 70.7 and 135.6 kJ/mol.¹³ These BDEs show the biggest increase, 92.9 kJ/mol, from $m = 2$ to $m = 3$; the increases from $m = 1$ to $m = 2$ is 64.9 kJ/mol and from $m = 3$ to $m = 4$ is 32.6 kJ/mol. As shown in Table 3, the BDEs per benzene unit reach a maximum value for $m = 3$. Moreover, the sequential BDEs show a more prominent maximum for $m = 3$, indicating that $[\text{Fe}_6-(\text{C}_6\text{H}_6)_3]^-$ is the anion of highest stability.

3f. Ionization Energies and Electron Affinities. Electron deletion from $\text{Fe}_6-(\text{C}_6\text{H}_6)_3$ and $\text{Fe}_6-(\text{C}_6\text{H}_6)_4$, both with $M = 13$ GSs, was also studied. After structural and electronic relaxation, it was found that $[\text{Fe}_6-(\text{C}_6\text{H}_6)_3]^+$ and $[\text{Fe}_6-(\text{C}_6\text{H}_6)_4]^+$ present GSs with $M = 12$, and producing adiabatic IEs of 4.60 and 4.42 eV, respectively, which are considerably smaller than

those of the bare Fe_6 (6.15 eV) and benzene (9.08 eV) molecules, but they are nearer to the former, suggesting that the electron is principally removed from the Fe_6 particle. As pointed out by Kurikawa et al., these IE reductions reflect signatures of $d-\pi$ bonding interactions.¹ Effectively, in $\text{Fe}_6-(\text{C}_6\text{H}_6)_3$ the electron is removed from the HOMO^\dagger level, lying at -2.99 eV, which shows major 3d contributions highly localized on the atomic sites of the Fe_6 core; some minor π contributions also appear on the benzene units, a nonbonding behavior between Fe_6 and the benzene units is also shown (see Figure 3). This HOMO^\dagger electron is weakly bonded on the complex. These features account for the relatively low IE of the $\text{Fe}_6-(\text{C}_6\text{H}_6)_3$ complex. A similar behavior occurs on $\text{Fe}_6-(\text{C}_6\text{H}_6)_4$ where the electron is also deleted from the HOMO^\dagger , showing major 3d components and small π contributions on benzene **c**; see Figure 4. These results should be compared with those obtained for $\text{Fe}_6-(\text{C}_6\text{H}_6)$ and $\text{Fe}_6-(\text{C}_6\text{H}_6)_2$, which have IEs of 5.31 and 4.90 eV, respectively,¹³ revealing that the IEs decrease as m increases, reaching a lowest value for $m = 4$.

Electron addition to the $M = 13$ GS of $\text{Fe}_6-(\text{C}_6\text{H}_6)_3$ produces, after full relaxation, a $M = 14$ GS for the $[\text{Fe}_6-(\text{C}_6\text{H}_6)_3]^-$ anion. The energy difference between these states, including ZPE, produces an EA, 1.02 eV, which is markedly smaller than the EA of Fe_6 , 1.61 eV, signifying that the extra electron is more weakly bonded in the $[\text{Fe}_6-(\text{C}_6\text{H}_6)_3]^-$ ion, which is due to repulsion effects and to the fact that the electron goes into the LUMO^\dagger level of the neutral complex (see Figure 3), showing a low bond behavior. The π contribution on benzene **c** and the bonding between one axial and one equatorial Fe atom (see Figure 3) account for some stabilization of the added electron. Electron addition also yields an $M = 14$ GS for $[\text{Fe}_6-(\text{C}_6\text{H}_6)_4]^-$, and the adiabatic EA, 1.13 eV, matches with the measured value, 1.1 ± 0.1 eV.⁴ The bond signatures of the LUMO^\dagger , Figure 4, between Fe_6 and benzene **d**, account for the shortening of the $\text{Fe}-\text{C}$ bonds showed by the anion; see Table 2b.

3g. Vibrational Analysis: $\text{Fe}_6-(\text{C}_6\text{H}_6)_3$, $[\text{Fe}_6-(\text{C}_6\text{H}_6)_3]^+$, and $[\text{Fe}_6-(\text{C}_6\text{H}_6)_3]^-$. The estimated IR spectrum of $\text{Fe}_6-(\text{C}_6\text{H}_6)_3$, reported in Figure 5Sc and in Table 1S of the Supporting Information, shows two main properties. First, it presents vibrational resonances near those of bare benzene, and some forbidden IR modes of benzene become IR-active in the reduced symmetry of the complex, which, differently from benzene has a dipole moment of 1.09 D. These facts emerge by comparing the spectra of benzene, Figure 5Sb (Supporting Information), and $\text{Fe}_6-(\text{C}_6\text{H}_6)_3$. Specifically, the strong band at 738 cm^{-1} accounts for out-of-plane (oop) CH bend modes of the **a** and **b** units and is shifted to the blue, by 77 cm^{-1} , with respect to the value of free benzene, 661 cm^{-1} . The oop CH bend of **c** also is moved, by 74 cm^{-1} , to a higher value. These shifts to the blue are essentially mechanical effects, because the presence of the Fe_6 cluster on the benzene rings impedes the oop hydrogen bend, driving the frequency higher. The in-plane CH (ipch) bend modes of the **a** and **b** moieties correspond to the weak bands (≈ 6) lying at $987-993 \text{ cm}^{-1}$ and shifted to the red by $41-48 \text{ cm}^{-1}$. For **c**, the ipch modes lie at 991 and 997 cm^{-1} , with smaller intensities, (0.9) and (3.7), and with similar shifts to the red, 43 and 37 cm^{-1} . Values in parentheses are for the intensities in km/mol. The small bands (≤ 5.9) centered at $1422-1426 \text{ cm}^{-1}$ are assigned to in-plane-carbon ring distortion (ipc-*rd*) modes, and are shifted to the red by $47-50 \text{ cm}^{-1}$. The frequency decrease of the ipch and ipc-*rd* bands indicate weakened bonding in the benzene rings. Moreover, the symmetric ring stretching of free benzene, at 990 cm^{-1} , is IR inactive. In $\text{Fe}_6-(\text{C}_6\text{H}_6)_3$, this mode lies at 953 cm^{-1} , for

a and **b** in the out-of-phase way (while one ring shrinks the other expands), and becomes IR active, and for benzene **c**, it is positioned at 966 cm⁻¹ and also becomes IR active. These modes are displaced to the red, by 25–37 cm⁻¹, signifying also a weakening of the bonding in the benzene molecules.

The IR spectrum of Fe₆-(C₆H₆)₃ shows two strong bands [see Figure 5Sc (Supporting Information)]; the higher frequency of 3139 cm⁻¹ is for the CH symmetric stretching (sym str), of the **a** and **b** moieties. The CH sym str of **c** is placed at 3138 cm⁻¹ and also is IR active. The CH asymmetric stretching (asym str) modes are located at 3129–3134 cm⁻¹; they remain IR active but with weaker resonances (16–27.5) than in free benzene, where they appear at 3121 cm⁻¹ [see Figures 5Sb and 5Sc (Supporting Information)]. Small shifts to the blue, less than 13 cm⁻¹, are suffered by these sym and asym str modes. The other strongest band falls at 342 cm⁻¹, and it originates from the mixing of the vibrational modes of benzene with those of Fe₆. The IR spectrum of the Fe₆ cluster is shown in Figure 5Sa; see the Supporting Information section for more details.

The IR spectrum of [Fe₆-(C₆H₆)₃]⁺ is shown in Figure 6Sa (Supporting Information). The cation also possess a strong band, at 760 cm⁻¹, for the oop CH bending of **a** and **b**. For **c**, it lies at 779 cm⁻¹. These modes are shifted to the blue, by 99–118 cm⁻¹, more strongly than in the neutral. The ipch and ipc-rd bands and the symmetric ring stretching also are shifted to the red; see Table 2S and the Supporting Information. Another difference with the neutral is that in the cation the asym and sym CH str modes also are IR active, but they show very weak bands.

The IR spectrum of [Fe₆-(C₆H₆)₃]⁻ is shown in Figure 6Sb of the Supporting Information; see also Table 3S in the Supporting Information. The most marked feature is the absence of the ipc-rd modes at the middle of the spectrum. In fact, these modes, which are IR active in benzene, become IR forbidden in the anion. The strongest band of this anion falls, as in the neutral complex, at the top of the spectrum, assigned to the sym CH str of **a** and **b**. As compared with the neutral, the oop CH bending shows smaller shifts to the blue and the ipch modes are moved more strongly to the red.

3h. Vibrational Analysis: Fe₆-(C₆H₆)₄, [Fe₆-(C₆H₆)₄]⁺, and [Fe₆-(C₆H₆)₄]⁻. The IR spectrum of Fe₆-(C₆H₆)₄ shows a large increase of vibrational modes, IR forbidden in benzene, that become IR active in the complex. These features can be observed in Figure 7S and in Table 4S of the Supporting Information. In fact, as it was found for Fe₆-(C₆H₆)₃, the tetramer also presents resonances near those of the free benzene molecule. For instance, the oop CH bends for the **a**, **b**, and **c** moieties also are shifted to the blue. However, the oop CH bend for the fourth benzene **d** was found at the 651 cm⁻¹ moderate band, and instead of being shifted to the blue, it is shifted to the red by about 10 cm⁻¹, implying a considerable reduction of the mechanical impedance, discussed above, for the CH bend. The ipch bend modes located at the 995–1006 cm⁻¹ weak band are displaced to the red by 29–40 cm⁻¹. Also the ipc-rd and the symmetric ring stretching modes are shifted to the red by about 23–49 cm⁻¹ and by 23–40 cm⁻¹, respectively. One of the strongest bands of this complex is situated in the high frequency region and originates from the addition of several asymmetric CH stretching modes. The other strongest band falls in the low frequency region, at 339 cm⁻¹, and is a mixture of benzene and Fe₆ vibrational modes.

The IR spectrum of the [Fe₆-(C₆H₆)₄]⁺ ion also shows a considerable increase of IR active vibrational modes, which otherwise are IR forbidden in the isolated benzene moiety. As can be observed in Figure 7Sb and in Table 5S of the Supporting Information section, some regions of this cation show more active IR modes than the neutral complex, which is clearly exemplified by the bands located at 300–400 cm⁻¹ (containing mixed Fe₆–benzene vibrations) and at 1400–1500 cm⁻¹ (which is the region of the ipc-rd modes). But at 900–1000 cm⁻¹, the bands are clearly weaker than in the neutral. Also the [Fe₆-(C₆H₆)₄]⁺ cation, as the neutral, shows resonances near those of neutral benzene, but with key differences in the frequency shifts and in the intensities for the prototypical IR bands. For example, the oop CH bend modes in the cation are more strongly shifted to the blue, and also the asymmetric and symmetric CH stretching modes are IR active in the cation, but they show weaker bands, as compared to the neutral complex where strongest bands occur for these modes.

The IR spectrum for the *M* = 14 GS of [Fe₆-(C₆H₆)₄]⁻ shows, as does the *m* = 3 anion, an enhancement in the intensities of the vibrational bands (see Figure 7Sc and Table 6S in the Supporting Information) and also with the distinction that some ipc-rd bands lying at the middle, \cong 1470 cm⁻¹, of the spectrum are IR active on this anion. Note that these modes are absent on the *m* = 3 anion. Thus, these ipc-rd modes, IR active in benzene, also are IR active on [Fe₆-(C₆H₆)₄]⁻. Even so, this spectrum is also different from that of the *m* = 4 neutral and cationic species, the main difference resides in the fact that it presents a smaller amount of IR resonances, mainly in the 1000–1500 cm⁻¹ region. However, the anion exhibits, as does the neutral, the strongest resonances at the top of the IR spectrum, which are growing from the addition of some symmetric and asymmetric CH stretching modes. See the discussion in the Supporting Information for more details on the IR spectra of these neutral and charged complexes.

4. Conclusions

The GS geometries of neutral and charged Fe₆-(C₆H₆)_{*m*}, *m* = 3 and 4, complexes were determined by means of the BPW91/6-311++G(2d,2p) method. In the *M* = 13 GS of Fe₆-(C₆H₆)₃ each benzene unit is adsorbed on one Fe site, forming six Fe–C bonds, and the structure of Fe₆ is preserved, but showing more distortion than in the isolated Fe₆ particle. Fe₆-(C₆H₆)₄ presents an even more distorted geometry, which is due to the repulsion of the adsorbed benzene moieties on the surface of the cluster, producing slightly distorted Fe–C η^6 coordinations and the formation of a lower one, η^2 , for the fourth benzene molecule, being more weakly bonded to the Fe₆ cluster. The d– π interactions are reflected by the estimated adiabatic IEs of the complexes, since they are smaller than that of bare Fe₆. Indeed, delocalization effects, through the network of Fe–C bonds, of the most external electrons of Fe₆-(C₆H₆)_{3,4} account for this behavior. The EAs are also reduced, as compared with the EA of Fe₆. The vibrational analysis reveals the presence of IR bands near those of free benzene, and several forbidden IR modes of benzene become IR active in the reduced symmetry of the complexes; the amount of this type of mode that becomes IR active in the complexes increases with *m*, and the cations (anions) show the biggest (smallest) amount of IR active bands. Conversely, some IR bands of benzene turn IR inactive in the complexes.

Acknowledgment. Financial support from Project PAPIIT IN-102308 from DGAPA-UNAM is acknowledged. Supercom-

puter facilities from DGSCA-UNAM are strongly appreciated. Valuable discussions with Oscar Gonzalez-Antonio are deeply thanked.

Supporting Information Available: Some MOs, of major spin, for the GS of $\text{Fe}_6-(\text{C}_6\text{H}_6)_3$ are shown in Figure 1S. The MOs, of minor spin, for the GS of $\text{Fe}_6-(\text{C}_6\text{H}_6)_3$ are shown in Figure 2S. Some MOs, of major spin, for the GS of $\text{Fe}_6-(\text{C}_6\text{H}_6)_4$ are shown in Figure 3S. The MOs of lower energy, of major spin, for $\text{Fe}_6-(\text{C}_6\text{H}_6)_4$ are contained Figure 4S. Also is reported a vibrational analysis for the neutral and charged species of $\text{Fe}_6-(\text{C}_6\text{H}_6)_3$ and $\text{Fe}_6-(\text{C}_6\text{H}_6)_4$; the vibrational frequencies for each case are reported in Tables 1S–6S and the IR spectra in Figures 5S–7S. This material is available free of charge via the Internet at <http://pubs.acs.org>.

References and Notes

- (1) Kurikawa, T.; et al. *Organometallics* **1999**, *18*, 1430.
- (2) Nakajima, A.; Kaya, K. *J. Phys. Chem. A* **2000**, *104*, 176.
- (3) Duncan, M. A. *Int. J. Mass Spectrom.* **2008**, *272*, 99.
- (4) Zheng, W.; Eustis, S. N.; Li, X.; Nilles, J. M.; C.; Thomas, O. C.; Bowen, K. H.; Kandalam, A. K. *Chem. Phys. Lett.* **2008**, *462*, 35.
- (5) Bansmann, J.; et al. *Surf. Sci. Rep.* **2005**, *56*, 189–275.
- (6) Eberhardt, W. *Surf. Sci.* **2002**, *500*, 242.
- (7) Chen, B.; Castleman, A. W., Jr.; Ashman, C.; Khanna, S. N. *Int. J. Mass Spectrom.* **2002**, *220*, 171.
- (8) Castro, M. *Int. J. Quantum Chem.* **1997**, *64*, 223.
- (9) Castro, M.; Jamorski, C.; Salahub, D. R. *Chem. Phys. Lett.* **1997**, *271*, 133–142.
- (10) Gutsev, G. L.; Bauschlicher, C. W., Jr. *J. Phys. Chem. A* **2003**, *107*, 7013.
- (11) Castro, M. *Chem. Phys. Lett.* **2007**, *435*, 322–326.
- (12) Valencia, I.; Chávez, V.; Castro, M. *J. Phys. Chem. A* **2008**, *112*, 5028.
- (13) Valencia, I.; Guevara-García, A.; Castro, M. *J. Phys. Chem. A* **2009**, *113*, 6222–6238.
- (14) Becke, A. D. *Phys. Rev. A* **1988**, *38*, 3098.
- (15) Perdew, J. P.; Wang, Y. *Phys. Rev.* **1992**, *45*, 13244.
- (16) Wachters, A. J. H. *J. Chem. Phys.* **1970**, *52*, 1033.
- (17) Hay, P. J. *J. Chem. Phys.* **1977**, *66*, 4377.
- (18) Raghavachari, K.; Trucks, G. W. *J. Chem. Phys.* **1989**, *91*, 1062.
- (19) Frisch, M. J. Gaussian 03, Revision D.01; Gaussian Inc.: Wallingford, CT, 2004.
- (20) Billas, I. M. L.; Chatelain, A.; de Heer, W. A. *Science* **1994**, *265*, 1682.
- (21) Cox, D. M.; Trevor, D. J.; Whetten, R. L.; Rohlfing, E. A.; Kaldor, A. *Phys. Rev. B* **1985**, *32*, 7290.
- (22) Yand, S.; Knickelbein, M. B. *J. Chem. Phys.* **1990**, *93*, 1533.
- (23) Wang, L.-S.; Li, X.; Zhang, H.-F. *Chem. Phys.* **2000**, *262*, 53.
- (24) (a) Moore, C. E. *Analysis of Optical Spectra, NSRDS-NBS 34*; National Bureau of Standards: Washington, DC, 1971. (b) Weast, R. C. *Handbook of Chemistry and Physics*; CRC Press: Boca Raton, FL, 1980; Vol. 61, p , E-69. (c) Robinson, J. W. *Handbook of Spectroscopy*; CRC Press: Boca Raton, 1974; Vol. 1, p 257.
- (25) Rabilloud, F. *J. Chem. Phys.* **2005**, *122*, 134303.
- (26) Imura, K.; Ohoyama, H.; Kasai, T. *Chem. Phys.* **2004**, *301*, 183.
- (27) Meyer, F.; Khan, I. A.; Armentrout, P. B. *J. Am. Chem. Soc.* **1995**, *117*, 9740.
- (28) Pandey, R.; Rao, B. K.; Jena, P.; Newsam, J. M. *Chem. Phys. Lett.* **2000**, *321*, 142.
- (29) Sun, X.; et al. *J. Appl. Phys.* **2007**, *101*, 09G256.

JP906131G